TEMPO and RTILs for the Sustainable Development of TEMPO - mediated Alcohol Electrooxidation

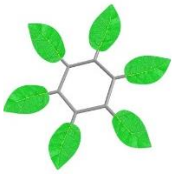

Astrid Delorme

Thesis submitted to the University of Nottingham for the degree of Doctor of Philosophy

September 2019

Abstract

In this thesis, TEMPO-mediated alcohol electrooxidation in room-temperature ionic liquids (RTILs) is described and it is shown that the reactivity and selectivity of the electrocatalytic oxidations can be manipulated by design of the solvent medium. Moreover, higher reaction kinetics and selectivity are obtained in bis(trifluoromethanesulfonyl)imide ($[NTf_2]^-$)-based RTILs than in acetonitrile, often the solvent-of-choice in indirect alcohol electrooxidations.

Electrolytic TEMPO-mediated alcohol oxidations are performed using RTILs in a flow-electrolysis system. Excellent yields and reaction selectivity are achieved, demonstrating the opportunities of replacing volatile molecular solvents and extraneous electrolytes in efficient electrolyses of alcohol oxidations.

Furthermore, by increasing the functionality of the RTIL medium the chemical input as well as the waste formation can be reduced in TEMPO-mediated alcohol oxidations. The use of a stoichiometric base is avoided in the paired electrosynthesis where the base is generated *in situ*, through the electroreduction of a protic RTIL at the counter electrode in parallel with the alcohol oxidation at the working electrode.

Declaration

This thesis is the result of my own investigations, and is not being concurrently submitted in candidature for any degree

Signed____

Date____________________

Acknowledgements

Firstly, I would like thank my supervisors Darren Walsh, Peter Licence and Victor Sans for the guidance in the development of my PhD project and also for their continuous support throughout my PhD. A lot of the success of this project was due to their insightful advices.

I also want to thanks all the past and present members of the Licence and the Walsh group, which have made my time during my PhD very enjoyable. This includes my master project mentor Rebecca Blundell for inspiring me to pursue a PhD. I especially want to thank my dedicated weekend-lab-buddy, Meike Leu, for not only making sure that we got work done, but also making weekend-work abit more fun. I want to express particular thanks to Neelam Mughal, Andreas Weilhard, Lais Dias Ferreira and Sean Goodwin for their advices throughout my PhD and for proof-reading my thesis which has been immensely valuable.

I must also extend my thanks to my placement supervisor, Jochem Zoetelief, who provided me the opportunity to work in a completely different field from my PhD, which has really sparked my interest for environmental research.

Finally, I am incredibly grateful for the support given by my family in so many different ways. My mum, for always encouraging and supporting me, even in the toughest of times during my PhD. And my siblings, who are all pursuing their own ambitions in their own unique ways and are truly a source of inspiration.

Abbreviations and Symbols

TEMPO	2,2,6,6-tetramethylpiperidine-1-oxyl
CV	Cyclic voltammogram
i	Current, A
J	Current density, A cm^{-2}
i_{p}	Peak current, A
$i_{\mathrm{p,a}}$	Anodic peak current, A
$i_{\mathrm{p,c}}$	Cathodic peak current, A
E	Potential, V
$E_{\mathrm{p,a}}$	Anodic peak potential, V
$E_{\mathrm{p,c}}$	Cathodic peak potential, V
$E_{\mathrm{T},\frac{1}{2}}$	Half-wave potential of TEMPO/TEMPO^{+} redox couple, V
ΔE	Peak potential difference, V
n	Number of electrons
A	Electrode surface area, cm^{2}
D	Diffusion coefficient, cm^{2} s^{-1}
D_{T}	Diffusion coefficient of TEMPO, cm^{2} s^{-1}
D_{A}	Diffusion coefficient of alcohol, cm^{2} s^{-1}
C	Concentration, mol dm^{-3}
C_{T}	Concentration of TEMPO, mol dm^{-3}
C_{A}	Concentration of alcohol, mol dm^{-3}
k	Apparent reaction rate constant, dm^{3} mol^{-1} s^{-1}
v	Scan rate, V s^{-1}
F	Faraday’s constant, 96485 C mol^{-1}
m	Amount of substance in moles, mol

t	Time, s or min
Q_v	Voltammetric flow rate, cm^3 min^{-1}
QRE	Quasi-reference electrode
IL	Ionic liquid
RTIL	Room temperature ionic liquid
TSIL	Task specific ionic liquid
α	Kamlet-Taft hydrogen bond donating ability
β	Kamlet-Taft hydrogen bond accepting ability
π^*	Kamlet-Taft dipolarity/polarizability effect
ESI-MS	Electrospray ionisation mass spectrometry
m/z	Mass to charge transfer
NMR	Nuclear magnetic resonance
PFG-NMR	Pulsed field gradient nuclear magnetic resonance
ppm	Parts per million
δ	Chemical shifts, ppm
IR	Infrared spectroscopy
ν_{max}	Wavenumber
GC-MS	Gas chromatography mass spectrometry
GC-FID	Gas chromatography flame ionisation detection
VOC	Volatile organic compound
pK_{aH}	Acid dissociation constant of conjugate acid (logarithmic scale)
dmFc	Decamethylferrocene
$[C_nC_1Im]^+$	1-alkyl-methylimidazolium
$[C_nC_1Pyrr]^+$	1-alkyl-1-methylpyrrolidinium
$[C_4HIm]^+$	1-butylimidazolium
$[NR_1R_2R_3R_4]^+$	*N, N, N, N* – tetraalkylammonium
$[PR_1R_2R_3R_4]^+$	*N, N, N, N* – tetraalkylphosphonium
$[NTf_2]^-$	Bis(trifluoromethanesulfonyl)imide

$[PF_6]^-$	Hexafluorophosphate
$[OTf]^-$	Trifluoromethanesulfonate
$[DCA]^-$	Dicyanamide
$[TEMPOOSO_3]^-$	2,2,6,6-tetramethylpiperidine-1-oxyl-4-sulfate

Table of Contents

List of Figures

List of Tables

List of Schemes

1. Introduction

1.1. Alcohol Oxidations

Alcohol oxidation is one of the most important reactions in organic chemistry. Carbonyl compounds formed from alcohol oxidations are used in the industrial manufacture of pharmaceuticals, fragrances and food additives. The synthesis of some classes of drugs, such as prostaglandins and steroids, require a high number of oxidations.[1, 2] Despite the importance of carbonyl functional groups, the scale-up of alcohol oxidations remains problematic and is often avoided by industry, especially within the pharmaceutical industry.[1] In a review regarding the types of reactions used for the preparation of drug candidate molecules by industrial experts from GlaxoSmithKline, Pfizer and AstraZeneca, it was stated that only 3.9% of the reactions studied were oxidations. Of these, the most common was sulfur oxidation, followed closely by alcohol oxidation.[3]

One example of a particularly oxidation-rich process that was used on industrial scale, is the synthesis of cortisone acetate from deoxycholic acid, which was operated in the 1950s and 1960s on a multi-hundred kilogram scale, with 11 separate synthetic steps.[2] The first step involved oxidation of the secondary alcohol to its corresponding ketone, and CrO_3 was used as the oxidant. However, hexavalent chromium is toxic and carcinogenic. Due to stricter regulations, the use of hexavalent chromium on industrial scale has reduced significantly since the 1980s.[2, 4] Today, two of the most commonly used alcohol oxidations carried out by Pfizer's medicinal chemists at industrial scale are the Swern oxidation and oxidation with tetra-*N*-propylammonium perruthenate (TPAP).[5]

The Swern oxidation drives oxidation of primary alcohols to aldehydes, using oxalyl chloride ($(COCl)_2$) dimethyl sulfoxide (DMSO) and a base such as trimethylamine (Et_3N).[2] For example it is used in the synthesis of the anticancer drug, camptothecin, in which the primary alcohol group is oxidised to yield the important aldehyde intermediate, see Scheme 1.14.[2, 6]

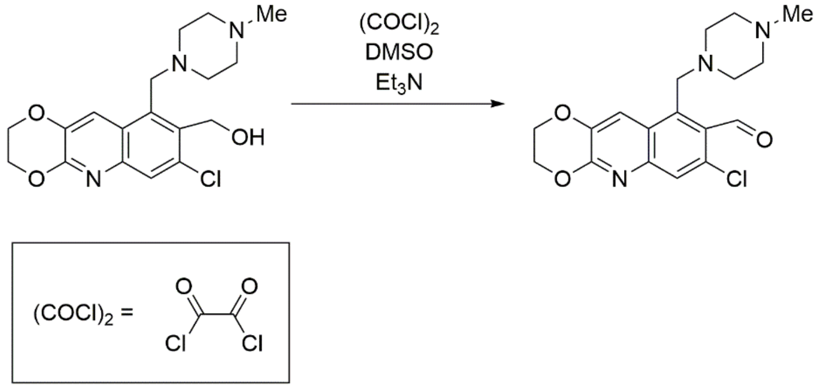

Scheme 1.14: Synthesis of aldehyde intermediate of camptothecin using the Swern protocol.[2]

While the Swern oxidation avoids the use of CrO_3, drawbacks include the generation of a large amounts of CO_2, dimethyl sulfide and CO.[2] Furthermore, an activated form of dimethyl sulfoxide, DMSO, is required, which can lead to violent and exothermic reactions, so the reaction is carried out at –60 °C. Furthermore, the choice of the reagent to activate DMSO is crucial for high conversions. The best performing activators, in terms of product yields and minimal by-product formation, are thionyl chloride and oxalyl chloride. Oxalyl chloride, however, is moisture sensitive, toxic and its vapour is a powerful irritant.[7]

In recent years, the use of metals in catalytic oxidations, and in particular for the oxidation of secondary alcohols, has received increased attention; a noteworthy example is the use of TPAP in combination with the co-oxidant *N*-methylmorpholine-*N*-oxide, NMO, for the preparation of a macrolide antibiotic (Scheme 1.15).[2, 8]

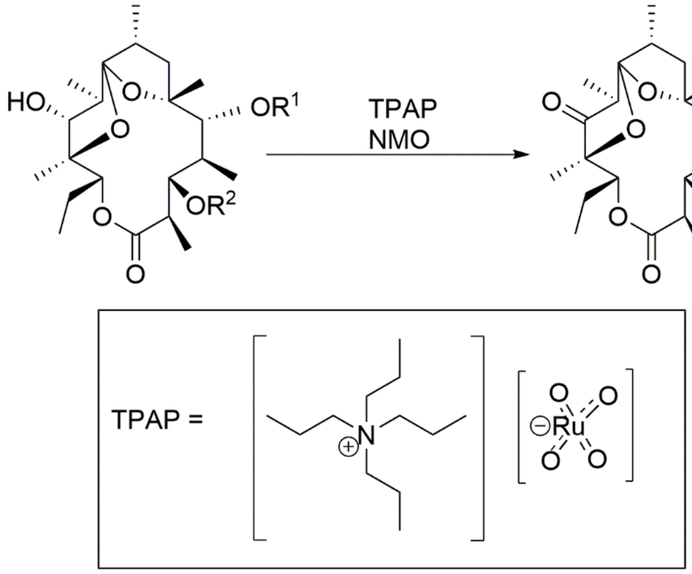

Scheme 1.15: Example of oxidation of a secondary alcohol functionality in the synthesis of a macrolide antibiotic using TPAP and NMO.[8]

The stoichiometric use of TPAP generates a considerable amount of waste. However, TPAP can be used in catalytic amounts when combined with the co-oxidant NMO.[2, 8] TPAP is a strong oxidant and is infrequently used for the oxidation of primary alcohols, as it can cause over-oxidation to the corresponding carboxylic acid. The presence of other reactive groups or bonds, such as amines, could also be problematic when using TPAP catalysts and by-products can be formed.[2]

Overall there is relatively few atom efficient, chemoselective and environmentally acceptable alcohol oxidation methods performed at industrial scale. The discovery of new, sustainable and scalable oxidations would greatly increase the flexibility in synthetic design and provide a more direct route in obtaining carbonyl groups.[1, 2, 5, 9-11]

1.1.1. TEMPO-mediated alcohol oxidations

The oxidised form of 2,2,6,6-tetramethylpiperidine-1-oxyl (TEMPO) and its derivatives are powerful, metal-free and environmentally sustainable reagents for the catalytic oxidation of primary and secondary alcohols to their corresponding carbonyl compounds. It tolerates other oxidisable groups and rarely leads to over-oxidation of products.[10]

While TEMPO-mediated alcohol oxidations have been known for more than a quarter of a century the reaction mechanism is still being explored.[12-16] It is known that the first step is to oxidise the radical TEMPO to its active oxoammonium cation (TEMPO$^+$) form. The oxidation of TEMPO to TEMPO$^+$ can be achieved electrochemically or using a secondary oxidant. Then, at least two steps are involved. In the first step an adduct between TEMPO$^+$ and the alcohol is formed. In the second step the adduct decomposes to form the carbonyl product and the reduced form of TEMPO (Scheme 1.16).[13, 16-18]

Typically, the reaction is performed under alkaline conditions, in which TEMPO exhibits strong stereoselectivity towards the oxidation of primary alcohols over secondary alcohols. This selectivity has been attributed to steric effects in the formation of the alcohol-TEMPO$^+$ adduct. The stability of these intermediates decreases with sterically crowded complexes, and gives a rationale for why primary alcohols are kinetically more favourable than secondary alcohols. A fundamental change in selectivity is observed when the oxidation is carried out under acidic conditions. Here, the mechanism has been proposed to be a bimolecular hydride transfer which favours the more electron rich secondary alcohols over primary alcohols, as illustrated in Scheme 1.16. Furthermore, TEMPO-mediated alcohol oxidations under acidic conditions are significantly slower than those under basic conditions.[15, 19, 20]

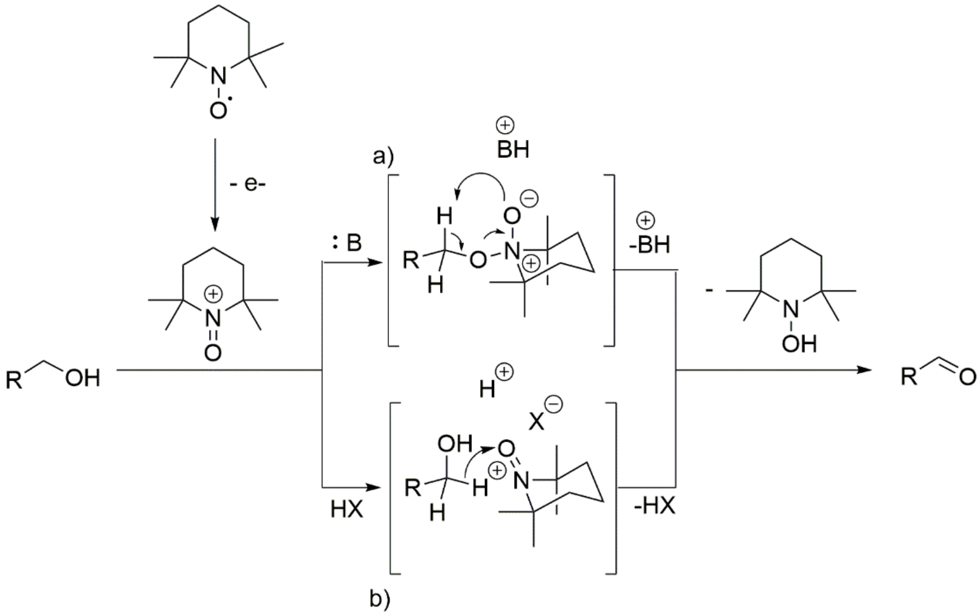

Scheme 1.16: Proposed mechanism for TEMPO-mediated oxidation of alcohols under a) basic conditions and b) acidic conditions.[18]

Under alkaline conditions, the rate of reaction is highly dependent on the concentration and the pK_{aH} of the base used in the reaction (or the pH in aqueous media). The greater the pH, concentration or pK_{aH} of the base used in the reaction the greater the rate of reaction, for both secondary and primary alcohols.[18, 21] The strong base dependency can be explained by the Brönsted equilibrium between the base and the alcohol, as well as between the hydroxylamine form of TEMPO and the base. Furthermore, deprotonation of the alcohol and hydroxylamine by the base is considered to be the rate-determining step (Scheme 1.17).[13, 21]

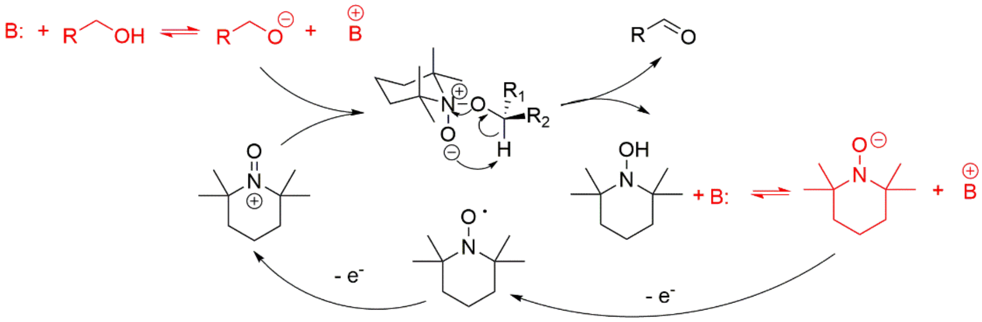

Scheme 1.17: TEMPO-mediated alcohol oxidation showing the rate-determining steps highlighted in red, which are the deprotonation of the alcohol and the deprotonation of the hydroxylamine by the base.[13]

Most of industrial oxidation processes that use TEMPO and its derivatives apply Anelli-Montanari type conditions.[22] For example, Pfizer use Anelli-Montanari conditions together with 4-hydroxy-TEMPO to convert bisnoralcohol to bisnoraldehyde (an intermediate to preogesterone). In this method, bleach is added in excess as part of the secondary oxidation together with an oxidant such as hypobromite, see Scheme 1.18.[1, 22, 23, 24]

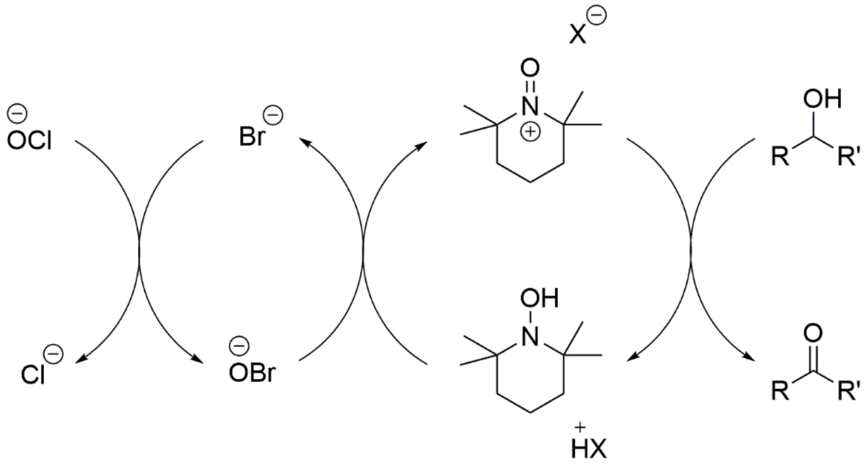

Scheme 1.18: Anelli-Montanari protocol where an alcohol substrate is oxidised by the oxoammonium salt, to yield a carbonyl product and the hydroxylamine species which is oxidised back to the oxoammonium salt with a halide and hypochlorite co-oxidant.[22]

Although the use of bleach provides a cheap approach to TEMPO-mediated alcohol oxidations, bleach is not compatible with certain functional groups and often results in unwanted chlorinated by-products. Over the years, a variety of secondary oxidants have replaced bleach in the classic Anelli-Montanari oxidation. For example, O_2 has been used as the co-oxidant in a Cu/TEMPO-based catalytic system developed by Stahl and co-workers.[23, 24]

The electrochemical approach eliminates the requirement for additional molecular oxidants such as bleach and Cu, and ultimately simplifying product recovery and improving reaction selectivity. Despite these advantages, unfamiliarity with electrosynthetic methods, as well as the use of volatile organic compounds (VOC) and expensive supporting electrolytes, may be contributing to the slow uptake of electrosynthesis. To the best of our knowledge, only one industrial TEMPO-mediated alcohol oxidation has been reported.[15, 22, 25]

1.2. Electrosynthesis

Chemical transformations involve the transfer of electrons, where electrons of a substrate can be lost (oxidation) and electrons can be gained (reduction). In conventional organic syntheses, the transfer of electrons to or from a substrate is facilitated by a chemical reductant or oxidant. Electrodes may be regarded as heterogeneous catalysts that can accept and provide electrons. Compared to chemical oxidants/reductants, these electrodes are easily separated from the reaction mixture and products, which can reduce the overall amount of processing steps of a synthesis, improve the atom efficiency and reduce the amount waste generated.[26, 27] Electrosynthetic routes can also be compatible with a wide range of functional groups, have higher energy efficiency than thermal processes, and high selectivity, since the degree of oxidation and reduction is easily controlled by the electrode potential. Furthermore, the unique approaches in electrosynthesis may facilitate the discovery of unique processing routes and new molecule syntheses.[28]

Existing synthetic transformations based on chemical reagents can often be ‘re-engineered’ and the chemical reagent replaced with a suitable electrode process.[27] For example, the synthesis of complex terpenes are often formed though unsustainable and impractical allylic C-H oxidations. As an example, 15 equivalents of CrO_3·pyridine are used for the allylic oxidation of valencene to the valued nootkatone, the principal aroma from grapefruit.

The conditions developed by Baran and co-workers employ *N*-hydroxyphtalimide as a catalyst which undergoes anodic oxidation to a highly reactive oxygen-centred radical, which then performs the allylic C-H oxidation of a substrate (Scheme 1.19). It has also been shown that this protocol can easily be scaled up to the100-g scale and has a wide substrate scope.

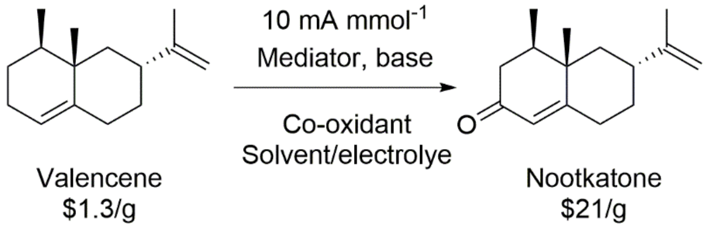

Scheme 1.19: Allylic C-H oxidation of valencene to nootkatone using, example of conditions, tert-butylhydroperoxide as co-oxidant, pyridine as the base, acetonitrile as the solvent and $LiClO_4$ as the electrolyte.[29]

Using an electrochemical route often eliminates the need for excess amounts of toxic reagents and minimises the use of solvents and aqueous media for the work-up (as is typically needed to remove unreacted Cr(VI)). To verify the improved environmental footprint and efficiency, the conditions used by Baran and co-workers were compared against the commonly used Cr(IV) mediated allylic C-H oxidation methods. It was found that the electrochemical route improved the process green score, PGS, (a metric used to evaluate the greenness of a process) by nearly 50% compared to that of the Cr(IV)-mediated allylic C-H oxidation.[29]

The wide-spread use of electrosynthesis has, however, previously been limited in the user-friendliness, availability and accessibility of the techniques and apparatus. The lack of electrosynthesis in laboratories is believed to be due to the perceived complex and unfamiliar reaction set-up which includes a potentiostat, divided/undivided cell, electrode composition, experiment type and the seemingly endless number of reaction variables, such as electrolyte and cell type.[30-33] However, electrosynthetic methods are currently undergoing a renaissance, and more techniques and instruments are becoming available.[30]

1.2.1. Electrolysis Cells

Recently, Aubé and co-workers have reported a very practical and simple set-up for the C-H electrooxidation of complex polycyclic lactams. They used a repurposed cell-phone charger as the power supply and a #7 mechanical pencil lead as electrodes (Scheme 1.20).[34] This simple set-up has some limitations, as the potential and current are not as easily controlled, but it demonstrates the simplicity of electrosynthesis.[30, 34]

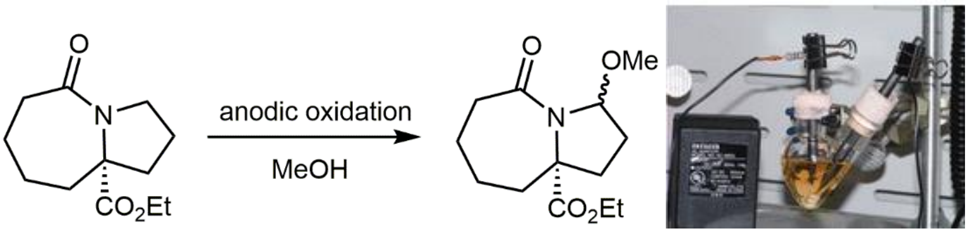

Scheme 1.20: Synthesis of functionalised polycyclic lactams by Aubé and co-workers using a repurposed mobile phone charger and a pencil for the anodic oxidation.[33, 34]

The use of commercially available cells, electrodes and electrolytes could make the use of electrosynthesis more attractive.[33] A few groups and companies have worked together to produce ‘easy-to-use’ electrochemical cells. For example Baran and co-workers, together with IKA, have developed a compact electrochemical kit (Electrasyn) to enable easy access to electrochemistry by chemists who are not experts in electrochemistry.[35, 36]

In the past 15 years, there has been a growing interest in the application in microflow synthesis because of its ability to deliver high selectivity and high conversions in a single pass. This concept has also extended into the field of electrochemistry. There is now a number of commercially-available, flow-through microreactor systems for organic electrosynthesis.[27, 32, 37, 38] Examples include the Ammonite cells developed by Cambridge Reactor Design Ltd and the Asia flux module fabricated by Syrris Ltd.[39] Efficient, selective and clean reactions have been performed in these cells. For example, Brown and co-workers used the Ammonite15 cell to perform the methoxylation of *N*-formylpyrrolidine. This reaction proceeds *via* a reactive intermediate in methanol produced at a carbon/polymer anode. At the cathode (stainless steel), methanol is reduced to hydrogen and methoxide, which then reacts with the intermediate formed at the anode. The overall reaction is formally a dehydrogenative coupling (Scheme 1.21). The reaction was used on a multi-gram scale, operated with inexpensive auxiliary equipment, and achieved high conversions and reaction selectivity in a single pass. Furthermore, the cell is straightforward to use, can be used with a simple power unit and is easy to dismantle, clean and reassemble.[40]

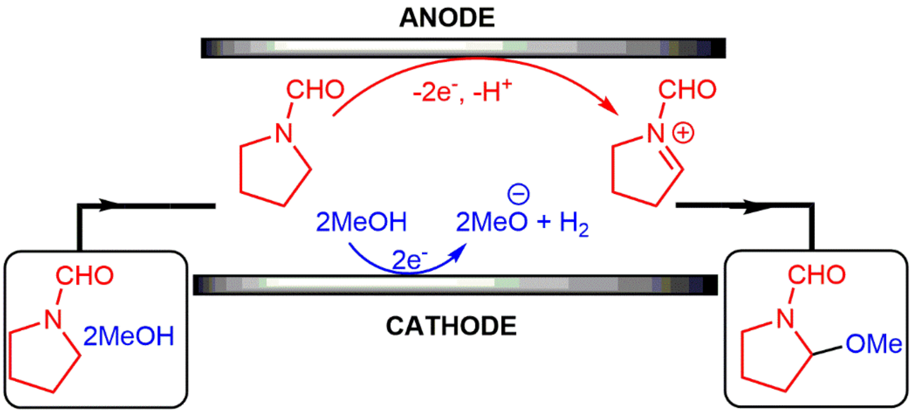

Scheme 1.21: Anodic methoxylation of *N*-formylpyrrolidine in a microfluidic electrolysis cell.[39]

A more detailed discussion of electrochemical cells for electrosynthesis can be found in Section 2.1.3., including flow electrolysis cells.

1.2.2. TEMPO-mediated Alcohol Electrooxidations: Current Work and Challenges.

Semmelhack and co-workers were the first to report the use of TEMPO as a selective and efficient redox catalyst for the electrooxidation of primary and secondary alcohols in 1983.[15] TEMPO undergoes direct electron transfer at the electrode surface and is known to form the reactive TEMPO$^+$ intermediate. Since its discovery, the redox activity of TEMPO coupled with its good catalytic performance, has spawned continual interest in the indirect anodic oxidation of alcohols employing TEMPO or its derivatives as a sustainable alternative for alcohol oxidations.[15, 17]

The chemoselectivity of TEMPO as well as the selectivity associated with electrosynthesis is particularly valuable in the oxidation of diols and carbohydrates derived from renewable sources such as glycosides in terms of obtaining pharmaceutically important products.[41] Schäfer and co-workers used TEMPO-mediated electrooxidations to convert methyl-glycosides and disaccharides into the corresponding uronic acid derivatives. The primary alcohols were oxidised selectively under potentiostatic conditions, leaving secondary alcohols and other functional groups intact, see Scheme 1.22. Good conversions and selectivities with a good substrate scope were obtained.[42]

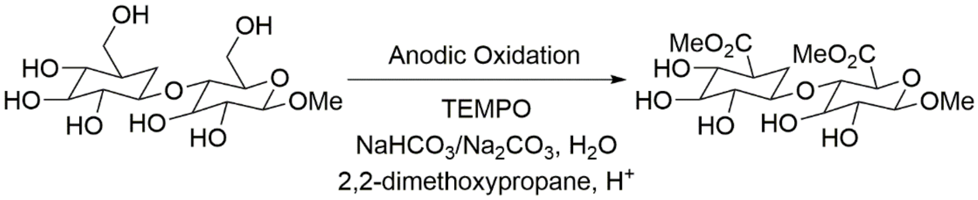

Scheme 1.22: Selective oxidation of methyl glycoside derivative with TEMPO and anodic oxidation.[42]

The Anelli-Montanari conditions in which the hypobromite oxidant together with excess bleach as the co-oxidant replaced the electrooxidation. However, under these conditions the bleach and the intermediate bromide can react with sensitive functional groups. In addition, the work-up of polar uronic acids from aqueous sodium halide solutions is challenging. The use of electrooxidation of TEMPO is advantageous, not only in terms of eliminating the chemical oxidants, but also because the electrodes do not interfere with the oxidation, ensuring good substrate scope, selectivity, ‘clean’ reactions and comparatively simple product recovery.[42]

The TEMPO-mediated electrooxidation has also been implemented in industrial processes. Betula Extractives is a commercial pilot plant part of The Actives Factory (Minnesota, US) which provides a cost-effective, safe and efficient method of converting betulin to betulin-28-aldehyde using TEMPO-mediated electrooxidation of betulin (Scheme 1.23). Betulin is a triterpene which is extracted from the bark of white birch.[24] It is a precursor to betulinic acid, which is a valued substance ($570/g) known for its anti-tumour activity against melanoma and anti-HIV activity in phocytic cells.[43] The synthesis is a one-step method that typically affords about 95% of betulin-28-aldehyde, and 5% unreacted starting material, leaving the secondary alcohol group intact. Their electrochemical undivided set-up is composed of a 2500 cm^3 Duran reaction which is equipped with an electrode bank of 3 flat platinum gauze anodes (50 x 50 mm) and 2 copper plate cathodes of the same size, clamped through 3 mm Teflon spacers and heating mantles.[44]

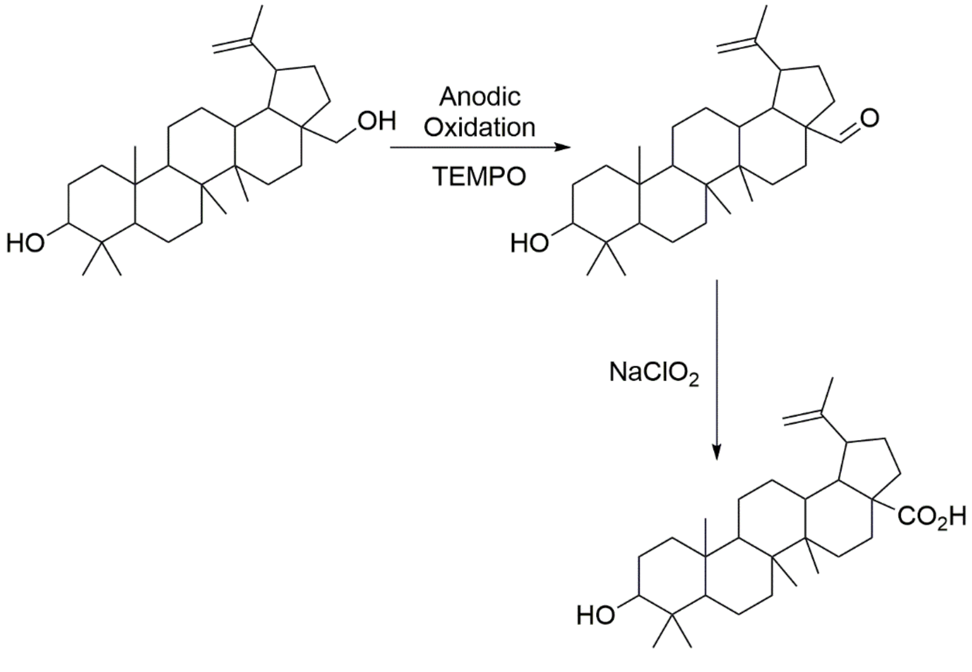

Scheme 1.23: Oxidation of betulin to botulin-28-aldehyde mediated by TEMPO and then conversion of botulin-28-aldehyde to the valuable betulinic acid.[24]

This process demonstrates the industrial feasibility of selective TEMPO-mediated electrooxidations.[24] Some significant drawbacks with this process are, however, that the process temperature is 70 °C for the reason to provide better solubility of betulin, TEMPO is not recovered, nor is the electrolyte (*p*-toluenesulfonate) used in the processs.[45]

Besides the poor recyclability of TEMPO in TEMPO-mediated electrooxidation of alcohols, the poor solubility of TEMPO in aqueous media limits its synthetic applicability. TEMPO bearing ionic tags have been synthesised in order to increase their solubility in aqueous electrolyte solutions.[33, 46] This problem can also be circumvented through the use of a biphasic solvent mixtures, wherein a halide in the aqueous phase undergoes oxidation, which can then oxidise TEMPO (which is in the organic phase) at the aqueous-organic interface.[47] Such biphasic system is illustrated in Scheme 1.24.[33, 47]

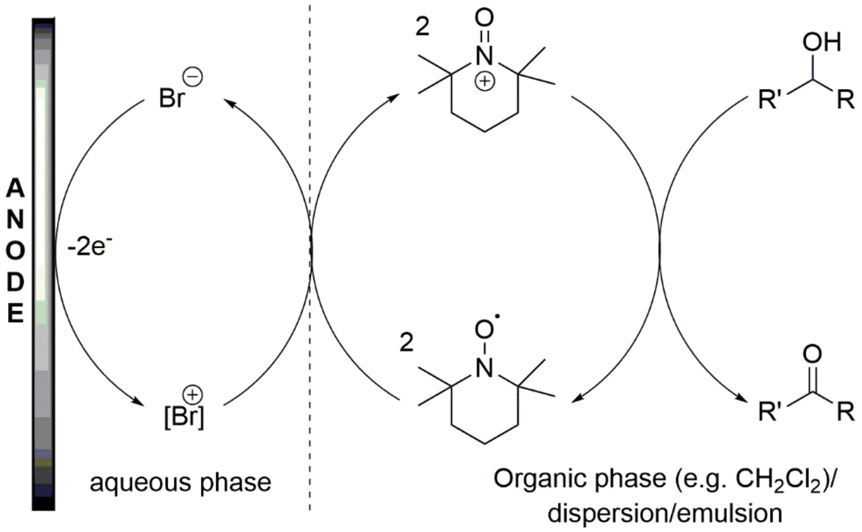

Scheme 1.24: biphasic system for TEMPO-mediated electrooxidation of alcohols.[33, 47]

Typically, in TEMPO-mediated alcohol oxidations the interconversion between TEMPO and TEMPO$^+$ occurs at a relatively high potential compared to that between the hydroxylamine form of TEMPO (TEMPOH, see scheme 1.12) and TEMPO. To take advantage of the low potential of the hydroxylamine form of TEMPO and TEMPO, Stahl and co-workers developed a cooperative electrocatalytic system using Cu(II) and TEMPO (Scheme 1.25).[33, 48]

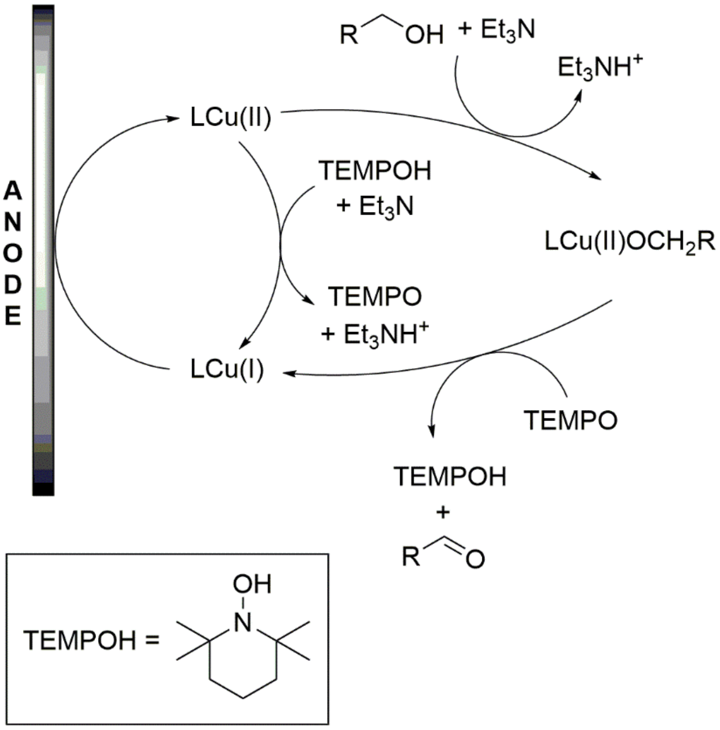

Scheme 1.25: Cooperative electrocatalytic alcohol oxidation with TEMPO/Cu system.[33, 48]

The use of electrochemistry in combination with TEMPO can offer a sustainable route for alcohol oxidation, yet, some challenges remain which limit their use together. These challenges include the requirement of a solvent-electrolyte system, which is typically composed of an electrochemically unstable VOC, such as acetonitrile, and the addition of an electrolyte. Ionic liquids, ILs, have received much attention in electrochemical applications, due in part to their dual functionality of being both solvents and electrolytes. ILs are also known to have excellent solvation properties, which is attractive since TEMPO is found to be poorly soluble in aqueous-electrolyte systems. Furthermore, the tunability properties of ILs, which will be described in the following section, could also be advantageous in terms of influencing the electrode potential required to oxidise TEMPO and tailoring the reactivity of TEMPO in alcohol oxidations.

1.3. Ionic Liquids

A generally accepted definition of ILs is that they are salts with a melting point below 100 ^{O}C. However, this is just an arbitrary limit used to differentiate ILs from high temperature molten salts. The term 'room temperature ionic liquid' (RTIL) is frequently applied to ILs where the melting point is less than 25 °C.[49, 50] ILs are generally composed of bulky asymmetrical cations which are coupled with a range of different anions, ranging from simple halides to large anions such as bis(trifluoromethanesulfonyl)imide. The low packing efficiencies of these ions, as well as the delocalisation of charge reduces the coulombic interaction between ions and hence the melting point of the salt. The majority of IL research have been based on quarternary ammonium, phosphonium, imidazolium and pyridinium cations with large, charge-diffuse inorganic counterions, examples of IL structures are shown in Table 1.2.[51]

Table 1.2: Examples of structures and abbreviations of cations and anions of commonly used ILs.

Abbreviations	Structure	Name
$[C_4C_1Im]^+$	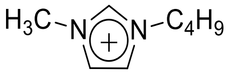	1-butyl-3-methylimidazolium
$[N_{4,4,4,1}]^+$	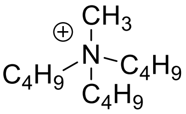	Tributyl(methyl)ammonium
$[P_{6,6,6,14}]^+$	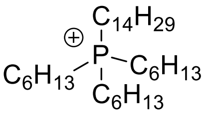	Tributyl(tetradecyl)phosphonium
$[NTf_2]^-$	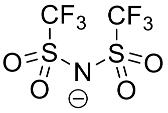	Bis(trifluoromethanesulfonyl)imide
$[PF_6]^-$	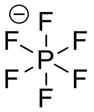	Hexafluorophosphate

Since the first discovery of ILs in 1914, the field of IL has received an increased amount of interest, due in part to the green chemistry movement.[51, 52] The main driving forces behind research into ILs is the potential advantage of substituting traditional industrial solvents, most of which are VOCs, with non-volatile ILs. This has led to ILs often being perceived as potential ‘green’ alternatives to the traditional solvents used today.[53, 54]

There is an immense number of ILs, with at least a million binary ILs and 10^{18} ternary ILs potentially possible.[55] Due to this diversity, ILs are being investigated for applications in areas as diverse as hypergolic rocket fuel,[56, 57] biomedical sensors,[58] batteries for energy storage[59, 60] and pharmaceuticals.[61] The use of ILs has also spread to industrial processes, for example the BASF^{TM} use ILs in the BASIL (Biphasic Acid Scavenging utilising Ionic Liquids) process. It is clear that the modern use of ILs have evolved far beyond being just reaction media.[55]

Due to the increasingly diverse group of ILs with a range of different and unique properties, it is a difficult task to give a general overview of the properties of ILs. However, there are a few properties that do apply to most ILs, such as that they consist solely of ions, have a near-zero vapour pressure and they are typically one order of magnitude more viscous than water or conventional solvents.[50] The following section outlines some of the properties of ILs relevant to this thesis.

1.3.1 Properties of ILs

1.3.1.1. Solvation

Alongside their negligible vapour pressure, a key property which contributes to ILs being regarded as 'green' alternatives to VOCs is their outstanding solvation ability. Among the most important features of an IL to be considered as a solvent are the specific interactions occurring between the IL and the dissolved substrate. Possible intermolecular interactions between the IL and the solute include Coulombic interactions, van der Waals forces, dipole interactions, H-bonding and π-π interactions.[62] Consequently, as ILs can provide a diverse range of potential solute-solvent interactions types, they are known to dissolve a variety of materials including cellulose,[63] carbon dioxide,[64] wool keratin fibres,[65] polymers[66] and proteins.[67, 68] The solvation ability will vary between different ILs for a given solute as a result of different solvent-solute interactions as the IL is varied. As such, a solute freely soluble in one IL may be insoluble in another.[50]

For commonly used molecular solvents, the solvent-solute interactions are usually measured through the polarity of the solvent as expressed through its dielectric constant. The dielectric constants of ILs is not commonly used to describe the solvation properties and other scales are used.[62] Primary solvent features of ILs include the H-bond donating capabilities of the cation, H-bond accepting functionality in the anion, and π-π interactions.[50] A number of empirical solvatochromic parameters have been suggested to quantify the molecular-microscopic solvent properties of ILs.[69] Kamlet, Taft and co-workers developed a method which uses a set of solvatochromic probes which allow the assessment of different parameters for the same solvent.[70, 71] The Kamlet-Taft parameters are now widely used to describe the solvent properties of ILs in terms of the H-bond basicity (β), H-bond acidity (α), and dipolarity/polarizability effect (π^*) of the ILs.[72-75]

It is important to note that the β, α and π^* of the anion and cation will depend on the cation-anion charge transfer (from the anion to the cation). For example, the β of one anion, such as [DCA]$^-$ will be one value when combined with one cation but can change drastically when combined with another cation, as a result of the different cation-anion interactions. The differences in the β and α parameters of the ionic components as ion-combinations are varied are illustrated in Scheme 1.26.[72, 76, 77]

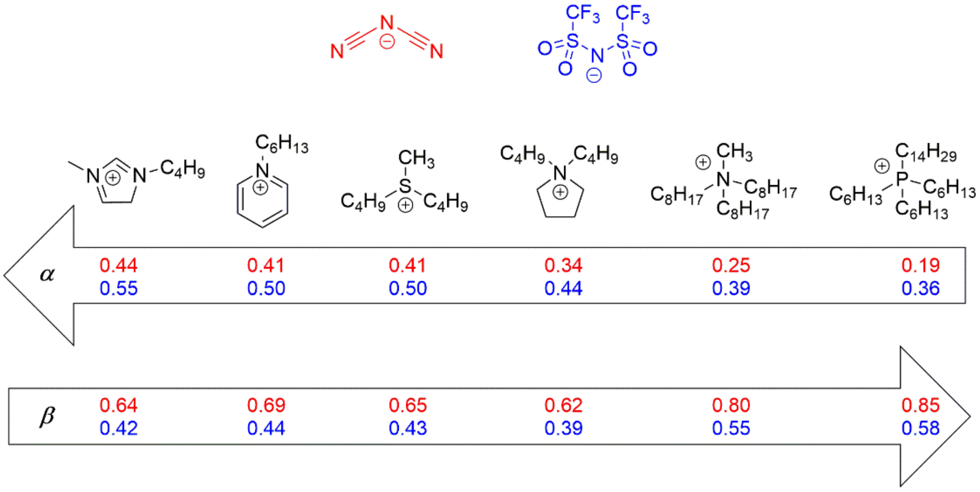

Scheme 1.26: Comparison of structural effects of the cation on the β of $[DCA]^-$ (red) and $[NTf_2]^-$ (blue) based ILs. The influence of the cations on the α of the two anions is also shown.[72]

Furthermore, ILs are not solely limited to act as an 'innocent' solvent medium, but can also act as a reagent, catalyst activator or even a catalyst. For example, improved rate and selectivity of Diels-Alder cycloadditions were observed in a range of ILs compared to many conventional molecular solvents.[62, 78, 79]

1.3.1.2. Tunability

Another attractive property of ILs is their tunability, that is, by changing the nature of the ions present in an IL, it is possible to tune the resulting chemical and physical properties of the IL for desirable functions. It has been found that by varying the length of the alkyl chain attached to the imidazolium ring of an imidazolium based IL, the physical properties, such as viscosity, hydrophobicity, pH-dependency and melting points, can be fine-tuned.[50, 80-82]

This tunability is significant in controlling reactions or optimising a process using ILs.[62] For example, Etzold and co-workers, discovered that the electrocatalytic properties of IL-modified Pt/Carbon catalysts can be regulated by systematically tuning the structures of the ILs at a molecular level. This observation also led to the realisation that the cationic alkyl chain holds the key to obtaining an optimised oxygen-reduction reaction catalyst.[83]

Further modification of the properties can be achieved by introducing a functionality as an integral part of the IL.[84] Davis and co-workers coined the term task-specific ionic liquid (TSIL), which may be defined as ILs in which a functional group is covalently anchored to the cation or/and anion of the IL. The types of added functional groups are diverse, ranging from ILs containing imidazolium cations with long appended fluorous tails[85] and urea based ILs.[86] For example, an urea functionality on an imidazolium based IL, as shown in Figure 1.1, has been successfully used for the extraction of metal ions from aqueous solutions.[86] Clearly, the range of TSILs is limited only by the imaginations of the chemists.[86, 87] This tunability has made ILs available for a range of applications.[51]

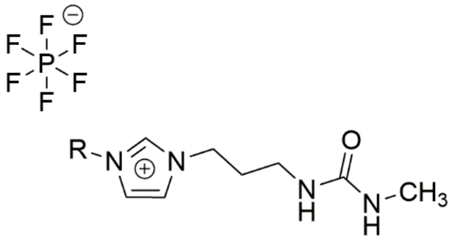

Figure 1.1: Example of a TSIL which is a functionalised imidazolium based IL with urea functionality which can act as metal ligating moieties.[86]

In recent years, some toxicological environmental concerns associated with ILs have arisen, mainly due to their synthetic pathways and the potential environmental hazards if accidentally released into the environment. However, considering the diversity, ILs can be designed to be environmentally benign, and so remain potential candidates for sustainable chemistry.[55]

1.3.1.3. Viscosity

The viscosity of ILs can range from as low as 10 mPa·s to as high as 500 mPa·s at room temperature. As a comparison, the viscosity of pure water is 1 mPa·s and for acetonitrile the viscosity is 0.3 mPa·s.[88, 89] The choice of anions has been shown to significantly alter the viscosity of the IL, e.g. dicyanamide anion based ILs are typically less viscous than the bis(trifluoromethanesulfonyl)imide based ILs. Changing the length of the substituent alkyl chains of the cation can also be used to manipulate viscosity. This has been explained to be a result of increased and stronger van der Waals forces between the cations in the liquid.[89]

1.3.1.4. Electrochemical Properties

Since ILs are composed of ions, they are intrinsically conductive. While they have an abundance of charge carriers, these viscous liquids exhibit low rates of mass transport.[88] In addition to the high viscosity, ion pairing and aggregation are believed to reduce the amount of available charge carriers and therefore lowering the conductivity of the overall IL. The conductivity of ILs are still comparable to those of organic solvents with added supporting electrolyte and are therefore possible candidates for electrochemical applications.[90]

Wide electrochemical windows of the media is important for a variety of electrochemical applications, such as in the development of stable batteries.[91] One of the advantages of RTILs is their large electrochemical window. For example, the commonly-used imidazolium based RTILs have an electrochemical window of about 5-6 V, which is greater than the 2-3 V electrochemical window of a typical aqueous system. Impurities in the solvent can significantly decrease the range of its electrochemical window. For instance, the presence of halide impurities can decrease the anodic current quite significantly. Water and oxygen are also known to drastically reduce the electrochemical window of the solvent at both the cathodic and anodic limit as a result of water oxidation occurring at low potential and the oxygen/water reduction potential occurs at not so low potential.[92]

Many ILs have found applications in electrochemistry, such as being electrolytes in lithium batteries, electric double-layer capacitors and dye-sensitized solar cells.[89] Typically VOCs such as acetonitrile are used in electrolyte-solvent systems found in e.g. dye-sensitised photoelectrochemical cells. However, the high vapour pressure associated with conventional organic solvents, especially under conditions where considerable solar heating may take place, is problematic. Recently, much effort has been devoted to identifying and characterising electrochemically stable and non-volatile ILs that can replace these organic solvents in photoelectrochemical cells.[93, 94] Furthermore, replacing conventional solvent-electrolyte systems in electrochemical applications can simplify experimental set-up and minimise waste as a result of replacing a two-component system (solvent and electrolyte) with the one-component IL system with dual functionality.[88]

1.3.3. TEMPO and RTILs

A handful of studies on the electrochemical behaviour of TEMPO in RTILs have been conducted, and showcase that the behaviour of TEMPO in RTILs is similar to that in acetonitrile and water.[13, 21, 95-98] In addition, Doherty and co-workers observed that the global rate constant of TEMPO-mediated alcohol oxidation was a factor of six larger in *N*-butyl-*N*-methyl pyrrolidinium than in acetonitrile, despite the fact that mass transfer was slower in the RTIL.[13] These studies have showcased the possibility of replacing conventional solvent-electrolyte systems with ILs in efficient TEMPO-mediated alcohol electrooxidation. Considering the tunability power of ILs the selectivity and reactivity could potentially be tuned *via* the IL media, which would add further value to TEMPO-mediated alcohol oxidations in ILs.

Computational and electron paramagnetic resonance spectroscopy (EPR) analyses have demonstrated that the physicochemical properties of TEMPO can been tuned *via* the IL media. Computational analysis, conducted by Gryn’ova and Coote, have discovered a significant stabilising interaction between the nitroxyl radical on TEMPO and a remote negative charge (in the absence of any conjugation or hyperconjugation and at long-range separations of over 5 Å).[99, 100] TEMPO is also commonly used as a spin probe in EPR measurements, and so a few studies have looked into the effect of the dissolution of TEMPO in different ILs on the mobility of the radical.[101-104] Strehmel and co-workers, observed some relationship between the differences in the hyperfine coupling of the EPR spectra, to the hydrogen bond accepting ability of the anion (β value of the Kamlet–Taft parameters), when TEMPO is dissolved in ILs bearing small anions such as $[BF_4]^-$ and $[PF_6]^-$.[101] They also observed that when TEMPO is dissolved in ILs containing the bulkier anion $[NTf_2]^-$ with a more delocalized charge, the coupling does not show any correlation to the Kamlet-Taft parameters.

1.4. Aims and Objectives

The aim of this thesis is to study the combination of three potential 'green' solutions for the development of sustainable alcohol oxidations- organocatalysis, electrosynthesis and ionic liquids. A summary of the techniques used in this thesis is described in chapter 2. The approach follows the order:

- In chapter 3, cyclic voltammetry is used to probe the redox properties of the TEMPO/TEMPO$^+$ redox couple as the RTIL media is varied in order to gain an insight of TEMPO-RTIL interactions. Voltammetric analysis is also used to investigate the influence of the TEMPO-RTIL interaction on the kinetics of TEMPO-mediated alcohol electrooxidations. The alcohol selectivity of TEMPO in different RTIL media are also investigated, to see if there is potential to control the selectivity *via* the RTIL media. The RTIL media systems are also compared to the commonly used acetonitrile-electrolyte systems.

- In chapter 4 two different electrolysis setups are investigated for the TEMPO-mediated alcohols electrooxidations in RTILs. Various conditions, such as the RTIL media and applied currents, are varied in order to give an insight of the optimum conditions needed for TEMPO-mediated alcohol electrooxidations in RTIL, and how the reaction can be tuned at preparative scale *via* the RTIL.

- In chapter 5 the amount of chemical input and waste of TEMPO-mediated alcohol oxidations in ILs is minimised. The use of stoichiometric base is eliminated by incorporating the base as the cationic component of the IL. Water reduction which is commonly used as the counter-electrode reaction, is replaced by the reduction of the cation of the IL to generate the base required for the alcohol oxidation. A TEMPO-based IL is synthesised and the recovery and reuse of TEMPO is considered.

1.5. References

1. Q. Cao, L. M. Dornan, L. Rogan, N. L. Hughes and M. J. Muldoon, *Chem. Commun.*, 2014, **50**, 4524-4543.

2. S. Caron, R. W. Dugger, S. G. Ruggeri, J. A. Ragan and D. H. B. Ripin, *Chem. Rev.*, 2006, **106**, 2943-2989.

3. J. S. Carey, D. Laffan, C. Thomson and M. T. Williams, *Org. Biomol. Chem.*, 2006, **4**, 2337-2347.

4. Z. Kowalski and M. Gollinger-Tarajko, *Waste Manage.*, 2003, **23**, 771-783.

5. K. Alfonsi, J. Colberg, P. J. Dunn, T. Fevig, S. Jennings, T. A. Johnson, H. P. Kleine, C. Knight, M. A. Nagy, D. A. Perry and M. Stefaniak, *Green Chem.*, 2008, **10**, 31-36.

6. F. G. Fang, D. D. Bankston, E. M. Huie, M. Ross Johnson, M.-C. Kang, C. S. LeHoullier, G. C. Lewis, T. C. Lovelace, M. W. Lowery, D. L. McDougald, C. A. Meerholz, J. J. Partridge, M. J. Sharp and S. Xie, *Tetrahedron*, 1997, **53**, 10953-10970.

7. L. De Luca, G. Giacomelli and A. Porcheddu, *J. Org. Chem.*, 2001, **66**, 7907-7909.

8. A. B. Jones, *J. Org. Chem.*, 1992, **57**, 4361-4367.

9. C. Dai, J. Zhang, C. Huang and Z. Lei, *Chem. Rev.*, 2017, **117**, 6929-6983.

10. R. A. Sheldon and I. W. C. E. Arends, *J. Mol. Catal. A: Chem.*, 2006, **251**, 200-214.

11. R. A. Sheldon, I. W. C. E. Arends, G.-J. ten Brink and A. Dijksman, *Acc. Chem. Res.*, 2002, **35**, 774-781.

12. S.-y. Kishioka and A. Yamada, *Electrochim. Acta*, 2006, **51**, 4582-4588.

13. C. Comminges, R. Barhdadi, A. P. Doherty, S. O'Toole and M. Troupel, *J. Phys. Chem. A*, 2008, **112**, 7848-7855.

14. R. A. Green, J. T. Hill-Cousins, R. C. D. Brown, D. Pletcher and S. G. Leach, *Electrochim. Acta*, 2013, **113**, 550-556.

15. M. F. Semmelhack, C. S. Chou and D. A. Cortes, *J. Am. Chem. Soc.*, 1983, **105**, 4492-4494.

16. M. F. Semmelhack, C. R. Schmid and D. A. Cortés, *Tetrahedron Lett.*, 1986, **27**, 1119-1122.

17. M. Rafiee, B. Karimi and S. Alizadeh, *ChemElectroChem*, 2014, **1**, 455-462.

18. M. Rafiee, K. C. Miles and S. S. Stahl, *J. Am. Chem. Soc.*, 2015, **137**, 14751-14757.

19. W. F. Bailey, J. M. Bobbitt and K. B. Wiberg, *J. Org. Chem.*, 2007, **72**, 4504-4509.

20. M. Shibuya, F. Pichierri, M. Tomizawa, S. Nagasawa, I. Suzuki and Y. Iwabuchi, *Tetrahedron Lett.*, 2012, **53**, 2070-2073.

21. R. Barhdadi, C. Comminges, A. P. Doherty, J. Y. Nédélec, S. O'Toole and M. Troupel, *J. Appl. Electrochem.*, 2007, **37**, 723-728.

22. R. Ciriminna, M. Ghahremani, B. Karimi and M. Pagliaro, *ChemistryOpen*, 2017, **6**, 5-10.

23. A. Porcheddu, E. Colacino, G. Cravotto, F. Delogu and L. De Luca, *Beilstein J. Org. Chem.*, 2017, **13**, 2049-2055.

24. R. Ciriminna and M. Pagliaro, *Org. Process Res. Dev.*, 2010, **14**, 245-251.

25. D. S. P. Cardoso, B. Šljukić, D. M. F. Santos and C. A. C. Sequeira, *Org. Process Res. Dev.*, 2017, **21**, 1213-1226.

26. D. Pletcher, R. Greff, R. Peat, L. M. Peter and J. Robinson, in *Instrumental Methods in Electrochemistry*, eds. D. Pletcher, R. Greff, R. Peat, L. M. Peter and J. Robinson, Woodhead Publishing, Cambridge, 1st edn., 2001, ch. 3, pp. 76-112.

27. J. E. Taylor, M. A. Kulandainathan, C. E. Hotchen and F. Marken, in *Modern electrosynthetic methods in organic chemistry*, eds. F. Marken and M. Atobe, CRC Press Boca Raton, 1st edn., 2018, ch. 1, pp. 1-44.

28. C. Sequeira and D. Santos, *J. Braz. Chem. Soc.*, 2009, **20**, 387-406.

29. E. J. Horn, B. R. Rosen, Y. Chen, J. Tang, K. Chen, M. D. Eastgate and P. S. Baran, *Nature*, 2016, **533**, 77.

30. E. J. Horn, B. R. Rosen and P. S. Baran, *ACS Cent. Sci.*, 2016, **2**, 302-308.

31. D. Pletcher, *Electrochem. Commun.*, 2018, **88**, 1-4.

32. D. Pletcher, R. A. Green and R. C. D. Brown, *Chem. Rev.*, 2018, **118**, 4573-4591.

33. M. Yan, Y. Kawamata and P. S. Baran, *Chem. Rev.*, 2017, **117**, 13230-13319.

34. K. J. Frankowski, R. Liu, G. L. Milligan, K. D. Moeller and J. Aubé, *Angew. Chem., Int. Ed.*, 2015, **54**, 10555-10558.

35. N. Fu, G. S. Sauer and S. Lin, *Nat. Protoc.*, 2018, **13**, 1725-1743.

36. M. Yan, Y. Kawamata and P. S. Baran, *Angew. Chem., Int. Ed.*, 2018, **57**, 4149-4155.

37. J. T. Hill-Cousins, J. Kuleshova, R. A. Green, P. R. Birkin, D. Pletcher, T. J. Underwood, S. G. Leach and R. C. Brown, *ChemSusChem*, 2012, **5**, 326-331.

38. J. Kuleshova, J. T. Hill-Cousins, P. R. Birkin, R. C. D. Brown, D. Pletcher and T. J. Underwood, *Electrochim. Acta*, 2011, **56**, 4322-4326.

39. R. A. Green, R. C. D. Brown and D. Pletcher, *J. Flow Chem.*, 2016, **6**, 191-197.

40. R. A. Green, R. C. D. Brown, D. Pletcher and B. Harji, *Org. Process Res. Dev.*, 2015, **19**, 1424-1427.

41. V. Kren and L. Martinkova, *Curr. Med. Chem.*, 2001, **8**, 1303-1328.

42. M. Schämann and H. J. Schäfer, *Eur. J. Org. Chem.*, 2003, **2003**, 351-358.

43. J. Zhao, R. Li, A. Pawlak, M. Henklewska, A. Sysak, L. Wen, J.-E. Yi and B. Obmińska-Mrukowicz, *In Vivo*, 2018, **32**, 1081-1088.

44. *US Pat.*, WO/2006/105357, 2006.

45. A. Khotkevych, personal communication, May, 2019.

46. J. Kubota, Y. Shimizu, K. Mitsudo and H. Tanaka, *Tetrahedron Lett.*, 2005, **46**, 8975-8979.

47. A. Palma, J. Cárdenas and B. A. Frontana-Uribe, *Green Chem.*, 2009, **11**, 283-293.

48. A. Badalyan and S. S. Stahl, *Nature*, 2016, **535**, 406.

49. R. Wibowo, S. E. W. Jones and R. G. Compton, *J. Chem. Eng. Data*, 2010, **55**, 1374-1376.

50. J. L. Anthony, J. F. Brennecke, J. D. Holbrey, E. J. Maginn, R. A. Mantz, R. D. Rogers, P. C. Trulove, A. E. Visser and T. Welton, in *Ionic Liquids in Synthesis*, eds. P. Wasserscheid and T. Welton, Wiley VCH, Weinheim, 1st edn., 2003, ch. 3, pp. 41-126.

51. J. S. Wilkes, in *Ionic Liquids in Synthesis*, eds. P. Wasserscheid and T. Welton, Wiley VCH, Weinheim, 1st edn., 2003, ch. 1, pp. 1-6.

52. P. Anastas and N. Eghbali, *Chem. Soc. Rev.*, 2010, **39**, 301-312.

53. R. D. Rogers and K. R. Seddon, *Science*, 2003, **302**, 792.

54. J. P. Hallett and T. Welton, *Chem. Rev.*, 2011, **111**, 3508-3576.

55. M. Freemantle, *Chem. Eng. News Arch.*, 1998, **76**, 32-37.

56. S. Schneider, T. Hawkins, M. Rosander, G. Vaghjiani, S. Chambreau and G. Drake, *Energy Fuels*, 2008, **22**, 2871-2872.

57. T. Liu, X. Qi, S. Huang, L. Jiang, J. Li, C. Tang and Q. Zhang, *Chem. Commun.*, 2016, **52**, 2031-2034.

58. S.-H. Zhang, F.-X. Wang, J.-J. Li, H.-D. Peng, J.-H. Yan and G.-B. Pan, *Sensors*, 2017, **17**, 2621.

59. M. Watanabe, M. L. Thomas, S. Zhang, K. Ueno, T. Yasuda and K. Dokko, *Chem. Rev.*, 2017, **117**, 7190-7239.

60. M. Kar, O. Tutusaus, D. R. MacFarlane and R. Mohtadi, *Energy Environ. Sci.*, 2019, **12**, 566-571.

61. J. L. Shamshina, S. P. Kelley, G. Gurau and R. D. Rogers, *Nature*, 2015, **528**, 188-189.

62. T. Welton, *Coord. Chem. Rev.*, 2004, **248**, 2459-2477.

63. R. P. Swatloski, S. K. Spear, J. D. Holbrey and R. D. Rogers, *J. Am. Chem. Soc.*, 2002, **124**, 4974-4975.

64. Z. Lei, C. Dai and B. Chen, *Chem. Rev.*, 2014, **114**, 1289-1326.

65. H. Xie, S. Li and S. Zhang, *Green Chem.*, 2005, **7**, 606-608.

66. N. Winterton, *J. Mater. Chem.*, 2006, **16**, 4281-4293.

67. D. Sate, M. H. A. Janssen, G. Stephens, R. A. Sheldon, K. R. Seddon and J. R. Lu, *Green Chem.*, 2007, **9**, 859-867.

68. A. P. S. Brogan and J. P. Hallett, *J. Am. Chem. Soc.*, 2016, **138**, 4494-4501.

69. A. F. M. Cláudio, L. Swift, J. P. Hallett, T. Welton, J. A. P. Coutinho and M. G. Freire, *Phys. Chem. Chem. Phys.*, 2014, **16**, 6593-6601.

70. M. J. Kamlet, J. L. Abboud and R. W. Taft, *J. Am. Chem. Soc.*, 1977, **99**, 6027-6038.

71. M. J. Kamlet and R. W. Taft, *J. Am. Chem. Soc.*, 1976, **98**, 377-383.

72. S. Spange, R. Lungwitz and A. Schade, *J. Mol. Liq.*, 2014, **192**, 137-143.

73. A. F. M. Claudio, L. Swift, J. P. Hallett, T. Welton, J. A. P. Coutinho and M. G. Freire, *Phys. Chem. Chem. Phys.*, 2014, **16**, 6593-6601.

74. L. Crowhurst, R. Falcone, N. L. Lancaster, V. Llopis-Mestre and T. Welton, *J. Org. Chem.*, 2006, **71**, 8847-8853.

75. L. Crowhurst, R. Falcone, N. L. Lancaster, V. Llopis-Mestre and T. Welton, *J. Org. Chem.*, 2006, **71**, 8847-8853.

76. S. Men, D. S. Mitchell, K. R. J. Lovelock and P. Licence, *ChemPhysChem*, 2015, **16**, 2211-2218.

77. R. K. Blundell and P. Licence, *Phys. Chem. Chem. Phys.*, 2014, **16**, 15278-15288.

78. T. Fischer, A. Sethi, T. Welton and J. Woolf, *Tetrahedron Lett.*, 1999, **40**, 793-796.

79. P. Ludley and N. Karodia, *Tetrahedron Lett.*, 2001, **42**, 2011-2014.

80. W. R. Carper, A. Dölle, C. G. Hanke, C. Hardacre, A. Leuchter, R. M. Lynden-Bell, Z. Meng, G. Palmer and D. J. Richter, in *Ionic Liquids in Synthesis*, eds. P. Wasserscheid and T. Welton, Wiley VCH, Weinheim, 1st edn., 2003, ch. 4, pp. 127-173.

81. A. Deyko, K. R. J. Lovelock, J.-A. Corfield, A. W. Taylor, P. N. Gooden, I. J. Villar-Garcia, P. Licence, R. G. Jones, V. G. Krasovskiy, E. A. Chernikova and L. M. Kustov, *Phys. Chem. Chem. Phys.*, 2009, **11**, 8544-8555.

82. C. M. Gordon, J. D. Holbrey, A. R. Kennedy and K. R. Seddon, *J. Mater. Chem.*, 1998, **8**, 2627-2636.

83. G.-R. Zhang, T. Wolker, D. J. S. Sandbeck, M. Munoz, K. J. J. Mayrhofer, S. Cherevko and B. J. M. Etzold, *ACS Catal.*, 2018, **8**, 8244-8254.

84. J. H. Davis, C. M. Gordon, C. Hilgers and P. Wasserscheid, in *Ionic Liquids in Synthesis*, eds. P. Wasserscheid and T. Welton, Wiley VCH, Weinheim, 1st edn., 2003, ch. 2, pp. 7-40.

85. T. L. Merrigan, E. D. Bates, S. C. Dorman and J. H. Davis Jr, *Chem. Commun.*, 2000, **20**, 2051-2052.

86. A. E. Visser, R. P. Swatloski, W. M. Reichert, R. Mayton, S. Sheff, A. Wierzbicki, J. J. H. Davis and R. D. Rogers, *Chem. Commun.*, 2001, **1**, 135-136.

87. J. H. Davis, *Chem. Lett.*, 2004, **33**, 1072-1077.

88. D. Silvester and R. G. Compton, *J. Phys. Chem.*, 2006, **220**, 1247-1274.

89. P. Wasserscheid and T. Welton, *Ionic Liquids in Synthesis*, eds. P. Wasserscheid and T. Welton, Wiley VCH, Weinheim, 1st edn., 2003, ch. 9, pp. 348-356.

90. H. Tokuda, S. Tsuzuki, M. A. B. H. Susan, K. Hayamizu and M. Watanabe, *J. Phys. Chem. B*, 2006, **110**, 19593-19600.

91. O. Mizrahi, N. Amir, E. Pollak, O. Chusid, V. Marks, H. Gottlieb, L. Larush, E. Zinigrad, D. Aurbach, *J. Electrochem. Soc.*, 2008, **155**, 103-109.

92. M. V. Fedorov and A. A. Kornyshev, *Chem. Rev.*, 2014, **114**, 2978-3036.

93. M. Gorlov and L. Kloo, *Dalton Trans.*, 2008, **20**, 2655-2666.

94. T. Tsuda and C. Hussey, *Electrochem. Soc. Interface*, 2007, **16**, 42-49.

95. A. C. Herath and J. Y. Becker, *Electrochim. Acta*, 2008, **53**, 4324-4330.

96. T. Hirashita, M. Nakanishi, T. Uchida, M. Yamamoto, S. Araki, I. W. C. E. Arends and R. A. Sheldon, *ChemCatChem*, 2016, **8**, 2704-2709.

97. N. Jiang and A. J. Ragauskas, *Tetrahedron Lett.*, 2005, **46**, 3323-3326.

98. X.-E. Wu, L. Ma, M.-X. Ding and L.-X. Gao, *Synlett*, 2005, **4**, 607-610.

99. G. Gryn’ova and M. L. Coote, *J. Am. Chem. Soc.*, 2013, **135**, 15392-15403.

100. G. Gryn'ova, D. L. Marshall, S. J. Blanksby and M. L. Coote, *Nat. Chem.*, 2013, **5**, 474.

101. V. Strehmel, S. Berdzinski and H. Rexhausen, *J. Mol. Liq.*, 2014, **192**, 153-170.

102. V. Strehmel, A. Laschewsky, R. Stoesser, A. Zehl and W. Herrmann, *J. Phys. Org. Chem.*, 2006, **19**, 318-325.

103. M. A. M. Noel, R. D. Allendoerfer and R. A. Osteryoung, *J. Phys. Chem.*, 1992, **96**, 2391-2394.

104. R. Stoesser, W. Herrmann, A. Zehl, V. Strehmel and A. Laschewsky, *ChemPhysChem*, 2006, **7**, 1106-1111.

2. Experimental and Review of Techniques

2.1. Electrochemical Techniques

Electrochemical techniques were used throughout this research project to understand the electrochemistry of TEMPO and aid development of preparative-scale electrolysis. In this section, the electrochemical techniques are reviewed and their applicability to this project is described.

2.1.1. Cyclic Voltammetry

Cyclic voltammetry is used in the characterisation of electrochemical processes. Qualitative and quantitative information can be obtained within a few seconds. The speed and ease of experimentation makes cyclic voltammetry the first method of choice for many electrochemists.[1, 2] Generally, a three-electrode cell made up of a working electrode, counter electrode and a reference electrode is used to record a cyclic voltammogram (CV). A typical three-electrode cell set-up is shown in Figure 2.1. The potential difference between the working electrode and reference electrode is controlled and current flows between the working and counter electrodes, so that negligible current passes through the reference electrode. This is important as it ensures that the reference electrode remains at a constant potential throughout the cyclic voltammetry, allowing comparison of systems using the same reference electrode scale.[3-5]

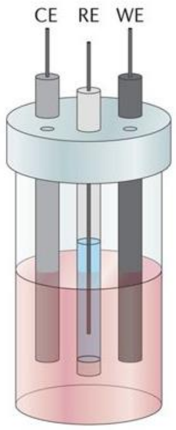

Figure 2.1: Typical set-up of a three-electrode system for cyclic voltammetry, constituting a working electrode, a counter electrode and a reference electrode.[6]

Figure 2.2 shows a CV of the one-electron redox couple R/O. First, the potential at the working electrode is ramped from an initial value, E_i, to a higher potential, E_λ, and then scanned back to a final value, E_f. The current, *i*, passing through the working electrode is recorded as the potential is changed, resulting in an *i*-*E* voltammogram. As the potential is swept positive of the electrode, a potential is reached which drives the transfer of an electron from the electroactive substrate to the electrode, causing an increase in current and oxidation of the substrate to its oxidised form. The current reaches a maxima at an oxidation potential $E_{p,a}$, where the current is dependent on the delivery of additional un-oxidised substrate *via* diffusion from the bulk solution. As the potential is scanned more positive the rate of diffusion of un-oxidised substrate becomes slower, resulting in a decrease in current as the potential is increased and a characteristic anodic peak current,

$i_{p,a}$, is formed. When E_λ, is reached, the potential scan direction is reversed and the potential is scanned towards negative potentials. The oxidised species is then reduced to its original form at the electrode and yields the cathodic peak at $E_{p,c}$ with a peak current of $i_{p,c}$.[3, 8, 9]

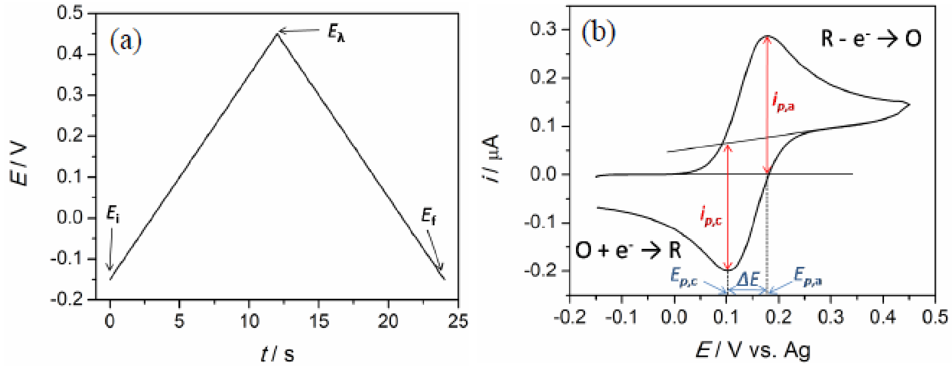

Figure 2.2: Typical cyclic voltammogram of a one-electron TEMPO/TEMPO$^+$ redox couple, where a) the potential is ramped from E_i to E_λ and then reversed back to E_f. b) As the potential is ramped to positive potentials the electroactive species, R, is oxidised to O, resulting in an increase in current. The current is limited by the mass transport of the electroactive species to the electrode and a peak is formed.[7]

If the electron transfer is fast and reversible at the electrode surface, the i-E curve in a cyclic voltammogram can be described by the Nernst equation (Equation 2.1). The Nernst equation relates the potential of an electrochemical cell to the standard potential (E^0) and the relative activities of the oxidised and reduced form of an electroactive species in the system at equilibrium. At low concentration of the electroactive species the activities can be replaced by the concentrations of oxidised and reduced form of the species (C_O and C_R respectively).

$$E = E^0 + \frac{RT}{nF} ln\left(\frac{C_R}{C_O}\right) \qquad (2.1)$$

Where F is Faraday's constant, R is the gas constant, n is the number of electrons and T is the temperature. The oxidation and reduction peaks are separated as a result of diffusion of the electroactive species to and from the electrode. The peak-to-peak separation, ΔE_p, for a one-electron Nernstian electrochemical reversible process is 59 mV. The half-wave potential between the oxidation and reduction peak of an electroactive species is in thesis referred to as, $E_{½}$.[8]

2.1.1.1.1. Reversibility

The reversibility of an electrochemical process is an important property that can be determined with cyclic voltammetry. In terms of thermodynamics, reversibility is when a process whose direction can be changed by an infinitesimal change in some variable, such as concentration, heat or pressure.[10] It is worth noting the differences between chemical reversibility and electrochemical reversibility of a system. Chemical reversibility describes the stability of the electroactive species upon oxidation and reduction. For example, an electroactive species can react chemically upon oxidation and is, in this case, not chemically reversible. If the potential is scanned back towards the starting potential, and the oxidised species is reduced back to its initial state, with no new reactions occurring, the reaction may be considered chemically reversible.[11]

Electrochemical reversibility describes the ability of a system to follow the Nernst equation and maintain Nernstian equilibrium at the electrode surface. Electrochemical reversibility depends on the electron transfer kinetics between electrode and the electroactive species. When the electron transfer is fast (electrochemical reversible) the Nernstian equilibrium is established instantaneously between the electrode and the species upon any change in applied potential. When the electron transfer is slow (electrochemical irreversible), and Nernstian equilibrium is not established instantaneously. For electrochemical irreversible systems more positive potentials (or negative) are required to observe oxidation (or reduction) reactions and thus giving rise to larger ΔE_p. In some cases, the electron transfer is neither facile or very sluggish, and the measured current involves appreciable conversion which is Nernstian, but is not fully Nernstian. These electrochemical systems are then referred to as quasi-reversible.

The electrochemical reversibility of a system depends upon the length of time of the measurement, the rate of change of the force driving the process, and how fast the system can re-establish Nernstian equilibrium. In other words, a reversible system can be obtained if the applied perturbation to the system is small enough, or if the system can attain equilibrium rapidly enough within the time of the measurement. The system can, however, become irreversible if for example the rate of change is large, such as using a high scan rate, v, and the system is too slow to attain the equilibrium at the electrode at that scan rate. Thus, a system may be electrochemically reversible in one experiment but irreversible in another.[11]

Sequential CV experiments can reveal whether a system is reversible or not under a range of conditions, and from CVs one can identify ‘signs’ of disequilibrium. For example, in an electrochemically reversible system the anodic and cathodic peak separation does not increase with increasing scan rate. In the irreversible case the separation of the peaks shows a dependency of the scan rate and the peak-to-peak separation of 59 mV become more ‘drawn out’.[11, 12]

2.1.1.2. Mass transport

Mass transport of an electroactive species is the transport of species to and from the electrode surface. The flux of an electroactive species to the electrode is a sum of migration, diffusion and convection, as illustrated in Figure 2.3.[13, 14]

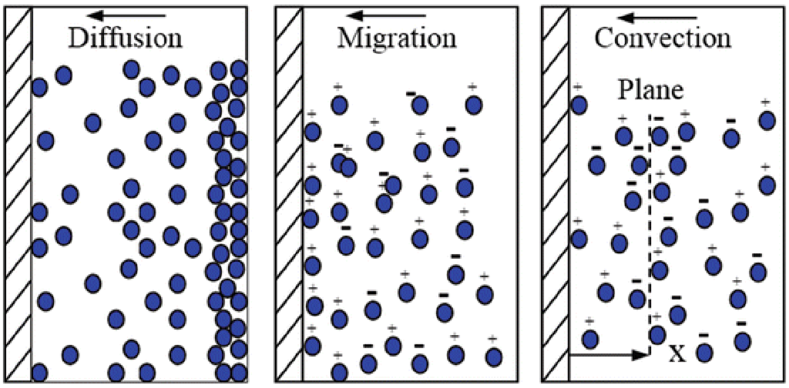

Figure 2.3: Illustration of modes of mass transport.[13]

Migration is the movement of charged particles in an electric field, diffusion is the movement of species down a concentration gradient and convection is the movement of species induced by mechanical means, *e.g.* stirring.[14, 15]

The consumption of an electroactive species at an electrode (e.g. by the oxidation of the species to its oxidised form) will initiate the development of the substrate concentration gradients near the electrode, which grows over time and is dependent on the scan rate and potential applied. The current obtained from a cyclic voltammetry measurement of an electroactive species is directly proportional to the flux of the species reaching the electrode surface.[16] The diffusion coefficient, *D*, of an electroactive species can be investigated through recording CVs of the substrate at different scan rates. The Randles-Sevçik relationship relates the peak currents obtained in CVs of an electroactive species with the scan rates. The diffusion coefficient of TEMPO in the different RTILs can be determined from the linear gradient by plotting i_p *vs* $v^{½}$, see Equation 2.2.[14]

$$i_p = 2.69 \times 10^{-5} n^{\frac{3}{2}} A D^{\frac{1}{2}} C v^{\frac{1}{2}} \qquad (2.2)$$

Where *n* is the number of electrons involved in the oxidation or reduction process, *A* is the electrode surface area and *C* is the concentration of the substrate. An alternative method to investigate the diffusion of an electroactive species is to carry out a chronoamperometric experiment. Chronoamperometry is a potential-step method where, the potential is stepped from a potential at which the substrate is not reduced or oxidised at the electrode to a potential past the $E_{p,a}$ or $E_{p,c}$ of the substrate, i.e. to a potential in the mass-transfer region.[17] As the potential step occurs, the current increases as a result of the electroactive substrate near the surface is reduced or oxidised. The current then decreases rapidly, the current response is dependent on how fast the substrate can diffuse to the electrode surface. Figure 2.4 frame a) shows the applied potential with time and frame b) shows the chronoamperometric response of an electroactive species.

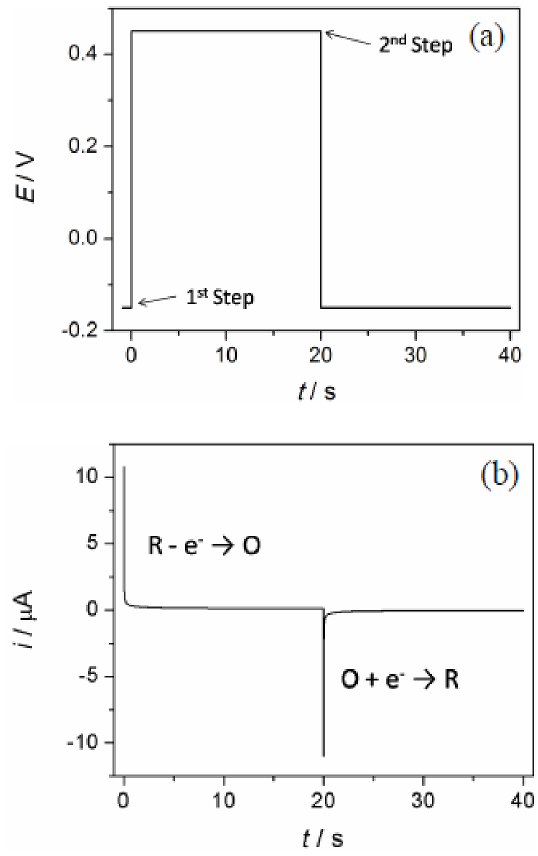

Figure 2.4: a) *E* plotted *vs t*, in the first step the potential is step from -0.15 V to 0.45 V. In the second step, the potential is stepped from 0.45 V to 0.15 V. b) Chronoamperometric response of an electroactive species recorded by stepping the potential from 0.00 V to 0.45 V.[7]

The tail off of current is described by the Cottrell equation, as shown in Equation 2.3.[17, 18]

$$i = \frac{nFAD^{\frac{1}{2}}C}{\pi^{\frac{1}{2}}t^{\frac{1}{2}}} \quad (2.3)$$

Where *t* is time. A plot of *i vs* $t^{-½}$ should yield a straight line with an intercept of 0. A linear Cottrell plot indicates that the redox reaction is diffusion limited and physical parameters of the electroactive substrate can be determined from the gradient. Such parameters include the diffusion coefficient of the substrate, the concentration or the number of electrons transferred. Usually only one of these parameters are unknown and can then be derived from the gradient of the linear relationship of i *vs* $t^{-½}$.[19]

2.1.2. Reference Electrode

A reference electrode is commonly used in electrochemical measurements so that the applied potential can be reported *vs* a specific reference.[3] In non-aqueous solvents, typically a quasi-reference electrode (QRE) is used, usually a metal wire such as Pt or Ag. The potential of the QRE is unknown and whenever the environment of the electrode is changed the potential is likely to change. Therefore, if a QRE is used, the potential of an internal reference redox couple, such as ferrocene, is recorded *in situ*. The potential of the QRE is then calibrated with the formal potential of the internal reference.[3, 20]

Ideally the redox potential of the internal reference should only be modestly affected by the solvent, and the redox couple must meet the criteria set by the IUPAC. IUPAC identified that the ferrocene/ferrocenium couple satisfies most of the requirements and is recommended to use in non-aqueous systems.[21, 22] Ferrocene is also often used as an internal reference system for comparison of redox processes in different RTILs.[20, 23-25] The reversible one-electron redox reactions of Fc/Fc^+ is shown in Figure 2.5.[21, 22]

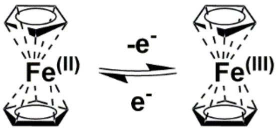

Figure 2.5: One-electron oxidation of Fc and reduction of Fc^+.[21]

However recent studies suggests that the Fc/Fc^+ is not an innocent species and its formal potential depends on solvation effects of the solvent and supporting electrolytes, which renders Fc/Fc^+ unsuitable for *in situ* reference purposes.[21, 26, 27] The search for a solvent-independent reference redox system for the comparison of redox potentials in RTILs has led to the conclusion that the decamethyl-substituted ferrocene, dmFc, is a superior redox standard to Fc.[27-29] The additional methyl groups on the cyclopentadienyl ring makes the $dmFc/dmFc^+$ redox couple more sterically hindered and therefore prevents any significant perturbing interactions between dmFc and other molecules in the solution.[28-30]

2.1.3. Electrolysis

Unlike electroanalytical techniques, such as cyclic voltammetry where the amount of products generated at both the working electrode and the counter electrode is not substantial, electrolysis can significantly alter the bulk concentrations of a solution.[31] There are two main ways to run an electrolysis experiment: galvanostatically or potentiostatically. In galvanostatic reactions, a constant current is passed through the cell, and the potential of the working electrode varies to maintain this current flow. In potentiostatic reactions, the potential is held constant (relative to that of a reference electrode) and a varying current flows through the cell.[1, 31]

It is important to note that in galvanostatic reactions, high voltages can arise if insufficient quantities of reagents are present to sustain the applied current, or if the mass transport of reagents to the electrodes is slow. High voltages can initiate, for example, solvent degradation and lead to side reactions and by-products. With the fixed potential in potentiostatic reactions, on the other hand, side products can be minimised and high reaction selectivity can be achieved. However, in potentiostatic reactions, the current will decrease as the substrate is consumed and consequently this will decrease the rate of reaction as the reaction proceeds.[16]

The choice of the two different methods will depend on the desired reaction itself, e.g. if a selective reaction is required but a lower conversion is not an issue then potentiostatic control would be the preferred choice. However, if a high conversion is required from the reaction, galvanostatic control would ensure that the reaction goes to completion by setting a high enough current. This could then come with a consequence of lower selectivity. Nonetheless, there are now growing number of different electroreactor set-ups which can ensure excellent selectivity of the reaction is achieved whilst the reaction is driven to completion. These set-ups include the use of flow electrolysis, undivided cells and divided cells.[16]

The charge, Q, needed for a full conversion is calculated using Faraday's law- assuming no competing electrode reactions, see Equation 2.4.[1, 32]

$$Q = mnF \quad (2.4)$$

Where *m* is the amount of substrate (in moles) to be oxidised/reduced in the reaction mixture. If the charge passed through the cell for a specific reaction is below the value determined by Faraday's law, full conversion cannot be achieved because not enough charge is passed through the cell to complete the reaction during the time of the electrolysis. If total charge passed is higher than the required charge then a competing reaction must be occurring at the working electrode to sustain the applied current because there is insufficient reactant in solution (e.g. the product is being degraded by over oxidation or the solvent/electrolyte is being oxidised).[1] With 100% Faradaic efficiency, better yields and cleaner products can be obtained, as the charge is fully consumed by the desired reaction and not by side-reactions. The choice of conditions will determine the success of an electrolysis in terms of faradaic efficiency and consequently yield of product, as well as in the reduction of side products.[1]

Moreover, in order to optimise the faradaic efficiency of an electrosynthetic process, it is crucial to take the counter electrode reaction into consideration. For each electron that is transferred at the working electrode, an electron will be transferred in the opposite direction at the counter electrode. For a high faradaic yield, the choice of counter electrode reaction needs to be one which does not generate electroactive species which can react with the desired products or with other reactants which could generate side-products and lower the faradaic efficiency of the electrolysis.[16]

Slow mass transport in the electrolysis solution can also be detrimental to the faradaic efficiency of the electrolysis, and many electroreactors are equipped with some type of agitator, such as a stirrer bar, to improve the rate of mass transport of reactants to electrode. The current is directly proportional to the flux of starting material, J, reaching the electrode surface, as described in Equation 2.5.[16]

$$i = nFAJ \qquad (2.5)$$

Thus with higher rate of mass transport a higher current can be obtained, and potentially better yield of products. Notably, if the mass transport is slow compared to the electrochemical reaction, then side-reactions will occur to maintain an applied current.[16, 32]

2.1.3.1. Bulk Electrolysis

High rate of conversion requires large electrode surface area to volume ratios. To achieve high electrode area to volume ratio, electrodes such as cylindrical reticulated vitreous carbon electrodes or platinum gauze are used.[2, 16] In some cells, the counter electrode is separated from the working electrode with a separator, such as a glass frit or an ion-selective membrane. This is necessary if, for example, the generated products or reactants at the working electrode side can be reduced/oxidised at the counter electrode or react with the products or reactant formed at the counter electrode. By separating the working and counter electrodes, the ‘chemistries’ at each electrode are separated and the possibility for producing side-products is lowered. A typical divided beaker cell for electrolysis is illustrated in Figure 2.6.[2, 5, 16]

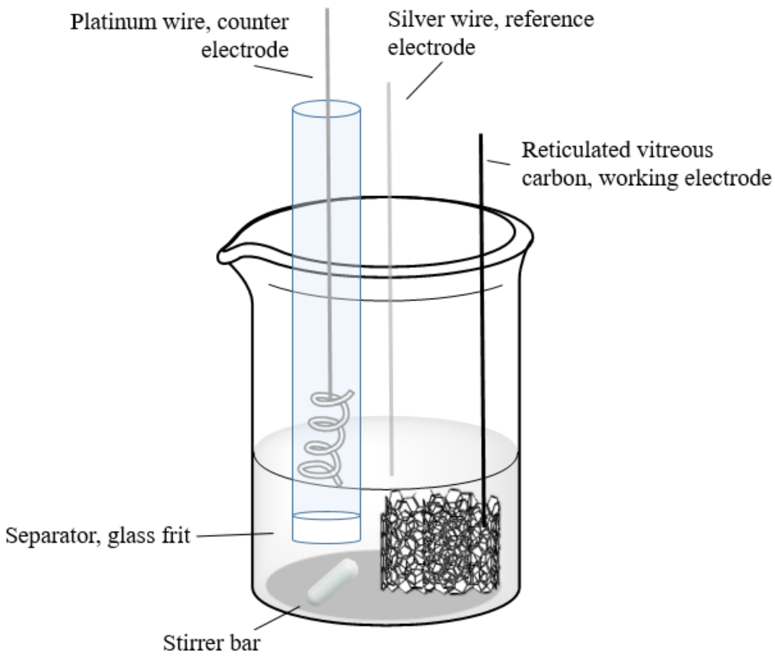

Figure 2.6: Typical divided beaker type electrolysis cell used for electrosynthesis with a separator (e.g. glass frit) separating the counter electrode from the working electrode.[2]

It should be noted that for every mole of electrons exchanged at the electrode surface there needs to be a transfer of 1 mole of ionic charge through the separator, and this charge transfer will also be accompanied by solvent from each of the cathode and anode compartments. Thus, mixing of the anolyte and catholyte solutions is inevitable, however the separator slows down the mixing. The extent of mixing will depend on pore dimensions and will increase with electrolysis time.[2]

Electrolysis with inefficient mass transport could give rise to the possibility of poorer performance of the electrolysis, through e.g. degradation of the solvent or slow homogeneous reactions. In bulk electrolysis it is, therefore, important to maximise the mass transport of the solution, and therefore the solutions are often stirred in a beaker cell set-up.[2]

2.6.1.2. Flow Electrolysis

In general, higher electrode area to reactant volume ratios are achieved in flow cells than in beaker electrolysis cells. These cells can be operated as divided or undivided cells. Figure 2.7 shows a schematic of a typical flow cell used in laboratories. These are commonly constituted of parallel electrode plate cells with path-length of only 1-3 cm.[2]

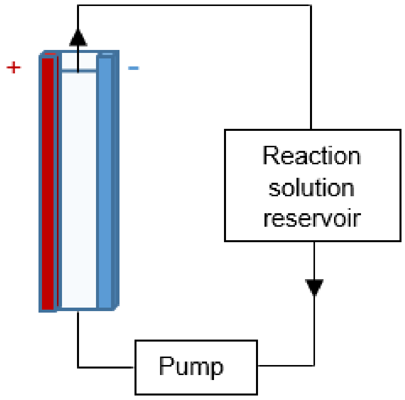

Figure 2.7: Typical flow cell for electrosynthesis with recycling of reactant solution.[2]

The reaction solution is usually passed through the electrode plates rapidly, to enhance the mass transfer of the reagents to the electrodes and keep the cell current high. The rate of conversion in terms of moles per second is therefore high. However, as the residence time of the reactant within the cell is short, the conversion in terms of moles in a single pass is low. By stacking or recycling the reactant solution in the cells the overall conversion is increased.[2] In principle, a high conversion in a single pass in a parallel plate electrolysis reactor can be achieved by using a lower flow rate of the reagent solution. However, lowering the flow rate also increases the possibility of side-reactions to occur. Lowering the flow rate could also initiate problems with reaction selectivity and the occurrence of side-products.[2]

A number of new flow electrolysis cells have been designed which produce selective reactions with high conversions and faradaic yields in a single pass of reagents without the need of stacking electrochemical cells. Syrris' Asia Electrochemistry Flow Chemistry system and the Cambridge Reactor Design's Ammonite cells are such examples and are shown in Figure 2.8.[2]

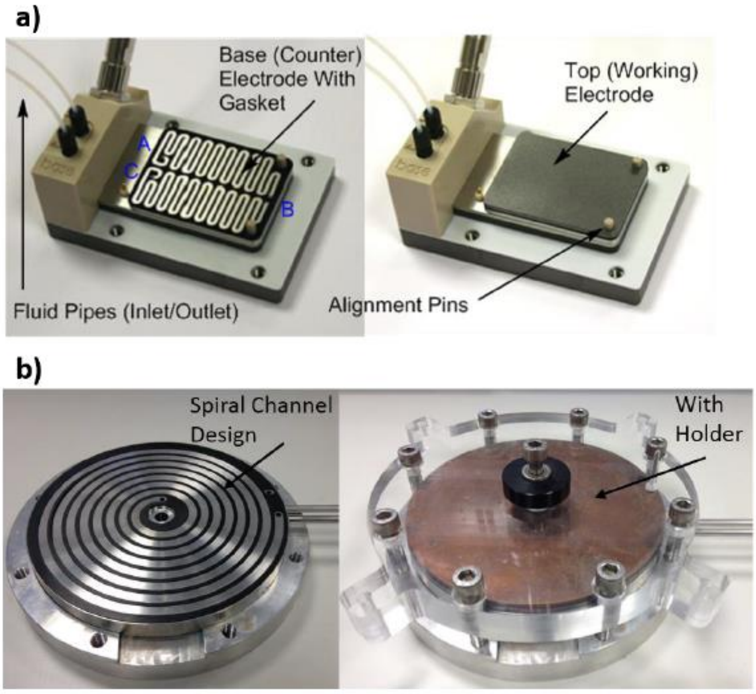

Figure 2.8: Extended channel length microflow electrolysis cells, a) cell with convoluted channel (Syrris) b) cell with spiral channel (Cambridge Reactor Design).[2]

These cells are similar to parallel plate reactors, but rather than increasing the residence time for higher conversions, the length of contact between the reactant solution and electrodes is extended, by creating longer channels between the electrodes. The Ammonite8 cell use carbon or platinum working electrodes, and the counter electrodes are stainless steel with grooves. A polymer spacer is used to form the interelectrode gap, and with this set-up a high electrode area to reactant volume is achieved. The Ammonite8 cell gives high conversions with flow rates up to 3 cm^3 min^{-1}, and for the methoxylation of *N*-formylpyrrolidine a rate of production of > 1 g hr^{-1} was observed.[2, 33]

In order to obtain high conversion in an extended channel flow electroreactor the concentration of the reactant must drop from the initial concentration at the cell inlet towards zero as the solution passes through the channels of the cell. Thus, in theory, the local current density of the reactant solution will decrease along the cell, as the reactant concentration drops, see Figure 2.9.

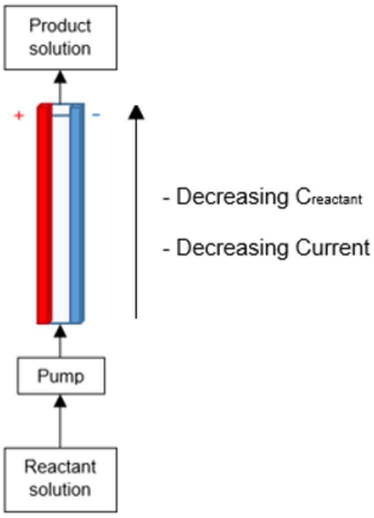

Figure 2.9: Schematic representation of full electrolysis in a single pass in an extended channel length flow cell.[2]

In order to obtain full conversion of reactant to product in a single pass in an extended channel cell, the charge passed through the cell must be large enough to convert all of the reagent within the time the reactant is in the electrolysis cell. The required current applied to the cell, i_{cell}, to obtain a conversion fraction of X can be determined using Faraday's law (assuming a 100% faradaic yield) as stated in Equation 2.6.

$$i_{cell} = nFQ_vC_{in}X \qquad (2.6)^{34}$$

Where Q_v is the volumetric flow rate of the reactant solution and C_{in} is the concentration of the reactant at the inlet. The concentration of reactant, the flow rate and applied current (if the electrolysis is conducted under galvanostatic conditions) will determine the fractional conversion of reactant and thus the rate of product formation from a single pass of reactant solution through the cell. Furthermore, in order to increase the rate of product formation, either the reactant concentration or the flow rate can be increased. Yet, if either of these parameters are increased, the applied current also needs to be increased for complete conversion in a single pass.[2]

As these flow cells are generally undivided cells, it is essential to consider the working and counter electrode reactions and possible reactions between the reactants and electro-generated species. Such reactions could lead to complex mixtures of side-products generating waste which might be difficult to separate from the desired product solution. These side reactions can significantly lower the faradaic efficiency of the electrolysis. Clean synthesis and high conversion is dependent on reactions at both the cathode and the anode, as well as possible homogeneous reactions between reactants and electrogenerated species, that neither contaminates the product stream nor consumes the reactant or product.[2]

2.2. Electrochemical Set-up

2.2.1. Cyclic Voltammetry

All CVs were performed using either an Autolab PGSTAT302 (EcoChemie, the Netherlands) or CHI760 potentiostat (From CH Instruments Austin, TX). A three-electrode electrochemical cell consisting of either a 3 mm diameter glassy carbon (GC) disk or 2 mm diameter Pt working electrode, a Pt-flag counter electrode, and Ag-wire quasi-reference electrode were used for electrochemical measurements. 5 mmol dm^{-3} decamethylferrocene (dmFc) was used as the internal standard during voltammetry studies. Prior to use, the GC or Pt electrode was polished using an aqueous suspension of 0.05-μm alumina and rinsed thoroughly with ultrapure H_2O. All solutions were deoxygenated prior to use by bubbling with Ar for at least 10 min. Compensation for uncompensated ohmic resistance was performed during each measurement using positive-feedback correction.

2.2.2. Flow Electrolyses

Flow electrolyses were performed in an Ammonite8 cell from Cambridge Reactor Design (Cambridgeshire, UK). Initially about 1 cm^3 of RTIL was pumped through the cell, the solution was then pumped through the cell at a set flow rate and electrolysis was carried out under constant current densities (0.5 mA cm^{-2}, 1 mA cm^{-2}, 1.5 mA cm^{-2} or 2 mA cm^{-2}). After the initial 1 cm^{3} of RTIL had passed through the cell the products were collected in a sample vial at the outlet of the cell. The products were collected from the cell outlet and were extracted into 5 cm^{3} of toluene or hexane for analysis by gas chromatography using a flame ionization detector.

2.2.3. Diffusion coefficients

PFG-NMR spectroscopic measurements for self-diffusion data were performed on a Bruker DPX-400 Spectrometer, working at 400.13 MHz (^{1}H). The pulse program ledbpgp2s (bipolar dosy experiment) was used with big delta = 149.9000m and little delta 5.000m, and experiments were run with 32 points and 16 scans for each. A solution of 0.6 mol dm^{-3} alcohol substrate and 2.4 mol dm^{-3} 2,6-lutidine or 1-butylimidazole in RTIL were added to the coaxial insert which was then added into the NMR tube with deuterated acetone. The measurements were repeated three times for each solution.

2.2.4. Gas Chromatography

Quantification of products were carried out on a TRACE$^{\text{TM}}$ 1310 Thermo Scientific$^{\text{TM}}$ gas chromatograph (GC) equipped with a flame ionization detector (FID). A Thermo Scientific$^{\text{TM}}$ TraceGOLD TG-17MS GC column with an inner diameter of 0.25 mm and a length of 30 m was used. A sample of 50 µcm^{3} was taken from the product solution and diluted. The product formation and reagent consumption were monitored by GC-FID or

GC-MS using the following procedure: an aliquot of 50 µcm^3 was collected from the product mixture. The neutral species, i.e. alcohol, aldehyde/ketone, 2,6-lutidine and tert-butylbenzene, were extracted into 5 cm^3 of toluene. The solutions were run on an autosampler splitless. The oven temperature began at 80 °C for 2 min and ramped to 120 ºC at 10 ºC min^{-1} and then kept at 180 ºC for 5 min, a solvent delay of 4 min was employed.

Four calibration standard solutions were prepared containing known amounts of tert-butylbenzene and varying concentrations of benzyl alcohol, benzaldehyde, 1-phenylethanol and acetophenone. These solutions were injected into the GC-FID. The peak area ratio of tert-butylbenzene and substrate was plotted *vs* the concentration of substrate, yielding a linear relationship. The gradient could then be used to calculate the experimental concentration of substrates from the electrolysis experiments, by dividing the experimental peak ratio of tert-butylbenzene and substrate with its respective gradient.

2.3. Materials and Characterisation

TEMPO (Sigma Aldrich, 98%), TEMPOL (Sigma Aldrich, 97%), hydrochloric acid (Fisher Scientific, 37% in water), sulphuric acid (Sigma Aldrich, 98%), 1-butylimidazole (Sigma Aldrich, 98%), 1-bromooctane (Sigma Aldrich, 99%), 1-methylimidazole (Sigma Aldrich ≥ 99%), benzyl alcohol (Sigma Aldrich, 99.8%), Tributylmethylphosphonium bis(trifluoromethanesulfonyl)imide methanesulfonate (IoLiTec, 97%), Tributylmethylphosphonium bis(trifluoromethanesulfonyl)imide chloride

(Sigma Aldrich, ≥ 98.0%), Trihexyl(tetradecyl)phosphonium bis(trifluoromethanesulfonyl)imide chloride (Sigma Aldrich, ≥ 95.0%), Trihexyl(tetradecyl)ammonium bis(trifluoromethanesulfonyl)imide bromide (Sigma Aldrich, ≥ 97.0%), 1-octanol (Acros Organics, 99%), 2-phenylethanol (Sigma Aldrich, 99%), 2-butanol (Sigma Aldrich, 99%), 4-nitrobenzyl alcohol (Acros Organics, 99%), 4-methoxyvenzyl alcohol (Sigma Aldrich, 98%), 4-bromobenzylalcohol (Sigma Aldrich, 99%), cinnamyl alcohol (Sigma Aldrich, 98%), 1-butanol (Sigma Aldrich, ≥ 99.5%), 1-ethyl-3-methyl dicyanamide (Sigma Aldrich, ≥ 98%), 1-ethyl-3-methyl chloride (Sigma Aldrich, 98.0%), 1-octyl-3-methylimidazolium chloride (Sigma Aldrich, ≥ 97.0%) and betulin (Sigma Aldrich, ≥ 98%) were used as received.

The ionic liquids and the Na[TEMPOOSO$_3$] salt were prepared according to literature procedures, and were fully characterized by ^{1}H, ^{13}C, ^{19}F and ^{31}P nuclear magnetic resonance spectroscopy, NMR, (recorded at room temperature on a Bruker DPX-400 Spectrometer) and electrospray ionisation mass spectrometry, ESI-MS, (Bruker MicroTOF spectrometer). All compounds were dried *in vacuo* (p ~10^{-4} – 10^{-6} mbar) and then stored under argon. The water content in the ILs were measured prior to electrochemical measurements using Karl-Fisher analysis, and when the water content was less than 200 ppm. The electrochemical measurements were conducted in ambient pressure and temperature.

2.3.1. 1-Ethyl-3-methylimidazolium bis(trifluoromethanesulfonyl)imide, $[C_2C_1Im][NTf_2]$[35, 36]

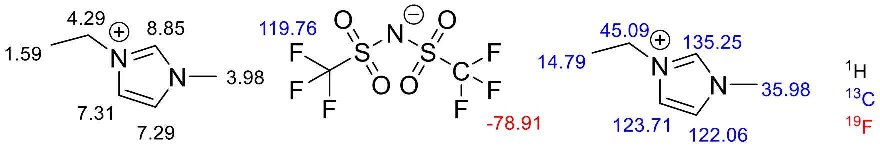

$[C_2C_1Im]Cl$ (36.0 g, 246 mmol) was dissolved in water (100 cm^3) and stirred. A solution of Li$[NTf_2]$ (84.9 g, 296 mmol) and water (50 cm^3) was added to the stirring solution, which was stirred overnight at room temperature. To the stirring solution a solution of $LiNTf_2$ (84.9 g, 296 mmol) and water (100 cm^3) was added. The solution was stirred overnight at room temperature. Dichloromethane (200 cm^3) was added to the mixture and the organic layer was washed with water (6 × 50 cm^3). The organic layer was separated and the solvent was removed under reduced pressure. The crude liquid was dried *in vacuo* at 40 °C for 12 hrs, to yield a clear viscous liquid (95 g, 99% yield).

^{1}H NMR (400 MHz, $CDCl_3$) δ ppm: 8.85 (s, 1 H), 7.31 (t, *J* =1.7 Hz, 1 H), 7.29 (t, *J* = 1.7 Hz, 1 H), 4.29 (q, *J* = 7.4 Hz, 2 H), 3.98 (s, 3 H), 1.59 (t, *J* = 7.4 Hz, 3 H).

^{13}C NMR (101 MHz, $CDCl_3$) δ ppm: 135.25, 123.71, 122.06, 119.76 (q, $^1J_{C-F}$ = 322 Hz, 2 C), 45.09, 35.98, 14.79.

^{19}F NMR (282 MHz, $CDCl_3$) δ ppm: -78.91 (s, 6 F).

ESI-MS (+ve) $[C_6H_{11}N_2]^+$: calcd 111.0917 m/z, found 111.0923 m/z.

ESI-MS (-ve) $[C_2F_6NO_4S_2]^-$: calcd 279.9178 m/z, found 279.9207 m/z.

Data in agreement with literature.[36]

2.3.2. 1-Octyl-3-methylimidazolium bromide, $[C_8C_1Im][Br]$[37]

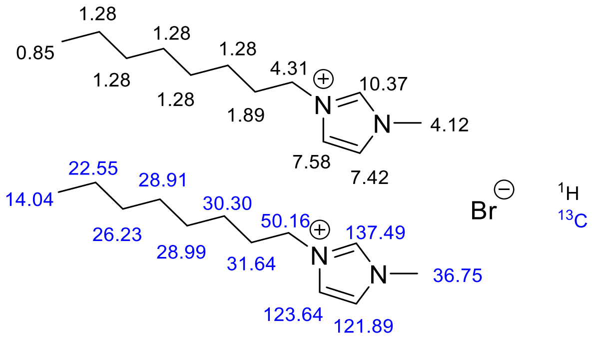

1-bromooctane (45.2 cm^3, 262 mmol) was added dropwise to a stirring mixture of 1-methylimidazole (17.4 cm^3, 218 mmol) and ethyl acetate (50.0 cm^3), at room temperature. The mixture was then stirred overnight at 40 °C. The solvent was removed under reduced pressure and the crude product was recrystallized from acetonitrile/ethyl acetate (approximately 2:1). The crude liquid was dried *in vacuo* at 50 °C for 12 h to yield a white solid product (44.2 g, 74%).

^{1}H NMR (400 MHz, $CDCl_3$) δ ppm: 10.37 (br. s, 1 H), 7.58 (t, *J* = 1.8 Hz, 1 H), 7.42 (t, *J* = 1.8 Hz, 1 H), 4.31 (t, *J* = 7.6 Hz, 2 H), 4.12 (s, 3 H), 1.89 (m, 2 H), 1.28 (m, 10 H), 0.85 (t, *J* = 7.6 Hz, 3 H).

^{13}C NMR (101 MHz, CDCl3) δ ppm: 137.49, 123.64, 121.89, 50.16, 36.75, 31.64, 30.30, 28.99, 28.91, 26.23, 22.55, 14.04.

ESI-MS (+ve) $[C_{12}H_{23}N_2]^+$: calcd 195.1856 m/z, found 195.1860 m/z.

Data in agreement to literature.[36, 37]

2.3.3. 1-Octyl-3-methylimidazolium bis(trifluoromethanesulfonyl)imide, $[C_8C_1Im][NTf_2]$[38]

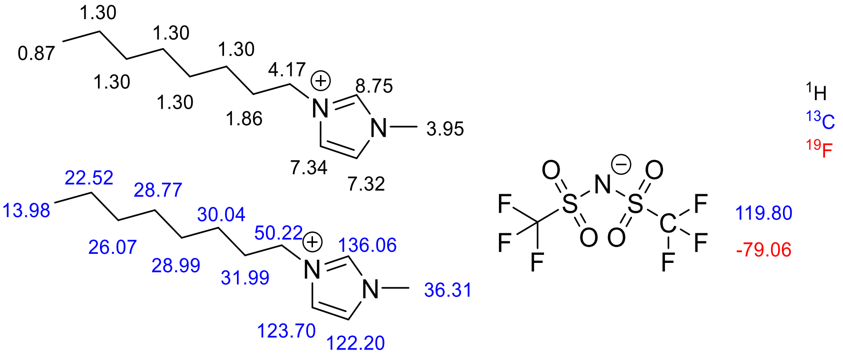

$[C_8C_1Im]Br$ (12.32 g, 44.8 mmol) was dissolved in water (100 cm^3) and stirred. A solution of $Li[NTf_2]$ (15.4 g, 53.8 mmol) and water (100 cm^3) was added to the stirring solution, which was stirred overnight at room temperature. Dichloromethane (150 cm^3) was added to the mixture and the organic layer was washed with water (4 × 50 cm^3). The organic layer was separated and the solvent was removed under reduced pressure. The crude liquid was dried *in vacuo* at 40 °C for 12 hrs, to yield a clear viscous liquid (21.0 g, 98%).

^{1}H NMR (400 MHz, $CDCl_3$) δ ppm: 8.75 (br. s, 1 H), 7.34 (t, J = 1.9 Hz, 1 H), 7.32 (t, J = 1.9 Hz, 1 H), 4.17 (t, J = 7.5 Hz, 2 H), 3.95 (s, 3 H), 1.86 (m, 2 H), 1.30 (m, 10 H), 0.87 (t, J = 7.5 Hz, 3 H).

^{13}C NMR (101 MHz, $CDCl_3$) δ ppm: 136.01, 123.73, 122.23, 119.80 (q, $^1J_{C-F}$ = 322 Hz, 2 C), 50.21, 36.30, 31.60, 30.04, 28.90, 28.78, 26.07, 22.53, 13.98.

^{19}F NMR (282 MHz, $CDCl_3$) δ ppm: -79.06 (s, 6 F).

ESI-MS (+ve) $[C_{12}H_{23}N_2]^+$: calcd 195.1856 m/z, found 195.1860 m/z.

ESI-MS (-ve) $[C_2F_6NO_4S_2]^-$: calcd 279.9178 m/z found 279.9176 m/z.

Data in agreement with literature.[38, 39]

2.3.4. 1-Octyl-3-methylimidazolium trifluoromethanesulfonate, $[C_8C_1Im][OTf]$[40]

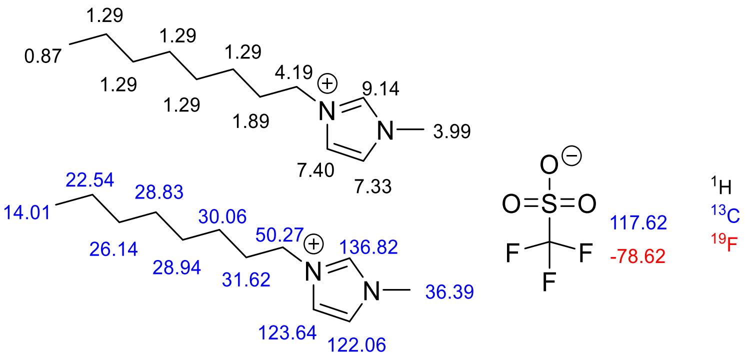

$[C_8C_1Im]Br$ (11.0 g, 40.0 mmol) was dissolved in water (50 cm^3) and stirred. A solution of LiOTf (9.36 g, 60.0 mmol) and water (50 cm^3) was added to the stirring solution, which was stirred overnight at room temperature. Dichloromethane (150 cm^3) was added to the mixture and the organic layer was washed with water (4 × 50 cm^3). The organic layer was separated and the solvent was removed under reduced pressure. The crude liquid was dried *in vacuo* at 40 °C for 12 hrs to yield clear viscous liquid (12.2 g, 88%).

^{1}H NMR (300 MHz, $CDCl_3$) δ ppm: 9.14 (br.s, 1 H), 7.40 (t, *J* = 1.8 Hz, 1 H), 7.33 (t, *J* = 1.8 Hz, 1 H), 4.19 (t, *J* = 7.6 Hz, 2 H), 3.99 (s, 3 H), 1.89 (m, 2 H), 1.29 (m, 10 H), 0.87 (t, *J* = 7.6 Hz, 3 H).

^{13}C NMR (75 MHz, $CDCl_3$) δ ppm: 136.82, 123.64, 122.06, 117.62 (q, $^1J_{C-F}$ = 322 Hz, 2 C), 50.27, 36.39, 31.62, 30.06, 28.94, 28.83, 26.14, 22.54, 14.01.

^{19}F NMR (282 MHz, CDC13) δ ppm: -78.62 (s, 3 F).

ESI-MS (+ve) $[C_{12}H_{23}N_2]^+$: calcd 195.1856 m/z, found 195.1868 m/z.

ESI-MS (-ve) $[C_1F_3O_3S_1]^-$: calcd 148.9526 m/z found 148.9519 m/z.

Data is in agreement with literature.[40]

2.3.5. 1-Octyl-3-methylimidazolium hexafluorophosphate, $[C_8C_1Im][PF_6]$[41, 42]

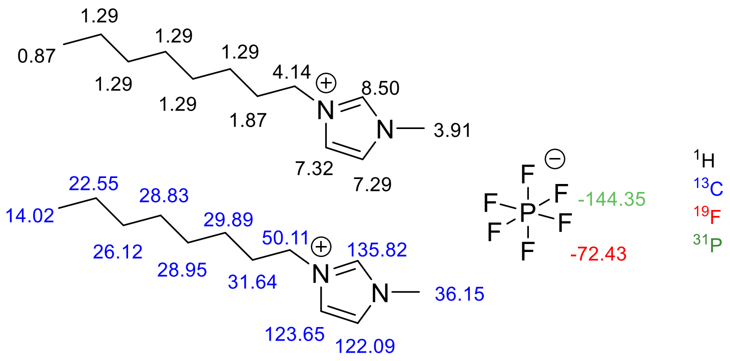

$[C_8C_1Im]Cl$ (17.0 g, 73.5 mmol) was dissolved in water (150 cm^3) and stirred. HPF_6 (60% in water, 13.0 cm^3, 88.2 mmol) was added dropwise to the stirring solution, which was stirred overnight at room temperature. Dichloromethane (150 cm^3) was added to the mixture and the organic layer was washed with water (4 × 50 cm^3). The organic layer was separated and the solvent was removed under reduced pressure. The crude liquid was dried *in vacuo* at 40 °C for 12 hrs to yield a clear viscous liquid (23.5 g, 94%).

^{1}H NMR (300 MHz, $CDCl_3$) δ ppm: 8.50 (br. s, 1 H), 7.32 (t, *J* = 1.8 Hz, 1 H), 7.29 (t, *J* = 1.8 Hz, 1 H), 4.14 (t, *J* = 7.5 Hz, 2 H), 3.91 (s, 3 H), 1.87 (m, 2 H), 1.29 (m, 10 H), 0.87 (t, *J* = 7.5 Hz, 3 H).

^{13}C NMR (75 MHz, $CDCl_3$) δ ppm: 135.82, 123.65, 122.09, 50.11, 36.15 31.64, 29.89, 28.95, 28.83, 26.12, 22.55, 14.02.

^{19}F NMR (282 MHz, $CDCl_3$) δ ppm: -72.43 (d, *J* = 711 Hz).

^{31}P NMR (121 MHz, $CDCl_3$) δ ppm: -144.35 (spt, *J* = 711 Hz).

ESI-MS (+ve) $[C_{12}H_{23}N_2]^+$: calcd 195.1856 m/z found 195.1862 m/z.

Data is in agreement with literature.[39, 42]

2.3.6. 1-Octyl-3-methylimidazolium dicyanamide, $[C_8C_1Im][DCA]$[43]

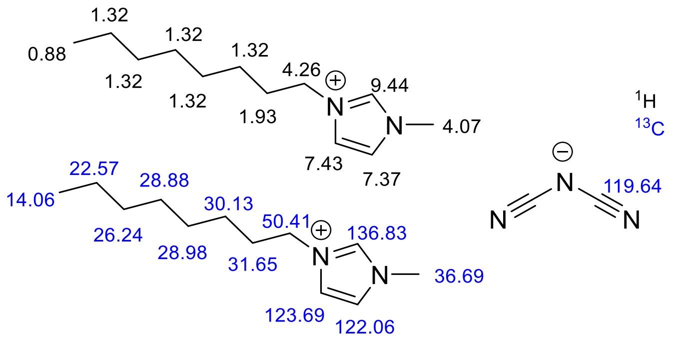

$[C_8C_1Im]Br$ (21.2 g, 77.0 mmol) was dissolved in water (50 cm^3) and stirred. A solution of $Na[N(CN)_2]$ (8.2 g, 92.0 mmol) and water (50 cm^3) was added to the stirring solution, which was stirred overnight at room temperature. Dichloromethane (150 cm^3) was added to the mixture and the organic layer was washed with water (4 × 50 cm^3). The organic layer was separated and the solvent was removed under reduced pressure. The crude liquid was dried *in vacuo* at 40 °C for 12 hrs to yield a clear viscous liquid (19.5 g, 98%).

^{1}H NMR (400 MHz, $CDCl_3$) δ ppm: 9.44 (br. s, 1 H), 7.43 (m, 1 H), 7.37 (m, 1 H), 4.26 (t, *J* = 7.4 Hz, 2 H), 4.07 (s, 3 H), 1.93 (m, 2 H), 1.32 (m, 10 H), 0.88 (t, *J* = 7.2 Hz, 3 H).

^{13}C NMR (101 MHz, $CDCl_3$) δ ppm: 136.83, 123.69, 122.06, 119.64, 50.41, 36.69, 31.65, 30.13, 28.98, 28.88, 26.24, 22.57, 14.06.

ESI-MS (+ve) $[C_{12}H_{23}N_2]^+$: calcd 195.1856 m/z found 195.1856 m/z.

Data in agreement with literature.[43, 44]

2.3.7. 1-Octyl-3-methylimidazolium tetrafluoroborate, $[C_8C_1Im][BF_4]$[39]

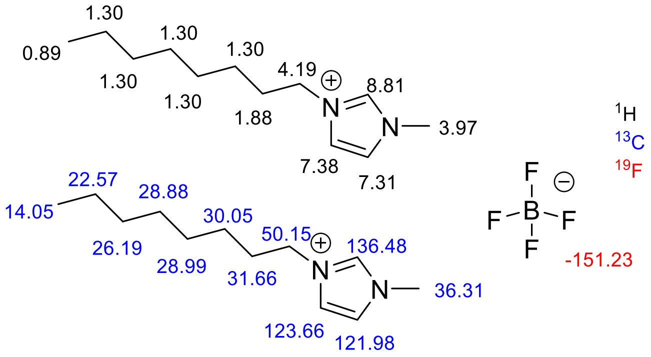

$[C_8C_1Im]Cl$ (34.0 g, 147 mmol) was dissolved in water (150 cm^3) and stirred. A solution of $Na[BF_4]$ (19.4 g, 177 mmol) and water (150 cm^3) was added to the stirring solution, which was stirred overnight at room temperature. Dichloromethane (150 cm^3) was added to the mixture and the organic layer was washed with water (4 × 50 cm^3). The organic layer was separated and the solvent was removed under reduced pressure. The crude liquid was dried *in vacuo* at 40 °C for 12 hrs to yield a clear viscous liquid (35.6 g, 86%).

^{1}H NMR (400 MHz, $CDCl_3$) δ ppm: 8.81 (br. s, 1 H), 7.38 (t, *J* = 1.8 Hz, 1 H), 7.31 (t, *J* = 1.8 Hz, 1 H), 4.19 (t, *J* = 7.5 Hz, 2 H), 3.97 (s, 3 H), 1.88 (m, 2 H), 1.30 (m, 10 H), 0.89 (t, *J* = 7.5 Hz, 3 H).

^{13}C NMR (101 MHz, $CDCl_3$) δ ppm: 136.48, 123.66, 121.98, 50.15, 36.31, 31.66, 30.05, 28.99, 28.88, 26.19, 22.57, 14.05.

^{19}F NMR (282 Hz, $CDCl_3$) δ ppm: -151.27 (br. s), -151.22 (br. s).

ESI-MS (+ve) $[C_{12}H_{23}N_2]^+$: calcd 195.1856 m/z found 195.1855 m/z.

Data is in agreement with literature.[39, 45]

2.3.8. 1-Octyl-1-methylpyrrolidinium bromide, $[C_8C_1Pyrr]Br$[46, 47]

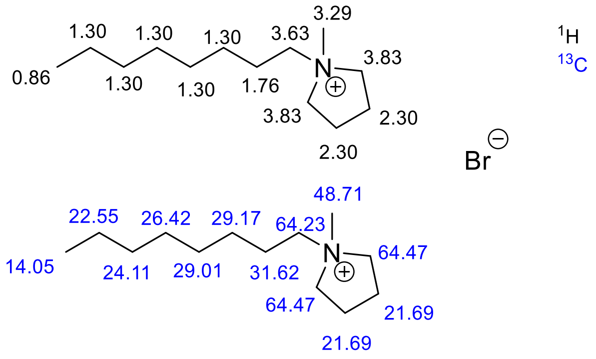

1-bromooctane (38.0 cm^3, 216 mmol) was added dropwise to a stirring mixture of 1-methylpyrrolidine (19.0 cm^3, 180 mmol) and ethyl acetate (15.0 cm^3), at room temperature, and the mixture was stirred overnight at 40 °C. The solvent was removed under reduced pressure and the crude product was recrystallized from acetonitrile/ethyl acetate. The white solid product was dried *in vacuo* at 50 °C for 12 h (32.6 g, 65%).

^{1}H NMR (400 MHz, $CDCl_3$) δ ppm: 3.83 (m, 4 H), 3.63 (m, 2 H), 3.29 (s, 3 H), 2.30 (m, 4 H), 1.76 (m, 2 H), 1.30 (m, 10 H), 0.86 (t, *J* = 7.4 Hz, 3 H).

^{13}C NMR (101 MHz, $CDCl_3$) δ ppm: 64.47, 64.23, 48.71, 31.62, 29.17, 29.01, 26.42, 24.11, 22.55, 21.69, 14.05.

ESI-MS (+ve) $[C_{13}H_{28}N]^+$: calcd 198.2216 m/z, found 198.2233 m/z.

Data in agreement with literature.[46, 47]

2.3.9. 1-Octyl-1-methylpyrrolidinium bis(trifluoromethanesulfonyl)imide, $[C_8C_1Pyrr][NTf_2]$[46]

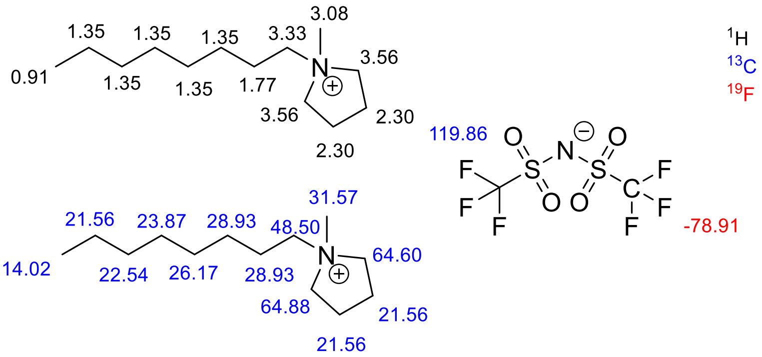

$[C_8C_1Pyrr]Br$ (5.8 g, 20.9 mmol) was dissolved in water (50 cm^3) and stirred. A solution of $Li[NTf_2]$ (7.2 g, 25.1 mmol) and water (50 cm^3) was added to the stirring solution, which was stirred overnight at room temperature. Dichloromethane (150 cm^3) was added to the mixture and the organic layer was washed with water (4 × 50 cm^3). The organic layer was separated and the solvent removed under reduced pressure. The clear liquid product was dried *in vacuo*, at 50 °C for 12 h (9.9 g, 100%).

^{1}H NMR (400 MHz , $CDCl_3$) δ ppm: 3.56 (m, 4 H), 3.33 (m, 2 H), 3.08 (s, 3 H), 2.30 (m, 4 H), 1.77 (m, 2 H), 1.35 (m, 10 H), 0.91 (t, J = 7.6 Hz, 3 H).

^{13}C NMR (101 MHz , $CDCl_3$) δ ppm: 119.86 (q, $^1J_{C\text{-}F}$ = 322 Hz, 2 C), 64.88, 64.60, 48.50, 31.57, 28.93, 26.17, 23.87, 22.54, 21.56, 14.02.

^{19}F NMR (282 MHz , $CDCl_3$) δ ppm: -78.91 (s, 6 F).

ESI-MS (+ve) $[C_{13}H_{28}N]^+$: calcd 198.2216 m/z, found 198.2229 m/z.

ESI-MS (-ve) $[C_2F_6NO_4S_2]^-$: calcd 279.9178 m/z, found 279.9234 m/z.

Data in agreement with literature.[46, 48]

2.3.10. Tributylmethylphosphonium bis(trifluoromethanesulfonyl)imide, $[P_{4,4,4,1}][NTf_2]$[46]

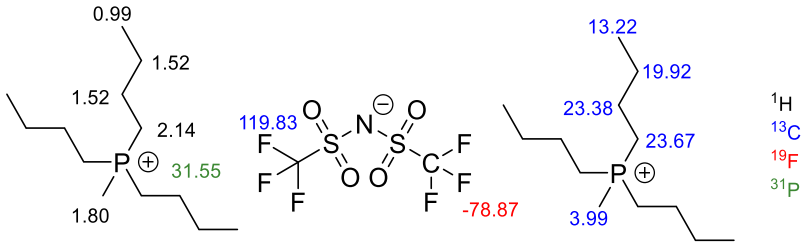

$[P_{4,4,4,1}][CH_3SO_3]$ (6.6 g, 20.1 mmol) was dissolved in chloroform (50 cm^3) and stirred. A solution of Li[NTf_2] (6.9 g, 24.1 mmol) and water (50 cm^3) was added to the stirring solution, which was stirred overnight at room temperature. Chloroform (150 cm^3) was added to the mixture and the organic layer was washed with water (4 × 50 cm^3). The organic layer was separated and the solvent removed under reduced pressure. The crude liquid was dried *in vacuo*, at 50 °C for 12 h to yield a clear liquid (8.5 g, 85%).

^{1}H NMR (300MHz, $CDCl_3$) δ ppm: 2.14 (m, 6 H), 1.80 (d, *J* = 12 Hz, 3 H), 1.52 (m, 12 H), 0.99 (t, *J* = 7.1, 9 H).

^{13}C NMR (75 MHz, $CDCl_3$) δ ppm: 119.83(q, $^{1}J_{C\text{-}F}$ = 321, 2 C), 23.67 (d, $J_{C\text{-}P}$ = 15.0 Hz, 1 C), 23.38 (d, $J_{C\text{-}P}$ = 4.5 Hz, 1 C), 19.92 (d, $J_{C\text{-}P}$ = 48.8 Hz, 1 C) 13.22, 3.99 (d, $J_{C\text{-}P}$ = 56.3, 1 C).

^{19}F NMR (282 MHz, $CDCl_3$) δ ppm: -78.87 (s, 6 F).

^{31}P NMR (121 MHz ,$CDCl_3$) δ ppm: 31.55 (s, 1 P).

ESI-MS (+ve) $[C_{13}H_{30}P]^{+}$: calcd 217.2080 m/z, found 217.2103 m/z.

ESI-MS (-ve) $[C_2F_6NO_4S_2]^{-}$: calcd 279.9178 m/z, found 279.9264 m/z.

Data is in agreement with literature.[49]

2.3.11. Tributylmethylammonium bis(trifluoromethanesulfonyl)imide, $[N_{4,4,4,1}][NTf_2]$[46]

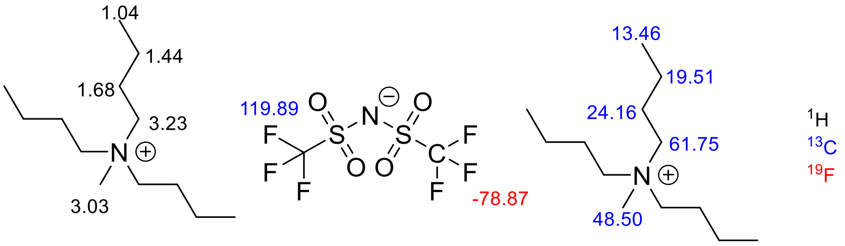

$[N_{4,4,4,1}]Cl$ (4.9 g, 20.8 mmol) was dissolved in chloroform (50 cm^3) and stirred. A solution of Li[NTf_2] (7.2 g, 25.0 mmol) and water (50 cm^3) was added to the stirring solution, which was stirred overnight at room temperature. Chloroform (150 cm^3) was added to the mixture and the organic layer was washed with water (4 × 50 cm^3). The organic layer was separated and the solvent removed under reduced pressure. The crude was dried *in vacuo*, at 40 °C for 12 h to yield a clear liquid (9.7 g, 97%).

^{1}H NMR (400 MHz, $CDCl_3$) δ ppm: 3.23 (m, 6 H), 3.03 (s, 3 H), 1.68 (m, 6 H), 1.44 (m, 6 H), 1.04 (t, *J* = 7.4 Hz, 9 H).

^{13}C NMR (101 MHz, $CDCl_3$) δ ppm: 119.89 (q, $^1J_{C\text{-}F}$ = 322 Hz, 2 C), 61.75, 48.50, 24.16, 19.51, 13.46.

^{19}F NMR (282 MHz, $CDCl_3$) δ ppm: -78.87 (s, 6 F).

ESI-MS (+ve) $[C_{13}H_{30}N]^+$: calcd 200.2373 m/z, found 200.2385 m/z.

ESI-MS (-ve) $[C_2F_6NO_4S_2]^-$: calcd 279.9178 m/z, found 279.9211 m/z.

Data in agreement with literature.[46, 50]

2.3.12. Trihexyl(tetradecyl)ammonium bis(trifluoromethanesulfonyl)imide, $[N_{6,6,6,14}][NTf_2]$[46]

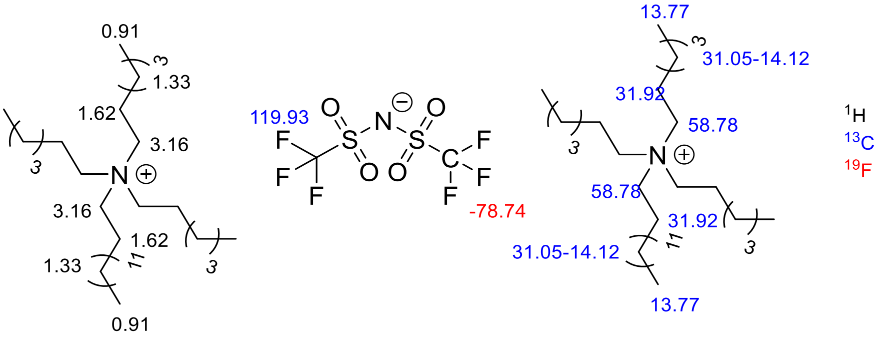

$[N_{6,6,6,14}]$Br (7.0 g, 15.1 mmol) was dissolved in chloroform (50 cm^3) stirred. A solution of Li$[NTf_2]$ (5.2 g, 18.1 mmol) and water (50 cm^3) was added to the stirring solution, which was stirred overnight at room temperature. Chloroform (150 cm^3) was added to the mixture and the organic layer was washed with water (4 × 50 cm^3). The organic layer was separated and the solvent removed under reduced pressure. The crude liquid was dried *in vacuo*, at 50 °C for 12 h to yield a clear viscous liquid (8.9 g, 89%).

^{1}H NMR (400 MHz, $CDCl_3$) δ ppm: 3.16 (m, 8 H), 1.62 (m, 8 H), 1.33 (m, 40 H), 0.91 (m, 12 H).

^{13}C NMR (101 MHz, $CDCl_3$) δ ppm: 119.93 (q, $^1J_{C\text{-}F}$ = 322 Hz, 2 C) 58.78, 31.92, 31.05, 29.68, 29.65, 29.60, 29.43, 29.36, 29.29, 28.97, 26.12, 25.80, 22.69, 22.33, 21.82, 14.12, 13.77.

^{19}F NMR (282 MHz, $CDCl_3$) δ ppm: -78.74 (s, 6 F).

ESI-MS (+ve) $[C_{32}H_{68}N]^+$: calcd 466.5346 m/z, found 466.5358 m/z.

ESI-MS (-ve) $[C_2F_6NO_4S_2]^-$: calcd 279.9178 m/z, found 279.9234 m/z.

Data in agreement with literature.[46, 51]

2.3.13. Trihexyl(tetradecyl)phosphonium bis(trifluoromethanesulfonyl)imide, $[P_{6,6,6,14}][NTf_2]$[52]

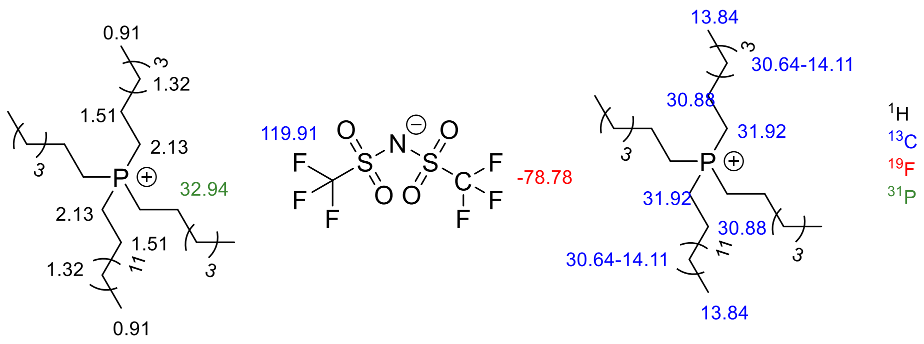

$[P_{6,6,6,14}]Cl$ (6.8 g, 13.1 mmol) was dissolved in chloroform (50 cm^3) and stirred. A solution of $Li[NTf_2]$ (4.5 g, 15.7 mmol) and water (50 cm^3) was added to the stirring solution, which was stirred overnight at room temperature. Chloroform (150 cm^3) was added to the mixture and the organic layer was washed with water (4 × 50 cm^3). The organic layer was separated and the solvent removed under reduced pressure. The crude liquid was dried *in vacuo*, at 50 °C for 12 h to yield a clear liquid (9.9 g, 99%).

^{1}H NMR (400 MHz, $CDCl_3$) δ ppm: 2.13 (m, 8 H), 1.51 (m, 16 H), 1.32 (m, 32 H), 0.91 (m, 12 H).

^{13}C NMR (101 MHz , $CDCl_3$) δ ppm: 119.91 (q, $^1J_{C\text{-}F}$ = 322 Hz, 2 C), 31.92, 30.88, 30.64, 30.49, 30.29, 30.15, 29.68, 29.65, 29.61, 29.49, 29.36, 29.25, 28.80, 22.69, 22.44, 22.28, 21.58, 21.54, 21.49, 18.96, 18.94, 18.49, 18.47, 14.11, 13.84.

^{19}F NMR (282 MHz, $CDCl_3$) δ ppm: -78.78 (s, 6 F).

^{31}P NMR (121 MHz, $CDCl_3$) δ ppm: 32.94 (s, 1 P).

ESI-MS (+ve) $[C_{32}H_{68}P]^+$: calcd 483.5053 m/z, found 483.5067 m/z.

ESI-MS (-ve) $[C_2F_6NO_4S_2]^-$: calcd 279.9178 m/z, found 279.9236 m/z.

Data in agreement with literature.[52]

2.3.14. Trihexyl(tetradecyl)phosphonium dicyanamide, $[P_{6,6,6,14}][DCA]$[52]

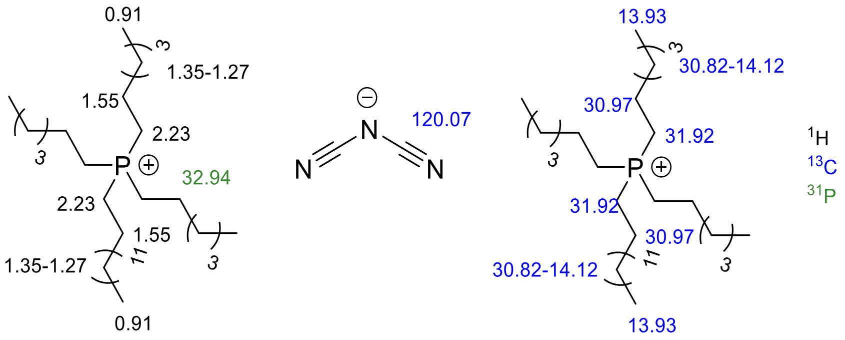

$[P_{6,6,6,14}]Cl$ (50.0 g, 95.9 mmol) was dissolved in chloroform (100 cm^3) and stirred. A solution of Na[DCA] (10.2 g, 115 mmol) and water (100 cm^3) was added to the stirring solution, which was stirred overnight at room temperature. Chloroform (150 cm^3) was added to the mixture and the organic layer was washed with water (4 × 50 cm^3). The organic layer was separated and the solvent removed under reduced pressure. The crude was dried *in vacuo*, at 50 °C for 12 h to yield a clear viscous liquid (51.2 g, 97%).

^{1}H NMR (400 MHz, $CDCl_3$) δ ppm: 2.23 (m, 8 H), 1.55 (m, 16 H), 1.35 (s, 14 H), 1.27 (m, 18 H), 0.91 (m, 12 H).

^{13}C NMR (101 MHz, $CDCl_3$) δ ppm: 120.07, 31.92, 30.97, 30.82, 30.68, 30.48, 30.34, 29.68, 29.65, 29.62, 29.52, 29.36, 29.29, 28.89, 22.69, 22.32, 21.74, 21.70, 21.65, 19.27, 19.25, 18.80, 18.78, 14.12, 13.93.

^{31}P NMR (121 MHz , $CDCl_3$) δ ppm: 32.94 (s, 1 P).

ESI-MS (+ve) $[C_{32}H_{68}P]^+$: calcd 483.5053 m/z, found 483.5055 m/z.

Data in agreement with literature.[52]

2.3.15. Tetrabutylammonium dicyanamide, $[N_{4,4,4,1}][DCA]$[53, 54]

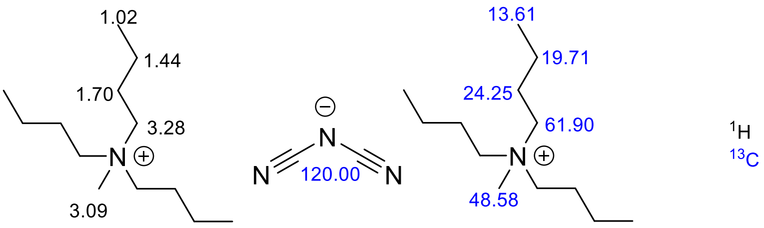

$[N_{4,4,4,1}]$Cl (88.5 g, 375 mmol) was dissolved in water (100 cm^3) and stirred. A solution of Na[DCA] (40.1 g, 450 mmol) and water (100 cm^3) was added to the stirring solution, which was stirred overnight at room temperature. Chloroform (150 cm^3) was added to the mixture and the organic layer was washed with water (4 × 50 cm^3). The organic layer was separated and the solvent removed under reduced pressure. The crude liquid was dried *in vacuo* at 50 °C for 12 h to yield a clear liquid product (88 g, 88% yield).

^{1}H NMR (400 MHz, $CDCl_3$) δ ppm: 3.28 (m, 6 H) 3.09 (s, 3 H), 1.70 (m, 6 H), 1.44 (m, 6 H), 1.02 (t, *J* = 7.8 Hz, 9 H).

^{13}C NMR (101 MHz, $CDCl_3$) δ ppm: 120.00, 61.90, 48.58, 24.25, 19.71, 13.61.

ESI-MS (+ve) $[C_{13}H_{30}N]^+$: calcd 200.2373 m/z, found 200.2369 m/z.

Data in agreement with literature.[55]

2.3.16. 1-butylimidazolium chloride, $[C_4HIm]Cl$[36]

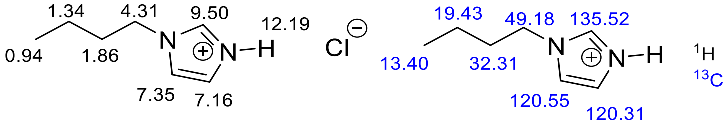

200 cm^3 of a 1 mol dm^{-3} aqueous solution of hydrochloric acid was added dropwise to a 200 cm^3 solution of 1 mol dm^{-3} aqueous solution of 1-butylimidazole. The temperature of the solution 1-butylimidazole solution was kept below 20 °C as the HCl solution was added. The mixture was then stirred at room temperature for 30 mins. The water was removed under reduced pressure and the crude was dried *in vacuo* at 40 °C for 12 h to yield a white crystalline solid product (31 g, 97%).

^{1}H NMR (400 MHz, $CDCl_3$) δ ppm: 12.19 (br. s, 1 H), 9.50 (m, 1 H), 7.35 (t, J = 1.8 Hz, 1 H), 7.16 (t, J = 1.8 Hz, 1 H), 4.31 (t, J = 7.3 Hz, 2 H), 1.86 (m, 2 H), 1.34 (m, 2 H), 0.94 (t, J = 7.4 Hz, 3 H).

^{13}C NMR (101 MHz, CDCl3) δ ppm: 135.52, 120.55, 120.31, 49.18, 32.31, 19.43, 13.40.

ESI-MS (+ve) $[C_7H_{13}N_2]^+$: calcd 125.1073 m/z found 125.1074 m/z.

Data in agreement with literature.[36]

2.3.17. Sodium (2,2,6,6-tetramethylpiperidin-*N*-oxyl)-4-sulfate, Na[$TEMPOOSO_3$][56]

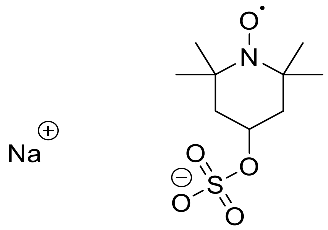

5 g of TEMPOL was ground to a fine powder and was then added in small portions to 10 cm^3 of concentrated (98%) H_2SO_4. The solution is stirred

for 20 mins and then transferred to a dropping funnel and added dropwise to a solution of aqueous $NaHCO_3$ (47.3 g in 500 cm^3 ultrapure water). The aqueous phase was washed twice with ethyl acetate (150 cm^3) to remove potentially unreacted TEMPOL or the hydrolysed reaction product. Water was removed under reduced pressure. Acetone (150 cm^3) was added to the slightly yellow coloured solid and the resulting dispersion was stirred until the solid was colourless (approximately 1 h). Acetone was removed from the filtrate under reduced pressure, to yield a dark-red waxy like solid (6.5 g, 82%).

ESI-MS (-ve) $[C_9H_{17}NO_5S]^-$: calcd 251.0833 m/z found 251.0835 m/z.

CHN Analysis: calcd. for Na[TEMPOOSO$_3$], ($NaC_9H_{17}NO_5S$): C 37.22%, H 5.90%, N 4.82% found: C 36.90%, H 6.60%, N 4.69%.

Data in agreement with literature.[56]

2.3.18. 1-butylimidazolium bis(trifluoromethanesulfonyl)imide, [C$_4$HIm][NTf$_2$][36]

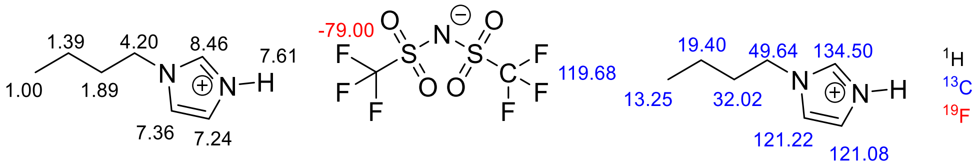

[C$_4$HIm]Cl (16.0 g, 0.2 mol) was dissolved in water (150 cm^3) and stirred. To the stirring solution a solution of Li[NTf$_2$] (34.5 g, 0.12 mol) and water (150 cm^3) was added. The solution was stirred overnight at room temperature. Dichloromethane (200 cm^3) was added to the mixture and the organic layer was washed with ultrapure water (4 × 50 cm^3). The organic layer was separated and the solvent was removed under reduced pressure. The crude liquid was dried *in vacuo* at 40 °C for 12 hrs to yield a clear viscous liquid (39.6 g, 98%).

^{1}H NMR (400 MHz, $CDCl_3$) δ ppm: 8.46 (m, 1 H), 7.61 (br. s, 1 H), 7.36 (t, *J* = 1.8 Hz, 1 H), 7.24 (t, *J* = 1.8 Hz, 1 H), 4.20 (t, *J* = 7.4 Hz, 1 H), 1.89 (m, 2 H), 1.39 (m, 2 H), 1.00 (t, *J* = 7.4 Hz, 3 H).

^{13}C NMR (101 MHz, CDCl3) δ ppm: 134.50, 121.22, 121.08, 119.68 (q, *J* = 322 Hz), 49.64, 32.02, 19.40, 13.25.

^{19}F NMR (282 MHz, $CDCl_3$) δ ppm: 79.00 (s, 6 F).

ESI-MS (+ve) $[C_7H_{13}N_2]^+$: calcd 125.1073 m/z found 125.1075 m/z.

ESI-MS (-ve) $[C_9H_{17}NO_5S]^-$: calcd 279.9178 m/z found 279.9184 m/z.

Data in agreement with literature.[36]

2.3.19. 1-butylimidazolium (2,2,6,6-tetramethylpiperidin-*N*-oxyl)-4-sulfate, $[C_4HIm][TEMPOOSO_3]$

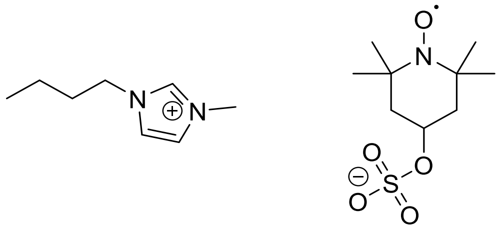

$Na[TEMPOOSO_3]$ (6.5 g, 0.02 mol) was dissolved in ultrapure water (50 cm^3) and stirred. To the stirring solution a solution of $[C_4HIm]Cl$ (3.2 g, 0.02 mol) and ultrapure water (50 cm^3). The solution was stirred overnight at room temperature. 1-butanol was (100 cm^3) was added to the mixture and washed once with ultrapure water (50 cm^3). The organic layer was separated and the solvent was removed under reduced pressure. The crude solid was dried *in vacuo* at 40 °C for 12 hrs to yield an orange waxy like solid (5.0 g, 67%).

ESI-MS (+ve) $[C_7H_{13}N_2]^+$: calcd 125.1073 m/z found 125.1080 m/z.

ESI-MS (-ve) $[C_9H_{17}NO_5S]^-$: 251.0833 m/z found 251.0833 m/z.

CHN Analysis: calcd. for $[C_4HIm][TEMPOOSO_3]$ ($C_{16}H_{30}N_3O_5S$): C 51.00%, H 8.05%, N 11.16% found: C 51.02%, H 8.17%, N 11.09%.

IR ν_{max} cm^{-1}: 2934.27, 1462.39, 1250.80, 1219.04, 1056.63, 964.46, 914.70, 861.42, 791.92, 628.80, 598.36, 561.91.

2.4. References

1. D. Pletcher, *Electrochem. Commun.*, 2018, **88**, 1-4.

2. D. Pletcher, R. A. Green and R. C. D. Brown, *Chem. Rev.*, 2018, **118**, 4573-4591.

3. A. J. Bard and L. R. Faulkner, in *Electrochemical methods : fundamentals and applications*, eds. A. J. Bard and L. R. Faulkner, John Wiley & Sons, New York, 2nd edn., 2001, ch. 1, pp. 1-43.

4. D. Pletcher, R. Greff, R. Peat, L. M. Peter and J. Robinson, in *Instrumental Methods in Electrochemistry*, eds. D. Pletcher, R. Greff, R. Peat, L. M. Peter and J. Robinson, Woodhead Publishing, Cambridge, 1st edn., 2001, ch. 1, pp. 15-41.

5. D. Pletcher, R. Greff, R. Peat, L. M. Peter and J. Robinson, in *Instrumental Methods in Electrochemistry*, eds. D. Pletcher, R. Greff, R. Peat, L. M. Peter and J. Robinson, Woodhead Publishing, Cambridge, 1st edn., 2001, ch. 11, pp. 356-387.

6. K. J. Lee, N. Elgrishi, B. Kandemir and J. L. Dempsey, *Nat. Rev. Chem.*, 2017, **1**, 0039.

7. A. W. Taylor, PhD Thesis, University of Nottingham, 2010.

8. N. Elgrishi, K. J. Rountree, B. D. McCarthy, E. S. Rountree, T. T. Eisenhart and J. L. Dempsey, *J. Chem. Educ.*, 2018, **95**, 197-206.

9. A. J. Bard and L. R. Faulkner, in *Electrochemical methods : fundamentals and applications*, eds. A. J. Bard and L. R. Faulkner, John Wiley & Sons, New York, 2nd edn., 2001, ch. 6, pp. 226-260.

10. J. Keeler and P. Wothers, in *Chemical structure and reactivity: an integrated approach*, eds. J. Keeler and P. Wothers, Oxford University Press, Oxford, 1st edn., 2008, ch. 7, pp. 201-260.

11. A. J. Bard and L. R. Faulkner, in *Electrochemical methods : fundamentals and applications*, eds. A. J. Bard and L. R. Faulkner, John Wiley & Sons, New York, 2nd edn., 2001, ch. 2, pp. 44-86.

12. D. Pletcher, R. Greff, R. Peat, L. M. Peter and J. Robinson, in *Instrumental Methods in Electrochemistry*, eds. D. Pletcher, R. Greff, R. Peat, L. M. Peter and J. Robinson, Woodhead Publishing, Cambridge, 1st edn., 2001, ch. 6, pp. 178-228.

13. N. Perez, in *Electrochemistry and Corrosion Science*, ed. N. Perez, Springer, Cham, 2nd edn., 2016, ch. 6, pp. 151-197.

14. A. J. Bard and L. R. Faulkner, in *Electrochemical methods : fundamentals and applications*, eds. A. J. Bard and L. R. Faulkner, John Wiley & Sons, New York, 2nd edn., 2001, ch. 4, pp. 137-155.

15. P. J. Wright and A. M. English, *J. Am. Chem. Soc.*, 2003, **125**, 8655-8665.

16. J. E. Taylor, M. A. Kulandainathan, C. E. Hotchen and F. Marken, in *Modern electrosynthetic methods in organic chemistry*, eds. F. Marken and M. Atobe, CRC Press Boca Raton, 1st edn., 2018, ch. 1, pp. 1-44.

17. A. J. Bard and L. R. Faulkner, in *Electrochemical methods : fundamentals and applications*, eds. A. J. Bard and L. R. Faulkner, John Wiley & Sons, New York, 2nd edn., 2001, ch. 5, pp. 156-225.

18. R. G. Compton, E. Laborda and K. R. Ward, in *Understanding voltammetry : simulation of electrode processes*, eds. R. G. Compton, E. Laborda and K. R. Ward, Imperial College Press, London, 2nd edn., 2014, ch. 4, pp. 71-97.

19. S. C. Petrovic and R. H. Hammericksen, *Electroanalysis*, 2002, **14**, 599-604.

20. A. A. J. Torriero, in *Electrochemistry in ionic liquids. Volume 1: Fundamentals.*, ed. A. A. J. Torriero, Springer, Cham, 1st edn., 2015, ch. 3, pp. 75-111.

21. G. Gritzner, in *Handbook of reference electrodes*, eds. G. Inzelt, A. Lewenstam and F. Scholz, Springer, Heidelberg, 1st edn., 2013, ch. 2, pp. 25-31.

22. G. Gritzner and J. Kůta, *Electrochim. Acta*, 1984, **29**, 869-873.

23. A. Lewandowski, L. Waligora and M. Galinski, *Electroanalysis*, 2009, **21**, 2221-2227.

24. A. A. J. Torriero, A. I. Siriwardana, A. M. Bond, I. M. Burgar, N. F. Dunlop, G. B. Deacon and D. R. MacFarlane, *J. Phys. Chem. B*, 2009, **113**, 11222-11231.

25. E. I. Rogers, D. S. Silvester, D. L. Poole, L. Aldous, C. Hardacre and R. G. Compton, *J. Phys. Chem. C*, 2008, **112**, 2729-2735.

26. M. J. A. Shiddiky, A. A. J. Torriero, C. Zhao, I. Burgar, G. Kennedy and A. M. Bond, *J. Am. Chem. Soc.*, 2009, **131**, 7976-7989.

27. A. A. J. Torriero, *Electrochim. Acta*, 2014, **137**, 235-244.

28. A. A. J. Torriero and P. C. Howlett, *Electrochem. Commun.*, 2012, **16**, 84-87.

29. L. Xiong, A. M. Fletcher, S. G. Davies, S. E. Norman, C. Hardacre and R. G. Compton, *Chem. Commun.*, 2012, **48**, 5784-5786.

30. N. Frenzel, J. Hartley and G. Frisch, *Phys. Chem. Chem. Phys.*, 2017, **19**, 28841-28852.

31. D. Pletcher, R. Greff, R. Peat, L. M. Peter and J. Robinson, in *Instrumental Methods in Electrochemistry*, eds. D. Pletcher, R. Greff, R. Peat, L. M. Peter and J. Robinson, Woodhead Publishing, Cambridge, 1st edn., 2001, ch. 7, pp. 229-250.

32. A. J. Bard and L. R. Faulkner, in *Electrochemical methods : fundamentals and applications*, eds. A. J. Bard and L. R. Faulkner, John Wiley & Sons, New York, 2nd edn., 2001, ch. 11, pp. 416-470.

33. R. A. Green, R. C. D. Brown, D. Pletcher and B. Harji, *Electrochem. Commun.*, 2016, **73**, 63-66.

34. R. A. Green, R. C. D. Brown and D. Pletcher, *J. Flow Chem.*, 2015, **5**, 31-36.

35. C. A. Velázquez, G. M. Lynn, V. Kumar, L. K. Keefer and S. V. Malhotra, *Synth. Commun.*, 2010, **40**, 1322-1332.

36. R. Bini, C. Chiappe, V. L. Mestre, C. S. Pomelli and T. Welton, *Org. Biomol. Chem.*, 2008, **6**, 2522-2529.

37. S. J. L. P. Perez and S. D. Arco, *J. Chin. Chem. Soc.*, 2014, **61**, 935-939.

38. S. V. Dzyuba and R. A. Bartsch, *ChemPhysChem*, 2002, **3**, 161-166.

39. G. Cravotto, L. Boffa, J.-M. Lévêque, J. Estager, M. Draye and W. Bonrath, *Aust. J. Chem.*, 2007, **60**, 946-950.

40. N. Papaiconomou, N. Yakelis, J. Salminen, R. Bergman and J. M. Prausnitz, *J. Chem. Eng. Data*, 2006, **51**, 1389-1393.

41. J. A. Willemse, B. C. B. Bezuidenhoudt and C. W. Holzapfel, *Synthesis*, 2006, **2006**, 2543-2550.

42. J. G. Huddleston, A. E. Visser, W. M. Reichert, H. D. Willauer, G. A. Broker and R. D. Rogers, *Green Chem.*, 2001, **3**, 156-164.

43. A. Deyko, K. R. J. Lovelock, J.-A. Corfield, A. W. Taylor, P. N. Gooden, I. J. Villar-Garcia, P. Licence, R. G. Jones, V. G. Krasovskiy, E. A. Chernikova and L. M. Kustov, *Phys. Chem. Chem. Phys.*, 2009, **11**, 8544-8555.

44. H. Srour, H. Rouault, C. C. Santini and Y. Chauvin, *Green Chem.*, 2013, **15**, 1341-1347.

45. X. Liu, X. Huang, Y. Wang, S. Huang and X. Lin, *Anal. Methods*, 2013, **5**, 2591-2601.

46. R. K. Blundell and P. Licence, *Chem. Commun.*, 2014, **50**, 12080-12083.

47. G. Chatel, C. Goux-Henry, N. Kardos, J. Suptil, B. Andrioletti and M. Draye, *Ultrason. Sonochem.*, 2012, **19**, 390-394.

48. M. Guncheva, M. Dimitrov, F. Napoly, M. Draye and B. Andrioletti, *J. Mol. Catal. B: Enzym.*, 2014, **102**, 72-80.

49. E. Rodil, A. Arce and A. Soto, *Thermochim. Acta*, 2018, **664**, 81-90.

50. É. Bossé, L. Berthon, N. Zorz, J. Monget, C. Berthon, I. Bisel, S. Legand and P. Moisy, *Dalton Trans.*, 2008, **7**, 924-931.

51. A. D. Ballantyne, A. K. Brisdon and R. A. W. Dryfe, *Chem. Commun.*, 2008, **40**, 4980-4982.

52. A. Cieniecka-Rosłonkiewicz, J. Pernak, J. Kubis-Feder, A. Ramani, A. J. Robertson and K. R. Seddon, *Green Chem.*, 2005, **7**, 855-862.

53. K. Tsunashima, S. Kodama, M. Sugiya and Y. Kunugi, *Electrochim. Acta*, 2010, **56**, 762-766.

54. P. S. Kulkarni, L. C. Branco, J. G. Crespo, M. C. Nunes, A. Raymundo and C. A. M. Afonso, *Chem. Eur. J.*, 2007, **13**, 8478-8488.

55. G. Thielemann and S. Spange, *New J. Chem.*, 2017, **41**, 8561-8567.

56. J. Winsberg, C. Stolze, A. Schwenke, S. Muench, M. D. Hager and U. S. Schubert, *ACS Energy Lett.*, 2017, **2**, 411-416.

3. Probing RTIL-TEMPO Interactions for Tuning the Reactivity and Selectivity of TEMPO-mediated Alcohol Oxidations

3.1. Introduction

The unique properties of RTILs offer clear advantages during the development of electrosynthetic processes, due to their stability and the fact that they can be used as both the solvent and electrolyte.[1, 2] A handful of studies on the electrochemical behaviour of TEMPO in RTILs have been conducted and demonstrate that the behaviour of TEMPO in RTILs is similar to its behaviour in acetonitrile and water, but some interesting differences are also observed.[3-7] For example, Doherty and co-workers observed that the global rate constant of TEMPO-mediated alcohol oxidation was larger by a factor of 6 in *N*-butyl-*N*-methyl pyrrolidinium than in acetonitrile.[3] These experiments demonstrate that not only is the use of RTILs advantageous in terms of eliminating the need for volatile molecular solvents and extraneous electrolytes, but also for improving the efficiency of the alcohol oxidations.

In recent years, RTILs have received increased attention due to their structural diversity.[8] By simply varying the structures of the ions or changing the combinations of anions and cations, the physicochemical properties such as density, viscosity, melting point and polarity can be tuned for specific functions.[9] For example, the rates of mass transfer of redox species to electrodes in RTILs can be changed significantly by altering the ionic composition of RTILs.[10]

The design of the RTILs can also have a marked effect on the physicochemical properties of solutes dissolved in RTILs. For example the redox reactions of 2,2-diphenyl-1-picylhydrazyl (DPPH)[11] and 1,2-diferrocenylethylene[12] in RTILs have been tailored by varying the RTIL anions. Furthermore, Men and co-workers were able to modify the catalytic activity of a palladium catalyst in a Suzuki cross-coupling reaction *via* the anionic tuning of cation-anion interactions within the RTIL.[13] In this context, the possibility of predicting and fine-tuning the reactivity and selectivity of TEMPO could potentially provide a mean to enhance the performance of TEMPO-mediated alcohol oxidations.

The work described in this chapter involves the use of cyclic voltammetry to probe TEMPO-RTIL interactions as the cations and anions of RTILs are varied. This work probes the affect of different RTIL anion-cation combinations on the redox properties of TEMPO, with an aim to determine if a degree of tunability of the reactivity and selectivity of TEMPO can be achieved *via* the design of the RTIL media.

3.2. Results and Discussion

TEMPO dissolved in RTILs may experience a range of intermolecular interactions, including van der Waals forces, hydrogen bonding, coulombic and dipole interactions.[14, 15] In order to investigate the impact of the solvation environment on the redox properties of the TEMPO/TEMPO$^+$ couple, TEMPO was dissolved in in a series of RTILs. The cations and anions used in this study are listed in Table 3.1.

Table 3.1: RTIL cations and anions used in this study

Abbreviation	**Structure**	**Name**
$[\mathrm{C}_n\mathrm{C}_1\mathrm{Pyrr}]^+$	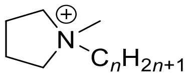	1-alkyl-1-methylpyrrolidinium
$[\mathrm{C}_n\mathrm{C}_1\mathrm{Im}]^+$	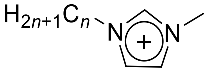	1-alkyl-3-methylimidazolium
$[\mathrm{NR}_1\mathrm{R}_2\mathrm{R}_3\mathrm{R}_4]^+$	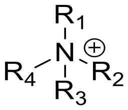	*N, N, N, N* – tetraalkylammonium
$[\mathrm{PR}_1\mathrm{R}_2\mathrm{R}_3\mathrm{R}_4]^+$	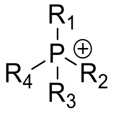	*N, N, N, N* – tetraalkylphosphonium
$[\mathrm{NTf}_2]^-$	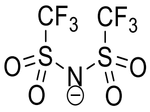	bis(trifluoromethanesulfonyl)imide
$[\mathrm{PF}_6]^-$	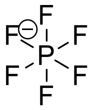	hexafluorophosphate
$[\mathrm{OTf}]^-$	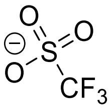	trifluoromethanesulfonate
$[\mathrm{DCA}]^-$	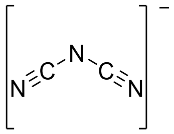	dicyanamide
$[\mathrm{MeOSO}_3]^-$	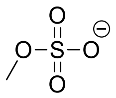	methylsulfate

A series of imidazolium-, pyrrolidinium-, phosphonium- and ammonium-based cations were selected. The positive charge is delocalized within the imidazolium ring, whereas for the pyrrolidinium and quaternary based cations the positive charge is more localised on the cationic centre,[16-18] which could influence the redox properties of the TEMPO/TEMPO$^+$ redox couple, *via* for example repulsive interactions between TEMPO$^+$ and the cation. Longer chain lengths of the imidazolium, quaternary phosphonium and quaternary ammonium based RTILs could offer additional shielding of the positive charge, but this will be dependent upon the degree of conformational flexibility.[17, 18] X-ray photoelectron spectroscopy, XPS, analysis conducted in the Licence group has shown that a large proportion of the alkyl chain of $[C_8C_1Pyrr]^+$ is 'pinned back' by the 5-membered heterocyclic ring. Consequently, the nitrogen core is much more exposed than in the case of $[N_{6,6,6,14}]^+$, where the central nitrogen is shielded by a layer of conformationally flexible long-chain hydrocarbons.[18]

The selected anions vary from small inorganic anions such as $[BF_4]^-$ and $[PF_6]^-$ to larger, mixed inorganic-organic anions, such as $[NTf_2]^-$. It has previously been shown that there is a strong correlation between the degree of cation-anion charge-transfer and the solvatochromically-determined hydrogen-bond basicity, β, of the anion. High β anions, such as halides, transfer a significant amount of charge to the cation, whilst the opposite is true for low β such as $[NTf_2]^-$.[19, 20] The strength of the anion-cation interactions may affect the possible interactions between the RTIL components and the TEMPO/TEMPO$^+$ redox species. Therefore, anions with a range of varying β were chosen to investigate whether the strength of the cation-anion interaction has an impact on the TEMPO/TEMPO$^+$ redox couple.

3.2.1. Redox Properties of TEMPO in RTILs

For all the RTILs, 10 mmol dm^{-3} of TEMPO dissolved almost instantly and for most RTILs the redox peaks of TEMPO/TEMPO$^+$ appeared within the electrochemical windows of the ILs. The exceptions to this were [C_8C_1Im]Cl, [C_8C_1Im]Br and [C_8C_1Im][OAc], in which their anodic limit was too short. The short electrochemical windows of halide and acetate based RTILs have previously been reported and is a result of the anions being more susceptible towards oxidation at the electrode.[8, 12] Figure 3.1 shows a CV of TEMPO dissolved in the RTIL [C_8C_1Pyrr][NTf_2].

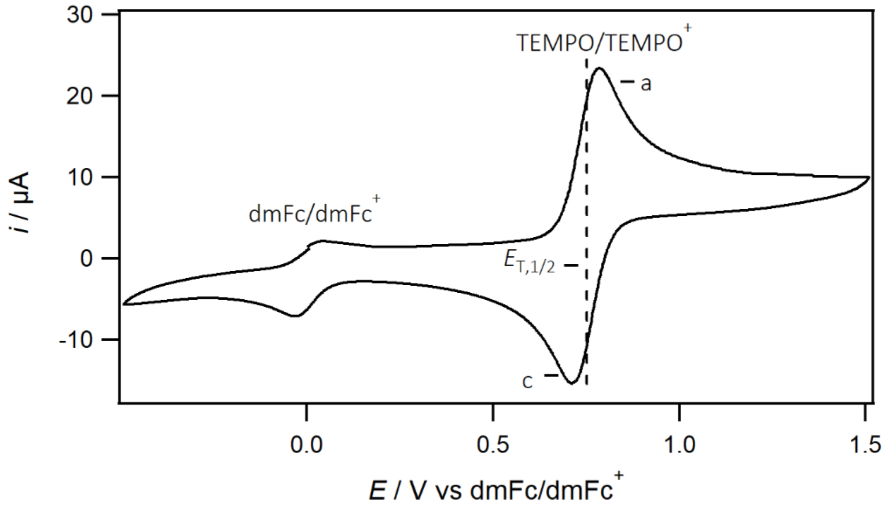

Figure 3.1: CV of 5 mmol dm^{-3} dmFc and 10 mmol dm^{-3} TEMPO in [C_8C_1Pyrr][NTf_2], recorded using a 3 mm diameter glassy-carbon electrode with scan rate of 50 mV s^{-1}. Dynamic iR drop compensation was used. Recorded at ambient temperature and pressure.

In Figure 3.1 an anodic peak, $i_{p,a}$, due to oxidation of TEMPO to TEMPO$^+$ can be seen at the anodic peak potential, $E_{p,a}$, = 0.79 V and a reduction peak, $i_{p,c}$, due to the reduction of TEMPO$^+$ to TEMPO can be seen at the cathodic peak potential, $E_{p,c}$ = 0.71 V. These peaks are labelled a and c, respectively. The half-wave potential of the TEMPO/TEMPO$^+$ redox couple, $E_{T,½}$ is shown as the dashed line in Figure 3.1 and is 0.75 V. The shape of the CV agrees with that reported previously in conventional solvents and in RTILs.[3-6] The CVs of TEMPO in each RTIL are shown in Figures A1-A15 in the Appendix. Table 3.2 summarises $E_{p,a}$, $E_{p,c}$, $E_{T,½,}$ ΔE_p, $i_{p,a,}$ $i_{p,c}$ and $i_{p,a}/i_{p,c}$ ratio obtained from cyclic voltammetry measurements of 10 mmol dm^{-3} TEMPO dissolved in different RTILs.

Table 3.2: Average $E_{p,a}$, $E_{p,c}$, $E_{T,½}$, ΔE_p, $i_{p,a}$, $i_{p,c}$ and $i_{p,a}/i_{p,c}$ ratio of the TEMPO/TEMPO$^+$ redox couple obtained from CVs measured at 5 mV s^{-1} of 10 mmol dm^{-3} TEMPO dissolved in different RTILs (measurments were repeated in triplicates). All potentials are relative to that of dmFc/dmFc$^+$. CVs recorded using a 3 mm diameter glassy-carbon electrode and at ambient temperature and pressure. Dynamic iR drop compensation was used.

Ionic Liquid	$E_{p, a}$, mV	$E_{p, c}$, mV	$E_{T,½}$, mV	ΔE_p, mV	$i_{p, a}$, µA	$i_{p, c}$ µA	$i_{p, a}/i_{p, c}$
[$N_{6,6,6,14}$][NTf_2]	853	681	767	172	+0.62	-0.59	1.05
[$N_{4,4,4,1}$][NTf_2]	852	684	768	168	+2.74	-2.75	1.00
[$N_{6,6,6,14}$][DCA]*	-	-	-	-	+1.95	-1.96	0.99
[$N_{4,4,4,1}$][DCA]	775	552	672	223	+3.24	-3.29	0.98
[$P_{4,4,4,1}$][NTf_2]	823	736	770	87	+1.22	-1.22	1.00
[$P_{6,6,6,14}$][NTf_2]	802	690	746	112	+3.65	-3.50	1.04
[$P_{6,6,6,14}$][DCA]	1018	851	670	167	+3.17	-2.77	1.14
[C_8C_1Pyrr][NTf_2]	786	711	749	75	+1.94	-1.80	1.08
[C_2C_1Im][NTf_2]	810	702	756	108	+14.4	-14.1	1.02
[C_2C_1Im][DCA]	764	653	709	111	+12.0	-12.0	1.00
[C_8C_1Im][NTf_2]	830	708	769	122	+5.55	-5.70	0.97
[C_8C_1Im][DCA]	722	631	677	91	+5.78	-5.27	1.10
[C_8C_1Im][BF_4]	731	634	683	97	+7.99	-8.18	0.98
[C_8C_1Im][OTf]	786	614	700	172	+5.19	-4.99	1.04
[C_8C_1Im][PF_6]	670	905	788	235	+2.43	-2.50	1.01

*dmFc did not dissolve in [$N_{6,6,6,14}$][DCA]

3.2.1.1. Reversibility of TEMPO in different RTILs

The most common way of characterising features of a redox species is in terms of its electrochemical reversibility, which essentially describes the rate of electron transfer between the electrode and the substrate. The electron transfer must be significantly greater than the rate of mass transport in order to maintain a Nernstian equilibrium at the electrode surface. A typical CV observed for a TEMPO/TEMPO$^+$ couple undergoing reversible electron transfer in the RTIL [C_2C_1Im][NTf_2] is shown in Figure 3.2 frame a. If, on the other hand, electron transfer is slow and consequently unable to maintain a Nernstian equilibrium at the electrode surface, it is electrochemically irreversible. The electron transfer is more difficult and therefore more 'extreme' potentials are required to drive the electron transfer.[21] An example of a CV recorded of an electrochemical irreversible TEMPO/TEMPO$^+$ redox reaction in the RTIL [$N_{6,6,6,14}$][NTf_2] is shown in Figure 3.2 frame b.

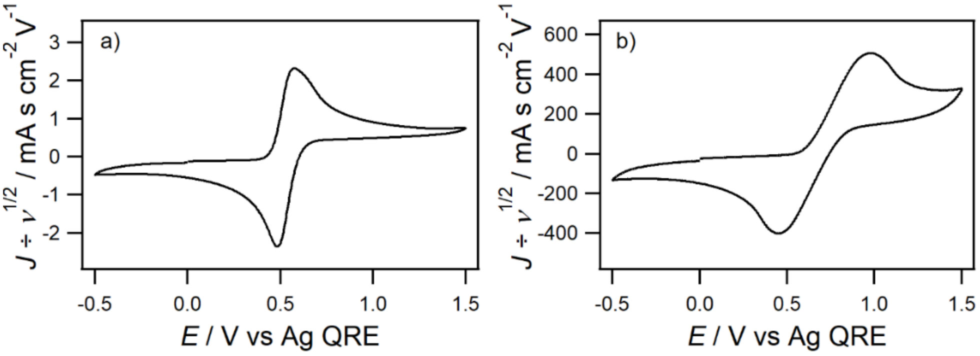

Figure 3.2: CV of 10 mmol dm^{-3} TEMPO undergoing a) reversible electron transfer in [C_2C_1Im][NTf_2] and b) irreversible electron transfer in [$N_{6,6,6,14}$][NTf_2]. CVs recorded using a 3 mm diameter glassy-carbon electrode with scan rate 50 mV s^{-1} at ambient temperature and pressure. Dynamic iR drop compensation was used.

In all TEMPO-RTILs solutions the anodic and cathodic peak ratios are all close to 1. However, the peak-to-peak separation, ΔE_p, was greater than the value expected for electrochemically-reversible systems involving the transfer of a single electron (59 mV), see Table 3.2. All the CVs were recorded using ohmic-drop compensation, this ensures that measured potential measured as a result of solution resistance is corrected. Consequently the high ΔE_p is attributed to sluggish electron-transfer kinetics across the electrode/RTIL interface.[22-24]

In the case of $[N_{6,6,6,14}][NTf_2]$, $[P_{6,6,6,14}][DCA]$, $[N_{4,4,4,1}][NTf_2]$, $[C_8C_1Im][PF_6]$ and $[C_8C_1Im][BF_4]$ an increase in peak separation is also noted as a function of scan rate. For example,**Figure 3.** Figure 3.3 frame a) and frame b) show normalised CVs of TEMPO in $[C_2C_1Im][NTf_2]$ and $[N_{6,6,6,14}][NTf_2]$ respectively. The CVs are normalised by converting *i* to $J/v^{1/2}$ in each *i*-*E* plots that were recorded with different scan rates.

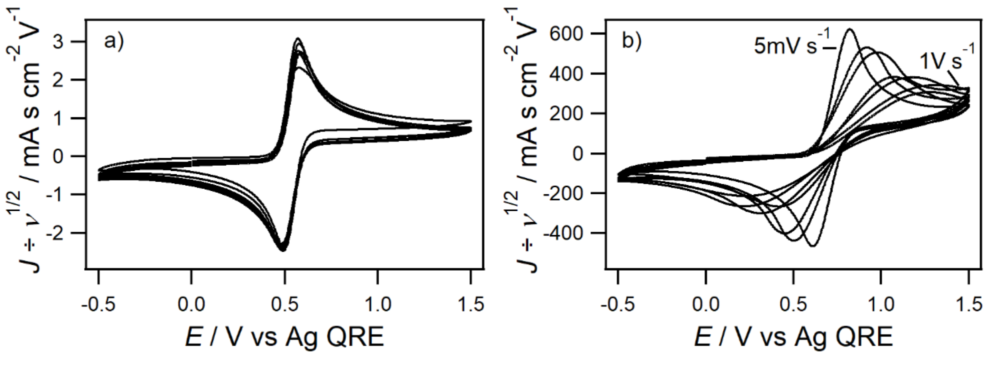

Figure 3.3: Normalised CVs of 10 mmol dm^{-3} of TEMPO dissolved in a) $[C_2C_1Im][NTf_2]$ and in b) $[N_{6,6,6,14}][NTf_2]$ recorded with scan rates 5, 25, 50, 100, 200, 500, 800 1000 mV s^{-1}. CVs recorded using a 3 mm diameter glassy-carbon electrode at ambient temperature and pressure. Dynamic iR drop compensation was used.

For reversible systems these normalised CVs should superimpose at all scan rates, as demonstrated in the CV of TEMPO in [C_2C_1Im][NTf_2] in **Figure 3.**Figure 3.3 frame a). The CV of TEMPO in [$N_{6,6,6,14}$][NTf_2] in Figure 3.3 frame b) clearly exhibits an irreversible system, the anodic peak potential is progressively shifted towards a more positive potential and *vice versa* for the anodic peak. Furthermore, the peak heights are lower at higher scan rate, when compared to those recorded at lower scan rates.[21] These differences in the electrochemical reversibility of TEMPO, suggests that the electron transfer rate is higher in [C_2C_1Im][NTf_2] than in [$N_{6,6,6,14}$][NTf_2].[25] In [$N_{6,6,6,14}$][NTf_2] the peaks of TEMPO/TEMPO$^+$ become more drawn out, resulting in larger ΔE_p and the peak currents are smaller at faster scan rates (50 mV s^{-1} to 1 V s^{-1}) than at slower scan rates (5 mV s^{-1}).

The peak currents in CVs of irreversible systems are also linearly dependent on the $v^{1/2}$. However, the peak currents of irreversible systems are also dependent on the transfer coefficient.[25] Figure 3.4 shows a plot of $i_{p,a}$ of TEMPO when dissolved in [C_2C_1Im][NTf_2] (frame a) and [$N_{6,6,6,14}$][NTf_2] (frame b) *vs* $v^{1/2}$.

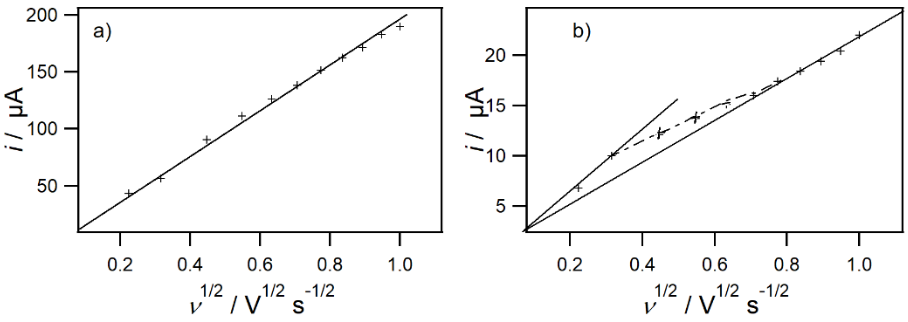

Figure 3.4: Plot of measured $i_{p,a}$ of 10 mmol dm^{-3} TEMPO at different scan rates *vs* $v^{1/2}$ dissolved in a) [C$_2$C$_1$Im][NTf$_2$] and in b) [N$_{6,6,6,14}$][NTf$_2$]. The measurements were done in triplicates and the graph represent the mean values of $i_{p,a}$ measured. CVs recorded using a 3 mm diameter glassy-carbon electrode at ambient temperature and pressure. Dynamic iR drop compensation was used.

Figure 3.4 frame a) shows that there is a good linear relationship of peak current and $v^{1/2}$ when TEMPO is dissolved in [C$_2$C$_1$Im][NTf$_2$], however when TEMPO is dissolved in [N$_{6,6,6,14}$][NTf$_2$] (frame b) there are two linear dependencies of $i_{p,a}$ with the $v^{1/2}$ - the first two data points corresponds to the $i_{p,a}$ measured at low scan rates (50 mV s^{-1} and 5 mV s^{-1}), and the last four data points are measured at high scan rates (700 mV s^{-1}, 800 mV s^{-1} ,900 mV s^{-1} and 1 V s^{-1}). The region where the electron transfer goes from reversible (at slow scan rates) to irreversible (fast scan rates) is known as quasi-reversible. This transition occurs when the relative rate of electron transfer with respect to mass transfer are comparable, and the Nernstian equilibrium is no longer maintained.[25] Most of the higher viscosity TEMPO-RTILs solutions demonstrated quasi-reversible behaviour. Since most of the RTIL-TEMPO solutions showed more reversible CVs at lower scan rates, a scan rate of 5 mV s^{-1} was used to conduct voltammetry analysis in this study. It has previously been shown that the electron transfer rates decrease with increasing viscosity in both conventional solvents and RTILs.[26-28] For example one study demonstrated slower electron transfer for the ferrocene/ferrocenium redox couple in viscous imidazolium-based RTILs.[29] This agrees well with this study where TEMPO/TEMPO$^+$ is clearly more reversible in the less viscous RTILs [C_2C_1Im][NTf_2] (31 mPa·s) than in the highly viscous [$N_{6,6,6,14}$][NTf_2] (585 mPa·s). The differences in reversibility is important to consider as faster electron transfer with electrodes is more advantageous for use as redox catalysts and electroactive materials as it leads to faster reactions and better faradaic selectivities.[30] Furthermore, higher viscosity of the RTIL will also slow down the mass transport of TEMPO/TEMPO$^+$ to the electrode, as well as the mixing and transfer of other reagents in the RTILs. Consequently, slower mass transport could slow down the overall TEMPO-mediated alcohol oxidations.[3, 4, 6]

3.2.1.2. Half-wave potential shifts of TEMPO/TEMPO$^+$ in RTILs

The most notable observation from the voltammetric studies of the TEMPO-RTIL solutions is the significant shift of $E_{T,½}$. ranging from 670 mV ([$P_{6,6,6,14}$][DCA]) to 788 mV ([C_8C_1Im][PF_6]). Figure 3.5 shows the shifts in $E_{T,½}$ as the anion of the RTIL media is varied and the cationic component is fixed as [C_8C_1Im]$^+$.

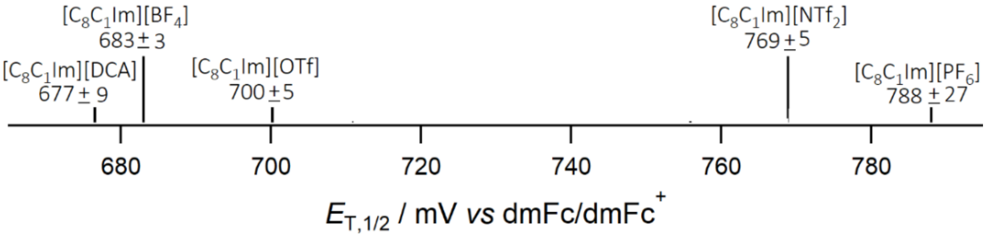

Figure 3.5: Measured $E_{T,½}$ of 10 mmol dm^{-3} TEMPO dissolved in $[C_8C_1Im]^+$ based RTILs with varying anions. The potentials are referenced to that of the dmFc/dmFc$^+$ redox couple. CVs recorded using a 3 mm diameter glassy-carbon electrode at 5 mV s^{-1} at ambient temperature and pressure. Dynamic iR drop compensation was used.

When TEMPO is dissolved in RTILs with high β anions, such as [DCA]$^-$, $E_{T,½}$ is lower compared to when TEMPO is dissolved in RTILs with low β anions, such as [NTf$_2$]$^-$. This may be rationalised as a result of the RTIL-anions with a higher β stabilise the electron-deficient TEMPO$^+$ more effectively than the RTIL-anions with low β. Thus, the potential required to oxidise TEMPO is lowered in RTILs with high β. A schematic of the cation-anion interactions and the competing anion-TEMPO$^+$ interactions is illustrated in Figure 3.6.

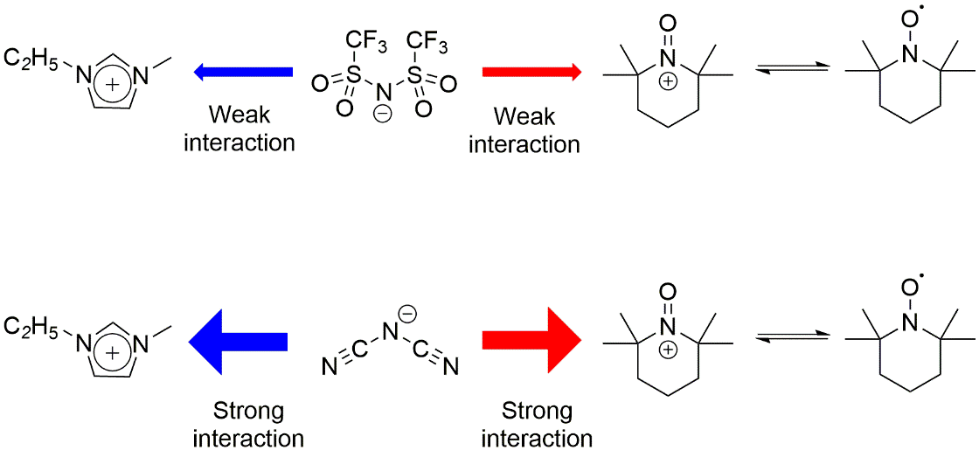

Figure 3.6: Schematic illustrating the influence of the anion on the magnitude of favourable interaction from anion to cation (blue arrow) and from anion to TEMPO$^+$ (red arrow) for a RTIL with low β (top structure) and a RTIL with high β (bottom structure).

The influence of the cation was also investigated and Figure 3.7 shows the influence of varying the cation on $E_{T,½}$ in RTILs containing [DCA]$^-$ and [NTf$_2$]$^-$ anions.

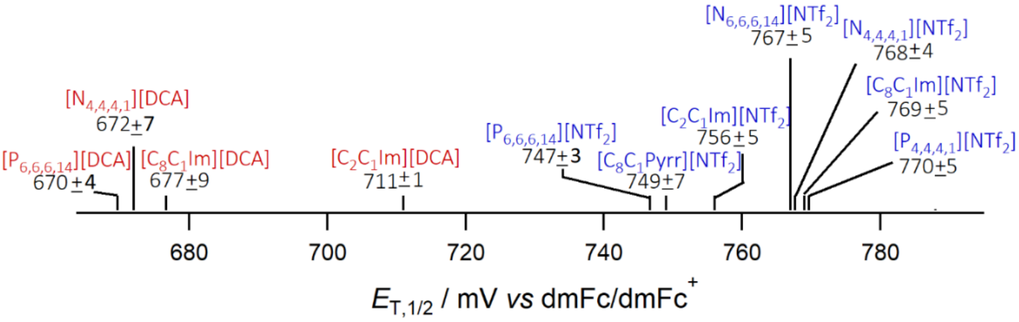

Figure 3.7: Measured $E_{T,½}$ of 10 mmol dm^{-3} TEMPO as the cation of the RTIL is varied in [NTf$_2$]$^-$ and [DCA]$^-$ based RTILs, highlighted in blue and red, respectively. The potentials are referenced to that of the dmFc/dmFc$^+$ redox couple. CVs recorded using a 3 mm diameter glassy-carbon electrode at 5 mV s^{-1} at ambient temperature and pressure. Dynamic iR drop compensation was used.

Again it is clear that the values for $E_{T,½}$ are lower when TEMPO is dissolved in [DCA]$^-$ based RTILs than when dissolved in [NTf$_2$]$^-$-based RTILs. Notably there are also some shifts of $E_{T,½}$ within each anion family. For the [DCA]$^-$ based RTILs, $E_{T,½}$ is lower in [P$_{6,6,6,14}$]$^+$, [N$_{4,4,4,1}$]$^+$ and [C$_8$C$_1$Im]$^+$ than in the presence of the imidazolium cation with short alkyl chains, [C$_2$C$_1$Im]$^+$.

In previously conducted XPS studies, it was observed that the small [C$_2$C$_1$Im]$^+$ structure with an 'exposed' delocalized charge enables more efficient cation-anion charge-transfer in the RTIL resulting in strong cation-anion interactions. By increasing the alkyl chain length as in [C$_8$C$_1$Im]$^+$ the cation-anion charge transfer significantly decreases and so the interaction is made weaker.[31] It has also been observed that the longer alkyl chains in [N$_{4,4,4,1}$]$^+$ and [P$_{6,6,6,14}$]$^+$ somewhat 'shield' the cationic core from the anionic charge-transfer, resulting in weaker cation-anion interactions within the RTIL.[31-33] Thus, it seems that weaker cation-anion interactions within a RTIL with high β increases the stabilisation of TEMPO$^+$ and therefore lower $E_{T,½}$ are observed in these RTILs, see the schematic in Figure 3.8.

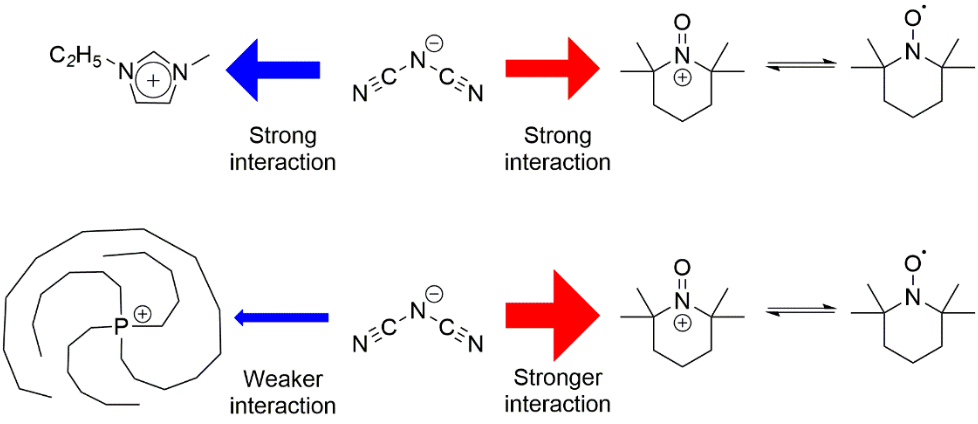

Figure 3.8: Schematic illustrating the influence of the anion on the magnitude of favourable interaction from anion to cation (blue arrow) and from anion to TEMPO$^+$ (red arrow) for a RTIL a small cation (top structure) and a RTIL with a bulky cation (bottom structure).

$[NTf_2]^-$ based RTILs were chosen as a RTIL family for analysis of cationic effect on TEMPO/TEMPO$^+$ redox properties, since they do not participate in significant charge-transfer from anion to cation.[17-19] Consequently it is expected that the cation would be more ‘available’ to interact with the TEMPO/TEMPO$^+$ redox species. For example, a repulsive interaction between TEMPO$^+$ and the cation could be expected. However no clear trend is observed in the $[NTf_2]^-$ family, which could suggest that cation-TEMPO or cation-TEMPO$^+$ is not a dominant interaction which affects $E_{T,½}$.

To investigate if the observed $E_{T,½}$ shifts correlate to the β and α Kamlet-Taft parameters, $E_{T,½}$ in all of the TEMPO-RTIL solutions are plotted against their corresponding β (values are taken from references 32 and 33), see Figure 3.9.

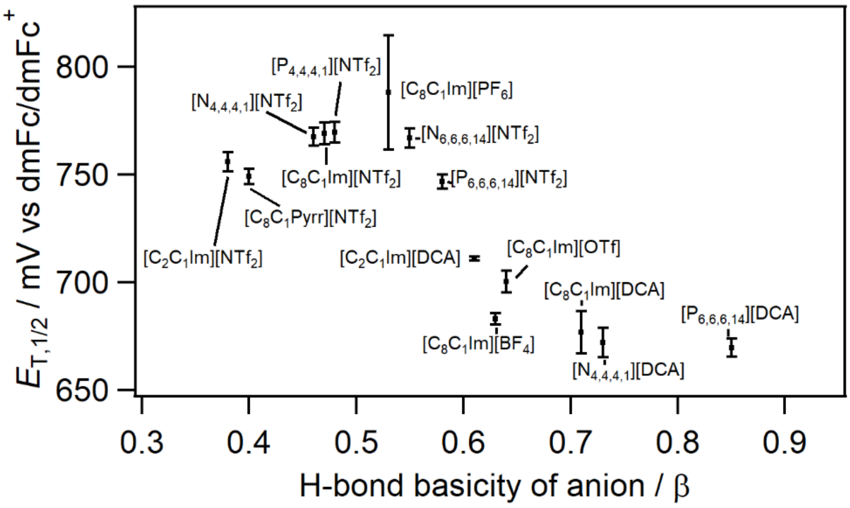

Figure 3.9: Measured $E_{T,½}$ of 10 mmol dm^{-3} TEMPO *vs.* β of the RTILs in which TEMPO is dissolved in.[32, 33] CVs recorded using a 3 mm diameter glassy-carbon electrode at 5 mV s^{-1} at ambient temperature and pressure. Dynamic iR drop compensation was used.

For RTILs with $\beta > 0.5$, the TEMPO/TEMPO$^+$ half-wave potential decreases linearly as β increases, indicating that the interaction between TEMPO$^+$ and RTIL-anions becomes stronger as β of the RTILs increases. In general, strongly interacting anions with high β stabilise TEMPO$^+$ and poorly coordinating anions with low β do not stabilise TEMPO$^+$ as efficiently.

To investigate the influence of α, $E_{T,½}$ is plotted against α of the RTILs in Figure 3.10.

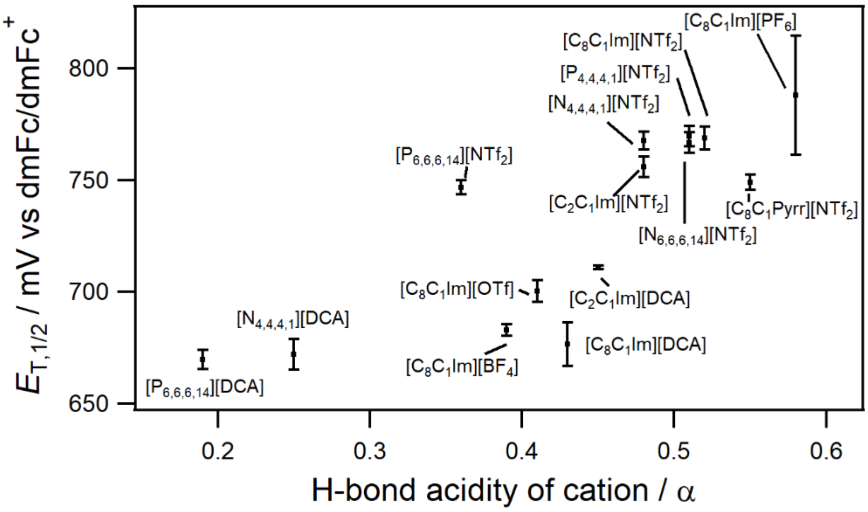

Figure 3.10: Measured $E_{T,½}$ of 10 mmol dm^{-3} TEMPO *vs.* α of the RTILs in which TEMPO is dissolved in.[32, 33] CVs recorded using a 3 mm diameter glassy-carbon electrode at 5 mV s^{-1} at ambient temperature and pressure. Dynamic iR drop compensation was used.

$E_{T,½}$ increases as α of the RTILs increases. However, as TEMPO is dissolved in [NTf$_2$]$^-$ based RTILs, it appears that the modification of the cationic structure has a minimal impact on $E_{T,½}$. Most of the variation of $E_{T,½}$ are observed in the RTILs with higher β, such as [DCA]$^-$ and [OTf]$^-$, which participate in greater charge-transfer between anion to cation.[17-19] Thus it appears to be that the cation and α of the RTIL does not influence the TEMPO/TEMPO$^+$ redox couple directly, but indirectly through the interaction with its paired anion. A small, exposed cation with a high α can attenuate the interaction of the anion-TEMPO$^+$, through a stronger interaction with the anion. If the anion-cation interaction is made weaker by e.g. increasing the size of the cation or decreasing α, the perturbation of the anion-TEMPO$^+$ interaction is less, so a lower $E_{T,½}$ is observed.

The shifts in $E_{T,½}$ could influence the overall TEMPO-mediated alcohol oxidation in RTIL media and thus the choice of RTIL media could provide a mean of controlling the reactivity of TEMPO in alcohol oxidations. However it is also important to consider the mass transport in the RTIL media and the heterogenous electron transfer kinetics as these factors are likely to influence the overall reaction rate.[5, 22]

3.2.1.3. Diffusion of TEMPO in RTILs

Fast diffusion of TEMPO to the electrode is important for efficient and selective TEMPO-mediated electrooxidations. Chronoamperometric experiments were carried out to investigate the diffusion of TEMPO in RTILs. The diffusion coefficients of quasi- or irreversible systems derived from the Cottrell equation is more accurate than those derived from the Randles-Sevçik equation, as the Cottrell equation does not require the system to be fully reversible, which is a requirement for the Randles-Sevçik equation.[34] Figure 3.11 frame a) shows the chronoamperometric response of TEMPO in $[C_2C_1Im][NTf_2]$ and frame b) the plot of i *vs* $t^{1/2}$.

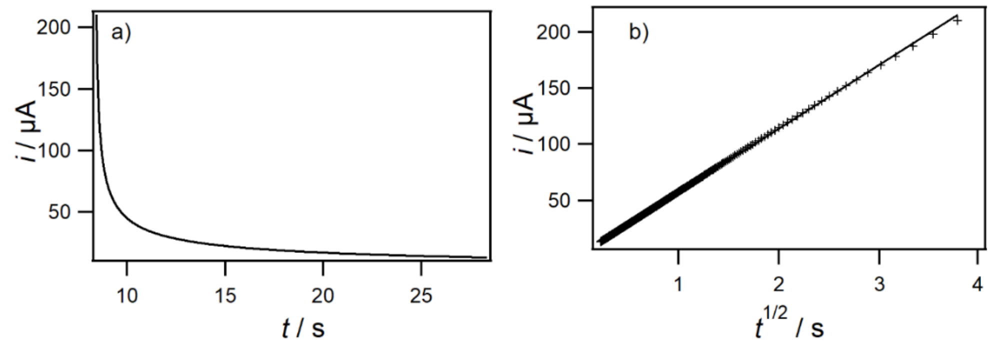

Figure 3.11: a) Chronoamperometric response of 10 mmol dm^{-3} TEMPO at a constant potential of 0.2 V *vs.* $E_{T,1/2}$ for the oxidation of TEMPO to $TEMPO^+$ in $[C_2C_1Im][NTf_2]$, and b) *i* plotted *vs*. $t^{1/2}$. The current was measured for 20 seconds. The measurements were done in ambient temperature and pressure.

The linear Cottrell plot indicates that the redox reaction is diffusion limited and the diffusion coefficient of TEMPO, D_T, in RTILs can be calculated from the gradient, see Equation 2.3. D_T for TEMPO in each RTIL is shown in Table 3.3.

Table 3.3: D_T determined using Cottrell relationship with the measured current of a single step chronoamperometric measurement at an applied potential of 0.2 V *vs.* $E_{T,1/2}$ for the oxidation of 10 mmol dm^{-3} TEMPO to TEMPO$^+$ and the current was measured for 20 seconds. The measurements were done in triplicates at ambient temperature and pressure.

Ionic Liquid	**D_T / 10^{-7} cm^2 s^{-1}**
[C_8C_1Im][DCA]	2.35 ± 1.21
[C_8C_1Im][OTf]	1.77 ± 0.25
[C_8C_1Im][PF_6]	1.07 ± 0.25
[C_8C_1Im][NTf_2]	2.37 ± 0.16
[C_8C_1Im][BF4]	1.82 ± 0.83
[C_2C_1Im][NTf_2]	4.49 ± 3.36
[C_2C_1Im][DCA]	12.09 ± 0.74
[$N_{6,6,6,14}$][NTf_2]	0.28 ± 0.17
[$N_{4,4,4,1}$][NTf_2]	0.44 ± 0.22
[$P_{6,6,6,14}$][NTf_2]	1.80 ± 0.22
[$P_{4,4,4,1}$][NTf_2]	0.96 ± 0.21
[$N_{4,4,4,1}$][DCA]	0.38 ± 0.14
[$N_{6,6,6,14}$][DCA]	0.28 ± 0.04
[$P_{6,6,6,14}$][DCA]	0.21± 0.03
[C_8C_1Pyrr][NTf_2]	2.08 ± 0.30

D_T is lower in the more viscous RTILs such as [$N_{6,6,6,14}$][NTf_2] (585.08 mPa·s) than in RTILs with low viscosity such as [C_8C_1Im][NTf_2] (90 mPa·s). Figure 3.12 shows that D_T is proportional to $1/\eta$, with a relatively linear relationship. This indicates that the hydrodynamic radius of TEMPO did not change significantly with changes in the RTIL viscosity.[35] Since catalytic currents are dependent on mediator mass transport, these differences in D_T are informative in order to understand the differences in catalytic performance of TEMPO-mediated alcohol oxidations in electrolysis, which will be discussed in more detail in chapter 4.

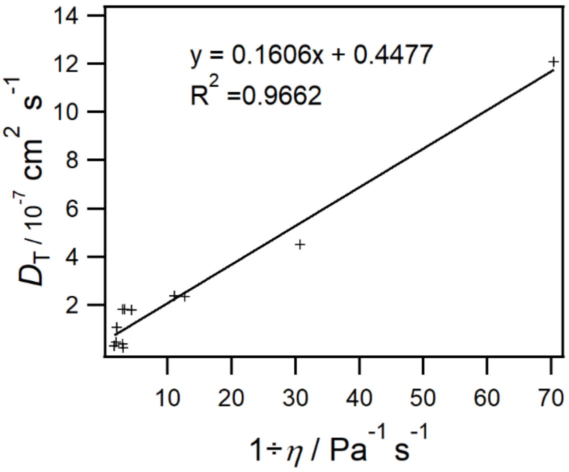

Figure 3.12: D_T obtained from Cottrell's relationship of 10 mmol dm^{-3} TEMPO *vs.* 1/η of the RTILs, at ambient temperature and pressure.

D_T can be used to determine the heterogeneous electron transfer rate constant, k^0, together with Equation 2.7.[22]

$$\psi = \frac{\left(\frac{D_{T+}}{D_T}\right)k^0}{\left[D_{T+}\pi\nu\left(\frac{nF}{RT}\right)\right]^{1/2}} \qquad (2.7)$$

Where ψ is the kinetic parameter of the electron transfer, which can be estimated using ΔE_p.[22] The exchange coefficient, α, is estimated to be 0.5 and the ratio of D_T^+/D_T is assumed to be equal to 1.. Using D_T from Table 3.3 and ΔE_p from Table 3.2. k^0 could be determined in each RTIL-TEMPO solution, see Table 3.4.[21, 22, 25]

Table 3.4: k^0 determined from CVs of solutions containing 10 mmol dm^{-3} TEMPO in RTIL media and D_T in the respective RTIL media. CVs recorded using a 3 mm diameter glassy-carbon electrode at 5 mV s^{-1} at ambient temperature and pressure. Dynamic iR drop compensation was used.

Ionic Liquid	**k^0 / 10^{-5} cm s^{-1}**
$[N_{6,6,6,14}][NTf_2]$	0.21 ± 0.09
$[N_{4,4,4,1}][NTf_2]$	0.33 ± 0.03
$[N_{4,4,4,1}][DCA]$	0.12 ± 0.05
$[P_{4,4,4,1}][NTf_2]$	2.92 ± 0.02
$[P_{6,6,6,14}][NTf_2]$	2.74 ± 0.23
$[P_{6,6,6,14}][DCA]$	2.56 ± 0.35
$[C_8C_1Pyrr][NTf_2]$	12.67 ± 0.11
$[C_2C_1Im][NTf_2]$	6.84 ± 0.05
$[C_2C_1Im][DCA]$	18.41 ± 0.10
$[C_8C_1Im][NTf_2]$	2.53 ± 0.09
$[C_8C_1Im][DCA]$	5.37 ± 0.08
$[C_8C_1Im][BF_4]$	4.16 ± 0.07
$[C_8C_1Im][OTf]$	1.35 ± 0.03
$[C_8C_1Im][PF_6]$	0.33 ± 0.12

As a reference, k^0 values for quasi-reversible system typically lies within the range 0.3 cm s^{-1} $\leq k^0 \geq 2 \times 10^{-5}$ cm s^{-1}.[21] Slow electron transfer could limit the overall reaction rate of TEMPO-mediated electroxidation of alcohols. As can be observed from Table 3.4 the lowest k^0 values are observed for the RTILs that are generally more viscous, e.g. $[N_{6,6,6,14}][NTf_2]$ and

[C_8C_1Im][PF_6]. The relationship between k^0 and the viscosity of the RTIL is shown in Figure 3.13.

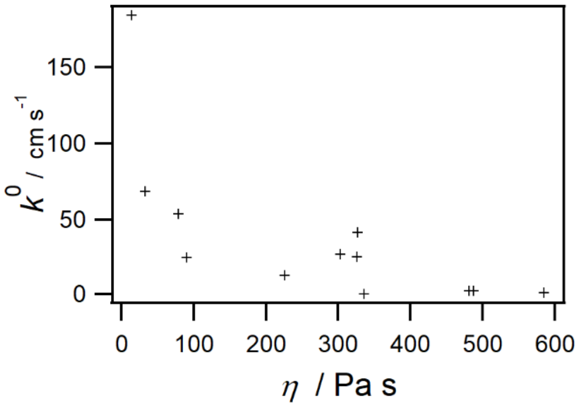

Figure 3.13: Relationship between k^0 of 10 mmol dm^{-3} TEMPO in different RTIL with η of the RTIL media. CVs recorded using a 3 mm diameter glassy-carbon electrode at 5 mV s^{-1} at ambient temperature and pressure. Dynamic iR drop compensation was used.

k^0 in general decreases as the viscosity of the media increases, which has previously been reported for RTIL media. It is believed that with more viscous RTIL the solvent molecules at the electrode need to orientate and move relative to each other as the electron transfer is occurring. Bulkier RTILs structures orientate slower and hence a lower electron transfer is observed.[36]

3.2.2. TEMPO-mediated Alcohol Oxidation in RTILs.

The electrochemical oxidation or reduction of an electroactive species often produces reactive intermediates that can undergo homogeneous chemical reactions. TEMPO is an example of such reaction, wherein the oxidation of TEMPO transforms the stable TEMPO radical into the reactive TEMPO$^+$, which can then react with an alcohol substrate.[37] The electrode process is referred to as an EC mechanism (an electron transfer followed by a chemical reaction).[38, 39] Figure 3.14 shows a CV of a solution containing TEMPO in $[C_8C_1Im][NTf_2]$ (red line) and a CV of a solution containing TEMPO, benzyl alcohol and $[C_8C_1Im][NTf_2]$ (blue line), which illustrates the current response of a system in which an EC mechanism is operative.

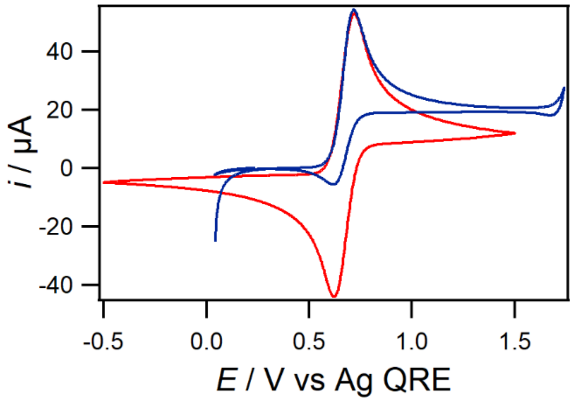

Figure 3.14: CVs of 0.06 mol dm^{-3} TEMPO (red line) and with 2.4 mol dm^{-3} benzyl alcohol (blue line) in $[C_8C_1Im][NTf_2]$. CVs recorded using a 3 mm diameter glassy-carbon electrode with a scan rate of 5 mV s^{-1} and at ambient temperature and pressure. Dynamic iR drop compensation was used.

The CV of the solution containing only TEMPO in $[C_8C_1Im][NTf_2]$ displays the oxidation peak of TEMPO and the reduction peak of TEMPO$^+$. The forward scan (0.0 V to 1.7 V vs Ag QRE) of CV of the solution with benzyl alcohol shows the oxidation peak of TEMPO which forms the intermediate TEMPO$^+$ (electron-transfer step). As the scan is reversed the reduction peak almost disappears. The reason for the disappearance of the reduction peak is a result of TEMPO$^+$ reacting with the alcohol (chemical-reaction step), so there is no TEMPO$^+$ to be reduced at the electrode.[37, 40] In the absence of base, it is likely that the autoprotolysis of the alcohol generates the alcoholate, see Scheme 3.1.[4]

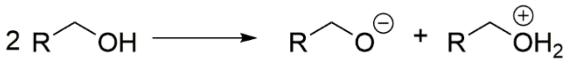

Scheme 3.1: autoprotolysis of an alcohol substrate to generate the alcoholate.[4]

From Figure 3.15 it can be seen that as the scan rate is increased from 5 mV s^{-1} to 50 mV s^{-1}, the reduction peak reappears.

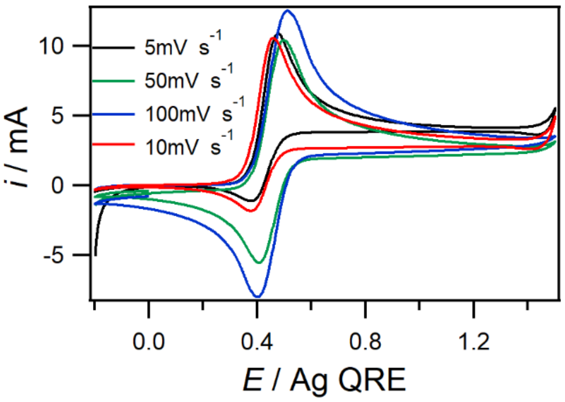

Figure 3.15: CVs of 0.06 mol dm^{-3} TEMPO and 0.6 mol dm^{-3} benzyl alcohol in [C_8C_1Im][NTf_2] measured at scan rates 5 mV s^{-1}, 10 mV s^{-1}, 50 mV s^{-1} and 100 mV s^{-1}. CVs recorded using a 3 mm diameter glassy-carbon electrode at ambient temperature and pressure. Dynamic iR drop compensation was used.

The reduction peak reappears because the chemical step of the reaction between TEMPO$^+$ and benzyl alcohol is now slower than the electron transfer at the higher scan rates, and consequently TEMPO$^+$ can be reduced to TEMPO at the electrode. Therefore, by simply varying the scan rate, it is possible to investigate the rate of the chemical reaction of the electrochemically generated TEMPO$^+$.[38, 39] When only TEMPO and benzyl alcohol are present in [C_8C_1Im][NTf_2], TEMPO$^+$ reacts with the alcohol to form benzaldehyde and the hydroxylamine form of TEMPO (see Scheme 3.2). Thus TEMPO is not regenerated in this EC reaction.

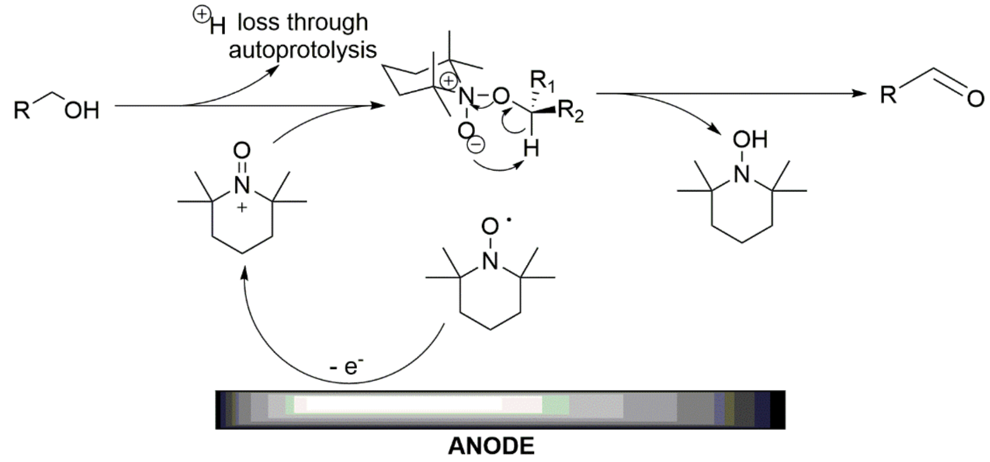

Scheme 3.2: Mechanism of EC reaction of TEMPO and an alcohol substrate, without a base.

In this project, the focus is on the catalytic TEMPO-mediated alcohol oxidation, where TEMPO is regenerated through the introduction of a base to the TEMPO, alcohol and RTIL solutions. Figure 3.16 shows the CV of a solution containing 2,6-lutidine (base), TEMPO and benzyl alcohol in [C_8C_1Im][NTf_2].

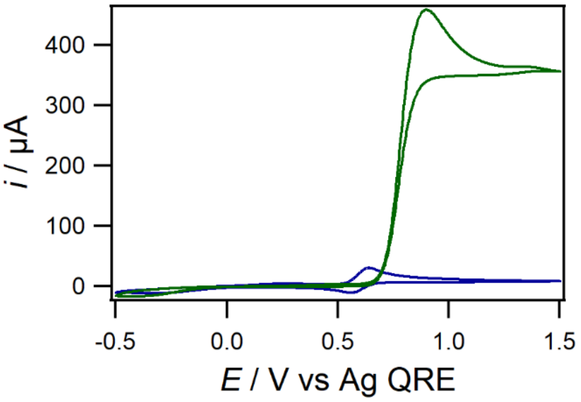

Figure 3.16: CVs of 0.06 mol dm^{-3} TEMPO and 0.6 mol dm^{-3} benzyl alcohol (blue line), with 2.4 mol dm^{-3} 2,6-lutine (green line) in [C_8C_1Im][NTf_2]. CVs recorded using a 3 mm diameter glassy-carbon electrode with scan rate of 5 mV s^{-1} and at ambient temperature and pressure. Dynamic iR drop compensation was used.

The sharp increase in the oxidation current yielding a catalytic current, i_{cat}, in the CV indicates that TEMPO is being recycled and that TEMPO can be used catalytically in the presence of a base. Cyclic voltammetry experiments are used in this section to investigate the effects using different RTIL media, changing the alcohol concentrations and altering the pK_{aH} of the base on the kinetics of the catalytic TEMPO mediated alcohol oxidation are investigated by measuring i_{cat}.[39, 41]

Figure 3.17 shows the effects of adding benzyl alcohol and 2,6-lutidine on the voltammetry of TEMPO in [C_8C_1Im][NTf_2]. In this instance, ferrocene (Fc) was used as the internal standard, due to the instability of decamethylferrocene in air. The green line is the CV of a solution containing TEMPO in the RTIL. Addition of 2.0 mmol dm^{-3} 2,6-lutidine to the TEMPO-RTIL solution causes $i_{p,a}$ and $i_{p,c}$ to increase, due to the slight decrease in viscosity of the RTIL (blue line).[3, 4] Upon addition of benzyl alcohol to the TEMPO-IL solution (red line) a slight increase in $i_{p,a}$ and decrease in $i_{p,c}$ is observed. The decrease in $i_{p,c}$ suggests that some of the TEMPO$^+$ was reduced back to TEMPO by the alcohol oxidation. However, this effect is only observed at low scan rates (< 50 mV s^{-1}), suggesting that TEMPO is relatively stable and only react very slowly in the presence of alcohol. When TEMPO, benzyl alcohol, and 2,6-lutidine are present together, $i_{p,a}$ increases drastically and $i_{p,c}$ decreases to a negligible level, as a result of the catalytic reaction between TEMPO$^+$ and benzyl alcohol producing benzaldehyde.[3, 4] The increase in the anodic peak current is due to the regeneration of TEMPO by the alcohol oxidation, and the disappearance of the cathodic peak is due to the consumption of TEMPO$^+$ by the alcohol oxidation.

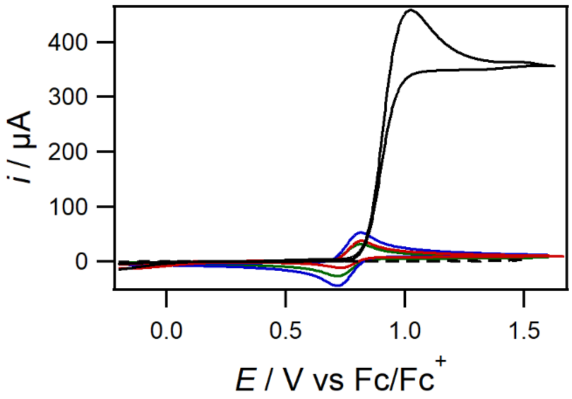

Figure 3.17: CV of 0.06 mol dm^{-3} TEMPO (green). The red line is the CV of 0.06 mol dm^{-3} TEMPO + 0.6 mol dm^{-3} benzyl alcohol. The blue line is the CV of 0.06 mol dm^{-3} TEMPO + 2.0 mol dm^{-3} 2,6-lutidine. The black line is the CV of 0.06 mol dm^{-3} TEMPO + 0.6 mol dm^{-3} benzyl alcohol + 2.0 mol dm^{-3} 2,6-lutidine. CVs recorded using a 3 mm diameter glassy-carbon electrode with scan rate of 5 mV s^{-1} and at ambient temperature and pressure. Dynamic iR drop compensation was used, and [C_8C_1Im][NTf_2] was used as the solvent.

3.2.2.1. TEMPO-mediated Alcohol Oxidations in Different RTIL media

Significant differences were observed in the catalytic currents as the TEMPO-mediated alcohol oxidations were conducted in different RTIL media, for example, CVs of 2,6-lutidine, benzyl alcohol, and TEMPO recorded using [C_2C_1Im][NTf_2] and [C_2C_1Im][DCA] as the solvent are compared in Figure 3.18.

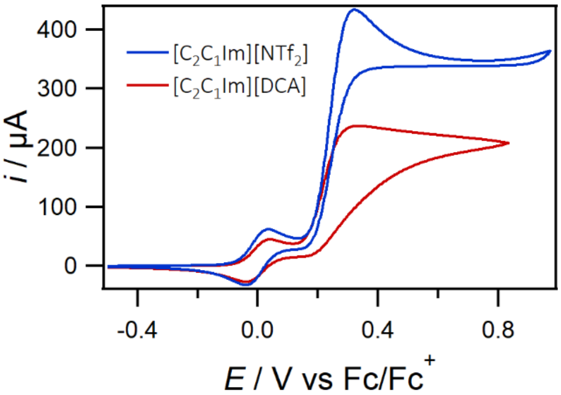

Figure 3.18: CVs of 0.06 mol dm^{-3} TEMPO, 0.6 mol dm^{-3} benzyl alcohol and 2.4 mol dm^{-3} 2,6-lutidine in[C_8C_1Im][NTf_2] (blue line) and [C_8C_1Im][BF_4] (red line). CVs recorded using a 3 mm diameter glassy-carbon electrode with scan rate of 5 mV s^{-1} and at ambient temperature and pressure. Dynamic iR drop compensation was used.

While the diffusion coefficient of benzyl alcohol, D_{BA}, in the [C_2C_1Im][DCA]/2.4 mol dm^{-3} 2,6-lutidine/0.6 mol dm^{-3} benzyl alcohol solution is slightly higher ($D_{BA} = 1.244 \times 10^{-10} \pm 0.061 \times 10^{-10}$ cm^2 s^{-1}) than in the [C_2C_1Im][NTf_2]/2.4 mol dm^{-3} 2,6-lutidine/0.6 mol dm^{-3} benzyl alcohol solution ($D_{BA} = 1.171 \times 10^{-10} \pm 0.055 \times 10^{-10}$ cm^2 s^{-1}), i_{cat}, is much higher in the [C_2C_1Im][NTf_2] solution than in the [C_2C_1Im][DCA] solution. Equation 3.1(shows the relationship between i_{cat} and D_{BA}.[41, 42] The increase in i_{cat} upon changing from [C_2C_1Im][DCA] to [C_2C_1Im][NTf_2] is higher than expected from Equation 3.1, indicating that changing the RTIL composition changes *k*.

$$i_{\mathrm{cat}} = nAFC_{\mathrm{T}}(D_{\mathrm{T}}kC_{\mathrm{A}})^{1/2} \qquad (3.1)^{41,\,40}$$

Where D_{T} is the diffusion coefficient of TEMPO in the reaction solution. In order to investigate if the chemical reaction kinetics of TEMPO-mediated alcohol oxidations is dependent on the RTIL media, Equation 3.1 was used to determine *k* in the different RTIL media.

3.2.2.2. Tuning the Reactivity of TEMPO with RTILs

Figure 3.19 shows CVs of solutions containing TEMPO, 2,6-lutidine and different concentrations of benzyl alcohol in [C_8C_1Im][NTf_2]. The catalytic current, i_{cat}, increases linearly with the square root of the alcohol concentration, $C_{\mathrm{A}}^{½}$, in agreement with Equation 3.1 (Figure 3.19 inset):[41, 42]

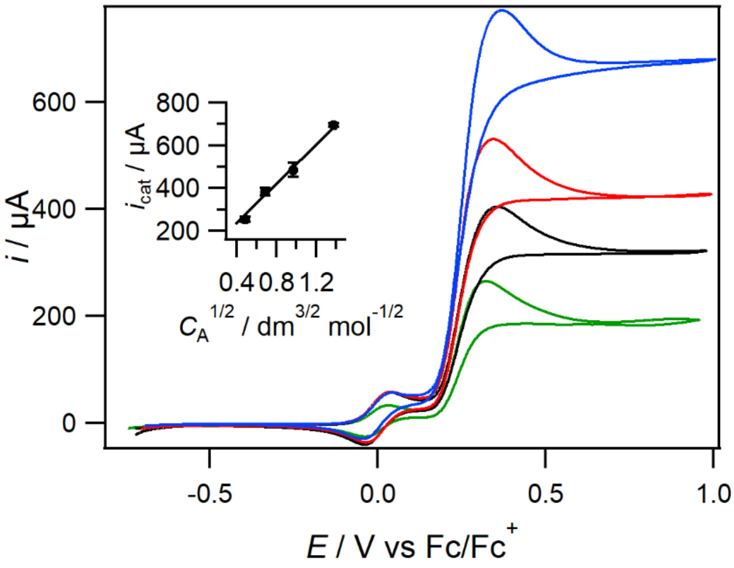

Figure 3.19: CVs of 0.06 mol dm^{-3} TEMPO, 2.4 mol dm^{-3} 2,6-lutidine dissolved in [C_8C_1Im][NTf_2] containing 0.3 mol dm^{-3} (green line), 0.6 mol dm^{-3} (black line), 1.2 mol dm^{-3} (red line) and 2.4 mol dm^{-3} (blue line) benzyl alcohol. The inset shows a graph of the peak current *vs* the square root of the alcohol concentration. CVs recorded using a 3 mm diameter glassy-carbon electrode with scan rate of 5 mV s^{-1} and at ambient temperature and pressure. Dynamic iR drop compensation was used.

All the TEMPO-RTIL systems with 2,6-lutidine and varying benzyl alcohol concentrations yielded i_{cat} that was linearly dependent on the square root of the benzyl alcohol concentration. k can be used as an indication of the efficiency of the catalytic cycle in the various RTILs and can be derived from the slope of the linear plot of the i_{cat} *vs* $C_A^{½}$. D_T in the reaction solution was not determined and throughout this project D_T is assumed to be the same as D_A. D_A in each RTIL was determined using pulsed field gradient nuclear magnetic resonance (PFG-NMR) spectroscopy (this method could not be used to determine D_T since TEMPO is paramagnetic).

Table 3.5 and Figure 3.20 shows the experimentally determined apparent rate constants of TEMPO-mediated alcohol oxidations in the different RTILs.

Table 3.5: *k* obtained from CVs of solutions of 2.4 mol dm^{-3} 2,6-lutidine, 0.06 mol dm^{-3} TEMPO and varying concentrations of benzyl alcohol in various RTILs. CVs recorded using a 3 mm diameter glassy-carbon electrode at 5 mV s^{-1} at ambient temperature and pressure. Dynamic iR drop compensation was used.

Ionic Liquid	**Apparent rate constant of benzyl alcohol oxidation / dm^3 mol^{-1} s^{-1}**
[C_2C_1Im][DCA]	0.245 ± 0.014
[C_8C_1Im][DCA]	0.116 ± 0.009
[C_8C_1Im][BF_4]	0.239 ± 0.005
[C_8C_1Im][OTf]	0.236 ± 0.000
[C_2C_1Im][NTf_2]	0.413 ± 0.001
[C_8C_1Pyrr][NTf_2]	0.520 ± 0.004
[$N_{4,4,4,1}$][NTf_2]	0.524 ± 0.016
[$P_{4,4,4,1}$][NTf_2]	0.434 ± 0.000
[C_8C_1Im][PF_6]	0.380 ± 0.000
[C_8C_1Im][NTf_2]	0.336 ± 0.004
[$P_{6,6,6,14}$][NTf_2]	0.743 ± 0.008
[$N_{6,6,6,14}$][NTf_2]	0.555 ± 0.000
[$P_{6,6,6,14}$][DCA]	0.059 ± 0.001

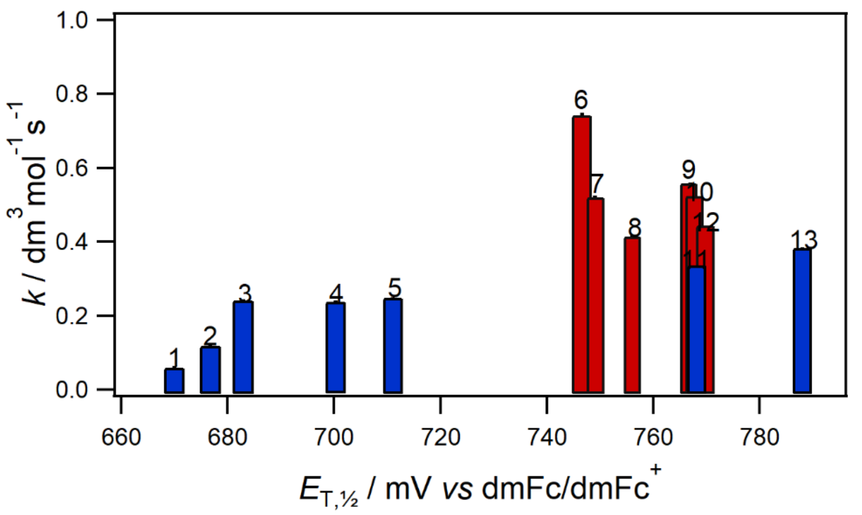

Figure 3.20: Correlation between $E_{T,½}$ and k. The maximum errors of k and $E_{T,½}$ are an average of ± 0.009 dm^{-3} mol^{-1} s^{-1} and ± 7 mV. The RTILs are 1- [$P_{6,6,614}$][DCA], 2-[C_8C_1Im][DCA], 3-[C_8C_1Im][BF_4], 4-[C_8C_1Im][OTf], 5-[C_2C_1Im][DCA], 6-[$P_{6,6,6,14}$][NTf_2], 7-[C_8C_1Pyrr][NTf_2], 8-[C_2C_1Im][NTf_2], 9-[$N_{6,6,6,14}$][NTf_2], 10-[$N_{4,4,4,1}$][NTf_2], 11-[C_8C_1Im][NTf_2], 12-[P4$_{,4,4,1}$][NTf_2], and 13-[C_8C_1Im][PF_6]. Solutions containing 0.06 mol dm^{-3} TEMPO, 2.4 mol dm^{-3} 2,6-lutidine and varying concentrations of benzyl alcohol in various RTIL media. CVs recorded using a 3 mm diameter glassy-carbon electrode with scan rate of 5 mV s^{-1} and at ambient temperature and pressure. Dynamic iR drop compensation was used.

Figure 3.20 shows that k generally decreases as the TEMPO-oxidation potential decreases. Here, k is generally higher in RTILs containing the low β and bulky [NTf_2]$^-$ anions (~0.5–0.8 dm^3 mol^{-1} s^{-1}, red bars in Figure 3.20) than in, for example, a RTIL with a high β such as [C_8C_1Im][DCA] (~0.1 dm^3 mol^{-1} s^{-1}). It is also important to note that although that RTILs such as [C_8C_1Im][PF_6] and [$N_{6,6,6,14}$][NTf_2] exhibited low k^0 (see table 3.4) a high k is observed, indicating that the low k^0 does not limit the overall rate of reaction. This decrease indicates that stabilization of TEMPO$^+$ by anions with higher β decreases the availability of TEMPO$^+$ to take part in the catalytic cycle, see Scheme 3.3. While any relationship between *k* and the RTIL cation identity is less clear, *k* is generally lower when using those liquids containing imidazolium cations, whereas use of the bulkier quaternary phosphonium- and ammonium-based RTILs leads to higher apparent rate constants. The more exposed charge on the imidazolium-based cations may disfavour formation of the positively charged TEMPO$^+$. These results demonstrate that it is possible to control the reactivity of TEMPO-mediated alcohol oxidations simply by changing the structure of the RTIL media.

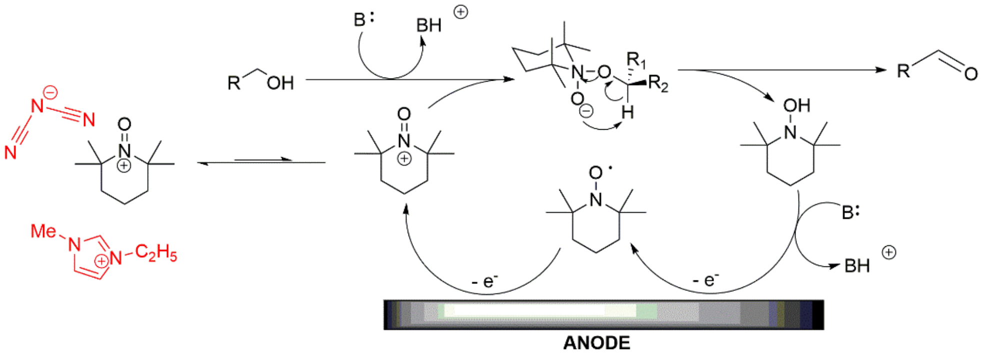

Scheme 3.3: Proposed mechanism of TEMPO-mediated alcohol in a RTIL with a high *β*, such as [C_2C_1Im][DCA] which stabilizes TEMPO$^+$ and lowers the availability of TEMPO$^+$ to participate in the catalytic cycle.

The RTILs with low *β* offer faster reaction kinetics, however it also comes with the cost of using a higher potential. Furthermore, a higher reaction potential is not only less energy efficient but it also increases the possibility of generating side-reactions.

3.2.2.3. *Kinetics of Primary and Secondary Alcohols*

The selectivity of TEMPO in different RTIL media were investigated by recording CVs of RTIL solutions containing TEMPO, the base -2,6-lutidine and the alcohols; benzyl alcohol, 1-phenylethanol, 1-octanol and 2-butanol, see structures in Figure 3.21.

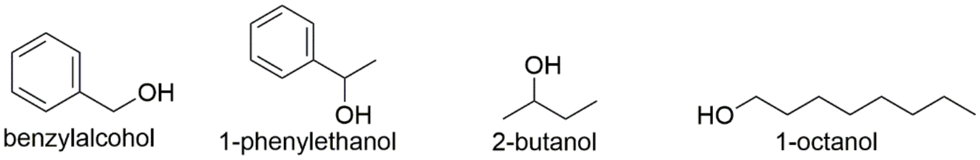

Figure 3.21: Alcohols used in this study.

Figure 3.22 shows CVs of solutions containing 2,6-lutidine, TEMPO with benzyl alcohol, 2-butanol, 1-octanol and 1-phenylethanol in $[C_8C_1Im][NTf_2]$.

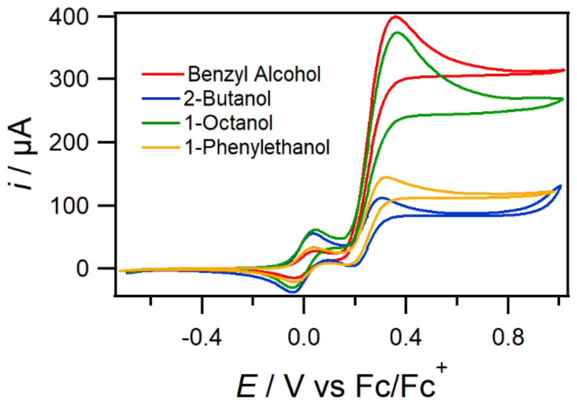

Figure 3.22: CVs of 2.4 mol dm^{-3} 2,6-lutidine, 0.06mol dm^{-3} TEMPO and 0.6 mol dm^{-3} benzyl alcohol, 1-phenylethanol, 1-octanol and 2-butanol in $[C_8C_1Im][NTf_2]$. CVs recorded using a 3 mm diameter glassy-carbon electrode with scan rate of 5 mV s^{-1} and at ambient temperature and pressure. Dynamic iR drop compensation was used.

The measured i_{cat} for the different RTIL solutions of alcohols follow the order 2-butanol < 1-phenylethanol < 1-octanol < benzyl alcohol. The 1-phenyl ethanol is a secondary alcohol, analogous to benzyl alcohol and is known to be more difficult to oxidise by TEMPO than benzyl alcohol due to the steric effects introduced by the secondary alcohol in the intermediate structure.[42-44] 2-butanol does not have the electron-rich aromatic ring and is consequently more difficult to oxidise than 1-phenylethanol.[7, 43-45] 1-octanol falls under the category of fatty alcohol, the physicochemical characteristics of this type of alcohols entail specific challenges, such as lower reactivity compared to benzyl alcohol, lower solubility in solvents and higher viscosity.[46] For example, 1-octanol did not dissolve in the shorter chained imidazolium based RTILs, such as $[C_2C_1Im][DCA]$ and $[C_2C_1Im][NTf_2]$, however dissolved in all of the other RTILs used in this study. Furthermore the pK_a of 1-octanol is higher than the pK_a of benzyl alcohol, thus benzyl alcohol is more easily deprotonated than 1-octanol by the base to from the reactive alcoholate intermediate.[5]

To investigate the rate of reactions of the different alcohols, the catalytic current was measured as the concentration of the alcohols were increased. Figure 3.23 shows the effect of varying the concentration of each alcohol in $[C_8C_1Im][NTf_2]$.

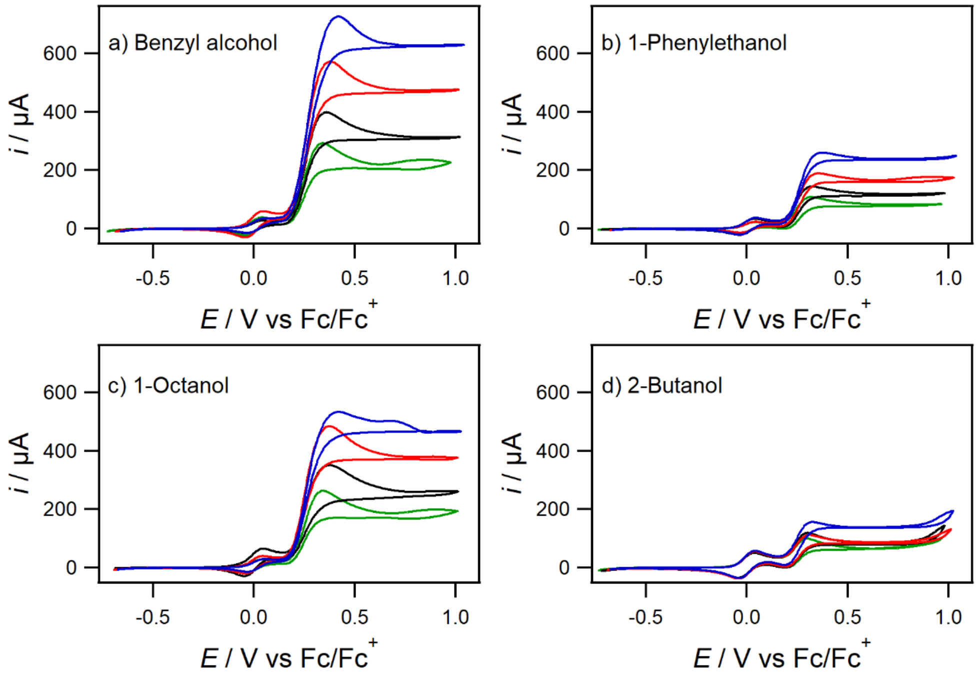

Figure 3.23: CVs of solutions of 2.4 mol dm^{-3} 2,6-lutidine, 0.06 mol dm^{-3} TEMPO and varying concentrations of a) benzyl alcohol, b) 1-phenylethanol, c) 1-octanol and d) 2-butanol in [C_8C_1Im][NTf_2]. All CVs are referenced to Fc/Fc$^+$ couple. CVs recorded using a 3 mm diameter glassy-carbon electrode with scan rate of 5 mV s^{-1} and at ambient temperature and pressure. Dynamic iR drop compensation was used.

Again, it is clear that the highest i_{cat} are obtained for benzyl alcohol, and the lowest i_{cat} are obtained for 2-butanol. Moreover, only a slight increase in current is observed as the concentration of 2-butanol is increased.

k in [C_8C_1Im][NTf_2] (blue bars) and [C_8C_1Im][DCA] (red bars) were calculated using Equation 3.1 and the gradients obtained from plotting the i_{cat} against $C_A^{½}$, these are shown in Figure 3.24.

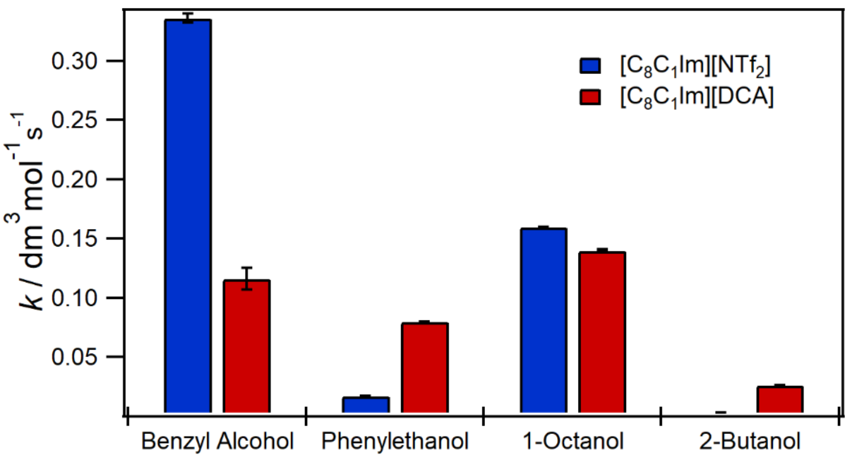

Figure 3.24: k obtained from CVs of solutions of 2.4 mol dm^{-3} 2,6-lutidine, 0.06 mol dm^{-3} TEMPO and varying concentrations of benzyl alcohol, 1-phenylethanol, 1-octanol and 2-butanol in [C_8C_1Im][NTf_2] (blue bars) and [C_8C_1Im][DCA] (red bars). CVs recorded using a 3 mm diameter glassy-carbon electrode with scan rate of 5 mV s^{-1} and at ambient temperature and pressure. Dynamic iR drop compensation was used.

k generally increases in the order 2-butanol < 1-phenylethanol < 1-octanol < benzyl alcohol, again due to the lower degree of steric hindrance during reaction of the alcohol. Figure 3.24 also shows that the [C_8C_1Im][NTf_2]/TEMPO system was more kinetically selective than the [C_8C_1Im][DCA]/TEMPO system in the oxidation of different alcohols. This different degree of discrimination between the RTILs indicates that the reaction selectivity can be tuned by the choice of RTIL media, which demonstrates some of the opportunities offered by RTIL/TEMPO solvent-electrocatalyst systems for selective alcohol oxidations.

Similar trends are also observed with [$P_{6,6,6,14}$][NTf_2], [$P_{6,6,6,14}$][DCA], [C_2C_1Im][NTf_2] and [C_2C_1Im][DCA] RTIL media, (note that 1-octanol did not dissolve in [C_2C_1Im][NTf_2] and [C_2C_1Im][DCA]), see Figure 3.25.

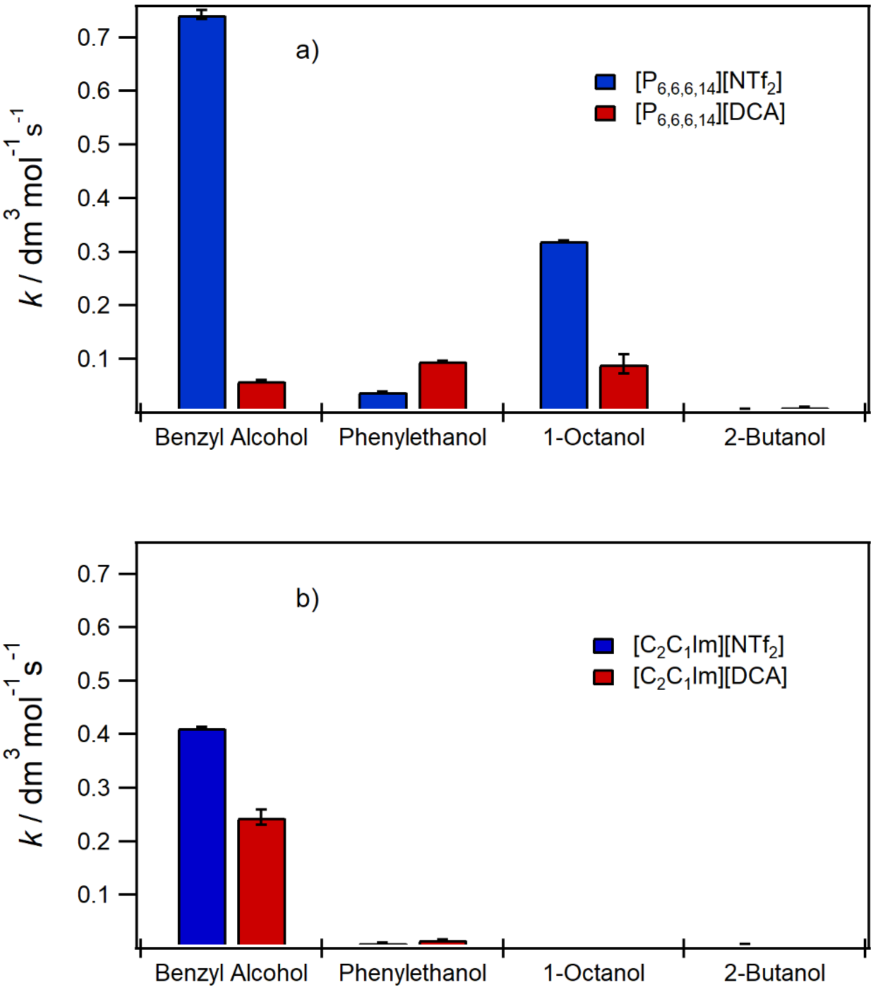

Figure 3.25: *k* obtained from CVs of solutions of 2.4 mol dm^{-3} 2,6-lutidine, 0.06 mol dm^{-3} TEMPO and varying concentrations of benzyl alcohol, 1-phenylethanol, 1-octanol and 2-butanol in a) [$P_{6,6,6,14}$][NTf_2] (blue bars) and [$P_{6,6,6,14}$][DCA] (red bars) and b) [C_2C_1Im][NTf_2] (blue bars) and [C_2C_1Im][DCA] (blue bars). CVs recorded using a 3 mm diameter glassy-carbon electrode with scan rate of 5 mV s^{-1} and at ambient temperature and pressure. Dynamic iR drop compensation was used. (note: 1-octanol did not dissolve in either [C_2C_1Im][NTf_2] nor [C_2C_1Im][DCA] and therefore no data was collected to determine *k* in the oxidation of 1-octanol).

The [NTf_2]$^-$ based RTILs shows better discrimination of primary and secondary alcohols compared to their [DCA]$^-$ analogues in terms of apparent rate constants. Interestingly, higher apparent rate constants were obtained with primary alcohols in all of the RTILs, apart from when using [$P_{6,6,6,14}$][DCA] as the media (*k* of the oxidation of 1-phenylethanol is higher than *k* obtained for the oxidation of benzyl alcohol).

The dependencies of *k* on the alcohol and RTIL media were investigated further by plotting *k* obtained for solutions containing either benzyl alcohol or 1-phenylethanol in the RTIL media [C_8C_1Im][NTf_2], [C_8C_1Im][DCA], [C_2C_1Im][NTf_2], [C_2C_1Im][DCA], [$P_{6,6,6,14}$][NTf_2] and [$P_{6,6,6,14}$][DCA] against β of the RTIL, see Figure 3.26.

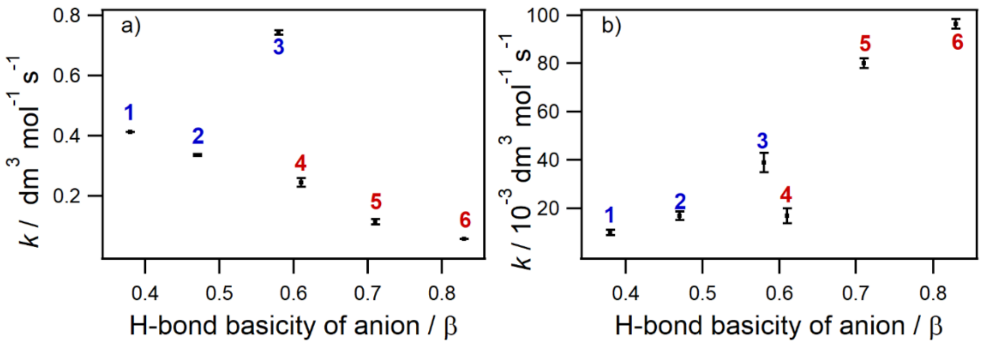

Figure 3.26: *k* obtained from CVs of solutions of 2.4 mol dm^{-3} 2,6-lutidine, 0.06 mol dm^{-3} TEMPO and varying concentrations of b) benzyl alcohol and a) 1-phenylethanol in 1-[C_2C_1Im][NTf_2], 2-[C_8C_1Im][NTf_2], 3-[$P_{6,6,6,14}$][NTf_2], 4-[C_2C_1Im][DCA], 5-[C_8C_1Im][DCA] and 6-[$P_{6,6,6,14}$][DCA] ([NTf_2]$^-$ based RTILs are highlighted in blue and [DCA]$^-$ based RTILs are highlighted in red), plotted against β of the RTILs.[32, 33] The cyclic voltammetry experiments were done in triplicates for each solution. CVs recorded using a 3 mm diameter glassy-carbon electrode with scan rate of 5 mV s^{-1} and at ambient temperature and pressure. Dynamic iR drop compensation was used.

In the case of the solutions containing benzyl alcohol, *k* decreases with increasing β of the RTIL. This trend can be explained by the increased stabilisation of TEMPO$^+$ by the anion of increasing *β* of the RTIL, as discussed previously. The calculated *k* for the solution containing 1-phenylethanol, on the other hand, increases with increasing *β* of the RTIL. A possible explanation for this trend is discussed below. Figure 3.27 shows CVs of two solutions- one containing 1-phenylethanol and the other containing benzyl alcohol in [C_8C_1Im][NTf_2] with 2.4 mol dm^{-3} 2,6-lutidine recorded at 50 mV s^{-1}.

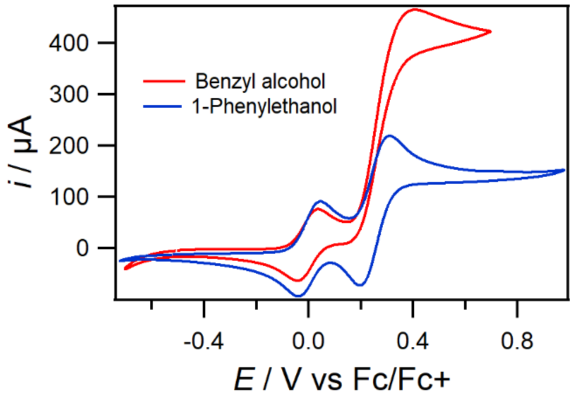

Figure 3.27: CVs of 2.4 mol dm^{-3} 2,6-lutidine, 0.06 mol dm^{-3} TEMPO and 0.6 mol dm^{-3} benzyl alcohol (red line) and 0.6 mol dm^{-3} 1-phenylethanol (blue line), recorded at 50 mV s^{-1}.

Comparing the CVs of the solutions containing benzyl alcohol and 1-phenylethanol, the initial observation is that the reduction peak of TEMPO$^+$ to TEMPO is observed in the CV of the solution containing 1-phenylethanol but not in the CV of the solution containing benzyl alcohol. The appearance of the reduction peak in the CV recorded for 1-phenylethanol, suggests that not all the TEMPO$^+$ produced at the electrode is consumed by chemical reaction and is therefore reduced at the electrode. Thus the reaction between

TEMPO$^+$ and 1-phenylethanol is slow compared to the reaction between TEMPO$^+$ and benzyl alcohol, since all of TEMPO$^+$ is consumed by the oxidation of benzyl alcohol. The slower kinetics of TEMPO-mediated oxidation of secondary alcohols is well-known and agrees well with recent mechanistic studies of TEMPO-mediated alcohol oxidations.[4, 7, 42]

The deprotonation steps of the alcohol and the hydroxyl amine species have previously been suggested to be the rate-limiting steps in TEMPO-mediated alcohol oxidations.[4, 5, 7] Doherty and co-workers, conducted a study in which the consumption of TEMPO$^+$ in an RTIL media and in acetonitrile was monitored at a rotating disk electrode as varying concentrations of alcohol and base were added to the solution. With this approach they developed a kinetic model which shows that the deprotonation of primary alcohols by the base is the rate-limiting step of TEMPO-mediated alcohol oxidation.[47, 48]

In another study conducted by Brown and co-workers, the deprotonation of the hydroxylamine species to regenerate TEMPO is proposed to be the rate-limiting step. Additionally, they suggest that the comproportionation of the hydroxylamine and TEMPO$^+$ is an important step in the regeneration of TEMPO during catalytic alcohol oxidation, see Scheme 3.4. This com/disproportionation of TEMPO has been shown to be highly pH dependent, as higher pH favours TEMPO regeneration, and leads to improved yields and turn-over of the reaction.[7, 48]

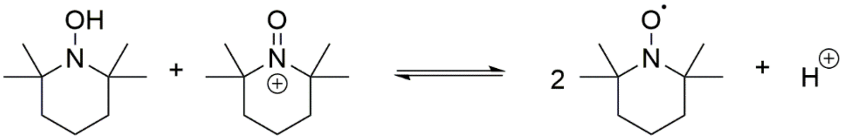

Scheme 3.4: com/disproportionation reaction between TEMPO$^+$ cation and hydroxylamine to regenerate TEMPO radical.[5]

The reduction peak of TEMPO$^+$ is observed in the CV of the 1-phenylethanol solution (Figure 3.27), suggesting that the reaction between TEMPO$^+$ and 1-phenylethanol is slow. It is worth noting that the reduction peak is observed at scan rates higher than 10 mV s^{-1}. Consequently, it is likely that the TEMPO$^+$-1-phenylethol reaction step does contribute to the overall rate of reaction and the base deprotonation steps are not the only ‘rate limiting steps’ in the overall oxidation of secondary alcohols, see Scheme 3.5.

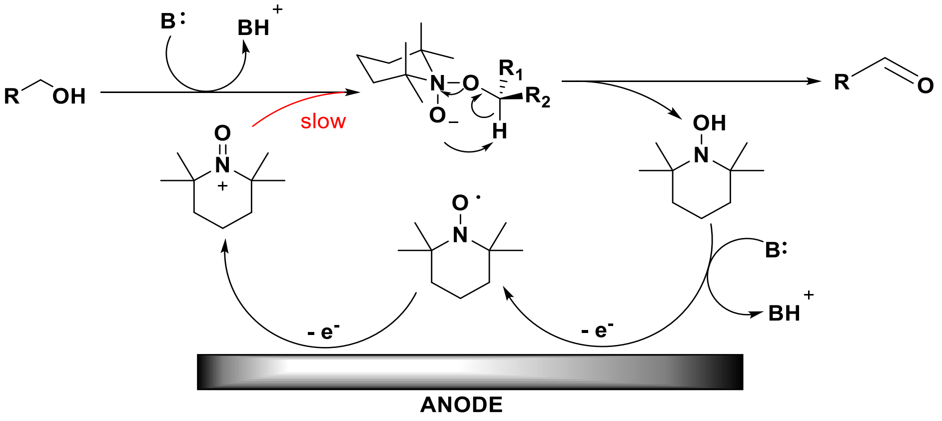

Scheme 3.5: proposed mechanism of secondary alcohol oxidations showing the possible rate limiting steps.

A possible explanation for the observed trend of increasing *k* for the TEMPO-mediated oxidation of secondary alcohols with increasing *β*, could be that the stabilization of TEMPO$^+$ by the RTIL anion can increase the lifetime of TEMPO$^+$ sufficiently in the solution so that the concentration of

$TEMPO^+$ is increased and pushes the equilibrium in Scheme 3.3. to the right and drives the alcohol oxidation. RTIL-alcohol and RTIL-alcoholate ion interactions could also be yielding the results observed in Figure 3.26. It is clear that k is dependent on the nature of the RTIL media and the alcohol, the reason for the observed trends in k as the substrate is changed from a primary to secondary alcohol is still unclear and needs further investigation.

Nonetheless, the dependencies of k on the RTIL media for both the oxidation of benzyl alcohol and secondary alcohols demonstrate that the overall rate of reaction can be controlled via the β of the RTIL, to such an extent that even the degree of selectivity can be controlled.

In the following section it is shown that the use of a strong base is required for the development of efficient TEMPO-mediated electrooxidation of both secondary and primary alcohols.

3.2.2. Effect of Base in TEMPO-Based Alcohol Oxidations in RTILs

The concentration and the pK_{aH} of the base is important for efficient TEMPO-mediated alcohol oxidations. Figure 3.28 shows the effect of increasing the concentration of 2,6-lutidine while maintaining constant benzyl alcohol and TEMPO concentrations.

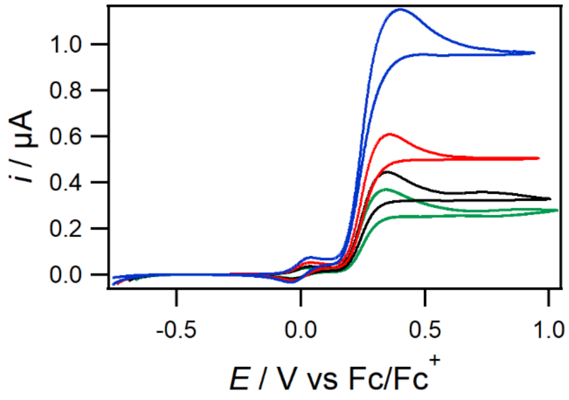

Figure 3.28: CVs of 0.06 mol dm^{-3} TEMPO, 0.6 mol dm^{-3} benzyl alcohol and 1.5 mol dm^{-3} (green line), 2 mol dm^{-3} (black line), 3 mol dm^{-3} (red line) and 4 mol dm^{-3} (blue line) 2,6-lutidine in [C_8C_1Im][NTf_2]. CVs recorded using a 3 mm diameter glassy-carbon electrode with scan rate of 5 mV s^{-1} and at ambient temperature and pressure. Dynamic iR drop compensation was used.

Figure 3.28 shows that i_{cat} increases with increasing concentration of 2,6-lutidine. As the concentration of 2,6-lutidine is increased, the viscosity decreases resulting in higher i_{cat} values. The increase in rates of mass transfer is evident by comparing the Fc/Fc$^+$ waves in the voltammograms. The relative increase in i_{cat} as the concentration of 2,6-lutidine increases is drastically higher than that of the Fc/Fc$^+$ peaks, demonstrating that the increase in the catalytic rate is due to a combination of the increased mass transfer in the solution and a higher k.

Voltammetric analysis was also conducted in reaction mixtures containing 2,4,6-collidine (pK_{aH} = 7.43) and pyridine (pK_{aH} =5.25), instead of 2,6-lutidine (pK_{aH} = 6.75) as the base, and Figure 3.29 shows that i_{cat} increases as the pK_{aH} of the base increases. These effects have been observed previously when using organic,[3, 4] aqueous[43] and RTIL media.[3, 4, 6] The increase in i_{cat} with increasing concentration and increasing pK_{aH} of the base is because both the alcohol and hydroxylammonium species are deprotonated more rapidly.[4]

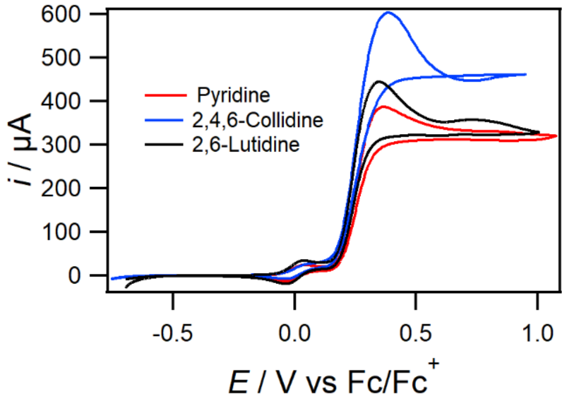

Figure 3.29: CVs of 0.06 mol dm^{-3} TEMPO, 0.6 mol dm^{-3}benzyl alcohol and 2.4 mol dm^{-3} of pyridine (pK$_{aH}$ =5.25, red line), 2,4,6-collidine (pK$_{aH}$ = 7.43, blue line) and 2,6-lutidine (pK$_{aH}$ = 6.75, black line). CVs recorded using a 3 mm diameter glassy-carbon electrode with scan rate of 5 mV s^{-1} and at ambient temperature and pressure. Dynamic iR drop compensation was used.

The dependence on base concentration was also investigated for solutions containing the secondary alcohol, 1-phenylethanol. Figure 3.30 shows CVs of solutions containing 1-phenylethanol, TEMPO and varying concentrations of 2,6-lutidine in [C_8C_1Im][NTf_2].

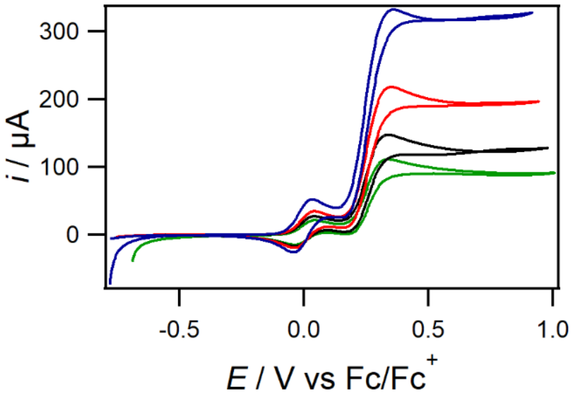

Figure 3.30: CVs of 0.06 mol dm^{-3} TEMPO, 0.6 mol dm^{-3} 1-phenylethanol and 1.5 mol dm^{-3} (green line), 2 mol dm^{-3} (black line), 3 mol dm^{-3} (red line) and 4 mol dm^{-3} (blue line) 2,6-lutidine in [C_8C_1Im][NTf_2]. CVs recorded using a 3 mm diameter glassy-carbon electrode with scan rate of 5 mV s^{-1} and at ambient temperature and pressure. Dynamic iR drop compensation was used.

Again, from Figure 3.30 it is clear that i_{cat} increases with increasing concentration of 2,6-lutidine. Figure 3.31 compares the increase of i_{cat} of solutions containing 1-phenylethanol and benzyl alcohol as the concentration of 2,6-lutidine increases in [C_8C_1Im][NTf_2].

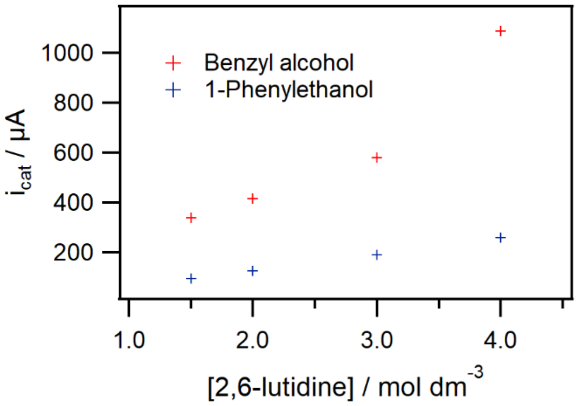

Figure 3.31: Measured i_{cat} from CVs recorded of solutions containing varying concentrations of 2,6-lutidine, 0.06 mol dm^{-3} TEMPO, 0.6 mol dm^{-3} 1-phenylethanol (blue markers) and 0.6 mol dm^{-3} benzyl alcohol (red markers) in [C_8C_1Im][NTf_2] *vs.* concentration of 2,6-lutidine in the solutions. CVs recorded using a 3 mm diameter glassy-carbon electrode with scan rate of 5 mV s^{-1} and at ambient temperature and pressure. Dynamic iR drop compensation was used.

Increasing the 2,6-lutidine concentration from 1.5 mol dm^{-3} to 4 mol dm^{-3} causes a 2.7- and a 3.2- fold increase in the measured i_{cat} of the solutions containing 1-phenylethanol and benzyl alcohol, respectively. The response in i_{cat} seems to be more sensitive to the increasing base concentrations in solutions containing benzyl alcohol compared to solutions containing 1-phenylethanol. This lower i_{cat} response, in the solutions containing 1-phenylethanol, due to increasing base concentration could be a consequence of the slower initial reaction between TEMPO$^+$ and 1-phenylethanol compared to the reaction between TEMPO$^+$ and benzyl alcohol, as proposed in Figure 3.27. As suggested in the previous section, the initial reaction between TEMPO$^+$ and 1-phenylethanol has a greater contribution to the overall rate of reaction compared to the benzyl alcohol oxidation. Therefore, *k* could be attenuated by the slower reaction between TEMPO$^+$ and 1-phenylethanol, and is not as influenced by the base as much as the oxidation of the benzyl alcohol.[4, 5]

3.2.5. TEMPO-mediated Alcohol Oxidations in Acetonitrile.

To allow comparison with the state of the art solvents, the kinetics of TEMPO-mediated alcohol oxidations in acetonitrile containing tetraethylammonium tetrafluoroborate, [TEA][BF_4], was investigated. Due to the lower viscosity of acetonitrile, mass transfer is typically faster in acetonitrile than in RTILs, resulting in more rapid and efficient electrooxidation if the chemical steps are fast. However, if the chemical reaction kinetics of alcohol oxidation in RTILs are faster than in acetonitrile, it could potentially compensate for the slower mass transfer in RTILs and yield a higher rate of catalysis.[4] Figure 3.32 shows catalytic benzyl-alcohol oxidation CVs recorded using acetonitrile/[TEA][BF_4] (dashed line) and [C_8C_1Im][NTf_2] (solid line), respectively.

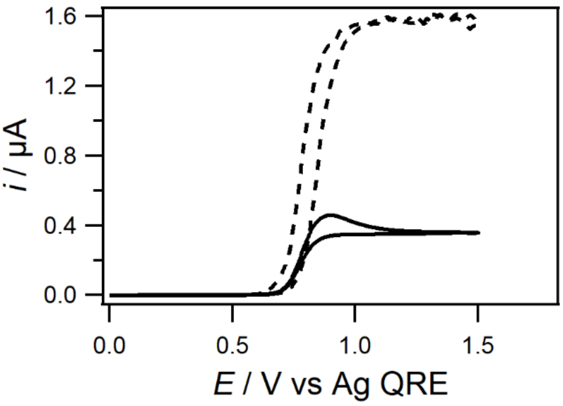

Figure 3.32: CVs of 0.06 mol dm^{-3} TEMPO, 0.6 mol dm^{-3} benzyl alcohol, and 2.4 mol dm^{-3} 2,6-lutidine in [C_8C_1Im][NTf_2] (solid line) and in acetonitrile containing 0.05 mol dm^{-3} [TEA][BF_4] (dashed line). CVs recorded using a 3 mm diameter glassy-carbon electrode with scan rate of 5 mV s^{-1} and at ambient temperature and pressure. Dynamic iR drop compensation was used.

i_{cat} in the acetonitrile system is greater than in the [C_8C_1Im][NTf_2] system, which reflects the relative mass-transport rates in the media. However, using the analysis described in Section 3.2.2.2 and Equation 3.1, it was derived that k = 0.336 ± 0.004 dm^3 mol^{-1} s^{-1} in [C_8C_1Im][NTf_2], compared to k = 0.249 ± 0.004 dm^3 mol^{-1} s^{-1} in acetonitrile containing 0.05 mol dm^{-3} [TEA][BF_4]. The concentration of [TEA][BF_4] in acetonitrile was increased to explore the role of the electrolyte in catalysis and for comparison [C_8C_1Im][DCA], [C_8C_1Im][NTf_2] and [C_8C_1Im][BF_4] were also investigated as electrolytes, see Figure 3.33.

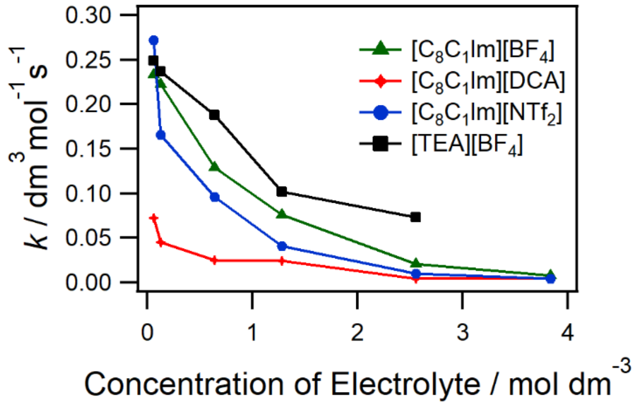

Figure 3.33: *k* obtained from CVs of solutions of 2.4 mol dm^{-3} 2,6-lutidine, 0.06 mol dm^{-3} TEMPO and varying concentrations of benzyl alcohol in acetonitrile containing various concentrations of [TEA][BF$_4$], [C$_8$C$_1$Im][BF$_4$], [C$_8$C$_1$Im][NTf$_2$] and [C$_8$C$_1$Im][DCA]. CVs recorded using a 3 mm diameter glassy-carbon electrode with scan rate of 5 mV s^{-1} and at ambient temperature and pressure. Dynamic iR drop compensation was used.

From Figure 3.33, it is clear that *k* decreases as the electrolyte concentration increases. These data suggest that increasing amounts of electrolyte increase interactions with TEMPO$^+$, making it less available to participate in the catalytic cycle. Similar decreases in *k* are observed when [C$_8$C$_1$Im][NTf$_2$], [C$_8$C$_1$Im][BF$_4$] and [C$_8$C$_1$Im][DCA] are used as dissolved electrolytes in acetonitrile at increasing concentrations (Figure 3.33) blue dots, green triangles, and red diamonds, respectively). Interestingly, *k* is generally lower when the solvent contained > 0.05 mol dm^{-3} electrolyte than in neat RTILs. However, near 0.05 mol dm^{-3} electrolyte, *k* is generally similar to that measured when using neat RTILs, suggesting that the ionic environment in the neat RTILs is similar to that in the dilute electrolytes.

Recent surface-force measurements have also indicated that RTILs behave as dilute electrolytes,[49] containing long-lived ion pairs, with relatively low numbers of free ions. However, there is some disagreement on the true "ionicity" of RTILs.[50-54] For example, Perkins and co-workers recently used computational models to conclude that RTILs behave not as dilute electrolytes, but as concentrated electrolytes, demonstrating that further work in this area is required.[55] While a lot more work on this topic is needed, the data described here suggest that electrochemical analyses such as that described here could potentially provide some new insights into the nature of RTILs.

3.3. Conclusion

In this study, the possibility of tuning the redox properties of TEMPO in terms of its reversibility and half-wave potentials simply by changing the RTIL media is demonstrated. The β of the RTIL has a significant impact on the half-wave potential of TEMPO/TEMPO$^+$, as a result of TEMPO$^+$ being stabilized by the higher β of the RTIL. This stabilization of TEMPO$^+$ results in lower half-wave potential and this stabilization of TEMPO$^+$ by the anionic component of the RTIL media has, to our knowledge, not been reported previously.

The variation in the degree of interaction between the RTIL solvent and the catalytically-active TEMPO$^+$ led to significant differences in catalytic activity of TEMPO during oxidation of alcohols in ionic liquids. The catalytic reaction apparent rate constant increased with increasing TEMPO/TEMPO$^+$ potential and could be correlated with decreasing β of the RTIL media. Comparison of k of the oxidation of four different alcohols substrates revealed different degrees of catalytic discrimination in the ionic liquids, confirming that the activity of TEMPO can be controlled by the choice of the ionic liquid. It is also significant that k for the oxidation reaction is larger in RTILs with low β than that observed in acetonitrile.

In the following chapter constant-current electrolysis is investigated in order to determine the efficiency and selectivity of the catalytic TEMPO-mediated alcohol oxidations in RTILs at preparative-scale.

3.4. References

1. M. Kathiresan and D. Velayutham, *Chem. Commun.*, 2015, **51**, 17499-17516.

2. A. Lahiri, N. Borisenko and F. Endres, *Top. Curr. Chem.*, 2018, **376**, 9.

3. R. Barhdadi, C. Comminges, A. P. Doherty, J. Y. Nédélec, S. O'Toole and M. Troupel, *J. Appl. Electrochem.*, 2007, **37**, 723-728.

4. C. Comminges, R. Barhdadi, A. P. Doherty, S. O'Toole and M. Troupel, *J. Phys. Chem. A*, 2008, **112**, 7848-7855.

5. R. A. Green, J. T. Hill-Cousins, R. C. D. Brown, D. Pletcher and S. G. Leach, *Electrochim. Acta*, 2013, **113**, 550-556.

6. A. C. Herath and J. Y. Becker, *Electrochim. Acta*, 2008, **53**, 4324-4330.

7. M. Rafiee, K. C. Miles and S. S. Stahl, *J. Am. Chem. Soc.*, 2015, **137**, 14751-14757.

8. J. S. Wilkes, in *Ionic Liquids in Synthesis*, eds. P. Wasserscheid and T. Welton, Wiley-VCH, Weinheim, 1st edn., 2003, ch. 1, pp. 1-6.

9. M. J. Earle and K. R. Seddon, in *Clean Solvents*, eds. M. A. Abraham and L. Moens, American Chemical Society, Washington, 2002, ch. 2, pp. 10-25.

10. M. C. Buzzeo, O. V. Klymenko, J. D. Wadhawan, C. Hardacre, K. R. Seddon and R. G. Compton, *J. Phys. Chem. A*, 2003, **107**, 8872-8878.

11. A. W. Taylor, S. Puttick and P. Licence, *J. Am. Chem. Soc.*, 2012, **134**, 15636-15639.

12. L. Xiong, A. M. Fletcher, S. G. Davies, S. E. Norman, C. Hardacre and R. G. Compton, *Chem. Commun.*, 2012, **48**, 5784-5786.

13. S. Men, K. R. J. Lovelock and P. Licence, *RSC Adv.*, 2015, **5**, 35958-35965.

14. C. Chiappe and D. Pieraccini, *J. Phys. Org. Chem.*, 2005, **18**, 275-297.

15. R. Sheldon, *Chem. Commun.*, 2001, **23**, 2399-2407.

16. V. Strehmel, S. Berdzinski and H. Rexhausen, *J. Mol. Liq.*, 2014, **192**, 153-170.

17. R. K. Blundell and P. Licence, *Phys. Chem. Chem. Phys.*, 2014, **16**, 15278-15288.

18. R. K. Blundell and P. Licence, *Chem. Commun.*, 2014, **50**, 12080-12083.

19. T. Cremer, C. Kolbeck, K. R. J. Lovelock, N. Paape, R. Wölfel, P. S. Schulz, P. Wasserscheid, H. Weber, J. Thar, B. Kirchner, F. Maier and H.-P. Steinrück, *Chem. Eur. J.*, 2010, **16**, 9018-9033.

20. S. Men, K. R. J. Lovelock and P. Licence, *Phys. Chem. Chem. Phys.*, 2011, **13**, 15244-15255.

21. D. Pletcher, R. Greff, R. Peat, L. M. Peter and J. Robinson, in *Instrumental Methods in Electrochemistry*, eds. D. Pletcher, R. Greff, R. Peat, L. M. Peter and J. Robinson, Woodhead Publishing, Cambridge, 1st edn., 2001, ch. 6, pp. 178-228.

22. A. J. Bard and L. R. Faulkner, in *Electrochemical methods : fundamentals and applications*, eds. A. J. Bard and L. R. Faulkner, John Wiley & Sons, New York, 2nd edn., 2001, ch. 11, pp. 416-470.

23. J. L. Anthony, J. F. Brennecke, J. D. Holbrey, E. J. Maginn, R. A. Mantz, R. D. Rogers, P. C. Trulove, A. E. Visser and T. Welton, in *Ionic Liquids in Synthesis*, eds. P. Wasserscheid and T. Welton, Wiley VCH, Weinheim, 1st edn., 2003, ch. 3, pp. 41-126.

24. J. P. Southall, H. V. S. A. Hubbard, S. F. Johnston, V. Rogers, G. R. Davies, J. E. McIntyre and I. M. Ward, *Solid State Ionics*, 1996, **85**, 51-60.

25. D. Pletcher, R. Greff, R. Peat, L. M. Peter and J. Robinson, in *Instrumental Methods in Electrochemistry*, eds. D. Pletcher, R. Greff, R. Peat, L. M. Peter and J. Robinson, Woodhead Publishing, Cambridge, 1st edn., 2001, ch. 3, pp. 76-112.

26. W. J. Miao, Z. F. Ding and A. J. Bard, *J. Phys. Chem. B*, 2002, **106**, 1392-1398.

27. X. Zhang, H. J. Yang and A. J. Bard, *J. Am. Chem. Soc.*, 1987, **109**, 1916-1920.

28. Z. J. Karpinski, S. Song and R. A. Osteryoung, *Inorg. Chim. Acta*, 1994, **225**, 9-14.

29. K. R. J. Lovelock, F. N. Cowling, A. W. Taylor, P. Licence and D. A. Walsh, *J. Phys. Chem. B*, 2010, **114**, 4442-4450.

30. J. E. Taylor, M. A. Kulandainathan, C. E. Hotchen and F. Marken, in *Modern electrosynthetic methods in organic chemistry*, eds. F. Marken and M. Atobe, CRC Press Boca Raton, 1st edn., 2018, ch. 1, pp. 1-44.

31. R. K. Blundell, A. E. Delorme, E. F. Smith and P. Licence, *Phys. Chem. Chem. Phys.*, 2016, **18**, 6122-6131.

32. A. F. M. Cláudio, L. Swift, J. P. Hallett, T. Welton, J. A. P. Coutinho and M. G. Freire, *Phys. Chem. Chem. Phys.*, 2014, **16**, 6593-6601.

33. S. Spange, R. Lungwitz and A. Schade, *J. Mol. Liq.*, 2014, **192**, 137-143.

34. A. J. Bard and L. R. Faulkner, in *Electrochemical methods : fundamentals and applications*, eds. A. J. Bard and L. R. Faulkner, John Wiley & Sons, New York, 2nd edn., 2001, ch. 5, pp. 156-225.

35. K. R. J. Lovelock, A. Ejigu, S. F. Loh, S. Men, P. Licence and D. A. Walsh, *Phys. Chem. Chem. Phys.*, 2011, **13**, 10155-10164.

36. A. A. J. Torriero, in *Electrochemistry in ionic liquids. Volume 1: Fundamentals.*, ed. A. A. J. Torriero, Springer, Cham, 1st edn., 2015, ch. 2, pp. 7-74.

37. M. F. Semmelhack, C. S. Chou and D. A. Cortes, *J. Am. Chem. Soc.*, 1983, **105**, 4492-4494.

38. D. Pletcher, *Electrochem. Commun.*, 2018, **88**, 1-4.

39. D. Pletcher, R. Greff, R. Peat, L. M. Peter and J. Robinson, in *Instrumental Methods in Electrochemistry*, eds. D. Pletcher, R. Greff, R. Peat, L. M. Peter and J. Robinson, Woodhead Publishing, Cambridge, 1st edn., 2001, ch. 7, pp. 229-250.

40. N. Elgrishi, K. J. Rountree, B. D. McCarthy, E. S. Rountree, T. T. Eisenhart and J. L. Dempsey, *J. Chem. Educ.*, 2018, **95**, 197-206.

41. J. M. Savéant, *Chem. Rev.*, 2008, **108**, 2348-2378.

42. M. Rafiee, B. Karimi and S. Alizadeh, *ChemElectroChem*, 2014, **1**, 455-462.

43. J. T. Hill-Cousins, J. Kuleshova, R. A. Green, P. R. Birkin, D. Pletcher, T. J. Underwood, S. G. Leach and R. C. Brown, *ChemSusChem*, 2012, **5**, 326-331.

44. J. Einhorn, C. Einhorn, F. Ratajczak and J.-L. Pierre, *J. Org. Chem.*, 1996, **61**, 7452-7454.

45. B. L. Ryland and S. S. Stahl, *Angew. Chem., Int. Ed. Engl.*, 2014, **53**, 8824-8838.

46. V. C. Corberán, M. E. González-Pérez, S. Martínez-González and A. Gómez-Avilés, *Appl. Catal., A*, 2014, **474**, 211-223.

47. R. Barhdadi, C. Comminges, A. P. Doherty, J. Y. Nedelec, S. O'Toole and M. Troupel, *J. Appl. Electrochem.*, 2007, **37**, 723-728.

48. C. Comminges, R. Barhdadi, A. P. Doherty, S. O'Toole and M. Troupel, *J. Phys. Chem. A*, 2008, **112**, 7848-7855.

49. M. A. Gebbie, M. Valtiner, X. Banquy, E. T. Fox, W. A. Henderson and J. N. Israelachvili, *Proc. Natl. Acad. Sci.*, 2013, **110**, 9674.

50. H. Tokuda, S.-J. Baek and M. Watanabe, *J. Phys. Chem. B*, 2005, **73**, 620-622.

51. M. Sha, H. Dong, F. Luo, Z. Tang, G. Zhu and G. Wu, *J. Phys. Chem. Lett.*, 2015, **6**, 3713-3720.

52. S. Perkin, M. Salanne, P. Madden and R. Lynden-Bell, *Proc. Natl. Acad. Sci.*, 2013, **110**, 4121.

53. M. A. Gebbie, M. Valtiner, X. Banquy, W. A. Henderson and J. N. Israelachvili, *Proc. Natl. Acad. Sci.*, 2013, **110**, 4122.

54. H. Weingärtner, *Angew. Chem., Int. Ed.*, 2008, **47**, 654-670.

55. A. A. Lee, D. Vella, S. Perkin and A. Goriely, *J. Phys. Chem. Lett.*, 2015, **6**, 159-163.

4. Electrolysis of TEMPO-mediated alcohol oxidations in RTILs

4.1. Introduction

The investigations conducted in chapter 3 gave an insight into the electrochemical properties of TEMPO-mediated alcohol oxidations in RTILs, which could be used as a guide for the development and optimisation of alcohol oxidations in RTILs at a preparative scale. Examples of bulk electrolysis of TEMPO-mediated alcohol oxidations exist both on laboratory scales[1-5] and at industrial scale,[6, 7] however these often have differing designs of electrochemical cells with varying performances.

In laboratories the typical set-up is either a divided or undivided beaker cell with carbon, graphite or platinum type material as the working electrode and a platinum or steel based material as the counter electrode.[5] For example, the electrolysis set-up used by Stahl and co-workers constituted an undivided cell with a hollow tube and a centralized rod of steel as the anode and an array of graphite rods as the cathode.[5] Doherty and co-workers performed TEMPO-mediated alcohol oxidations in an RTIL medium using a divided cell fitted with a fritted glass, with platinum grids as both the anode and cathode. Highly efficient electrolyses were achieved for a range of alcohols, demonstrating the applicability of RTILs in preparative scale electrolysis.[1, 2, 8]

Due to the generally high viscosity of RTILs, it is important to use or design an electrolysis cell which can maximise mass transport rates to and from electrode surfaces, in order to obtain good performance of the electrolysis in RTIL media.[9] Conducting the electrolyses in an electrochemical flow through cell that accommodate viscous RTIL media, could significantly increase the mass transport rates and therefore minimise the effect of the RTIL viscosity on the electrolysis performance. Recently, Ammonite flow electrolysis cells have become available. The Ammonite8 cell gives high conversions with flow rates of up to 3 cm^3 min^{-1}, allowing product formation at a rate of > 1 g hr^{-1} and Brown and co-workers used the Ammonite8 cell for the successful electrolysis of TEMPO-mediated oxidation of a range of alcohols in aqueous media.[10, 11] The use of such flow system may be beneficial in terms of improving mass transfer rates when conducting TEMPO-mediated alcohol oxidations in RTIL media.

In this chapter, flow and non-flow cells are investigated for the development of TEMPO-mediated alcohol oxidations in RTIL media at preparative scale. The electrochemical conditions, such as applied currents, reaction media and varying flow rates are explored in order to achieve electrolyses with optimum performance, in terms of high rates of conversion, fast electrolysis and high faradaic selectivity.

4.2. Results and Discussion

4.2.1. Bulk Electrolysis

The initial set-up used for bulk electrolysis in this project is shown in Figure 4.1. This set-up constitutes a reticulated vitreous carbon electrode as the working electrode, a platinum flag as the counter electrode and a silver wire as the quasi-reference electrode.

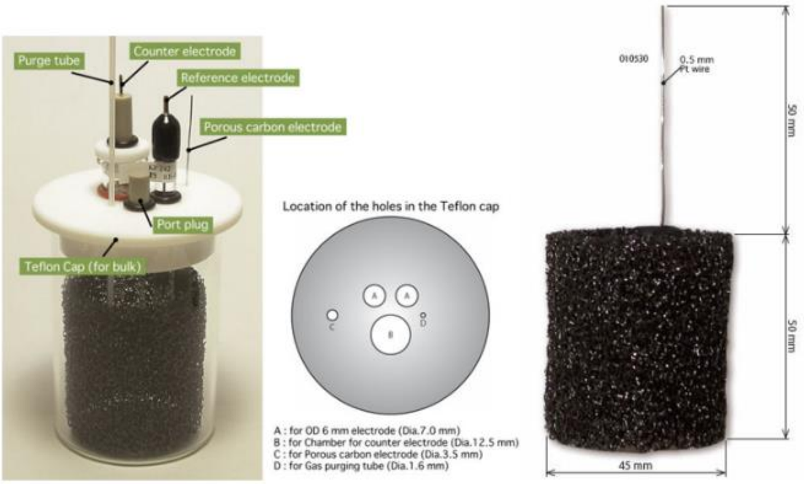

Figure 4.1: Set-up used for bulk electrolysis of the TEMPO-mediated alcohol oxidations in ILs.

For most of the examples of TEMPO-mediated alcohol oxidation electrolysis, water reduction is chosen for the counter-electrode reaction. The H_2 gas formed from the water reduction is considered to be a convenient and 'clean' counter electrode reaction, as it escapes the reaction mixture, and will therefore not contaminate the products.[2, 5, 10, 12] The counter electrode was, however, separated from the anolyte solution using a glass frit, as to prevent any possible by-products generated at the counter electrode from contaminating the anolyte solution and preventing reagents and products to be reduced at the counter electrode.[1, 4] Similar conditions and concentrations of materials used by Doherty and co-workers in their TEMPO-mediated alcohol oxidation bulk electrolyses were used as a guide for the electrolyses conducted in this study.[1] In the cathode compartment with the counter electrode, the catholyte solution consisted of a 10 cm^3 mixture of 4 cm^3 RTIL, 1 cm^3 water and 5 cm^3 acetonitrile, which allowed for the reduction of water at the counter electrode producing H_2 gas and OH^-. Thus, the protonated base crosses the frit and reacts with OH^- to form water and the base. The anolyte compartment constituted of a 10 cm^3 solution of 0.6 mol dm^{-3} benzyl alcohol, 0.06 mol dm^{-3} TEMPO and 2.4 mol dm^{-3} 2,6-lutidine dissolved in a RTIL. The anode and cathode reactions along with the overall alcohol oxidation is shown in Scheme 4.1.

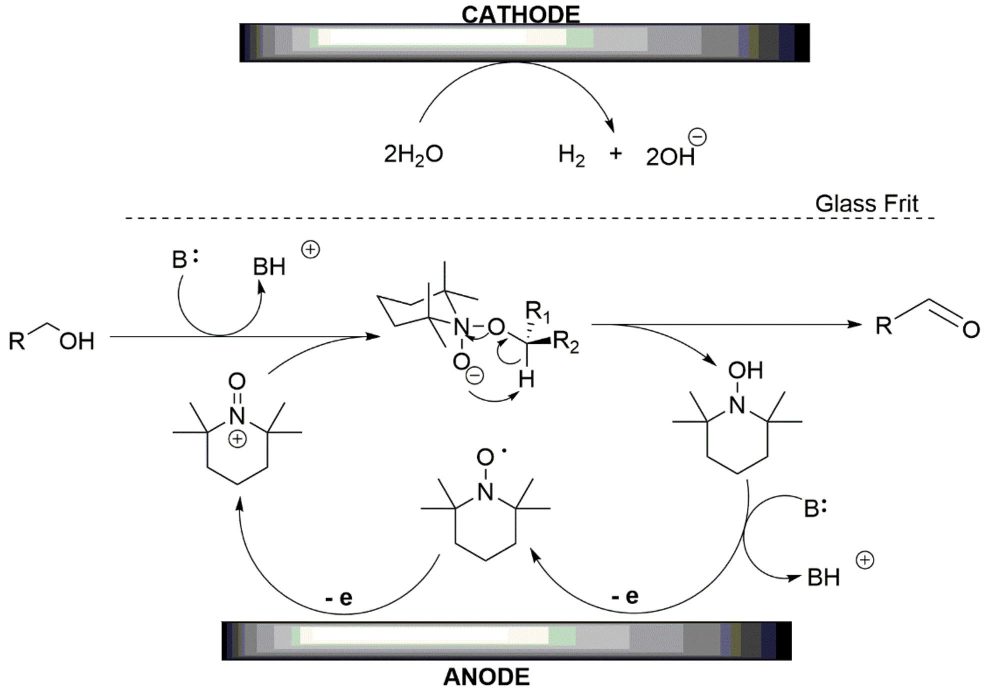

Scheme 4.1: Bulk electrolysis of TEMPO-mediated alcohol oxidation in a divided cell (anolyte and catholyte solutions are separated by a glass frit), where TEMPO is oxidised and regenerated at the reticulated vitreous carbon anode and water is reduced at the platinum flag cathode.

Initially the electrolysis was conducted with current control with low currents of 8-10 mA. Both the substrates and products, as well as potential by-products, were monitored periodically during electrolyses with GC-MS analysis. The electrolysis of benzyl alcohol in $[C_8C_1Im][NTf_2]$ at 10 mA yielded very stable potentials of around 0.6 V (vs. Ag QRE). After 5 hours of electrolysis at constant current of 10 mA, approximately 7% conversion of benzyl alcohol to benzaldehyde was observed. This low conversion is, however, unsurprising. Full conversion of reactants into products in an electrolysis is dependent on passing a large enough charge through the cell and for enough time. The cell current required for full conversion was determined by using Faraday's law (Equation 2.4).[13] For a 20 cm^3 solution with 0.6 mol dm^{-3} of alcohol, there will be 0.012 mol of alcohol, which requires 0.024 mol of electrons to be exchanged at the electrodes (each catalytic cycle in the TEMPO mediated alcohol oxidation needs 2 electrons). This means that by flowing 10 mA to the solution, this conversion should take 64 hours for the complete conversion. After 5 hours of electrolysis with an applied current of 10 mA, a 7.7% conversion is expected which is similar to the conversion obtained from the GC-MS analysis. Thus, a longer electrolysis time is needed for a higher conversion at an applied current of 10 mA, however with longer electrolysis time the possibilities of side reactions to occur also increases.[4]

The applied current was then increased to 50 mA in order to reduce the electrolysis time to 13 hrs for full conversion. However, with this increase in applied current, the measured potential of the system began shifting to higher potentials (2-4 V). The electrolysis was monitored for 37 hours with GC-MS analysis. There was an increase in conversion from benzyl alcohol to benzaldehyde up to an electrolysis time of 20 hrs and a maximum of 60% conversion was observed. There was also a clear depletion of TEMPO with time. In addition, the colour of the solution changed after 20 hrs of electrolysis, from a light orange coloured solution to a dark brown coloured solution. Previous studies have observed that the imidazolium cation is susceptible to oxidation to an imidazole radical species,[14, 15] which could be a competing reaction in the electrolysis. Considering that TEMPO is known to scavenge carbon-centred radicals,[16] if any imidazole radical is formed it will react with TEMPO, which would explain the loss of TEMPO.

The electrolysis was repeated with different currents, with potential control (at 0.3 V vs $E_{T,½}$), and the electrolysis was left for different lengths of time. However, the electrolyses only achieved conversions to benzaldehyde no higher than 50%. Similar responses were observed as different RTILs, including $[C_8C_1Im][OTf]$, $[C_8C_1Im][DCA]$, $[C_8C_1Im][PF_6]$, $[C_2C_1Im][NTf_2]$ and $[N_{4,4,4,1}][NTf_2]$, were used. In the TEMPO-mediated alcohol oxidation involving a 2 e^- oxidation, a 0.6 mol dm^{-3} solution of alcohol will result in a product solution with 1.2 mol dm^{-3} of protons. Efficient charge transport across the frit to the catholyte, where OH^- is formed, is needed to prevent a build-up of protons in the anolyte solutions which could cause side-reactions to occur. Another factor to consider is the size of the counter electrode- its active area needs to be larger than that of the anode, to reach a current limitation due to the anodic reaction.[12, 17, 18] The cathode compartment used in the set-up, shown in Figure 4.1, was replaced by a cathode cell which has a frit with larger surface area and a larger platinum counter electrode than the previously used counter electrode, see Figure 4.2.

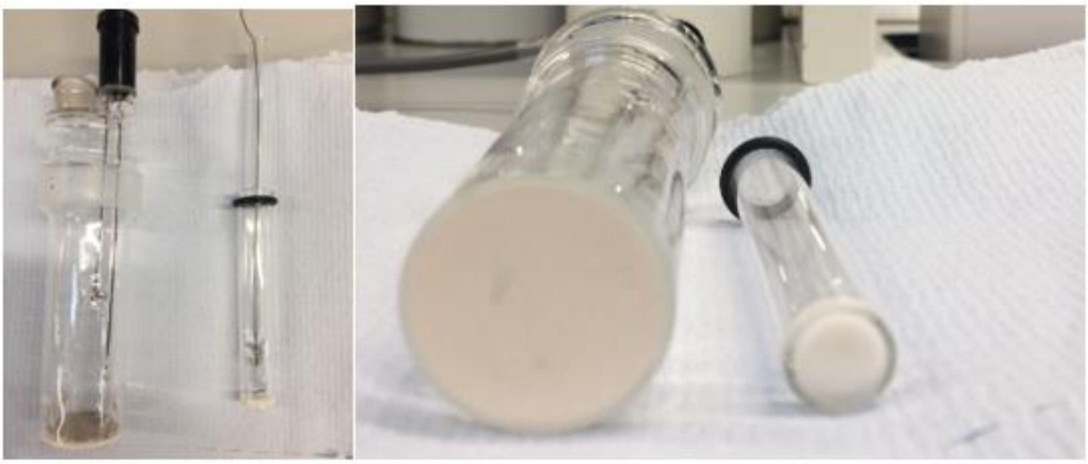

Figure 4.2: Larger cathode cell (to the left) and the glass frit with the platinum flag (to the right) that were used for the TEMPO-mediated alcohol oxidations.

Using the larger cathode cell, for the electrolysis of 0.6 mol dm^{-3} benzyl alcohol in [C_8C_1Im][NTf_2] with a constant current of 100 mA, a 91% conversion was obtained after 9 hrs of electrolysis. No apparent loss of TEMPO was observed in the GC-MS analysis. The electrolysis of benzyl alcohol was repeated in [C_8C_1Pyrr][NTf_2] and in [C_8C_1Im][DCA], and a 100% conversion of the alcohol was observed after 6.5 hrs of electrolysis, and about 95% conversion after 5.5 hours of electrolysis respectively. It is likely that the larger frit allowed better transfer of charges and protonated base, lowering the build-up of protonated base in the anolyte cell and potentially lowering the possibility of side-reactions to occur.

However, the success of the new electrolysis set-up was short-lived. The electrolyses were repeated in the [C_8C_1Im][NTf_2] and [C_8C_1Im][DCA] media but the potential shifted to higher potentials minutes after the electrolysis was started, TEMPO depletion was observed in the GC-MS analysis and the solutions changed colour from light orange to dark brown. This was believed to be due to the frit being blocked. While the frit was cleaned with aqua regia and burnt, no improvements were made in the electrolysis performance.

An undivided electrolysis set-up was then tested. The counter electrode (platinum grid) was submerged directly in the reaction solution and with 1 cm^3 of water added directly to the ‘anolyte’ solution. At 100 mA, the voltage response recorded was relatively stable. However, after about 4 hrs of electrolysis, the potential started to drift to higher potentials and a loss of TEMPO was observed in the GC-MS analysis. It is worth noting that with the undivided set-up it was difficult to ensure good stirring of the solution and at the same time making sure that the counter electrode did not get into contact with the working electrode. A better set-up was needed to perform the electrolysis in an undivided cell.

Clearly, good performance in a beaker cell requires efficient electrochemical reaction at both the working and counter electrodes, which subsequently require efficient transfer across the separator and high mass transfer rates to and from electrodes. The residence time of reactant and product in beaker electrolysis cells is typically hours and long electrolysis increases the possibility for degradation of performance due to slow homogenous side-reactions. In flow cells, on the other hand, the residence time in the cell is determined by the flow rate of reactant solution and is generally less than a few minutes. This significantly decreases the opportunity for unwanted competing chemistry.[17] In the following section the electrolysis performance of TEMPO-mediated alcohol oxidations in RTIL media is investigated using a flow electrochemical cell.

4.2.2. Flow Electrolysis

The extended channel flow electrolysis cell used in this study was an Ammonite8 cell developed by Cambridge Reactor Design, see Figure 4.3. The electrodes are composed of a carbon/PDVF polymer composite anode and stainless steel for the cathode, with the channel making up a volume of 1 cm^3.[3]

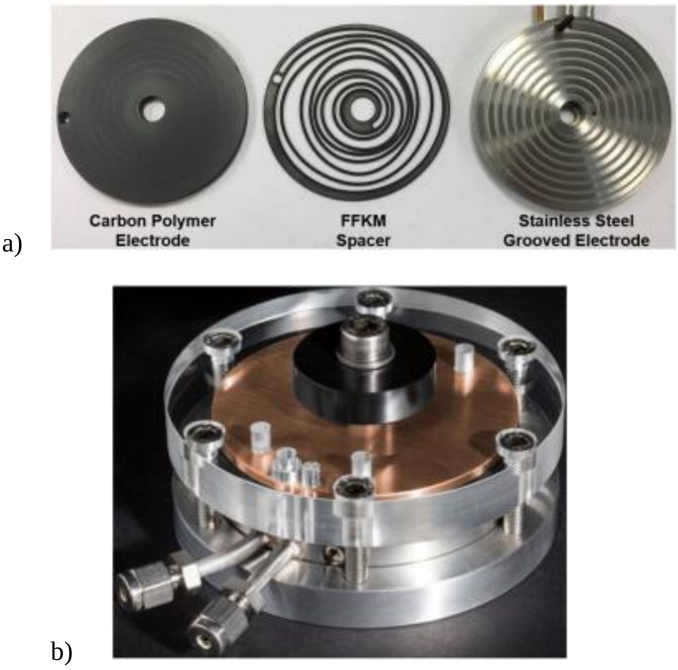

Figure 4.3: Ammonite8 flow electrolysis cell with spiral solution channel, a) the key components and b) the complete cell.[3]

The Ammonite8 cell is an undivided electrolysis cell and so water was added directly to the reaction mixture, for the water reduction at the counter electrode to occur. Although the Ammonite8 cell is a more 'closed' system compared to a beaker cell, the hydrogen evolution during electrolysis in the Ammonite cell does not block the flow cell, but it has previously been shown that the H_2 evolution improves the mass transfer of reactants in the cell and consequently improving the faradaic selectivity of TEMPO-mediated alcohol oxidations and overall electrolysis performance. The electrogenerated H_2 gas bubbles introduce turbulence along the channel, which increases the transfer of reagents to the electrodes. The H_2 evolution also increases the linear flow rate of solution.[19]

Similar electrolysis conditions, including alcohol and TEMPO concentrations that were used by Brown and co-workers in their flow electrolyses of TEMPO-mediated alcohol oxidations were used as a guide for the flow electrolyses in this study.[10, 11] The general procedure for the flow electrolysis of the TEMPO-mediated alcohol oxidation was: 5 cm^3 reaction mixture consisting of 0.2 mol dm^{-3} of alcohol, 2.4 mol dm^{-3} of 2,6-lutidine, 0.06 mol dm^{-3} TEMPO and 0.4 mol dm^{-3} tert-butylbenzene (as the internal standard for GC-FID analysis) in a RTIL. 1 cm^3 ultrapure water was then added to the reaction mixture. Since some of the RTILs are immiscible with water (e.g. $[NTf_2]^-$ based RTILs), the RTIL reaction mixture and water was mixed thoroughly to create an emulsion prior to introducing the mixture to the ammonite cell. Products emanating from the flow cell were recovered from the reaction mixture by solvent extraction into toluene and analysed using GC-FID analysis (see Appendix B.3).

In the following sections, the performance of TEMPO-mediated alcohol oxidations are investigated in terms of the applied current density, the flow rates, type of alcohol substrate (e.g. primary or secondary) and the reaction media.

4.2.2.1. Flow electrolysis conditions: Current Density

Figure 4.4 shows flow electrolysis data for TEMPO-mediated oxidation of benzyl alcohol to benzaldehyde in [C_8C_1Im][NTf_2] with varying applied current densities.

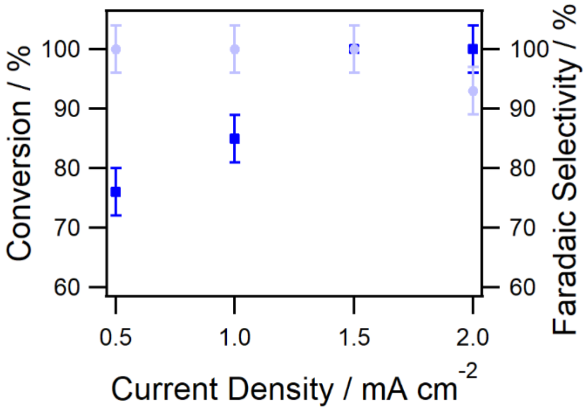

Figure 4.4: Measured conversions (blue squares) and faradaic selectivity (light blue dots) of flow electrolysis of solutions containing 0.2 mol dm^{-3} of benzyl alcohol, 2.4 mol dm^{-3} of 2,6-lutidine, 0.06 mol dm^{-3} TEMPO and 0.4 mol dm^{-3} tert-butylbenzene in [C_8C_1Im][NTf_2] using different applied current densities and a constant flow rate of 0.05 cm^3 min^{-1}. Conversions were determined by using GC-FID analysis and calibration curves of benzyl alcohol. Faradaic selectivity is based on concentration of unreacted benzyl alcohol and concentration of benzaldehyde (derived from calibration curves).

In order to achieve full conversion in a single pass, a large enough charge must be passed through the cell to convert all of the alcohol in the cell before it leaves the cell. The minimum cell current density required to convert all the alcohol in the reaction mixture, using an appropriate flow rate, can be determined using Faraday's law (Equation 2.6). For a 100% conversion of a reaction mixture containing 0.2 mol dm^{-3} alcohol and using a flow rate of 0.05 cm^3 min^{-1}, an applied current density of 1.6 mA cm^{-2} is required.[19]

If the applied current density is lower than 1.6 mA cm^{-2}, full conversion is not expected and if the current density is higher than 1.6 mA cm^{-2}, then a competing reaction might occur, e.g. degradation of solvent or overoxidation of product, resulting in side-products in the outlet stream.[19] As predicted, at current densities below the minimum cell current for full conversion (< 1.6 mA cm^{-2}), conversions of only 76-85% are observed in Figure 4.4. Furthermore, the faradaic selectivity decreases from 100% to 93% at the highest used current density of 2.0 mA cm^{-2}, indicating that there are competing reactions at higher current densities. Interestingly, the conversions are higher than predicted by Equation 2.6. For example, when using an applied current density of 0.5 mA cm^{-2} with a flow rate of 0.05 cm^3 min^{-1}, the predicted conversion of alcohol is 31%, which is much lower than the measured 76% conversion. This increase in performance of electrolysis has previously been observed in aqueous systems by Brown and co-workers and is believed to be due to the increased mass transfer in the channel as a result of H_2 gas bubbles forming.[3, 19]

4.2.2.2. Flow Electrolysis Conditions: Flow rates

Figure 4.5 shows electrolysis data of the oxidation of benzyl alcohol with an applied current of 1.5 mA cm^{-2} with varying flow rates.

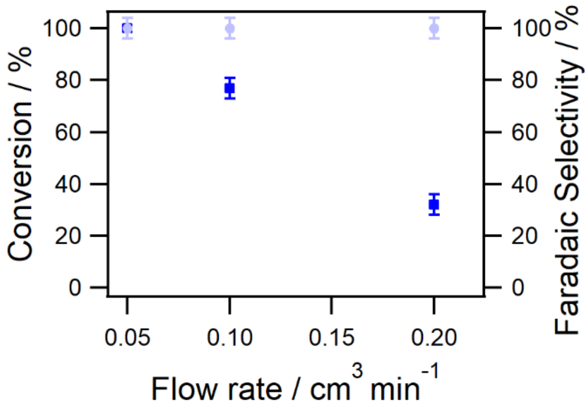

Figure 4.5: Measured conversions (blue squares) and faradaic selectivity (light blue dots) of flow electrolysis of solutions containing 0.2 mol dm^{-3} of benzyl alcohol, 2.4 mol dm^{-3} of 2,6-lutidine, 0.06 mol dm^{-3} TEMPO and 0.4 mol dm^{-3} tert-butylbenzene in [C_8C_1Im][NTf_2] using different flow rates at a constant applied current density of 1.5 mA cm^{-2}. Conversions were determined by using GC-FID analysis and calibration curves of benzyl alcohol. Faradaic selectivity is based on concentration of unreacted benzyl alcohol and concentration of benzaldehyde (derived from calibration curve).

A 100% conversion of benzyl alcohol is achieved at the slowest flow rate (0.05 cm^3 min^{-1}) and the conversions decrease as the flow rate increases. By increasing the flow rate, the residence time of the reaction mixture in the cell is decreased. With shorter residence time of the reaction mixture in the cell, a higher charge (and hence current) is needed for full conversion.[3, 19] Again, the conversions are greater than predicted by Equation 2.6, which is likely to be a result of perturbation due to H_2 gas bubble formation at the counter electrode.[19]

Figure 4.6 shows electrolysis data of TEMPO-mediated oxidation of benzyl alcohol in [C_8C_1Im][NTf_2] at a flow rate of 0.02 cm^3 min^{-1} and varying applied currents.

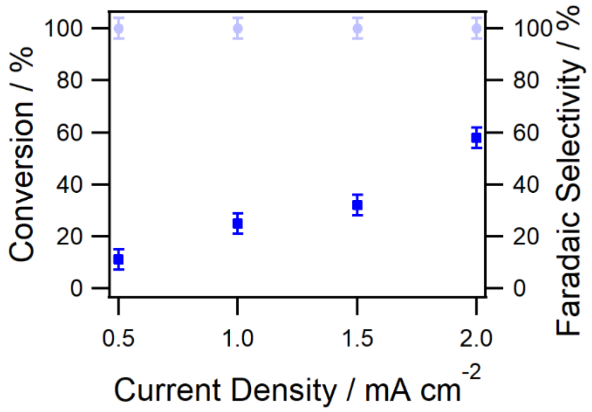

Figure 4.6: Measured conversions (blue squares) and faradaic selectivity (light blue dots) of flow electrolysis of solutions containing of 0.2 mol dm^{-3} of benzyl alcohol, 2.4 mol dm^{-3} of 2,6-lutidine, 0.06 mol dm^{-3} TEMPO and 0.4 mol dm^{-3} tert-butylbenzene in [C_8C_1Im][NTf_2] using a constant flow rate of 0.2 cm^3 min^{-1} and varying applied current densities. Conversions were determined by using GC-FID and calibration curves of benzyl alcohol. Faradaic selectivity is based on concentration of unreacted benzyl alcohol and concentration of benzaldehyde (derived from calibration curve).

The conversion of benzyl alcohol increases as the current is increased at a flow rate of 0.2 cm^3 min^{-1} with good faradaic selectivity. However, the conversions of benzyl alcohol are relatively low compared to when a flow rate of 0.05 cm^3 min^{-1} is used (see Figure 4.4).

From the above results, it can be concluded that the best conversions and faradaic selectivities for TEMPO-mediated oxidation of a mixture consisting of a 5 cm^3 solution of 0.2 mol dm^{-3} benzyl alcohol, 2.4 mol dm^{-3} 2,6-lutidine and 0.06 mol dm^{-3} TEMPO in [C_8C_1Im][NTf_2] and 1 cm^3 ultrapure water are obtained with a flow rate of 0.05 cm^3 min^{-1} with an applied current density of 1.5 mA cm^{-2}.

4.2.2.3. *Flow Electrolysis Conditions: Oxidation of Secondary Alcohols*

The electrolysis of the oxidation of 1-phenylethanol to acetophenone was investigated. Figure 4.7 shows the measured conversions of 1-phenylethanol and faradaic selectivity when performing the flow electrolysis of a mixture consisting of 5 cm^3 solution of 0.2 mol dm^{-3} 1-phenylethanol, 2.4 mol dm^{-3} 2,6-lutidine and 0.06 mol dm^{-3} TEMPO in $[C_8C_1Im][NTf_2]$ and 1 cm^3 ultrapure water.

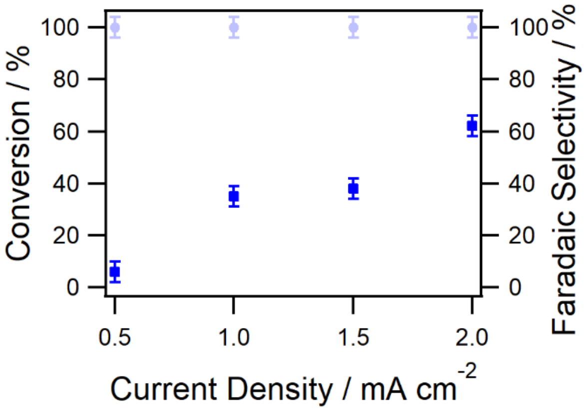

Figure 4.7: Measured conversions (blue squares) and faradaic selectivities (light blue dots) of flow electrolysis of solutions containing 0.2 mol dm^{-3} of 1-phenylethanol, 2.4 mol dm^{-3} of 2,6-lutidine, 0.06 mol dm^{-3} TEMPO and 0.4 mol dm^{-3} tert-butylbenzene in $[C_8C_1Im][NTf_2]$ using a flow rate of 0.05 cm^3 min^{-1} and different applied current densities. Conversions were determined by using GC-FID analysis and calibration curves of 1-phenylethanol. Faradaic selectivity is based on concentration of unreacted 1-phenylethanol and acetophenone (derived from calibration curve).

Both the conversions and faradaic selectivities of the electrooxidation of 1-phenylethanol are lower compared to the electrooxidation of its primary alcohol analogue- benzyl alcohol (see Figure 4.4). As discussed in chapter 3, *k* for the oxidation of secondary alcohols is lower than *k* for the oxidation of primary alcohols, which is reflected in the conversions obtained in the electrolysis of 1-phenylethanol and benzyl alcohol. This is due to a higher degree of steric hindrance of secondary alcohols compared to primary alcohols, which makes the formation of the intermediate between the alcohol and the oxoammonium cation less favourable with secondary alcohols and the rate of conversion is therefore lower for secondary alcohols.

The slightly lower faradaic conversions of the electrolysis of 1-phenylethanol compared to benzyl alcohol could also be a result of the lower rate of reaction of 1-phenylethanol oxidation. If the rate of oxidation is comparatively slow with the mass transport of the species in the solution, then the chemical reaction will not be able to consume the charge fast enough and other side-reactions are likely to occur instead.[12, 13, 20, 21] The rate of the chemical reaction and thus k is therefore important to consider in order to achieve clean electrosynthesis. In chapter 3, it was shown that k is dependent on the RTIL media, and in particular on β of the RTIL media. Thus in the following sections, the performance of the electrolysis in an RTIL with a higher β, such as [C_8C_1Im][DCA] is investigated.

4.2.2.4. Flow Electrolysis Conditions: RTIL media

Figure 4.8 compares flow electrolysis data for the oxidation of benzyl alcohol in [C_8C_1Im][NTf_2] and [C_8C_1Im][DCA] when applying different current densities.

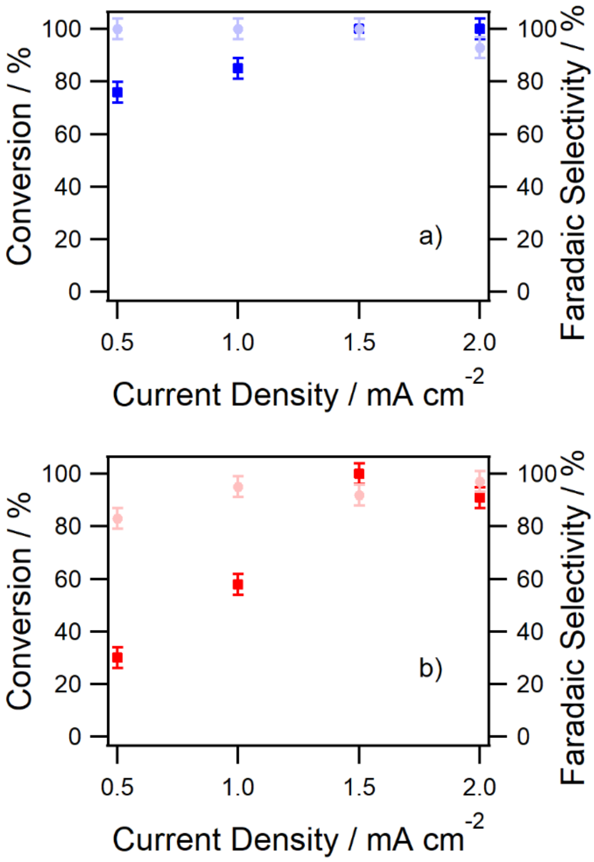

Figure 4.8: Measured conversions (squares) and faradic selectivities (dots) of flow electrolysis of solutions containing 0.2 mol dm^{-3} of benzyl alcohol, 2.4 mol dm^{-3} of 2,6-lutidine, 0.06 mol dm^{-3} TEMPO and 0.4 mol dm^{-3} tert-butylbenzene in a) [C_8C_1Im][NTf_2] (blue squares for conversions and light blue dots for selectivities) and b) [C_8C_1Im][DCA] (red squares for conversions and light red dots for selectivities) using a flow rate of 0.05 cm^3 min^{-1} and different applied current densities. Conversions were determined by using GC-FID analysis and calibration curves of benzyl alcohol. Faradaic selectivity is based on concentration of unreacted benzyl alcohol and concentration of benzaldehyde (derived from calibration curve).

Overall, better conversion and faradaic selectivities are observed when the reaction is performed in [C_8C_1Im][NTf_2] than when performed in [C_8C_1Im][DCA]. The differences in performance is likely to be due to a combination of faster mass transfer and reaction rates in [C_8C_1Im][NTf_2] (D_A

and k in $[C_8C_1Im][NTf_2]$ and $[C_8C_1Im][DCA]$ are shown in Table A1 and Table A5 in the Appendix, respectively). The lower faradaic selectivities when $[C_8C_1Im][DCA]$ is used as the reaction medium suggest that competing reactions occur in $[C_8C_1Im][DCA]$ even when low current densities are applied (< 1.6 mA cm^{-2}).

Electrolysis of a mixture of a primary and a secondary alcohol was then conducted to investigate the alcohol selectivities of TEMPO in RTIL media (Scheme 4.2). Table 4.1 shows flow electrolysis data for the oxidation of two RTIL reaction mixtures consisting of 0.1 mol dm^{-3} benzyl alcohol, 0.1 mol dm^{-3} 1-phenylethanol, 2.4 mol dm^{-3} 2,6-lutidine and 0.06 mol dm^{-3} TEMPO in $[C_8C_1Im][NTf_2]$ and $[C_8C_1Im][DCA]$.

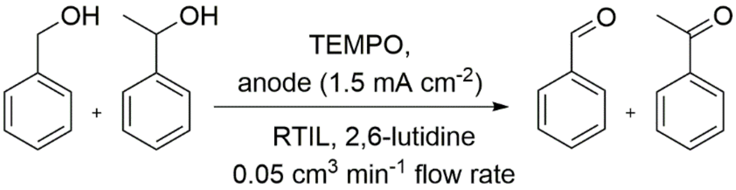

Scheme 4.2: Oxidation of benzyl alcohol and 1-phenylethanol to benzaldehyde and acetophenone, respectively.

Table 4.1: Measured conversions and alcohol selectivities of the flow TEMPO-mediated electrooxidation of a mixture consisting of 0.1 mol dm^{-3} benzyl alcohol, 0.1 mol dm^{-3} phenylethanol, 0.06 mol dm^{-3} TEMPO, 2.4 mol dm^{-3} 2,6-lutidine and 1 cm^3 water in $[C_8C_1Im][NTf_2]$ and $[C_8C_1Im][DCA]$ with a constant flow rate of 0.05 cm^3 min^{-1}.

Ionic Liquid	Conversion of benzyl alcohol[a] / %	Conversion of 1-phenylethanol[a] / %	Reaction selectivity of benzyl alcohol[b] / %
$[C_8C_1Im][NTf_2]$	96	16	83
$[C_8C_1Im][DCA]$	100	39	61

[a]Conversions were determined by using GC-FID analysis and calibration curves of benzyl alcohol, phenylethanol, benzaldehyde and acetophenone. [b]Alcohol selectivity of TEMPO-mediated alcohol oxidations.

A clear selectivity towards primary alcohols is observed, and the best selectivity is observed when the electrolysis is performed in [C_8C_1Im][NTf_2]. The selectivity is poorer when the electrolysis is performed in [C_8C_1Im][DCA]. This is in agreement with the voltammetry studies conducted in chapter 3, where it was shown, through *k*, that the [C_8C_1Im][NTf_2]/TEMPO system is more kinetically selective than the [C_8C_1Im][DCA]/TEMPO system in the oxidation of different alcohols.

4.2.3. Comparing Acetonitrile-Electrolyte Systems with RTILs

To investigate how the efficiency of the TEMPO-mediated alcohol oxidations in RTILs compares to that of alcohol oxidations in acetonitrile, flow electrolysis of benzyl alcohol oxidation was conducted in solutions of acetonitrile containing 1 mol dm^{-3} [C_8C_1Im][NTf_2] and 0.05 mol dm^{-3} [C_8C_1Im][NTf_2]. The conversions of benzyl alcohol and faradaic selectivities of the electrolysis of the TEMPO mediated oxidation of benzyl alcohol are shown in Figure 4.9.

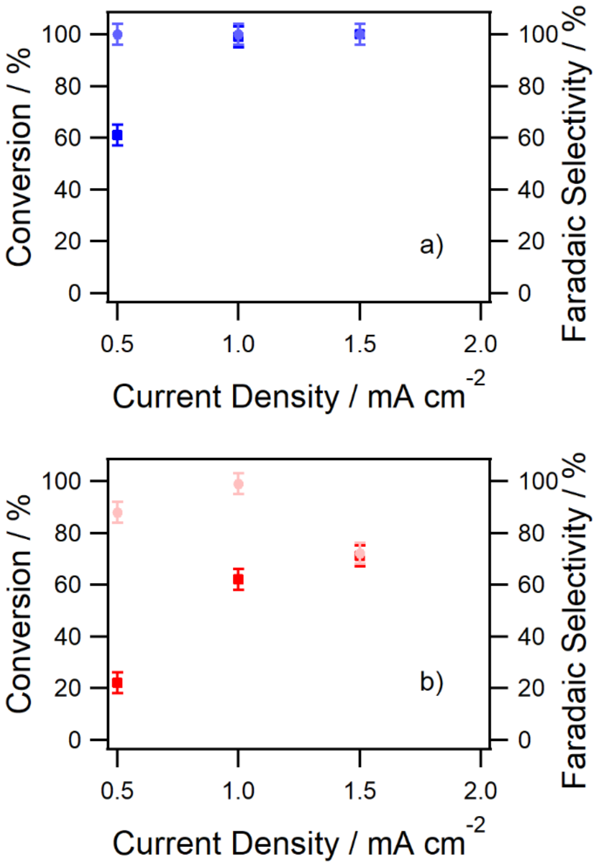

Figure 4.9: Measured conversions (squares) and faradaic selectivity (dots) of flow electrolysis of solutions containing 0.2 mol dm^{-3} of benzyl alcohol, 2.4 mol dm^{-3} of 2,6-lutidine, 0.06 mol dm^{-3} TEMPO and 0.4 mol dm^{-3} tert-butylbenzene in acetonitrile with a) 1 mol dm^{-3} $[C_8C_1Im][NTf_2]$ (blue squares for conversions and light blue dots for selectivities) and b) 0.05 mol dm^{-3} (red squares for conversions and light red dots for selectivities) using a constant flow rate of 0.05 cm^3 min^{-1} and different applied current densities. Conversions were determined by using GC-FID analysis and calibration curves of benzyl alcohol. Faradaic selectivity is based on concentration of unreacted benzyl alcohol and concentration of benzaldehyde (derived from calibration curve).

Despite the fact that $[C_8C_1Im][NTf_2]$ is more viscous than acetonitrile, the conversions are similar or only slightly lower (see Figure 4.4) than when the oxidation is performed in acetonitrile media containing either 0.05 mol

dm^{-3} or 1 mol dm^{-3} $[C_8C_1Im][NTf_2]$ (D_A in acetonitrile is $17.1 \times 10^{-10} \pm 0.5 \times 10^{-10}$ m^2 s^{-1}).

As shown in chapter 3, k of TEMPO-mediated oxidation of benzyl alcohol in $[C_8C_1Im][NTf_2]$ (0.336 dm^3 mol^{-1} s^{-1}) is significantly greater than k in a solution of 1 mol dm^{-3} $[C_8C_1Im][NTf_2]$ in acetonitrile (0.04 dm^3 mol^{-1} s^{-1}). The higher k in $[C_8C_1Im][NTf_2]$ seems to compensate for the slower mass transfer and results in comparative conversion as when the oxidation is performed in acetonitrile. This observation demonstrates the viability of replacing volatile organic solvents and electrolyte systems with RTILs as the media for TEMPO-mediated alcohol oxidations without the loss of efficiency of the reaction due to slower mass transfer.

Interestingly, from cyclic voltammetry studies summarised in Section 3.2.5., it was observed that k increased as the concentration of the electrolyte is decreased (see Figure 3.33) and k was calculated to be 0.272 dm^3 mol^{-1} s^{-1} for the solution containing 0.05 mol dm^{-3} $[C_8C_1Im][NTf_2]$ in acetonitrile. Thus, it would be expected that higher conversions would be obtained from solution containing 0.05 mol dm^{-3} $[C_8C_1Im][NTf_2]$ than the system with 1 mol dm^{-3} $[C_8C_1Im][NTf_2]$. Considering the observed lower faradaic selectivities for the solution containing 0.05 mol dm^{-3} $[C_8C_1Im][NTf_2]$, it is possible that this electrolyte loading is insufficient to ensure high conductivity in the cell. Poor conductivities in a solution could lead to both lower faradaic selectivities and lower conversions.[22]

The alcohol selectivity in the acetonitrile media was also compared with the $[C_8C_1Im][NTf_2]$ and the $[C_8C_1Im][DCA]$ media. The flow electrolyses data for the oxidation of a mixture of benzyl alcohol (blue bars) and 1-phenylethanol (red bars) are summarised in Figure 4.10.

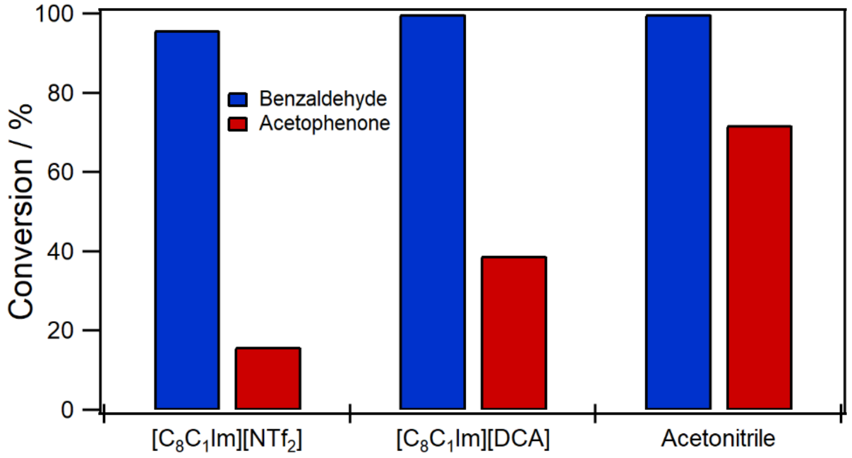

Figure 4.10: Measured conversions of benzyl alcohol (blue bars) and conversions of 1-phenylethanol (red bars) of the flow TEMPO-mediated electrooxidation of three mixtures consisting of 0.1 mol dm^{-3} benzyl alcohol, 0.1 mol dm^{-3} 1-phenylethanol, 0.06 mol dm^{-3} TEMPO, 2.4 mol dm^{-3} 2,6-lutidine and 1 cm^{3} water in $[C_8C_1Im][NTf_2]$, $[C_8C_1Im][DCA]$ and acetonitrile (with 1 mol dm^{-3} $[C_8C_1Im][NT_2]$ as the electrolyte) at a constant flow rate of 0.05 cm^{3} min^{-1} and with an applied current density of 1.5 mA cm^{-2}. Conversion were determined by using GC-FID analysis and calibration curves of benzyl alcohol and 1-phenylethanol.

The alcohol selectivity was very poor when the alcohol oxidation was performed in acetonitrile containing 1 mol dm^{-3} $[C_8C_1Im][NTf_2]$. In previous studies, it has been demonstrated that, despite the slower chemistry, secondary alcohols are oxidised efficiently with excellent conversions using the same conditions as for oxidation of the primary alcohol analogue. For example, Brown and co-workers demonstrated that the electrolysis of the primary alcohol 4-methoxybenzyl alcohol yielded 4-methoxybenzaldehyde with an 88% yield and electrolysis of the secondary alcohol analogue 1-(4-methoxyphenyl)ethanol yielded 92% of 1-(4-methoxyphenyl)ethanone, under the same conditions.[10] Stahl and co-workers showed that the TEMPO modified 4-acetamido-TEMPO, electrooxidation of benzyl alcohol and 1-phenylethanol yielded 88% of benzaldehyde and 88% acetophenone respectively (in two separate experiments) using identical conditions and electrolysis time.[5] These results show good reaction efficiency of oxidation secondary alcohols, however which consequently results in poor alcohol selectivity of TEMPO.

4.3. Conclusion

In this chapter, a beaker and a flow electrolysis cell were used to conduct the electrolysis of TEMPO-mediated alcohol oxidations in RTIL media. A direct comparison of the two types of cells is difficult due to the significant differences of the cell design and electrolysis conditions. With the divided beaker cell, however, it was clear that efficient transport of ions across the separator is essential for successful electrolyses. In addition, with electrolysis in beaker cells, the residence time of reactant and product in the cell is usually hours and this gives rise to the possibility for poor electrolysis performance due to slow homogenous reactions. In microflow cells, such as the Ammonite8, the residence time in the cell is determined by the flow rate of reactant solution and it is generally only a few minutes. This significantly decreases the opportunity for unwanted competing chemistry.[17]

Efficient and convenient electrolysis of TEMPO-mediated alcohol oxidations in RTIL media was achieved using flow electrolysis. The above results of the flow electrolyses not only demonstrates the possibility of substituting volatile organic solvent and electrolyte systems with the more electrochemically stable and non-volatile RTILs in TEMPO-mediated alcohol oxidations but also demonstrates the enhanced alcohol selectivity when RTILs are used as the media. Furthermore, it was confirmed that the voltammetry analyses discussed in chapter 3 can be used to support and guide the development of preparative-scale TEMPO-mediated alcohol oxidations in RTILs in that RTIL media with low β, such as $[NTf_2]^-$ based RTILs showed to be particularly advantageous in terms of the selectivity and the efficiency of the alcohol oxidation.

4.4. References

1. R. Barhdadi, C. Comminges, A. P. Doherty, J. Y. Nédélec, S. O'Toole and M. Troupel, *J. Appl. Electrochem.*, 2007, **37**, 723-728.

2. C. Comminges, R. Barhdadi, A. P. Doherty, S. O'Toole and M. Troupel, *J. Phys. Chem. A*, 2008, **112**, 7848-7855.

3. R. A. Green, R. C. D. Brown, D. Pletcher and B. Harji, *Electrochem. Commun.*, 2016, **73**, 63-66.

4. A. C. Herath and J. Y. Becker, *Electrochim. Acta*, 2008, **53**, 4324-4330.

5. M. Rafiee, K. C. Miles and S. S. Stahl, *J. Am. Chem. Soc.*, 2015, **137**, 14751-14757.

6. R. Ciriminna, M. Ghahremani, B. Karimi and M. Pagliaro, *ChemistryOpen*, 2017, **6**, 5-10.

7. *US Pat.*, WO/2006/105357, 2006.

8. F. Raynal, R. Barhdadi, J. Périchon, A. Savall and M. Troupel, *Adv. Synth. Catal.*, 2002, **344**, 45-49.

9. A. P. Doherty, *Curr. Opin. Electrochem.*, 2018, **7**, 61-65.

10. J. T. Hill-Cousins, J. Kuleshova, R. A. Green, P. R. Birkin, D. Pletcher, T. J. Underwood, S. G. Leach and R. C. Brown, *ChemSusChem*, 2012, **5**, 326-331.

11. D. Pletcher, R. A. Green and R. C. D. Brown, *Chem. Rev.*, 2018, **118**, 4573-4591.

12. J. E. Taylor, M. A. Kulandainathan, C. E. Hotchen and F. Marken, in *Modern electrosynthetic methods in organic chemistry*, eds. F. Marken and M. Atobe, CRC Press Boca Raton, 1st edn., 2018, ch. 1, pp. 1-44.

13. D. Pletcher, *Electrochem. Commun.*, 2018, **88**, 1-4.

14. J. P. Hallett and T. Welton, *Chem. Rev.*, 2011, **111**, 3508-3576.

15. V. Farmer and T. Welton, *Green Chem.*, 2002, **4**, 97-102.

16. P. J. Wright and A. M. English, *J. Am. Chem. Soc.*, 2003, **125**, 8655-8665.

17. R. A. Green, R. C. D. Brown and D. Pletcher, *J. Flow Chem.*, 2016, **6**, 191-197.

18. A. J. Bard and L. R. Faulkner, in *Electrochemical methods : fundamentals and applications*, eds. A. J. Bard and L. R. Faulkner, John Wiley & Sons, New York, 2nd edn., 2001, ch. 11, pp. 416-470.

19. R. A. Green, R. C. D. Brown and D. Pletcher, *J. Flow Chem.*, 2015, **5**, 31-36.

20. D. Pletcher, R. Greff, R. Peat, L. M. Peter and J. Robinson, in *Instrumental Methods in Electrochemistry*, eds. D. Pletcher, R. Greff, R. Peat, L. M. Peter and J. Robinson, Woodhead Publishing, Cambridge, 1st edn., 2001, ch. 7, pp. 229-250.

21. D. Pletcher, R. Greff, R. Peat, L. M. Peter and J. Robinson, in *Instrumental Methods in Electrochemistry*, eds. D. Pletcher, R. Greff, R. Peat, L. M. Peter and J. Robinson, Woodhead Publishing, Cambridge, 1st edn., 2001, ch. 11, pp. 356-387.

22. D. S. P. Cardoso, B. Šljukić, D. M. F. Santos and C. A. C. Sequeira, *Org. Process Res. Dev.*, 2017, **21**, 1213-1226.

5. Paired TEMPO-mediated Alcohol Oxidation in RTILs

5.1. Introduction

Tuning synthetic processes by introducing multi-functionality to each component, such as the solvent, supporting electrolyte or electrodes, could help minimise waste and improve energy efficiency.[1] For example, by using RTILs for TEMPO-mediated alcohol oxidations, the need for supporting electrolytes and volatile organic solvents may be eliminated.[2, 3] However, in the case of TEMPO-mediated alcohol oxidations, the need for a stoichiometric base remains a shortcoming with respect to waste minimisation and atom efficiency.

In this chapter, the generation of the necessary base *in situ*, *via* the electroreduction of a protic ionic liquid at the counter electrode is described. The protic ionic liquid is reformed as the electrogenerated base deprotonates the alcohol and the hydroxylamine (Scheme 5.1). Furthermore, by having the base incorporated within the ionic liquid itself, the ‘base’ can be reused by recycling the ionic liquid.

As discussed in chapter 4, water reduction is often chosen as the counter-electrode reaction in the electrolysis of TEMPO-mediated alcohol oxidations, producing H_2 and OH^-.[2, 4] Besides ensuring a flow of electrons through the cell, the cathode reduction of water brings little value to the overall alcohol oxidation. Thus, pairing the electroreduction of the protic ionic liquid with the alcohol oxidation not only eliminates the generation of reactive intermediates (e.g. protonated base and OH^-) and reduces the amount of waste produced, but it also allows a more efficient use of electrical current.[1]

The recyclability of TEMPO is also considered in this chapter, as the recovery and reuse of TEMPO with sustained high activity is important, yet this has been proven to be challenging.[5, 6] Previous studies have shown that the reactivity and selectivity of TEMPO-based ionic liquids behaves very similar to homogeneous TEMPO systems.[7-9] Furthermore, the solvation properties of the TEMPO-IL can be tailored through the design of the TEMPO-IL structure for desired outcomes such as simple product extraction as well as recovery of the TEMPO-IL.[10] For example, Wei and co-workers, demonstrated facile recovery and recyclability of their TEMPO-based ionic liquid, which retained excellent catalytic activity after being recycled 5 times, whereas the solution with TEMPO only has 5% of its catalytic activity after the same amount of recycling.[7]

Efficient and selective flow electrolysis of the electrooxidation of alcohols, with high conversions, were achieved using a system consisting of 1-butylimidazolium bis(trifluoromethanesulfonyl)imide, $[C_4HIm][NTf_2]$, as the recyclable solvent, electrolyte and protonated base, and 1-butylimidazolium TEMPO-4-sulfate, $[C_4HIm][TEMPOOSO_3]$[11] as the recyclable catalyst (structures are shown in Figure 5.1). The system was recycled up to 10 times with excellent catalytic activity.

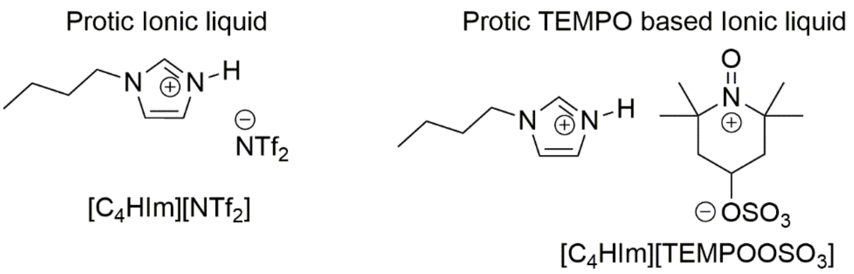

Figure 5.1: Structures of [C_4HIm][NTf_2] and [C_4HIm][TEMPOOSO$_3$]

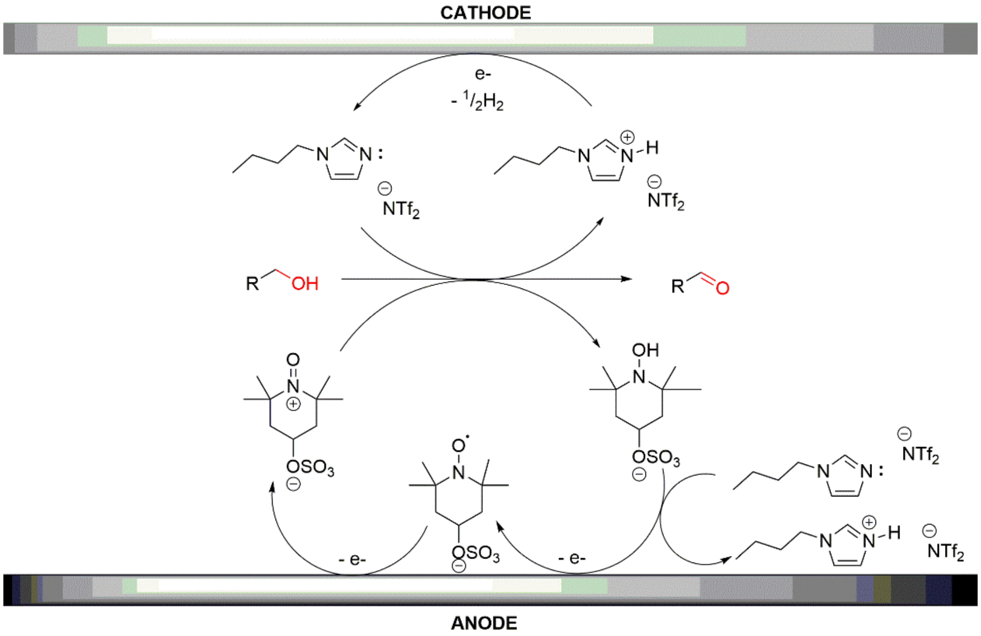

Scheme 5.1: Proposed alcohol electrooxidation with [C_4HIm][TEMPOOSO$_3$] at the anode, paired with the electroreduction of the cationic component of a protic ionic liquid, [C_4HIm][NTf_2] to generate the base, 1-butylimidazole, which deprotonates the alcohol and the hydroxylamine to regenerate the cation of [C_4HIm][NTf_2].

5.2. Results and Discussion

5.2.1. Reduction of Protonated Base in Paired TEMPO-mediated Alcohol Oxidation

Figure 5.2 shows the first and second sweeps of the CV of a solution containing 0.06 mol dm^{-3} TEMPO, 0.6 mol dm^{-3} benzyl alcohol and 2.4 mol dm^{-3} 1-butylimidazole in [C$_8$C$_1$Im][NTf$_2$].

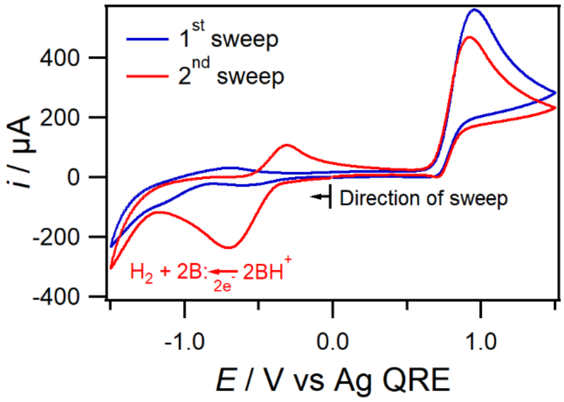

Figure 5.2: The first (blue line) and second sweep (red line) of a CV, with a starting potential at 0.0 V, recorded of a solution containing 0.06 mol dm^{-3} TEMPO, 0.6 mol dm^{-3} benzyl alcohol and 2.4 mol dm^{-3} 1-butylimidazole in [C$_8$C$_1$Im][NTf$_2$], recorded at a 2 mm Pt disk electrode and with a scan rate of 100 mV s^{-1}.

The starting potential was set to 0.0 V (vs Ag QRE), the potential was swept towards negative potential until -2.0 V was reached and was then swept towards positive potentials (to 2.0 V). No significant peaks are observed in the first sweep (blue line) until a potential of 0.8 V is reached, when alcohol oxidation occurs. As the TEMPO-mediated alcohol oxidation occurs, the base, B:, deprotonates the alcohol and the hydroxylamine, leaving the base protonated, BH$^+$ (see Scheme 5.1). The potential is then scanned back towards negative potentials, passing through the starting potential (0.0 V). A reduction peak at -0.8 V is observed in the second sweep (red line) corresponding to the reduction of BH^+ to B:.

By making the protonated base the cationic component of a RTIL medium, the base can be generated *in situ* by the electroreduction of the cation and thus eliminating the need for a stoichiometric base. Moreover, in having the protonated base as the cation of the RTIL medium there will be a large excess of protonated base that can be reduced at the counter electrode. This will ensure that the reduction occurring at the counter electrode will not limit the rate of the reaction occurring at the working electrode, lowering the possibility of side-reactions occurring.[12] To test this idea, $[C_4HIm][NTf_2]$, where $[C_4HIm]^+$ is the protonated form of 1-butylimidazole, was used. To investigate the possibility of improving the recyclability of TEMPO, $[C_4HIm][TEMPOOSO_3]$ was synthesised. However $[C_4HIm][TEMPOOSO_3]$ is solid at room temperature, so it was dissolved in $[C_4HIm][NTf_2]$.

5.2.2. Electrochemical Behaviour of $[C_4HIm][TEMPOOSO_3]$ in $[C_4HIm][NTf_2]$

Figure 5.3 frame a) shows a CV of 0.06 mol dm^{-3} $[C_4HIm][TEMPOOSO_3]$ dissolved in $[C_4HIm][NTf_2]$. An anodic peak due to oxidation of $[TEMPOOSO_3]^-$ to $[TEMPO^+OSO_3]^-$ can be seen at $E_{p,a}$, = 0.763 V (*vs* dmFc/dmFc$^+$), and a reduction peak due to the reduction of $[TEMPO^+OSO_3]^-$ to $[TEMPOOSO_3]^-$ can be seen at $E_{p,c}$ = 0.695 V (*vs* dmFc/dmFc$^+$). These peaks are labelled a and c, respectively in Figure 5.3. The shape of the CV agrees with that expected for TEMPO in conventional solvents and in RTILs.[2, 3, 13-15] The values for $E_{p,a}$, $E_{p,c}$, $E_{T,½}$, ΔE_p, $i_{p,a}$, $i_{p,c}$ and $i_{p,a}/i_{p,c}$ ratio are summarised in Table A.9 in the Appendix.

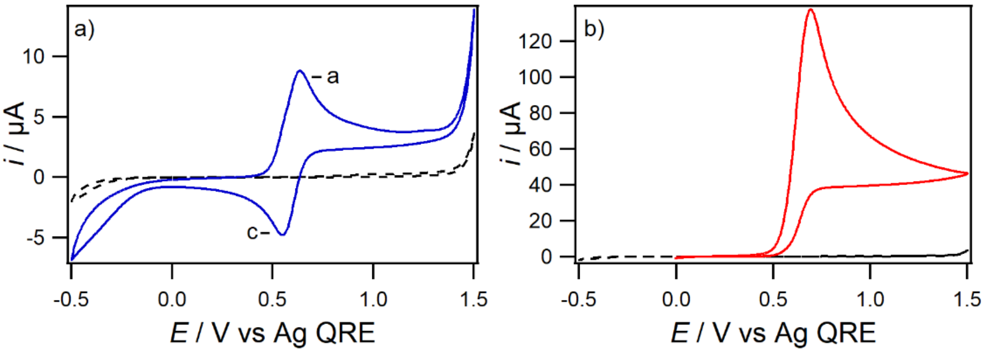

Figure 5.3: a) CV of 0.06 mol dm^{-3} [C_4HIm][TEMPOOSO$_3$] in [C_4HIm][NTf$_2$] (blue line). b) CV of 0.06 mol dm^{-3} [C_4HIm][TEMPOOSO$_3$] and 0.6 mol dm^{-3} benzyl alcohol in [C_4HIm][NTf$_2$]. The CV of the blank [C_4HIm][NTf$_2$] RTIL is shown (black dashed line). The CVs are recorded using a 3 mm diameter glassy carbon electrode with a scan rate of 5 mV s^{-1} and at ambient temperature and pressure. Dynamic iR drop compensation was used.

Figure 5.3 frame b) shows the effect of adding 0.6 mol dm^{-3} benzyl alcohol on the voltammetry of 0.06 mol dm^{-3} [C_4HIm][TEMPOOSO$_3$] in [C_4HIm][NTf$_2$]. Addition of benzyl alcohol causes $i_{p,a}$ to significantly increase and $i_{p,c}$ to decrease to a negligible level, as a result of the reaction between [TEMPO$^+$OSO$_3$] and benzyl alcohol, producing benzaldehyde. This catalytic response of TEMPO solutions with alcohol is typically not observed without the addition of base (see section 3.2.2.). The occurrence of the catalytic current without the addition of base is likely be a result that the protonated base is in equilibria with the base.[3, 15]

5.2.3. Kinetics of Alcohol Oxidations with $[C_4HIm][TEMPOOSO_3]$ in $[C_4HIm][NTf_2]$

The reaction kinetics of TEMPO-mediated alcohol oxidations using the $[C_4HIm][NTf_2]$-$[C_4HIm][TEMPOOSO_3]$ system were investigated by determining k using Equation 3.1. Figure 5.4 shows CVs of solutions containing 0.06 mol dm^{-3} $[C_4HIm][TEMPOOSO_3]$ and 0.3 mol dm^{-3}, 0.6 mol dm^{-3}, 1.2 mol dm^{-3}, 2.4 mol dm^{-3} benzyl alcohol in $[C_4HIm][NTf_2]$. i_{cat} increases linearly with $C_A^{½}$ in agreement with Equation 3.1 (Figure 5.4 insert).[16, 17]

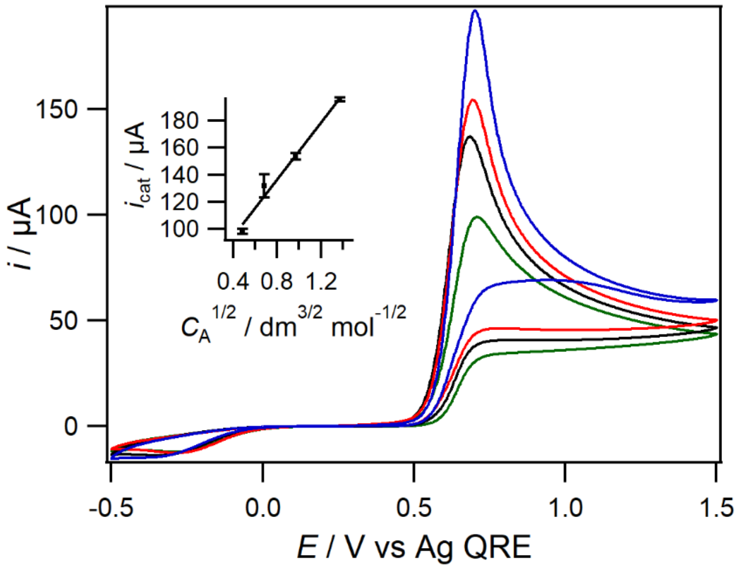

Figure 5.4: CVs of 0.06 mol dm^{-3} $[C_4HIm][TEMPOOSO_3]$ dissolved in $[C_4HIm][NTf_2]$ containing 0.3 mol dm^{-3} (green), 0.6 mol dm^{-3} (black), 1.2 mol dm^{-3} (red) and 2.4 mol dm^{-3} (blue) benzyl alcohol. The inset shows a graph of i_{cat} *vs* $C_A^{½}$. CVs recorded using a 3 mm diameter glassy-carbon electrode with scan rate of 5 mV s^{-1} and at ambient temperature and pressure. Dynamic iR drop compensation was used.

k was derived from the slope of the linear plot of i_{cat} *vs* $C_{\mathrm{A}}^{½}$ and D_{A} was determined from PFG-NMR spectroscopy. $k = 0.052 \pm 0.001$ dm^3 mol^{-1} s^{-1}, which is relatively low for TEMPO-mediated oxidation of benzyl alcohol conducted in RTILs. As a comparison k in a [C_8C_1Im][NTf_2]-TEMPO system is 0.336 dm^3 mol^{-1} s^{-1} ± 0.004 dm^3 mol^{-1} s^{-1}. In aprotic RTILs and conventional solvents an excess of base is needed to drive the reaction in TEMPO-mediated alcohol oxidations,[2, 3, 18] thus the low k in the [C_4HIm][NTf_2]-[C_4HIm][$TEMPOOSO_3$] system could be a result of the low concentration of base present in the solution. It is, however, expected that when performing electrolysis of the reaction mixture, more 1-butylimidazole base will be formed as a result of the reduction of the cationic component of [C_4HIm][NTf_2].

In order to investigate whether k can be increased, an excess of base was added to the [C_4HIm][NTf_2]-[C_4HIm][$TEMPOOSO_3$] system. Figure 5.5 shows the effect of adding 2.4 mol dm^{-3} 1-butylimidazole to the CVs of the solutions containing 0.06 mol dm^{-3} [C_4HIm][$TEMPOOSO_3$] with 0.3 mol dm^{-3}, 0.6 mol dm^{-3}, 1.2 mol dm^{-3}, 2.4 mol dm^{-3} benzyl alcohol in [C_4HIm][NTf_2].

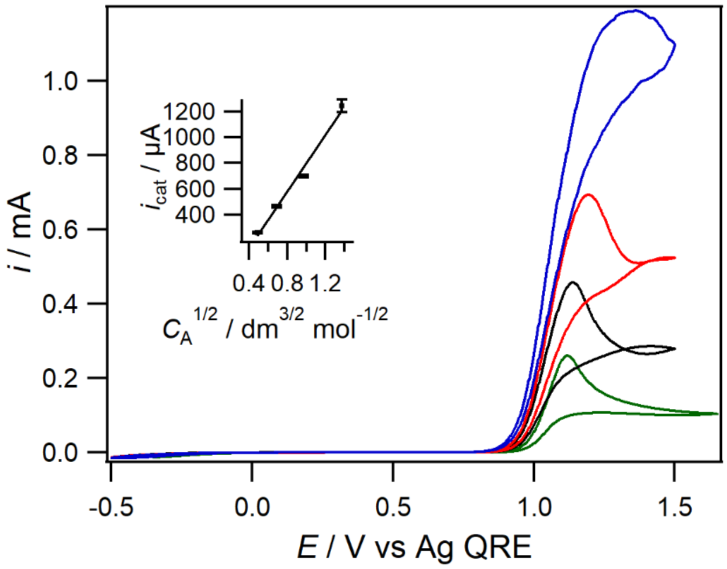

Figure 5.5: CVs of 0.06 mol dm^{-3} [C_4HIm][TEMPOOSO$_3$] and 2.4 mol dm^{-3} 1-butylimidzole dissolved in [C_4HIm][NTf$_2$] containing 0.3 mol dm^{-3} (green), 0.6 mol dm^{-3} (black), 1.2 mol dm^{-3} (red) and 2.4 mol dm^{-3} (blue) benzyl alcohol. The inset shows a graph of i_{cat} *vs* $C_A^{½}$. CVs recorded using a 3 mm diameter glassy-carbon electrode with scan rate of 5 mV s^{-1} and at ambient temperature and pressure. Dynamic iR drop compensation was used.

Figure 5.5 shows that i_{cat} of the CVs recorded for each solution are significantly greater than the i_{cat} of the CVs recorded for the solutions without the added base in Figure 5.4. The measured *k* increased from 0.052 ± 0.001 dm^3 mol^{-1} s^{-1} to a value of 2.37 ± 0.004 dm^3 mol^{-1} s^{-1} with the addition of 2.4 mol dm^{-3} 1-butylimidazole. This increase in i_{cat} and consequent increase in *k* is a result of both the alcohol and hydroxylamine species being deprotonated more rapidly.[2, 3, 15, 18] Although the addition of base adds another component to the [C_4HIm][TEMPOOSO$_3$]-[C_4HIm][NTf$_2$] system, it offers a faster electrocatalytic rate, which is important for achieving high faradaic yields.[19] Moreover, as demonstrated in Section 5.2.6, the additional 1-butylimidazole can easily be recovered from the product mixture and be recycled as $[C_4HIm][NTf_2]$.

5.2.4. Flow Electrolysis of the Paired TEMPO-mediated Alcohol Oxidation with the Reduction of $[C_4HIm]^+$

The flow electrolysis of benzyl alcohol to benzaldehyde, was performed in an Ammonite8 cell, with a flow rate of 0.05 cm^3 min^{-1} and a range of current densities. Products were extracted from the RTIL with toluene and analysed using GC-FID. The results are summarised in Figure 5.6.

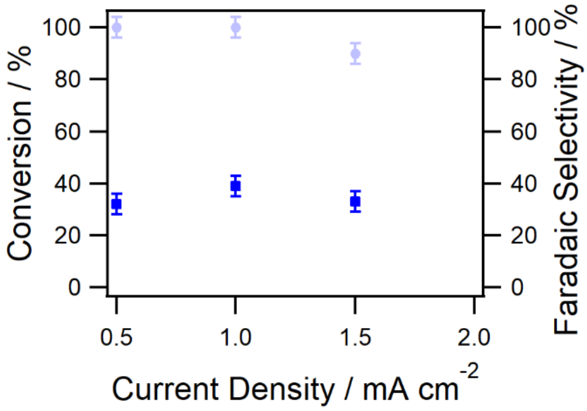

Figure 5.6: Measured conversions (blue squares) and faradaic selectivities (light blue dots) of flow TEMPO-mediated electrooxidation of 0.2 mol dm^{-3} benzyl alcohol with 0.06 mol dm^3 $[C_4HIm][TEMPOOSO_3]$ in $[C_4HIm][NTf_2]$ using a constant flow rate of 0.05 cm^3 min^{-1} and varying current densities. Conversions were determined by using GC-FID analysis and calibration curves of benzyl alcohol. Faradaic selectivity is based on concentration of unreacted benzyl alcohol and concentration of benzaldehyde (derived from calibration curves of benzaldehyde).

The minimum cell current density required for a 100% conversion of 0.2 mol dm^{-3} alcohol when using a flow rate of 0.05 cm^3 min^{-1} is 1.6 mA cm^{-}

^{2} (calculated using Equation 2.6). However, only a 33% conversion is obtained when a current density of 1.5 mA cm^{-2} is used. Notably, there is a decrease in faradaic selectivity from 100% to 90% when increasing the current density from 1.0 mA cm^{-2} to 1.5 mA cm^{-2}, suggesting that there are competing reactions at the higher current densities. As observed in the previous section the chemical reaction kinetics of TEMPO-mediated alcohol oxidations in the [C_4HIm][NTf_2]-[C_4HIm][$TEMPOOSO_3$] system is relatively slow, and it could be that the flow rate of 0.05 cm^3 min^{-1} may be too high for the chemical reaction. The flow rate was therefore lowered in an attempt to increase the conversion of benzyl alcohol while maintaining a good faradaic selectivity; the results are summarised in Figure 5.7.

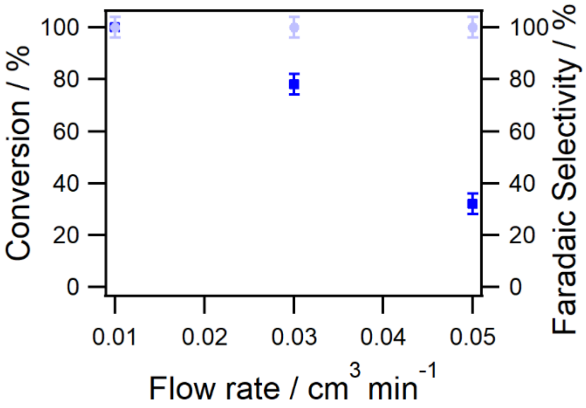

Figure 5.7: Measured conversions and faradaic selectivity of flow TEMPO-mediated electrooxidation of 0.2 mol dm^{-3} benzyl alcohol with 0.06 mol dm^{-3} [C_4HIm][TEMPOOSO3] in [C_4HIm][NTf_2] at constant applied current density of 0.5 mA cm^{-2}, measured using different flow rates. Conversions were determined by using GC-FID analysis and calibration curves of benzyl alcohol. Faradaic selectivity is based on concentration of unreacted benzyl alcohol and concentration of benzaldehyde (derived from calibration curves of benzaldehyde).

A 100% conversion with a 100% faradaic selectivity was observed with a flow rate of 0.01 cm^3 min^{-1} and with an applied current density of 0.5 mA cm^{-2}. With low flow rates the residence time of the reaction mixture in the electrolysis cell is increased. The need for long residence time could be due to the fact that this will generate more base as a result of the reduction of $[C_4Him]^+$ at the cathode. As discussed previously, the more base there is, more alcohol and hydroxylamine will be deprotonated and the overall rate of the alcohol oxidation will increase as a result.[2, 3]

To further confirm that the addition of base increases the rate of the reaction of TEMPO-mediated alcohol oxidation in the $[C_4HIm][NTf_2]$-$[C_4HIm][TEMPOOSO_3]$ system, 2.4 mol dm^{-3} 1-butylimidazole was added to a solution of 0.2 mol dm^{-3} benzyl alcohol, 0.06 mol dm^{-3} $[C_4HIm][TEMPOOSO_3]$ in $[C_4HIm][NTf_2]$. A 78% conversion of benyl alcohol with 100% faradaic yield was observed when the electrolysis was conducted with a flow rate of 0.05 cm^3 min^{-1} and with an applied current density of 1.0 mA cm^{-2}. This is approximately a two-fold increase in the conversion observed of the electrolysis conducted with the same conditions but without the added 1-butylimidazole (see Figure 5.6).

Further electrolysis experiments were performed to validate that the electrooxidation of benzyl alcohol does require a base, a counter electrode reaction and TEMPO itself for the electrooxidation of alcohols. All of the electrolyses illustrated in Scheme 5.2, Scheme 5.3, Scheme 5.4 and Scheme 5.5 were conducted with a flow rate of 0.05 cm^3 min^{-1} and 1.0 mA cm^{-2}.

- A 3% conversion of benzyl alcohol with a 79% faradaic selectivity was obtained from the electrolysis of a solution containing 0.2 mol dm^{-3} benzyl alcohol in [C$_4$HIm][NTf$_2$].

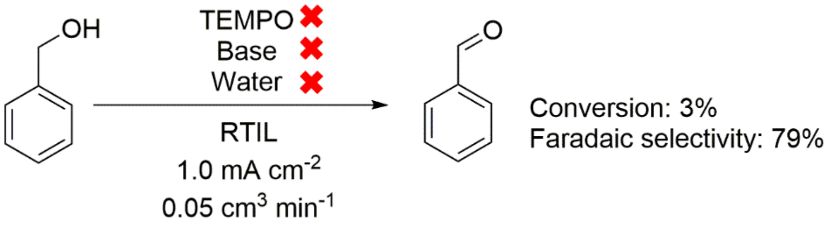

Scheme 5.2: Flow electrooxidation of 0.2 mol dm^{-3} benzyl alcohol in [C$_4$HIm][NTf$_2$] with a flow rate of 0.05 cm^3 min^{-1} and an applied current density of 1.0 mA cm^{-2}.

- An 18% conversion of benzyl alcohol with a 60% faradaic selectivity was obtained from the electrolysis of a solution containing 0.2 mol dm^{-3} benzyl alcohol and 0.06 mol dm^{-3} TEMPO in the aprotic RTIL [C$_8$C$_1$Im][NTf$_2$].

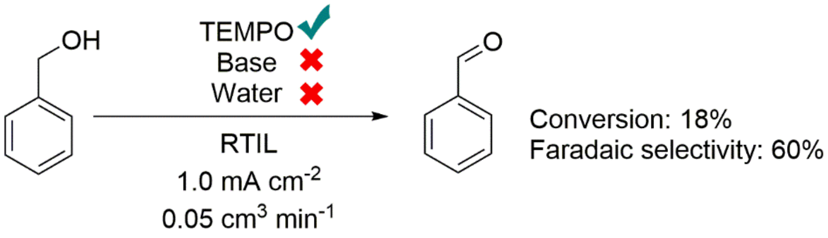

Scheme 5.3: Flow electrooxidation of 0.2 mol dm^{-3} benzyl alcohol and 0.06 mol dm^{-3} TEMPO in [C$_8$C$_1$Im][NTf$_2$] with a flow rate of 0.05 cm^3 min^{-1} and an applied current density of 1.0 mA cm^{-2}.

- A 10% conversion of benzyl alcohol with a 79% faradaic selectivity was obtained from the electrolysis of a solution containing 2.4 mol dm^{-3} 1-butylimidazole, 0.2 mol dm^{-3} benzyl alcohol and 0.06 mol dm^{-3} TEMPO in the aprotic RTIL [C$_8$C$_1$Im][NTf$_2$].

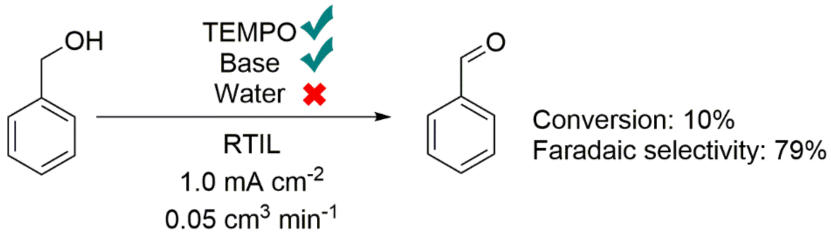

Scheme 5.4: Flow electrooxidation of 0.2 mol dm^{-3} benzyl alcohol, 0.06 mol dm^{-3} TEMPO and 2.4 mol dm^{-3} 1-butylimidazole in [C_8C_1Im][NTf_2] with a flow rate of 0.05 cm^3 min^{-1} and an applied current density of 1.0 mA cm^{-2}.

- An 85% conversion of benzyl alcohol with a 100% faradaic selectivity was obtained from the electrolysis of a 6 cm^3 solution containing 1 cm^3 water, 2.4 mol dm^{-3} 1-butylimidazole, 0.2 mol dm^{-3} benzyl alcohol and 0.06 mol dm^{-3} TEMPO in the aprotic RTIL [C_8C_1Im][NTf_2].

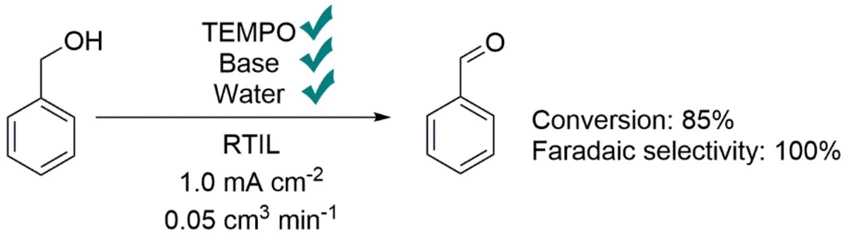

Scheme 5.5: Flow electrooxidation of a 6 cm^3 solution of 0.2 mol dm^{-3} benzyl alcohol, 0.06 mol dm^{-3} TEMPO and 2.4 mol dm^{-3} 1-butylimidazole in [C_8C_1Im][NTf_2] and 1 cm^3 water with a flow rate of 0.05 cm^3 min^{-1} and an applied current density of 1.0 mA cm^{-2}.

These experiments confirm the need for (1) a base to deprotonate the alcohol and hydroxylamine, (2) a counter electrode reaction (e.g. water or [C_4Him]$^+$ reduction), and (3) a TEMPO based catalyst in order to achieve both good conversions and faradaic selectivities.

5.2.5. Screening of Alcohol Substrates

A range of primary and secondary alcohols were oxidised using the [C_4HIm][TEMPOOSO_3]-[C_4HIm][NTf_2] system in order to investigate the selectivity and substrate scope of the system. Flow electrolysis data of solutions containing 0.2 mol dm^{-3} alcohol, 2.4 mol dm^{-3} 1-butylimidazole and 0.06 mol dm^{-3} [C_4HIm][TEMPOOSO_3] in [C_4HIm][NTf_2] with a flow rate of 0.05 cm^3 min^{-1} and 1.0 mA cm^{-2} applied current are summarised in Table 5.1.

Table 5.1: Measured conversions of flow TEMPO-mediated electrooxidation of various alcohols (0.2 mol dm^{-3}) with 0.06 mol dm^{-3} [C_4HIm][TEMPOOSO$_3$], 2.4 mol dm^{-3} 1-butylimidazole in [C_4HIm][NTf$_2$] using an applied current density of 0.5 mA cm^{-2} and a flow rate of 0.05 cm^3 min^{-1}.

Entry	Alcohol	Product	NMR conversion[a]
1	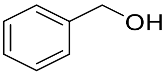	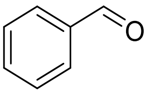	78 ± 1%
2	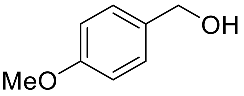	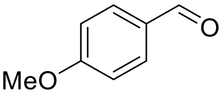	83 ± 8%
3	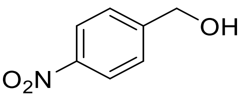	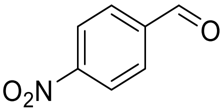	35 ± 6%
4	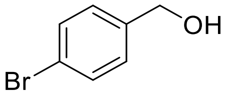	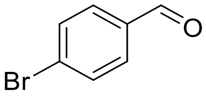	72 ± 1%
5	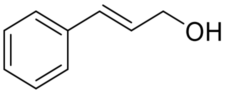	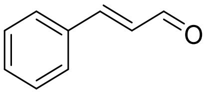	70 ± 5%
6	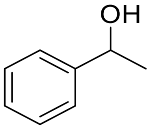	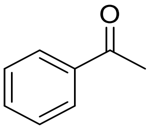	55 ± 2%
7	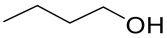	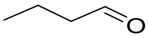	78 ± 4%
8	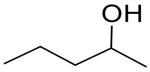	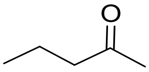	50 ± 6%
9	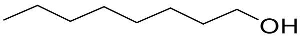	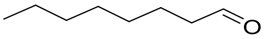	70 ± 5%
10	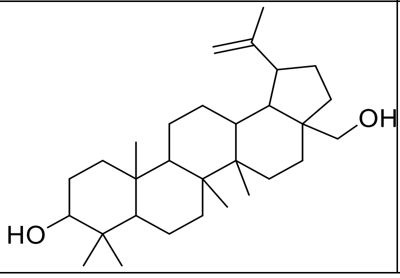	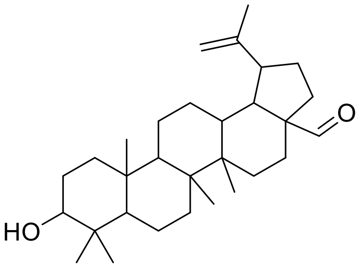	41 ± 4%

[a]Conversions are obtained from NMR spectra, comparing the starting material and the product. The electrolyses were done in triplicates and the conversions are an average.

In general, the benzylic alcohols are more easily oxidised than the aliphatic alcohols. The 4-methoxybenzyl alcohol (entry 2) oxidises slightly better than the benzyl alcohol (entry 1) which can be explained as a result of the electron donating methoxy group on 4-methoxybenzyl alcohol, resulting in more favourable deprotonation of the alcohol group compared to the non-substituted benzyl alcohol.[19-21]

Electron-poor benzylic alcohols such as 4-nitrobenzyl alcohol (entry 3) and 4-bromobenzyl alcohol (entry 4) showed poorer conversions.[20] The product mixture of the oxidation of 4-nitrobenzylalcohol was dark brown in colour (in contrast to the light orange coloured starting reactant mixture). Brown and co-workers have previously reported a particularly low conversion of 4-nitrobenzylalcohol when conducting the TEMPO-mediated alcohol oxidation electrolysis in the undivided Ammonite8 flow electrolysis cell. It was believed that the low conversion could be a result of the nitro group potentially reacting at the cathode.[14]

Under alkali conditions, TEMPO exhibits strong stereoselectivity towards the oxidation of primary alcohols over secondary alcohols.[22] This selectivity has been attributed to steric effect in the formation of the alcohol-TEMPO$^+$ adduct (see scheme 1.3).[17] The stability of these intermediates decreases with sterically crowded complexes, and gives a rationale for why primary alcohols are kinetically favoured over secondary alcohols. The slower chemistry of secondary alcohol oxidations is reflected in the conversions. This demonstrates that the [C_4HIm][NTf_2]-[C_4HIm][TEMPOOSO_3] system is selective towards primary alcohols over secondary alcohols.

For the alkyl alcohols, the yield of the carbonyl products decreases as the chain length of the alcohols increases. This decrease in conversion has previously been observed, and is understood to be a result of increasing degree of steric hindrance as the chain length increases.[14]

Betulin is a triterpene with both a primary and secondary alcohol group and is therefore interesting to study with this system in terms of the alcohol selectivity. Additionally, betulin is a precursor to the valuable betulinic acid which has anti-tumour activity against melanoma and anti-HIV activity in phocytic cells.[23, 24] Only a 41% conversion of betulin to betulin-28-aldehyde was observed and it should be noted that betulin did not fully dissolve in the 1-butylimidaozle and [C_4HIm][TEMPOOSO$_3$]-[C_4HIm][NTf$_2$] solution. In an attempt of increasing the solubility of betulin, the [NTf$_2$]$^-$ anion was exchanged to a [DCA]$^-$ anion. The solubility of betulin in [C_4HIm][DCA] was significantly higher, but electrolysis produced a 10% conversion. The lower conversion could be a result of the stronger interaction between the TEMPO$^+$ moiety and the [DCA]$^-$ anion, as observed in chapter 3. These results, however, demonstrate some promising prospects of designing an RTIL which can dissolve betulin but that also promote the oxidation to betulin-28-aldehyde.

5.2.6. Recyclability of [C_4HIm][TEMPOOSO$_3$] and [C_4HIm][TEMPOOSO$_3$]

The recyclability of the [C_4HIm][TEMPOOSO$_3$]-[C_4HIm][NTf$_2$] system was tested for the electrolysis benzyl alcohol to form benzaldehyde. Benzaldehyde was extracted together with 1-butylimidazole and unreacted benzyl alcohol from the [C_4HIm][TEMPOOSO$_3$]-[C_4HIm][NTf$_2$] system by distillation *in vacuo*. Fresh substrates were then recharged to the [C_4HIm][TEMPOOSO$_3$]- [C_4HIm][NTf$_2$] solution and the reaction solution was then subjected into the Ammonite8 cell to repeat the electrolysis. The procedure was repeated 10 times, and the concentrations of benzyl alcohol and benzaldehyde were monitored with GC-FID analysis. There was no significant loss of catalytic activity in the oxidation up to 10 times (Figure 5.8).

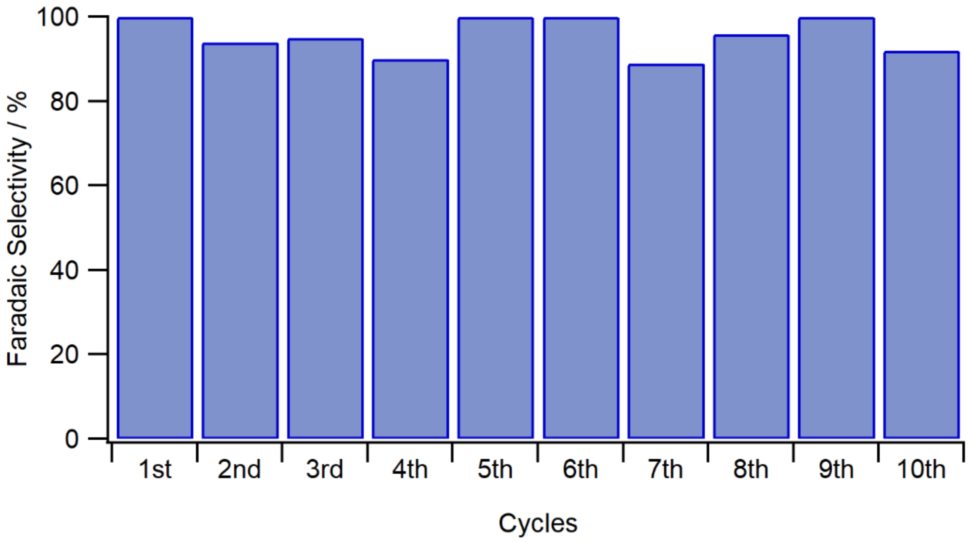

Figure 5.8: Faradaic selectivity of the recycling of the [C_4HIm][TEMPOOSO$_3$]-[C_4HIm][NTf$_2$] system for the oxidation of benzyl alcohol.

1-butylimidazole was distilled with benzaldehyde and recovered as [C_4HIm]Cl by washing the distilled organics with 1 mol dm^{-3} HCl. The product and starting material could be recovered from the organic layer. Li[NTf$_2$] was then added to the aqueous layer containing [C_4HIm]Cl to form [C_4HIm][NTf$_2$] through a simple metathesis. [C_4HIm][NTf$_2$] was then reused in the [C_4HIm][TEMPOOSO$_3$]-[C_4HIm][NTf$_2$] system. It should be noted that, even when 1-butylimidazole is not added and the electrolysis is conducted at 0.01 cm^3 min^{-1} with a current density of 0.5 mA cm^{-2}, it was found that some 1-butylimidazole was also distilled off together with the product.

Both $[C_4HIm][NTf_2]$ and $[C_4HIm][TEMPOOSO_3]$ are immiscible in commonly used non-polar organic solvents such as toluene and hexane, and thus, an alternative procedure to distillation *in vacuo* is solvent extraction of the carbonyl products. For example, octanal could be extracted from the $[C_4HIm][NTf_2]$-$[C_4HIm][TEMPOOSO_3]$ system with hexane. The organic layer was then treated with 1 mol dm^{-3} HCl acid in order to remove 1-butylimidazole and consequently make $[C_4HIm]Cl$. The aqueous $[C_4HIm]Cl$ solution was kept and $Li[NTf_2]$ was added to the solution to make $[C_4HIm][NTF_2]$. The organic layer was then dried over magnesium sulfate and the aldehyde and alcohol were recovered by removing the solvent under reduced pressure.

5.3. Conclusion

By maximising the functionality of the solvent and electrolyte media in TEMPO-mediated alcohol oxidations and using paired electrosynthesis, the need for a stoichiometric base and water is eliminated. Excellent conversions and faradaic selectivity with flow electrolysis were achieved at a flow rate of 0.01 cm^3 min^{-1} and 0.5 mA cm^{-2}. With the addition of 1-butylimidazole the electrolysis time can be reduced significantly and can be run at 0.05 cm^3 min^{-1}, with 1.0 mA cm^{-2} to produce relatively high conversions of 78%. The use of these multi-functional ILs does not lead to four major sources of waste which are typically generated in TEMPO-mediated alcohol electrooxidation: which are- organic solvent (if distillation is used for the work-up), electrolyte, catalysts and hazardous by-products, since 1-butylimidazole can be recycled as [C_4HIm][NTf_2].

5.4. References

1. T. Keijer, V. Bakker and J. C. Slootweg, *Nat. Chem.*, 2019, **11**, 190-195.

2. R. Barhdadi, C. Comminges, A. P. Doherty, J. Y. Nédélec, S. O'Toole and M. Troupel, *J. Appl. Electrochem.*, 2007, **37**, 723-728.

3. C. Comminges, R. Barhdadi, A. P. Doherty, S. O'Toole and M. Troupel, *J. Phys. Chem. A*, 2008, **112**, 7848-7855.

4. R. A. Green, R. C. D. Brown, D. Pletcher and B. Harji, *Electrochem. Commun.*, 2016, **73**, 63-66.

5. S.-i. Ohsugi, K. Nishide, K. Oono, K. Okuyama, M. Fudesaka, S. Kodama and M. Node, *Tetrahedron*, 2003, **59**, 8393-8398.

6. A. P. Thottumkara and T. K. Vinod, *Tetrahedron Lett.*, 2002, **43**, 569-572.

7. C. Zhu, L. Ji and Y. Wei, *Catal. Commun.*, 2010, **11**, 1017-1020.

8. T. Hirashita, M. Nakanishi, T. Uchida, M. Yamamoto, S. Araki, I. W. C. E. Arends and R. A. Sheldon, *ChemCatChem*, 2016, **8**, 2704-2709.

9. A. Fall, M. Sene, M. Gaye, G. Gómez and Y. Fall, *Tetrahedron Lett.*, 2010, **51**, 4501-4504.

10. Á. Molnár and A. Papp, *Coord. Chem. Rev.*, 2017, **349**, 1-65.

11. J. Winsberg, C. Stolze, A. Schwenke, S. Muench, M. D. Hager and U. S. Schubert, *ACS Energy Lett.*, 2017, **2**, 411-416.

12. R. A. Green, R. C. D. Brown and D. Pletcher, *J. Flow Chem.*, 2016, **6**, 191-197.

13. R. A. Green, J. T. Hill-Cousins, R. C. D. Brown, D. Pletcher and S. G. Leach, *Electrochim. Acta*, 2013, **113**, 550-556.

14. J. T. Hill-Cousins, J. Kuleshova, R. A. Green, P. R. Birkin, D. Pletcher, T. J. Underwood, S. G. Leach and R. C. Brown, *ChemSusChem*, 2012, **5**, 326-331.

15. A. C. Herath and J. Y. Becker, *Electrochim. Acta*, 2008, **53**, 4324-4330.

16. M. Rafiee, B. Karimi and S. Alizadeh, *ChemElectroChem*, 2014, **1**, 455-462.

17. C. Costentin and J.-M. Savéant, *ChemElectroChem*, 2014, **1**, 1226-1236.

18. M. Rafiee, K. C. Miles and S. S. Stahl, *J. Am. Chem. Soc.*, 2015, **137**, 14751-14757.

19. A. Badalyan and S. S. Stahl, *Nature*, 2016, **535**, 406.

20. J. Vandanapu and S. Rachuru, *Adv. Phys. Chem.*, 2012, **12**, 1-4.

21. F. d'Acunzo, P. Baiocco, M. Fabbrini, C. Galli and P. Gentili, *Eur. J. Org. Chem.*, 2002, **2002**, 4195-4201.

22. M. F. Semmelhack, C. S. Chou and D. A. Cortes, *J. Am. Chem. Soc.*, 1983, **105**, 4492-4494.

23. J. Zhao, R. Li, A. Pawlak, M. Henklewska, A. Sysak, L. Wen, J.-E. Yi and B. Obmińska-Mrukowicz, *In Vivo*, 2018, **32**, 1081-1088.

24. *US Pat.,* WO/2006/105357, 2006.

6. Concluding remarks

6.1. Summary

The aim of this project was to develop an insight into TEMPO-mediated alcohol electroxidations in RTILs and for the development of more sustainable alcohol oxidations than the traditional alcohol oxidation methods used currently. Electrochemical TEMPO-mediated oxidations in RTILs offer higher atom efficiency than in conventional alcohol oxidations in that (1) coupling electrochemistry with TEMPO minimizes the input of stoichiometric or hazardous reagents during oxidations, (2) the use of ionic liquids as the solvent and electrolyte reduces the amount of required reagents for the electrosynthesis.

In Chapter 3, tuning the redox properties of the TEMPO/TEMPO$^+$ couple *via* the simple modification of the RTIL media was described. This tuning of redox properties of TEMPO in turn affects the rates of alcohol oxidation in the RTILs, demonstrating that it is possible to tune the reactivity of TEMPO by judicious choice of the RTIL composition. Different degrees of discrimination of alcohol substrates were observed in different RTILs, offering the valuable possibility of tuning the selectivity of TEMPO in TEMPO-mediated alcohol electroxidations. It was also significant that the apparent rate constant for the oxidation reaction is larger in RTILs with low β, such as $[NTf_2]^-$ based RTILs, than in acetonitrile-electrolyte systems.

Electrolyses of TEMPO-mediated alcohol electroxidations using the Ammonite8 flow electrolysis cell were demonstrated in Chapter 4. Efficient, selective and high yielding electrolyses were achieved and the cell enabled good reproducibility of the electrolyses. Again, the TEMPO-mediated alcohol electroxidation in RTILs with low β was particularly advantageous for highly efficient processing, as predicted by the voltammetry described in Chapter 3. Electrolyses in RTIL media also demonstrated better alcohol selectivity than when using an acetonitrile-electrolyte system. Overall the electrolyses of TEMPO-mediated alcohol oxidations demonstrated that highly efficient and substrate selective alcohol oxidations can be carried out catalytically in the absence of secondary oxidants, volatile molecular solvents, and electrolyte salts.

In Chapter 5, the chemical input needed for alcohol oxidations was reduced further, by maximising the functionality of the RTIL media and using paired electrosynthesis. Efficient and selective flow electrolyses of TEMPO-mediated alcohol oxidations, using the $[C_4HIm][NTf_2]$-$[C_4HIm][TEMPOOSO_3]$ system as the catalyst, solvent, electrolyte and base, was demonstrated. The reduction of $[C_4HIm]^+$ at the counter-electrode eliminates the need of adding water, which reduces amount of waste produced and this paired electrosynthesis offers a more efficient use of electrical current compared to semi-reactions.[1] Furthermore the $[C_4HIm][NTf_2]$-$[C_4HIm][TEMPOOSO_3]$ was recycled up to 10 times and thus the use of these multi-functional ILs does not lead to four major sources of waste typically associated with TEMPO-mediated alcohol electroxidations: organic solvent, electrolyte, catalysts and hazardous by-products (if 100% faradaic selectivity is achieved).[2-5]

6.2. Outlook and future work

The voltammetry studies performed in Chapter 3 provide insights into the kinetics of TEMPO-mediated alcohol electroxidations in RTILs. An extension to this investigation would be to conduct a similar study performed by Doherty and co-workers, in which the mechanism of TEMPO-mediated oxidations of primary alcohols in the *N*-butyl-*N*-methyl pyrrolidinium bis(trifluoromethanesulfonyl)imide IL was investigated using cyclic voltammetry and rotating disk electrode voltammetry.[3] They were able to develop a kinetic model and identify the rate-limiting step of the reaction. Since clear differences were observed in the apparent rate constants of TEMPO-mediated oxidations of primary and secondary alcohols in $[DCA]^-$ and $[NTf_2]^-$ based RTILs in Chapter 3, it would be interesting to investigate whether the reaction mechanism and/or the rate determining steps vary in the different RTIL media and when using primary and secondary alcohol substrates.

Considering the large number of possible combinations and structures of ILs,[6] the prospects for developing other multi-tasking protic ionic liquids are exciting and could contribute more resource efficient processes as well as unlocking potentially new and innovative synthetic pathways. For example, as discovered in Chapter 5, the addition of base to the $[C_4HIm][NTf_2]$-

[C_4HIm][$TEMPOOSO_3$] system significantly increases the rate of reaction, thus the development of a protic RTIL which has a base functionality could be a solution to eliminating the addition of a base for fast electrolyses. Furthermore, for the industrially-relevant transformation of betulin to betulin-28-aldehyde it would be valuable to develop an RTIL which can dissolve betulin, whilst also promoting efficient TEMPO-mediated electroxidations.[7]

Initial investigations of using the [C_4HIm][NTf_2]-[C_4HIm][$TEMPOOSO_3$] system in another synthetically useful transformation have been conducted. As a proof-of-concept, the IL system was used to conduct the flow electrolysis of the electrosynthetic allylic C-H activation of phenyl cyclohexene to phenyl cyclohexanone, developed by Baran and co-workers.[8] By using the [C_4HIm][NTf_2]-[C_4HIm][$TEMPOOSO_3$] system and the Ammonite8 flow cell, the solvent (acetone), the base (pyridine), the electrolyte ($LiClO_4$) and the catalyst (Cl_4NHPI) was replaced with the recyclable [C_4HIm][NTf_2]-[C_4HIm][$TEMPOOSO_3$] system and approximately a 65% yield was obtained with a flow rate of 0.01 $cm^3\ min^{-1}$ and a constant applied current of 0.5 $mA\ cm^{-2}$. This demonstrates the versatility of the [C_4HIm][NTf_2]-[C_4HIm][$TEMPOOSO_3$] system and the possible prospects of using this system for other useful electroxidations requiring addition of a base.

6.3. References

1. T. Keijer, V. Bakker and J. C. Slootweg, *Nature Chemistry*, 2019, **11**, 190-195.

2. R. Barhdadi, C. Comminges, A. P. Doherty, J. Y. Nédélec, S. O'Toole and M. Troupel, *Journal of Applied Electrochemistry*, 2007, **37**, 723-728.

3. C. Comminges, R. Barhdadi, A. P. Doherty, S. O'Toole and M. Troupel, *The Journal of Physical Chemistry A*, 2008, **112**, 7848-7855.

4. J. T. Hill-Cousins, J. Kuleshova, R. A. Green, P. R. Birkin, D. Pletcher, T. J. Underwood, S. G. Leach and R. C. Brown, *ChemSusChem*, 2012, **5**, 326-331.

5. M. Rafiee, K. C. Miles and S. S. Stahl, *Journal of the American Chemical Society*, 2015, **137**, 14751-14757.

6. M. J. Earle and K. R. Seddon, in *Clean Solvents*, eds. M. A. Abraham and L. Moens, American Chemical Society, Washington, 2002, ch. 2, pp. 10-25.

7. *US Pat.,* WO/2006/105357, 2006.

8. E. J. Horn, B. R. Rosen, Y. Chen, J. Tang, K. Chen, M. D. Eastgate and P. S. Baran, *Nature*, 2016, **533**, 77.

Appendix

Appendix A contain supplementary figures and tables to the cyclic voltammetry studies described in chapter 3 and partly in chapter 5 of this thesis. Appendix B contain supplementary figures to electrolysis experiments descried in chapter 4 and chapter 5 of this thesis.

A.1-A.15 show CVs and chronoamperometric responses, which were used for the results discussed in chapter 3. The frames in Figures A.1-A.15 represent the:

a) CV of a solution constituting of 10 mmol dm^{-3} TEMPO and 5 mmol dm^{-3} decamethylferrocene, in the specified RTIL recorded with a scan rate of 5 mV s^{-1}

b) Normalised CVs of 10 mmol dm^{-3} of TEMPO dissolved in the specified RTIL with scan rates 5 mV s^{-1}, 50 mV s^{-1}, 100 mV s^{-1}, 200 mV s^{-1}, 500 mV s^{-1}, 800 mV s^{-1} and 1 V s^{-1}.

c) Chronoamperometric response of TEMPO at a constant potential, in the specified RTIL.

d) The i measured from the chronoamperometry measurement (in frame c)) plotted *vs* $t^{½}$.

e) CVs of 0.06 mol dm^{-3} TEMPO, 2.4 mol dm^{-3} 2,6-lutidine dissolved in the specified RTIL containing 0.3 mol dm^{-3}(green line), 0.6 mol dm^{-3}(black line), 1.2 mol dm^{-3} (red line) and 2.4 mol dm^{-3} (blue line) benzyl alcohol. The inset shows a graph of $i_{p,a}$ *vs* $C_A^{½}$.

f) CVs of 0.06 mol dm^{-3} TEMPO, 2.4 mol dm^{-3} 2,6-lutidine dissolved in the specified RTIL containing 0.3 mol dm^{-3}(green line), 0.6 mol dm^{-3}(black line), 1.2 mol dm^{-3} (red line) and 2.4 mol dm^{-3} (blue line) 1-phenylethanol. The inset shows a graph of $i_{p,a}$ *vs* $C_A^{½}$.

Tables A.1 – A.8 summarises the data of the diffusion coefficient of benzyl alcohol 1-phenylethanol, 1-octanol and butanol in solutions containing 0.6 mol dm^{-3} and 2.4 mol dm^{-3} 2,6-lutidine in an RTIL, obtained from PFG-NMR. The derived apparent rate constants of TEMPO-mediated oxidations of benzyl alcohol, 1-phenylethanol, 1-octanol and butanol are also summarised.

Figure A.16 shows a CV of 10 mmol dm^{-3} [BIm][$TEMPOOSO_3$] in [BIm][NTf_2] with 5 mmol dm^{-3} of dmFc. Table A.9 summarises the data obtained from the CV of [C_4HIm][$TEMPOOSO_3$]-[C_4HIm][NTf_2] system.

B.1 and B.2 show observations of electrolysis experiments conducted in the bulk electrolysis cell. Figure B.3 represent the four calibration curves used for GC-FID quantification of products and reactants.

Figure A.1: CVs and chronoamperometric responses in [C$_2$C$_1$Im][DCA] media

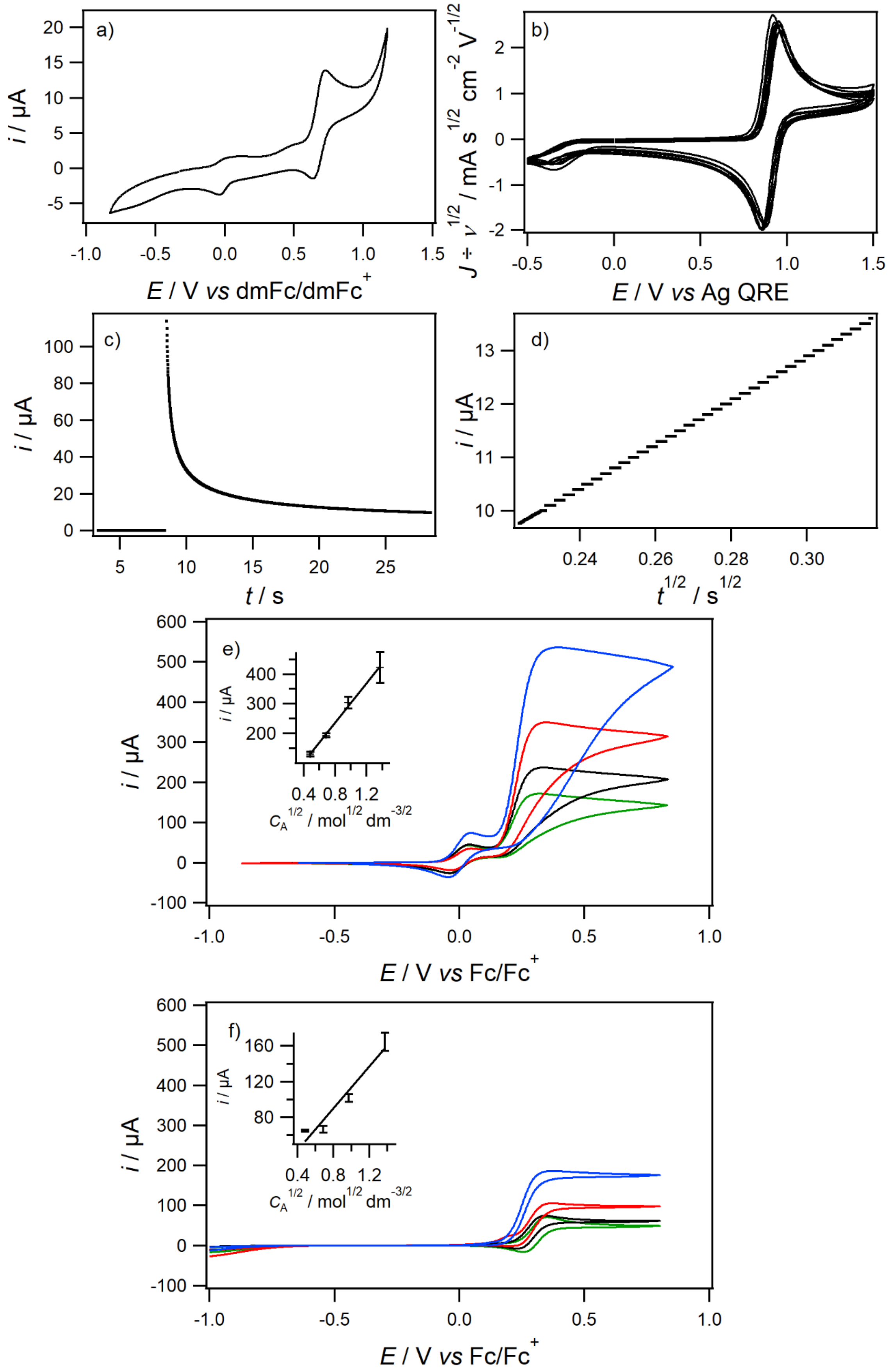

Figure A.2: CVs and chronoamperometric responses in [C_8C_1Im][DCA] media.

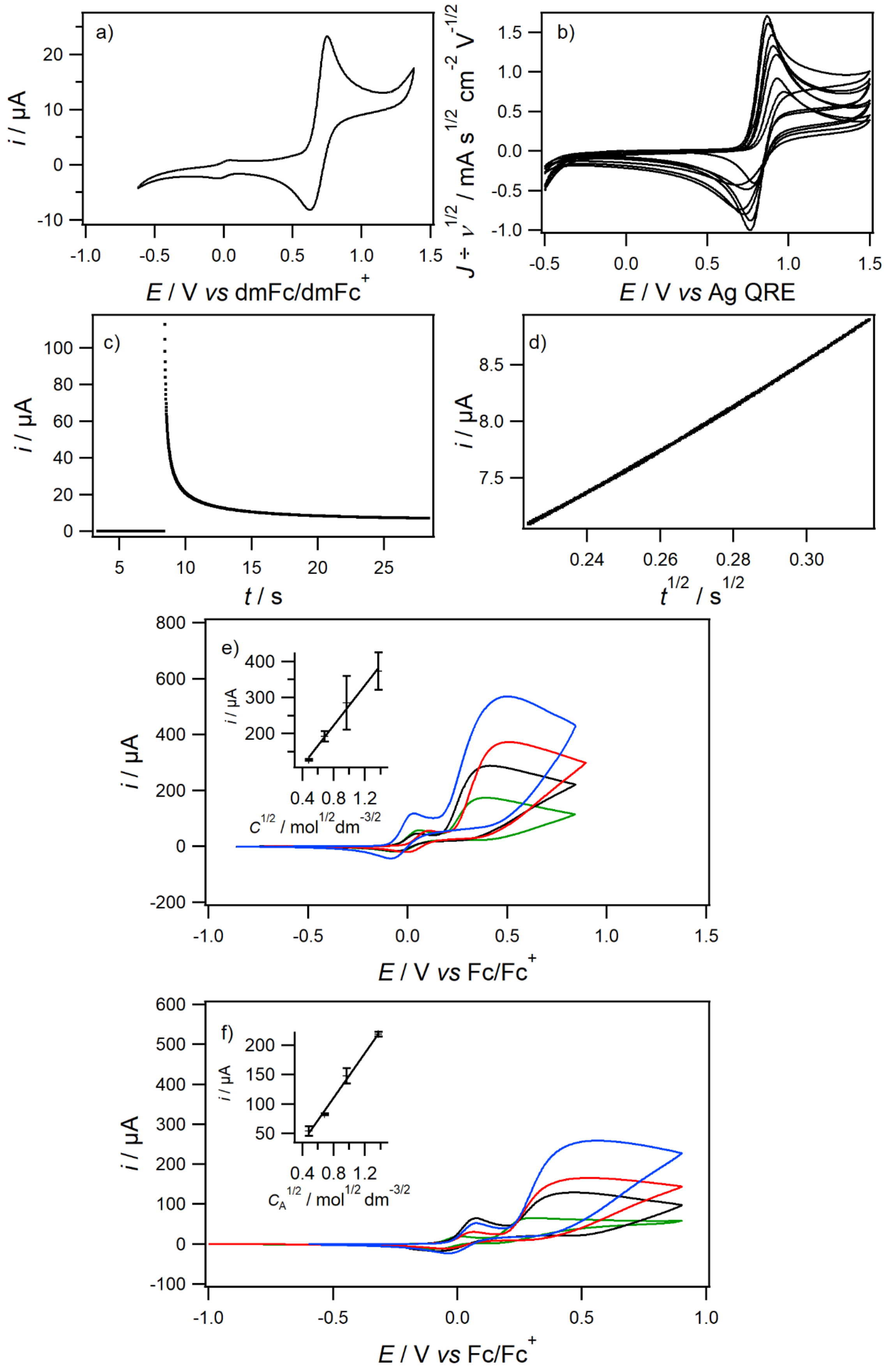

Figure A.3: CVs and chronoamperometric responses in [C_8C_1Im][BF_4] media.

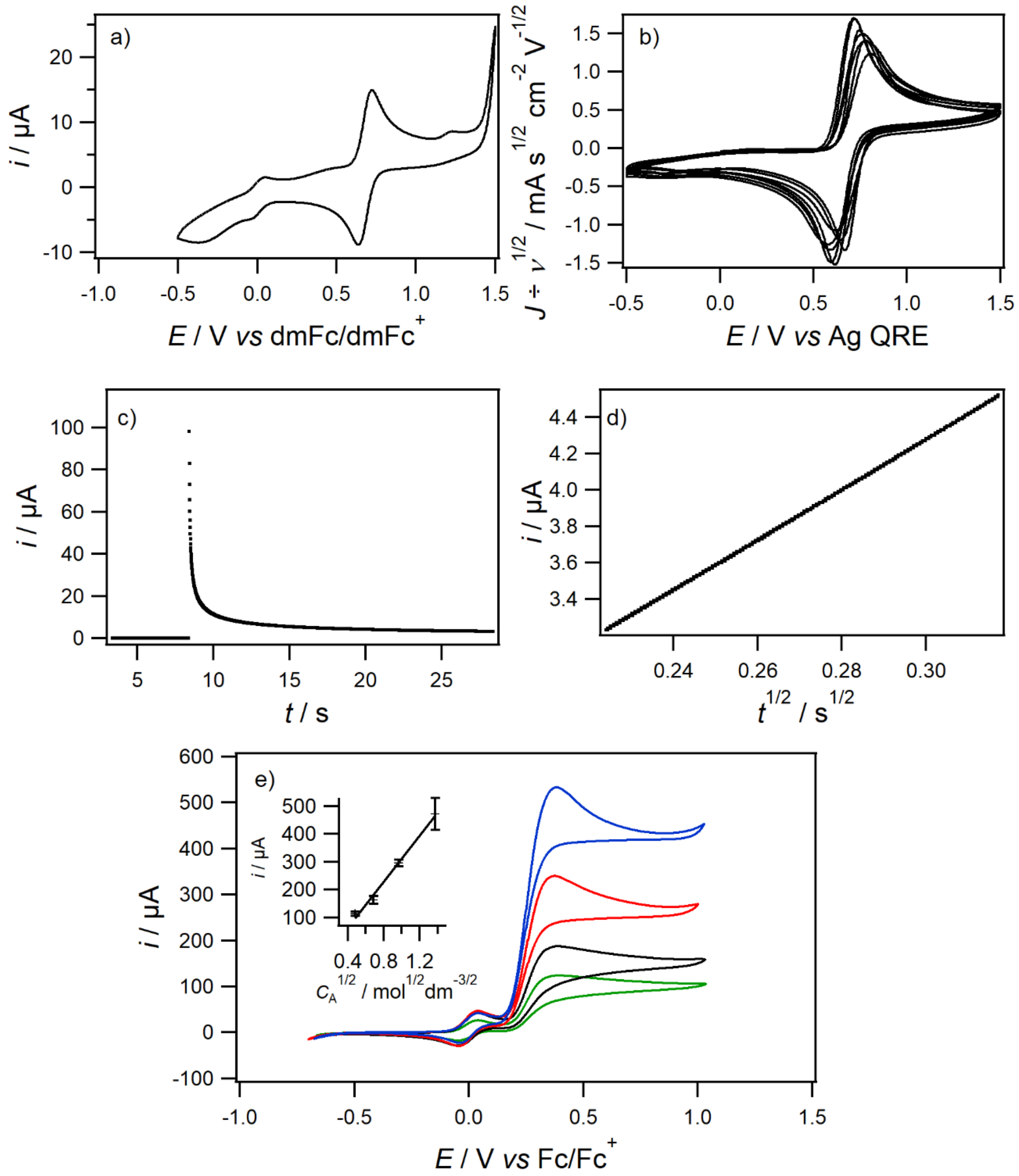

Figure A.4: CVs and chronoamperometric responses in [C_8C_1Im][OTf] media.

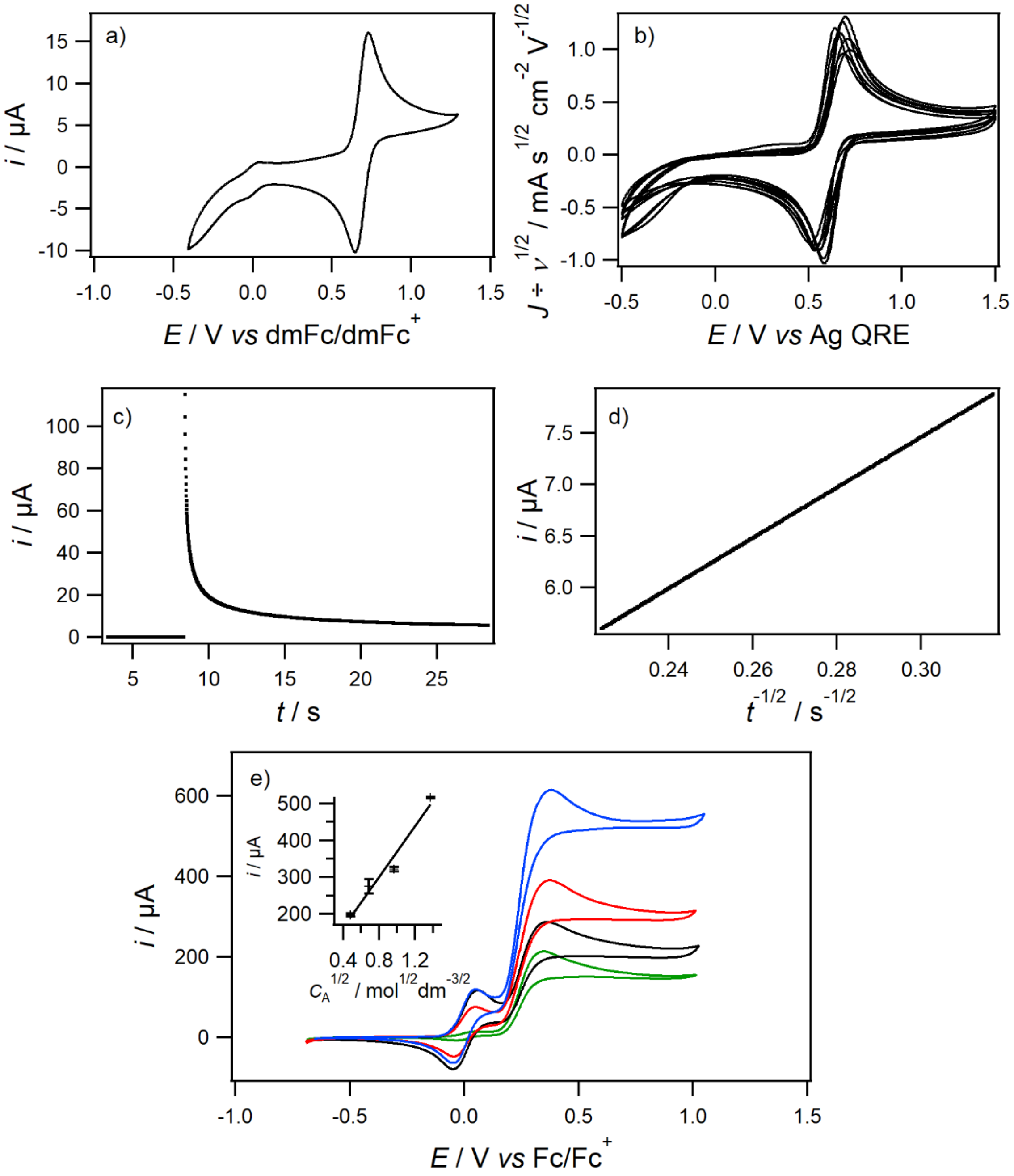

Figure A.5: CVs and chronoamperometric responses in [C_2C_1Im][NTf_2] media.

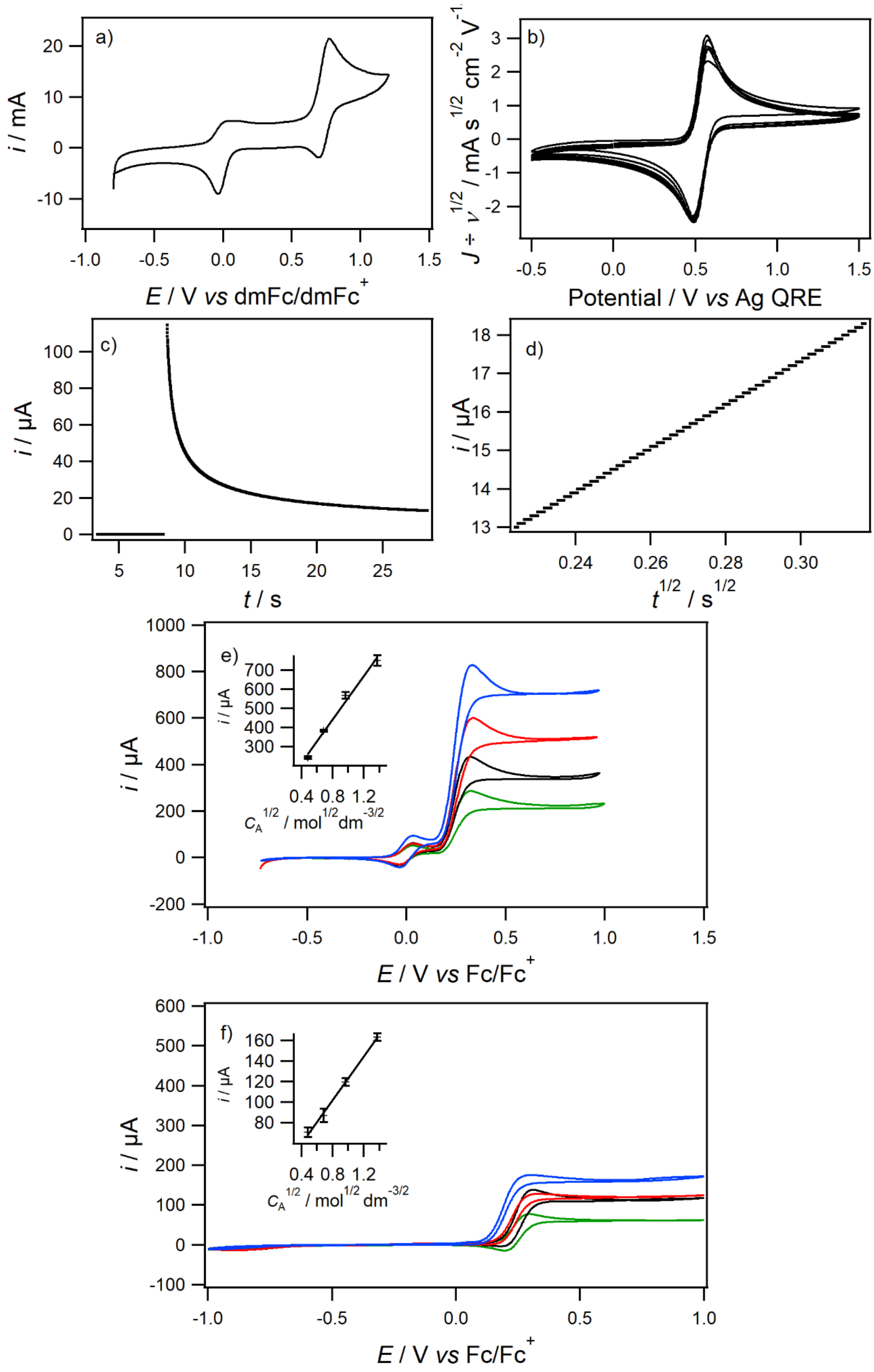

Figure A.6: CVs and chronoamperometric responses in $[C_8C_1Im][NTf_2]$ media.

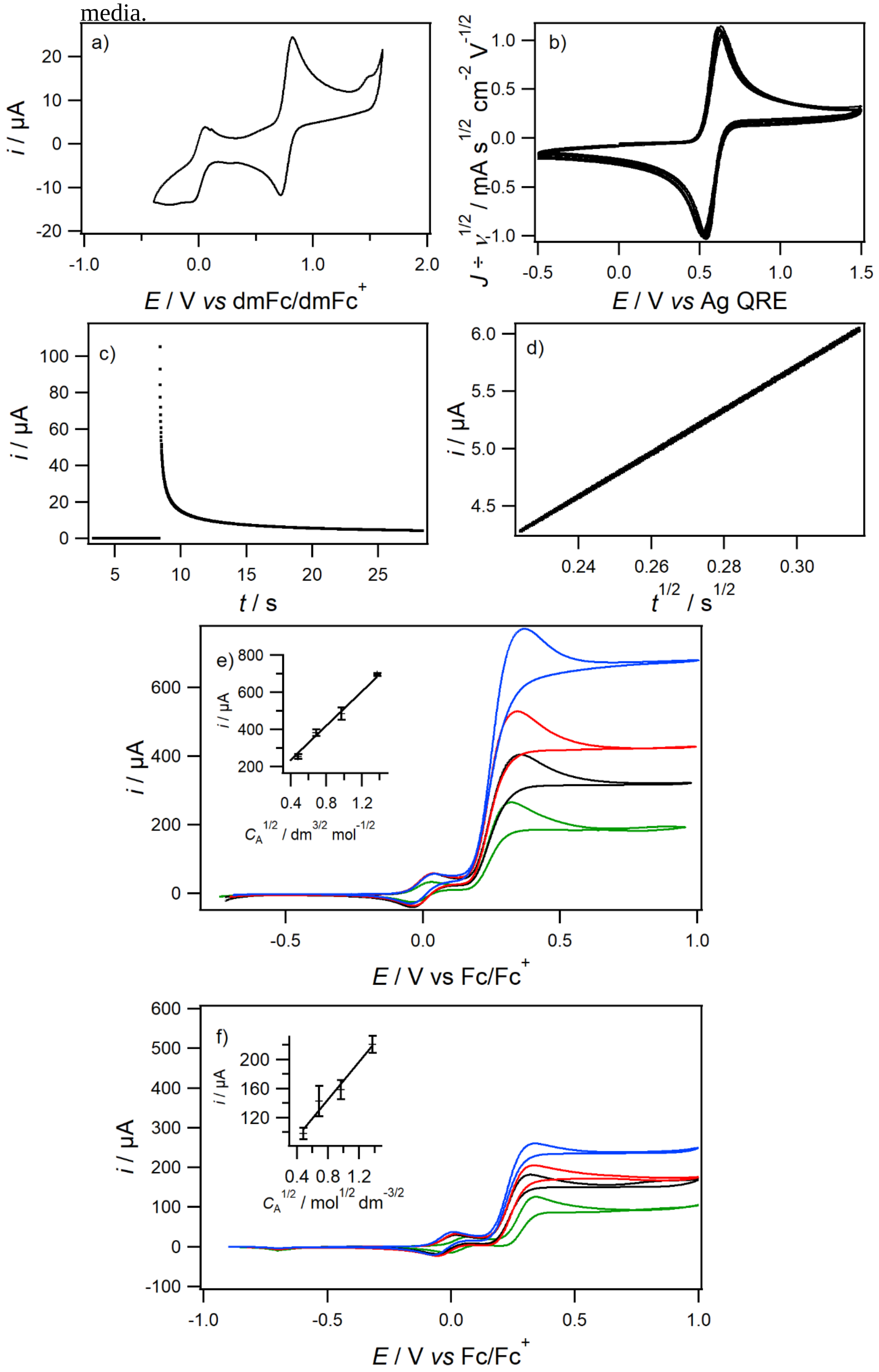

Figure A.7: CVs and chronoamperometric responses in [C_8C_1Im][PF_6] media.

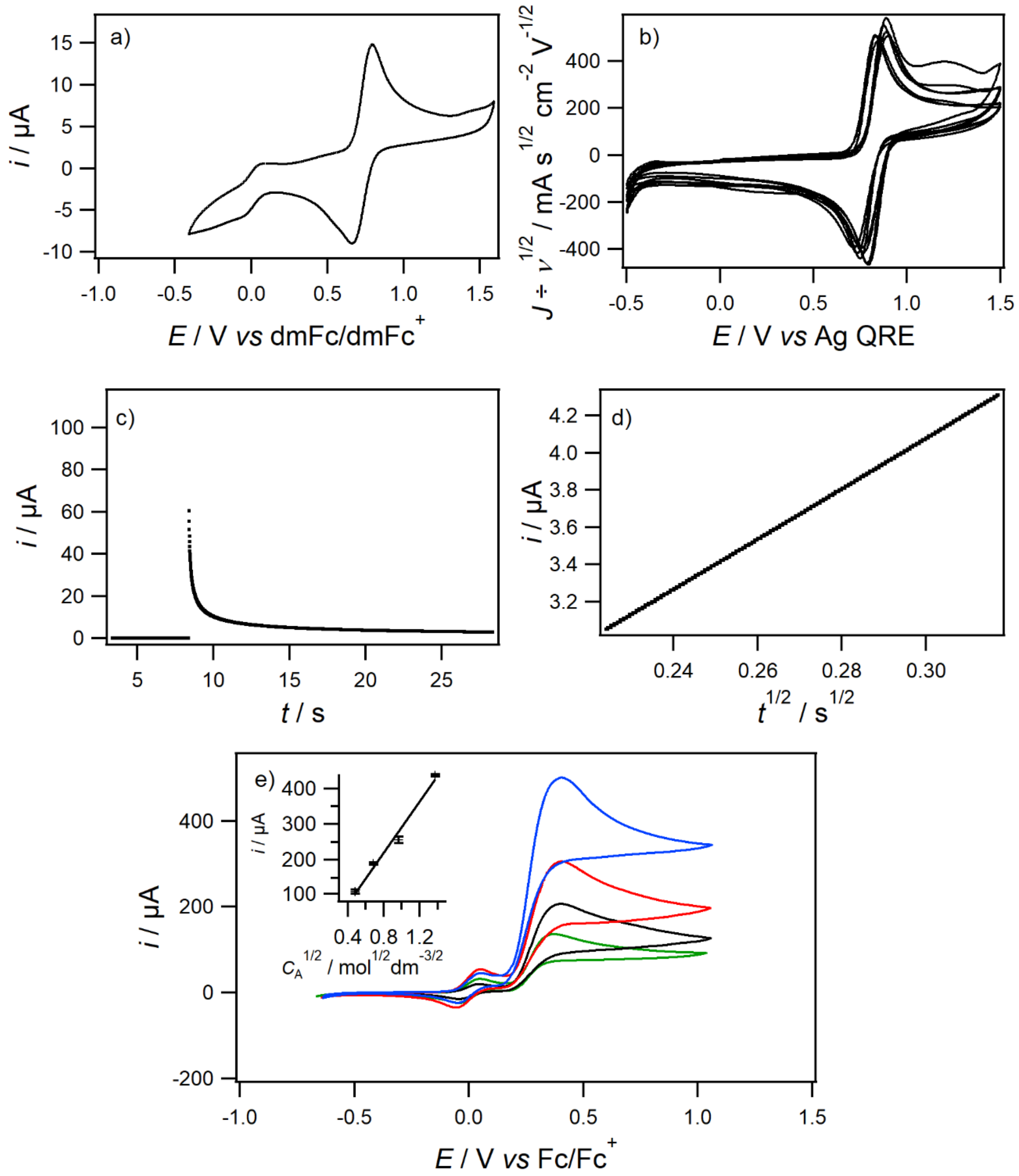

Figure A.8: CVs and chronoamperometric responses in [C_8C_1Pyrr][NTf_2] media.

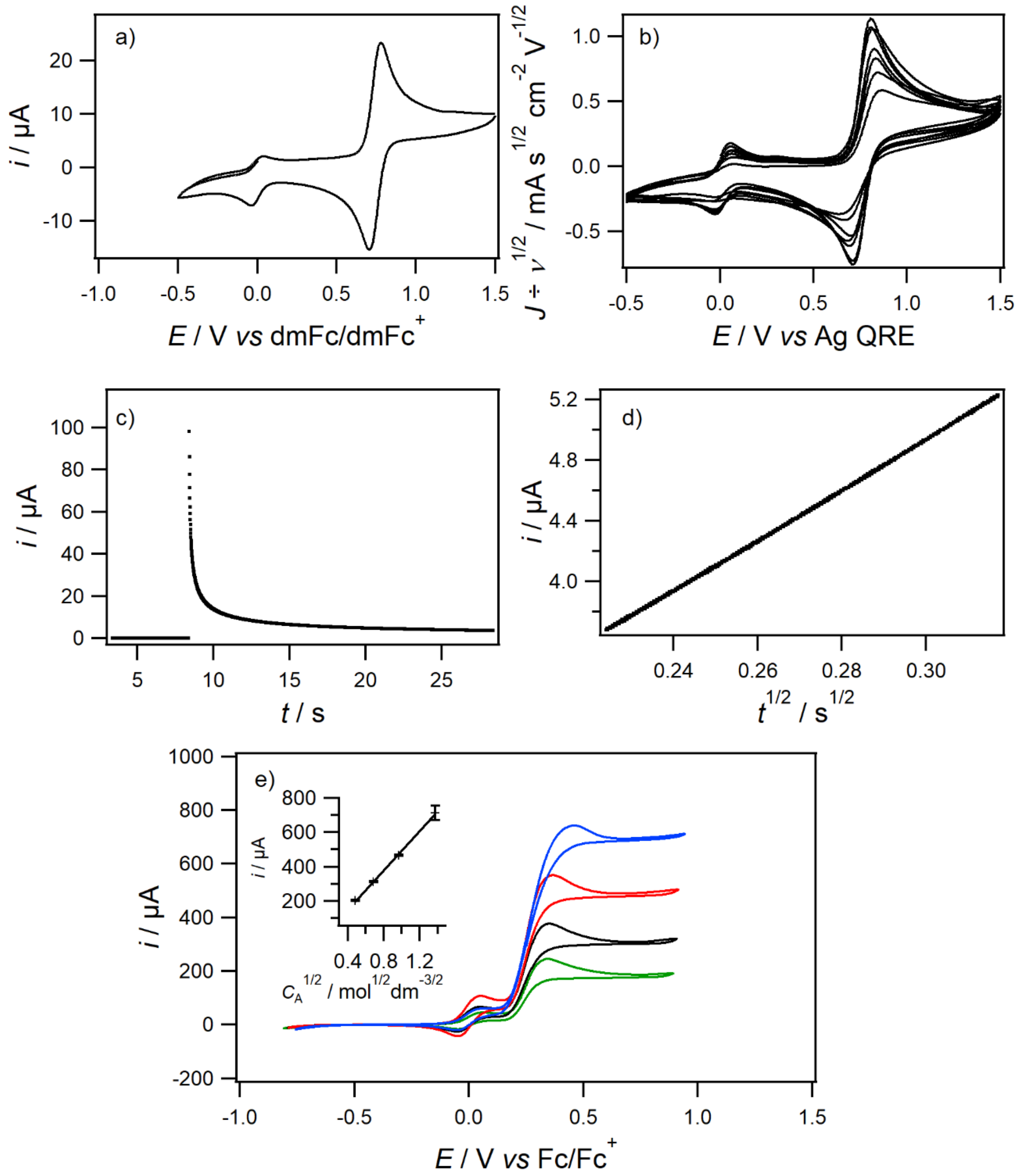

Figure A.9: CVs and chronoamperometric responses in [$N_{6,6,6,14}$][NTf_2] media.

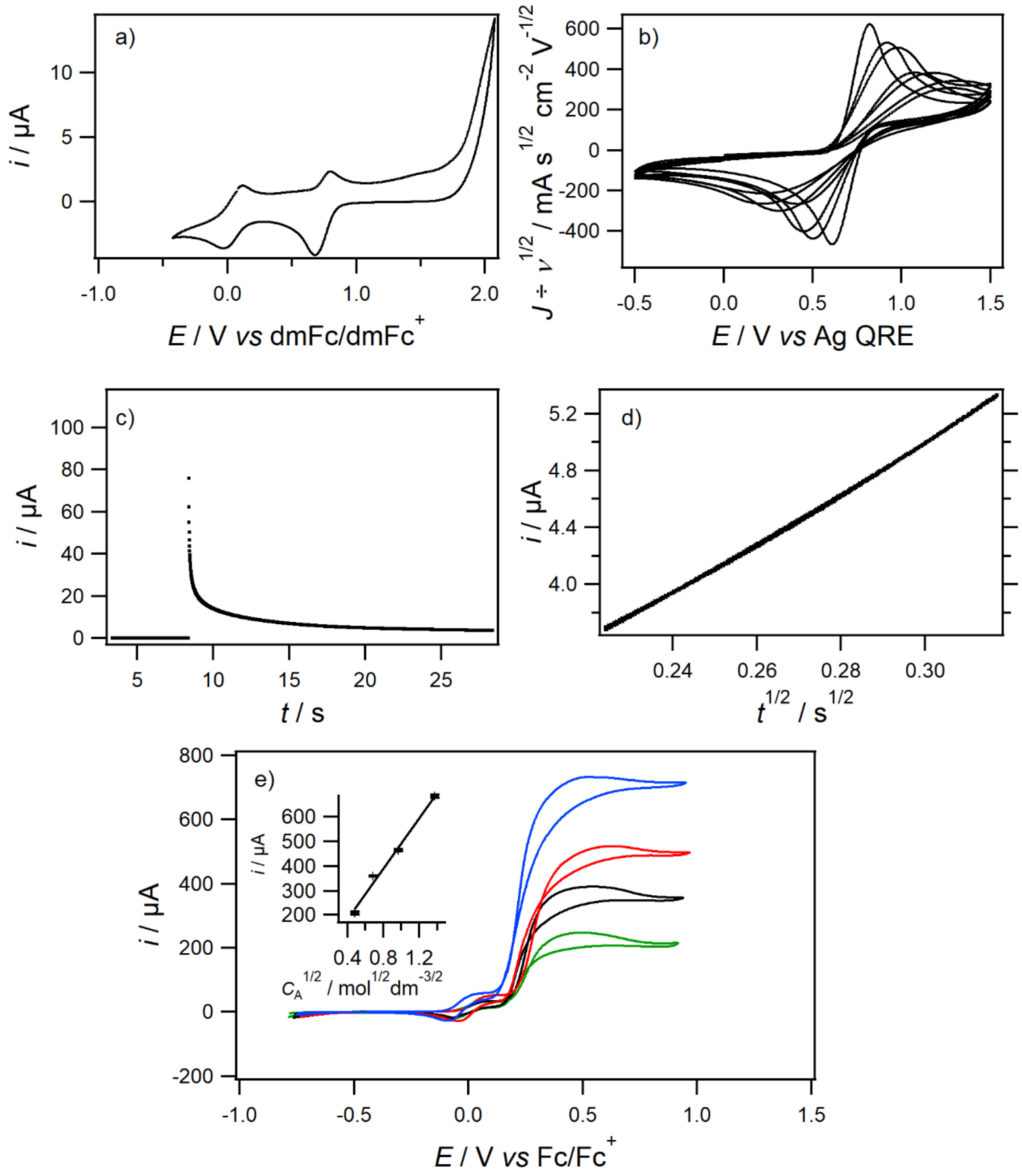

Figure A.10: CVs and chronoamperometric responses in [$N_{4,4,4,1}$][NTf_2] media.

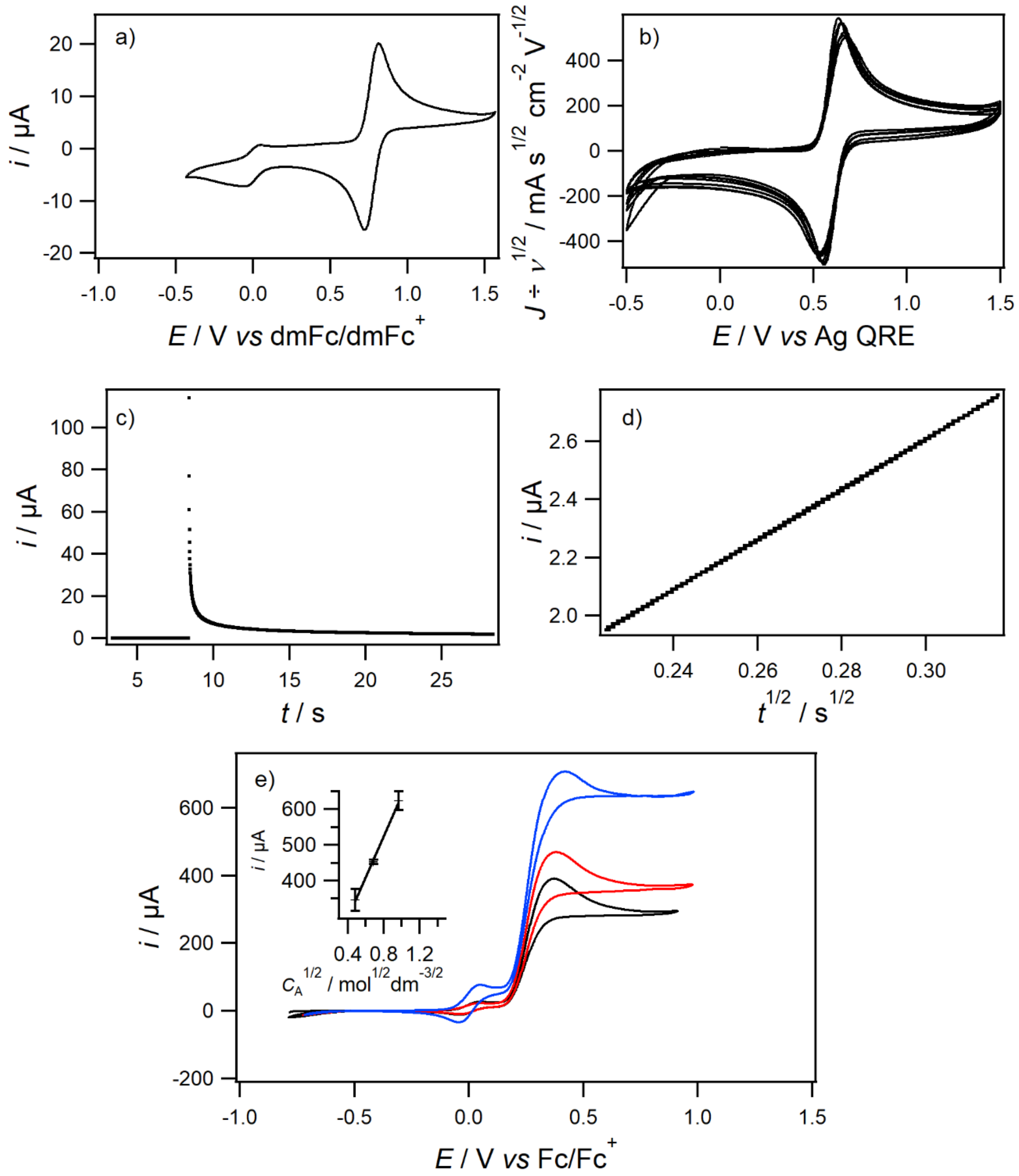

Figure A.11: CVs and chronoamperometric responses in $[P_{4,4,4,1}][NTf_2]$ media.

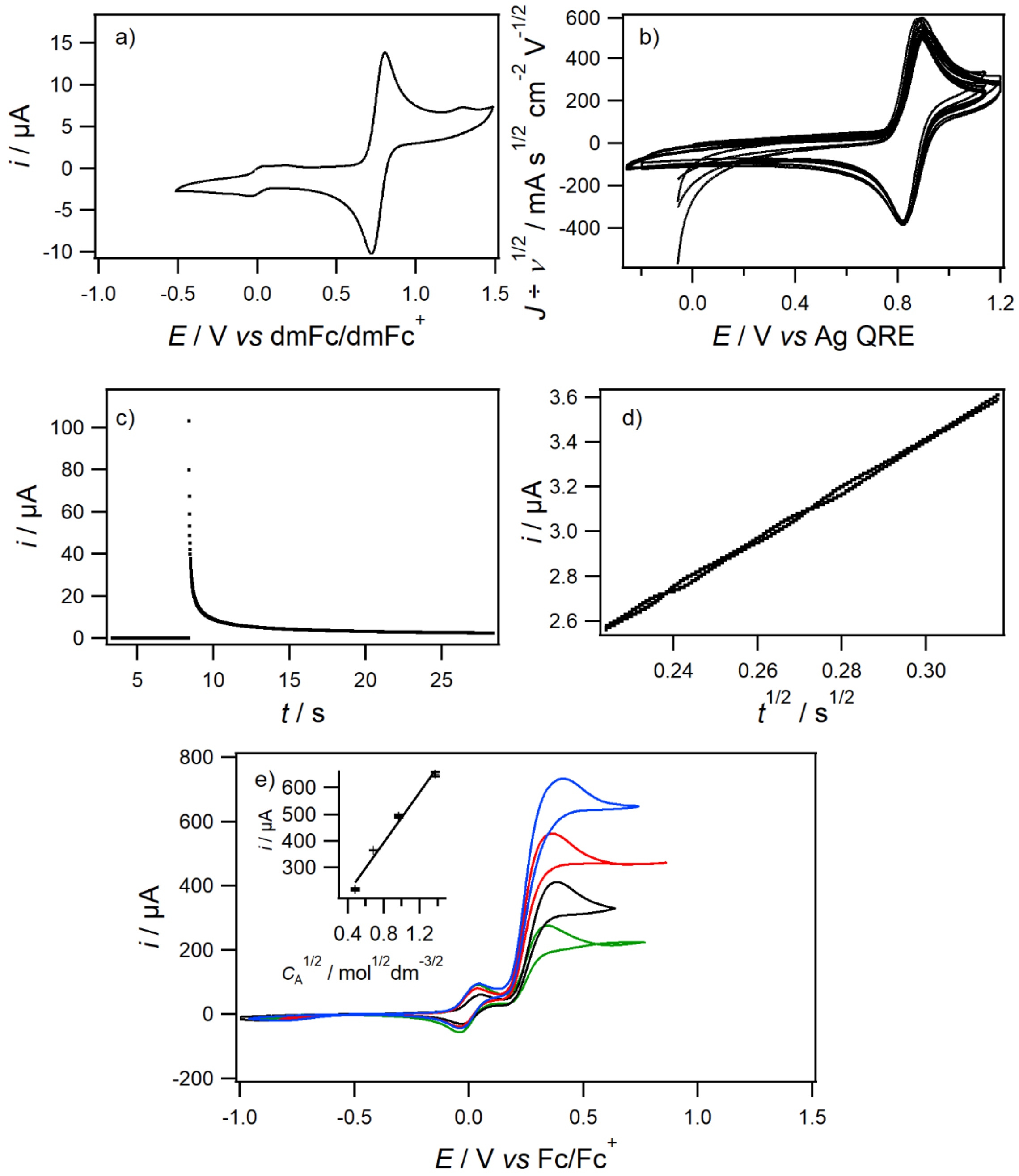

Figure A.12: CVs and chronoamperometric responses in [$P_{6,6,6,14}$][NTf_2] media.

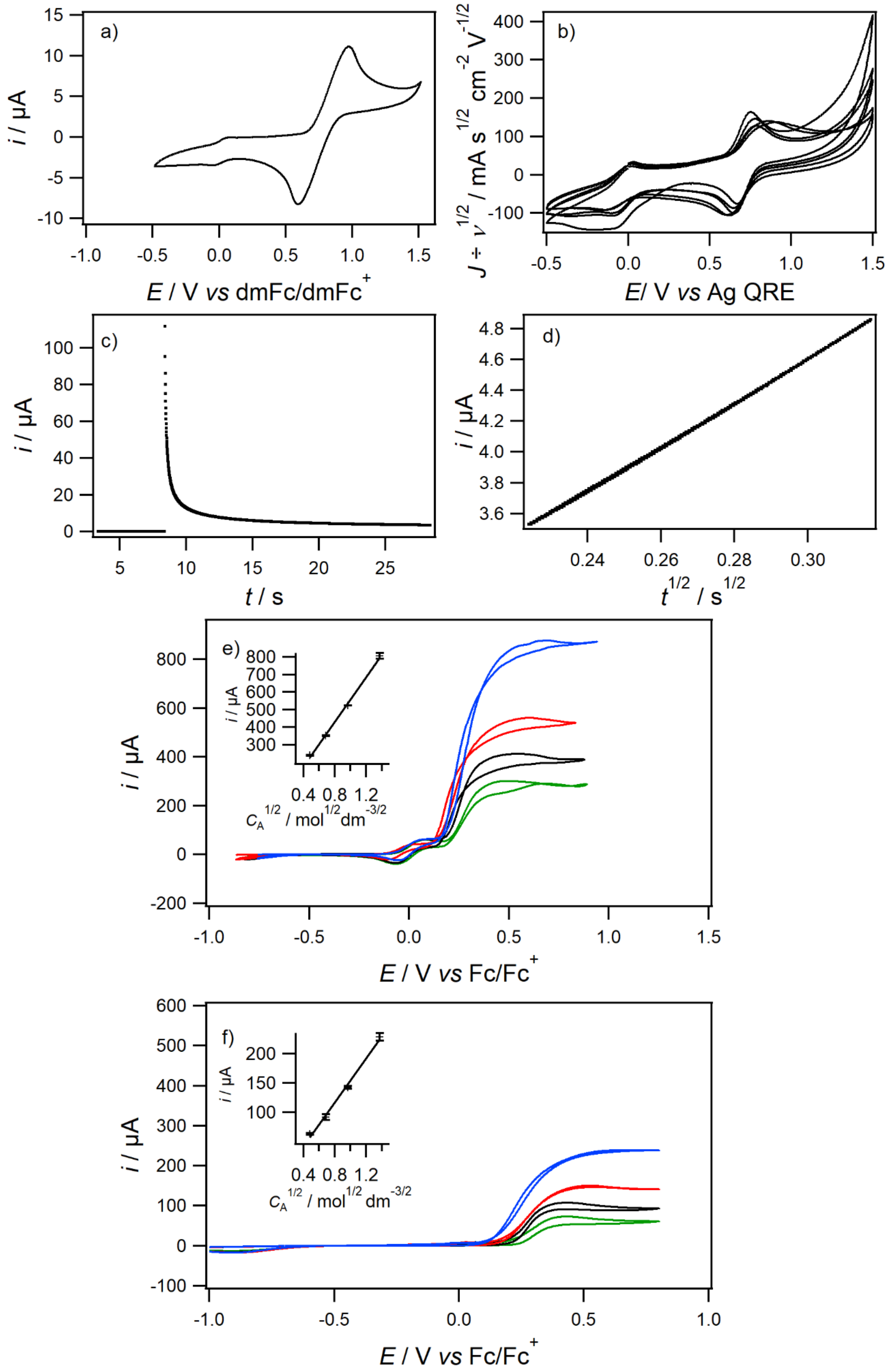

Figure A.13: CVs and chronoamperometric responses in [$P_{6,6,6,14}$][DCA] media.

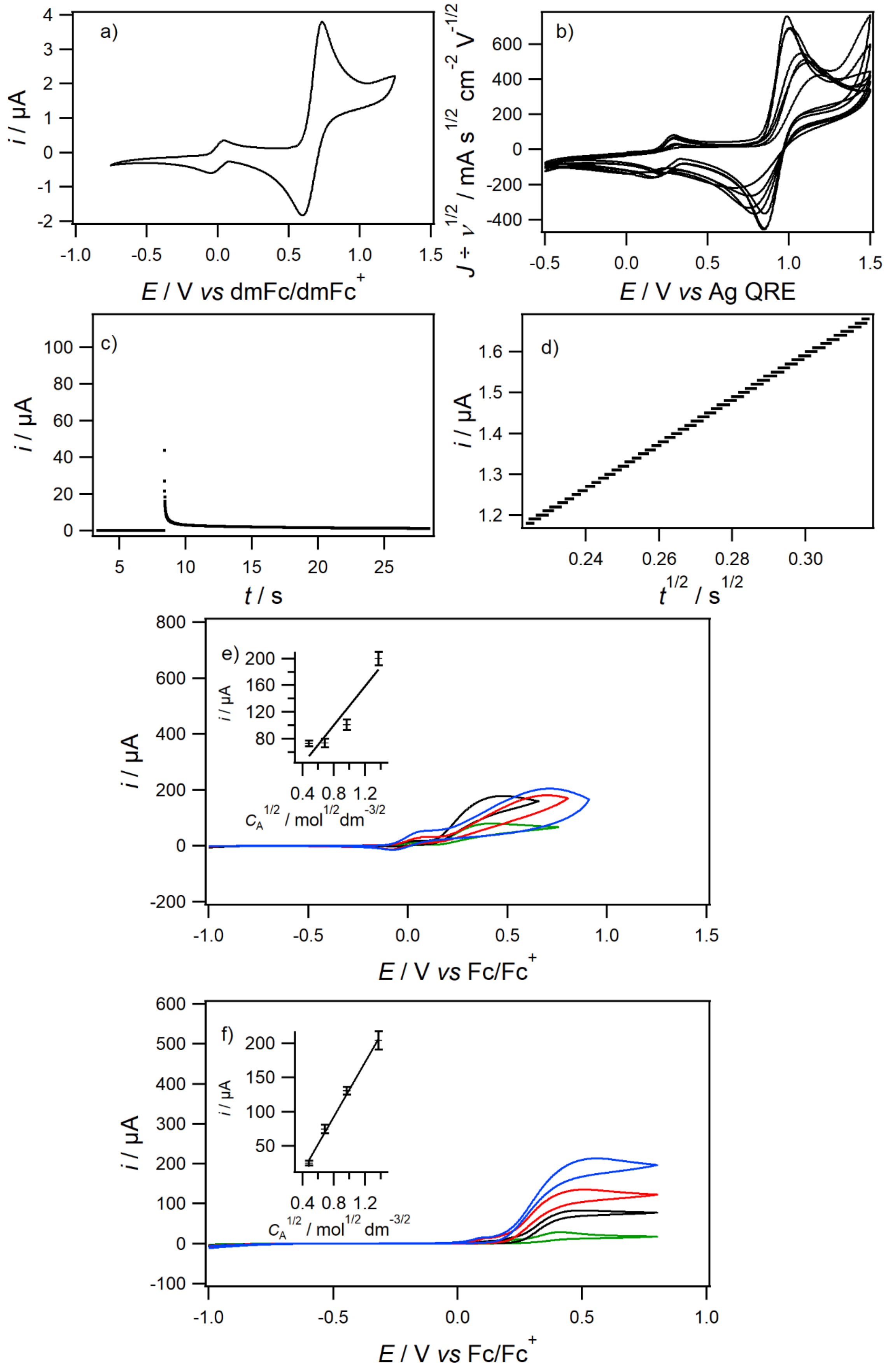

Figure A.14: CVs and chronoamperometric responses in [$N_{6,6,6,14}$][DCA] media.

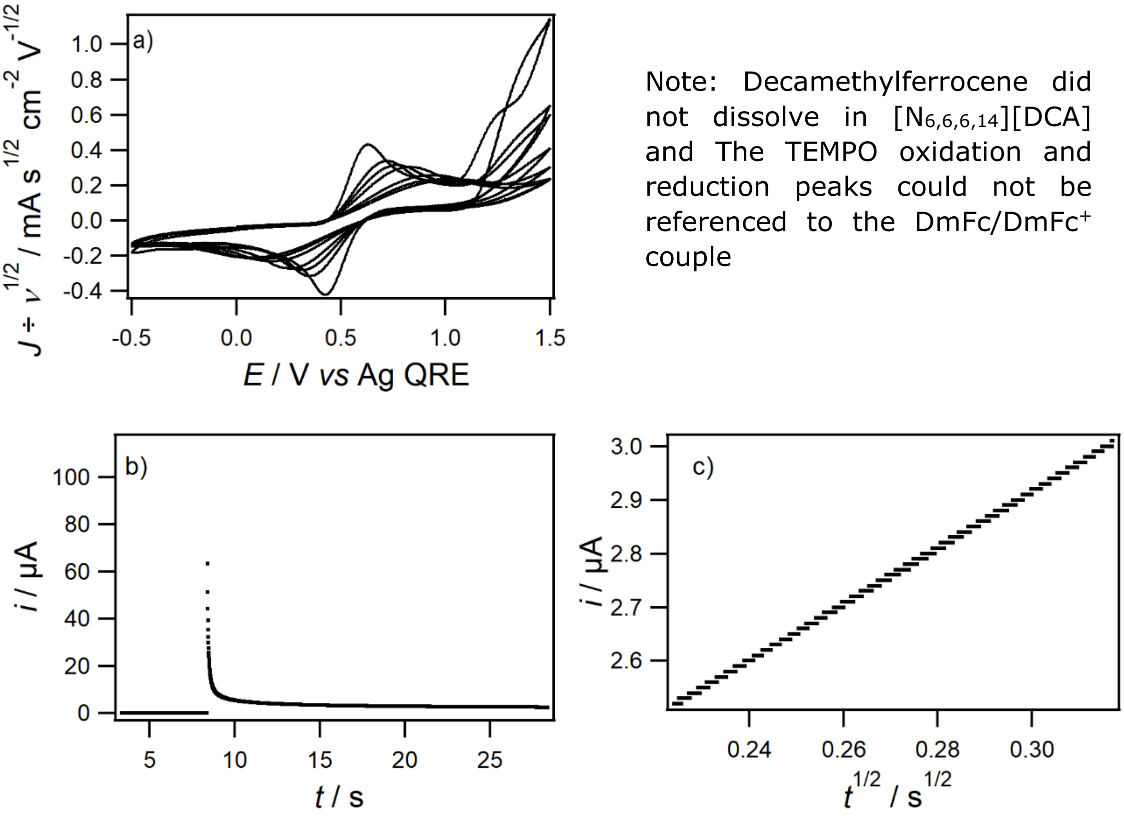

Note: Decamethylferrocene did not dissolve in [$N_{6,6,6,14}$][DCA] and The TEMPO oxidation and reduction peaks could not be referenced to the DmFc/DmFc$^+$ couple

Figure A.15: CVs and chronoamperometric responses in [$N_{4,4,4,1}$][DCA] media.

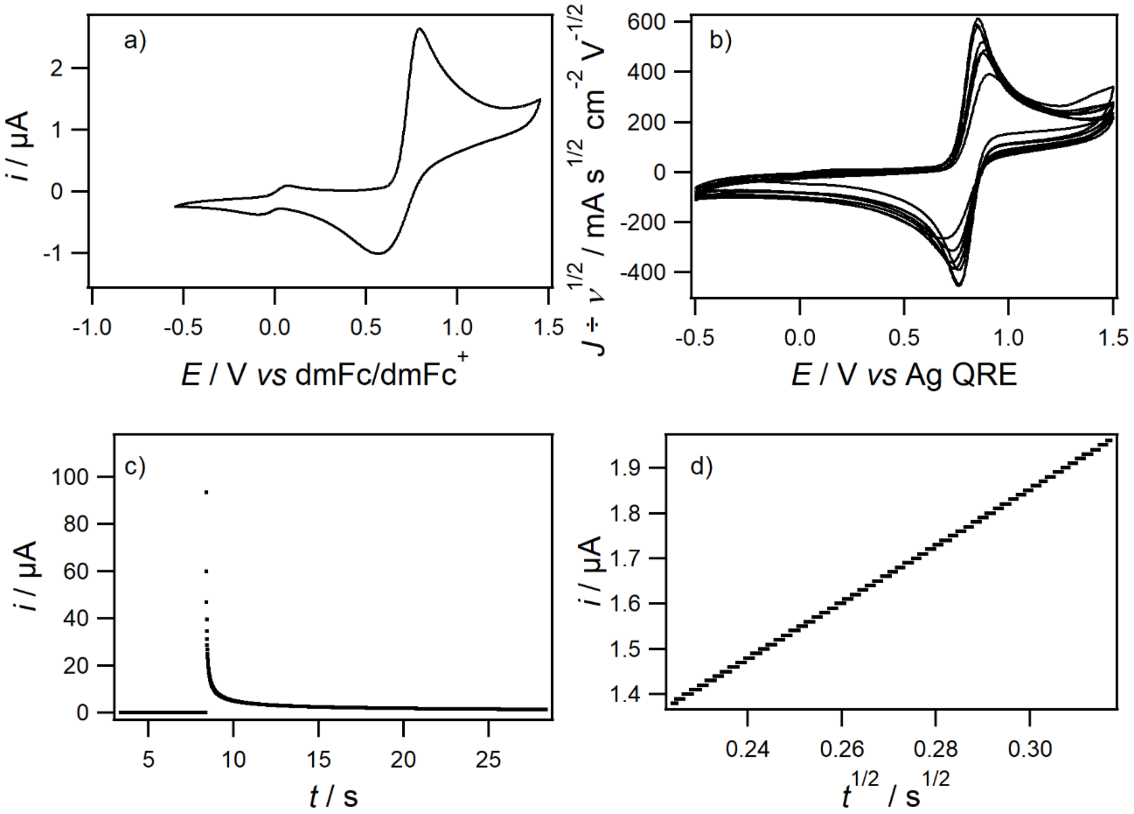

Table A.1: Average diffusion coefficients of 0.6 mol dm^{-3} benzyl alcohol in RTILs containing 2.4 mol dm^{-3} 2,6-lutidine, acquired from PFG-NMR measurements for self-diffusion data, working at 400.13 MHz (^{1}H).

Ionic Liquid	**Diffusion coefficient of Benzyl Alcohol / 10^{-10} m^2 s^{-1}**
$[C_2C_1Im][DCA]$	0.936 ± 0.102
$[C_8C_1Im][DCA]$	0.698 ± 0.128
$[C_8C_1Im][BF_4]$	0.626 ± 0.053
$[C_8C_1Im][OTf]$	0.673 ± 0.019
$[C_2C_1Im][NTf_2]$	1.171 ± 0.055
$[C_8C_1Pyrr][NTf_2]$	0.922 ± 0.044
$[N_{4,4,4,1}][NTf_2]$	0.562 ± 0.016
$[P_{4,4,4,1}][NTf_2]$	0.776 ± 0.009
$[C_8C_1Im][PF_6]$	0.511 ± 0.005
$[C_8C_1Im][NTf_2]$	0.936 ± 0.102
$[P_{6,6,6,14}][NTf_2]$	0.825 ± 0.080
$[N_{6,6,6,14}][NTf_2]$	0.690 ± 0.026
$[P_{6,6,6,14}][DCA]$	0.546 ± 0.052

Table A.2: Average diffusion coefficients of 0.6 mol dm^{-3} phenylethanol in RTILs containing 2.4 mol dm^{-3} 2,6-lutidine, acquired from PFG-NMR measurements for self-diffusion data, working at 400.13 MHz (^1H).

Ionic Liquid	**Diffusion coefficient of Phenylethanol / 10^{-10} m^2 s^{-1}**
[C_8C_1Im][DCA]	0.675 ± 0.001
[C_8C_1Im][NTf_2]	1.099 ± 0.024
[$P_{6,6,6,14}$][NTf_2]	0.806 ± 0.010
[$P_{6,6,6,14}$][DCA]	0.681 ± 0.029
[C_2C_1Im][DCA]	1.201 ± 0.021
[C_2C_1Im][NTf_2]	1.199 ± 0.032

Table A.3: Average diffusion coefficients of 0.6 mol dm^{-3} 2-butanol in RTILs containing 2.4 mol dm^{-3} 2,6-lutidine, acquired from PFG-NMR measurements for self-diffusion data, working at 400.13 MHz (^1H).

Ionic Liquid	**Diffusion coefficient of 2-Butanol / 10^{-10} m^2 s^{-1}**
[C_8C_1Im][DCA]	1.281 ± 0.059
[C_8C_1Im][NTf_2]	1.681 ± 0.009
[$P_{6,6,6,14}$][NTf_2]	1.565 ± 0.033
[$P_{6,6,6,14}$][DCA]	0.951 ± 0.045
[C_2C_1Im][DCA]	1.503 ± 0.006
[C_2C_1Im][NTf_2]	0.926 ± 0.017

Table A.4: Average diffusion coefficients of 0.6 mol dm^{-3} octanol in RTILs containing 2.4 mol dm^{-3} 2,6-lutidine, acquired from PFG-NMR measurements for self-diffusion data, working at 400.13 MHz (^{1}H).

Ionic Liquid	**Diffusion coefficient of Octanol / 10^{-10} m^{2} s^{-1}**
[C_8C_1Im][DCA]	0.332 ± 0.005
[C_8C_1Im][NTf_2]	1.029 ± 0.003
[$P_{6,6,6,14}$][NTf_2]	0.975 ± 0.101
[$P_{6,6,6,14}$][DCA]	0.581 ± 0.024
[C_2C_1Im][DCA]*	-
[C_2C_1Im][NTf_2]*	-

*1-Octanol did not dissolve in these RTILs

Table A.5: *k* obtained for TEMPO-mediated oxidation of benzyl alcohol in various RTIL media.

Ionic Liquid	**Apparent rate constant of benzyl alcohol oxidation / dm^3 mol^{-1} s^{-1}**
[C_2C_1Im][DCA]	0.245 ± 0.014
[C_8C_1Im][DCA]	0.116 ± 0.009
[C_8C_1Im][BF_4]	0.239 ± 0.005
[C_8C_1Im][OTf]	0.236 ± 0.000
[C_2C_1Im][NTf_2]	0.413 ± 0.001
[C_8C_1Pyrr][NTf_2]	0.520 ± 0.004
[$N_{4,4,4,1}$][NTf_2]	0.524 ± 0.016
[$P_{4,4,4,1}$][NTf_2]	0.434 ± 0.000
[C_8C_1Im][PF_6]	0.380 ± 0.000
[C_8C_1Im][NTf_2]	0.336 ± 0.004
[$P_{6,6,6,14}$][NTf_2]	0.743 ± 0.008
[$N_{6,6,6,14}$][NTf_2]	0.555 ± 0.000
[$P_{6,6,6,14}$][DCA]	0.059 ± 0.001

Table A.6: *k* obtained for TEMPO-mediated oxidation of 1-phenylethanol in various RTIL media.

Ionic Liquid	**Apparent rate constant of 1-phenylethanol oxidation / dm^3 mol^{-1} s^{-1}**
[C_8C_1Im][DCA]	0.080 ± 0.000
[C_8C_1Im][NTf_2]	0.017 ± 0.000
[$P_{6,6,6,14}$][NTf_2]	0.039 ± 0.000
[$P_{6,6,6,14}$][DCA]	0.096 ± 0.000
[C_2C_1Im][DCA]	0.017 ± 0.000
[C_2C_1Im][NTf_2]	0.010 ± 0.000

Table A.7: *k* obtained for TEMPO-mediated oxidation of 2-butanol in various RTIL media.

Ionic Liquid	**Apparent rate constant of 2-butanol oxidation / dm^3 mol^{-1} s^{-1}**
[C_8C_1Im][DCA]	0.026 ± 0.000
[C_8C_1Im][NTf_2]	0.003 ± 0.000
[$P_{6,6,6,14}$][NTf_2]	0.007 ± 0.000
[$P_{6,6,6,14}$][DCA]	0.011 ± 0.000
[C_2C_1Im][DCA]	0.002 ± 0.000
[C_2C_1Im][NTf_2]	0.008± 0.000

Table A.8: *k* obtained for TEMPO-mediated oxidation of 1-octanol in various RTIL media.

Ionic Liquid	**Apparent rate constant of 1-octanol oxidation / dm^3 mol^{-1} s^{-1}**
[C_8C_1Im][DCA]	0.140 ± 0.001
[C_8C_1Im][NTf$_2$]	0.160 ± 0.000
[$P_{6,6,6,14}$][NTf$_2$]	0.321 ± 0.000
[$P_{6,6,6,14}$][DCA]	0.090 ± 0.018
[C_2C_1Im][DCA]*	
[C_2C_1Im][NTf$_2$]*	

*1-Octanol did not dissolve in these RTILs

Figure A.16: CV of 5 mmol dm^{-3} dmFc and 10 mmol dm^{-3} [C_4HIm][TEMPOOSO$_3$] dissolved in [C_4HIm][NTf$_2$], recorded using a 3 mm diameter glassy-carbon electrode at 50 mV s^{-1}.

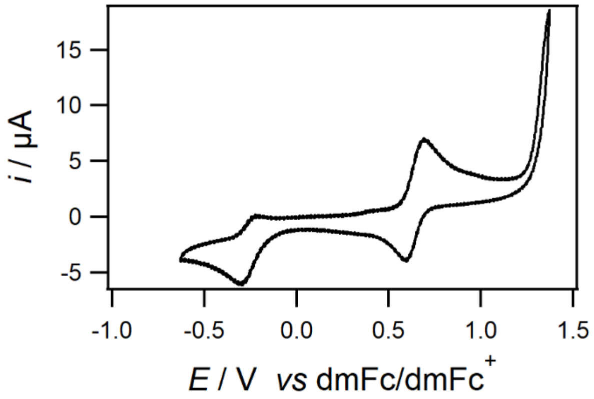

Table A.9: $E_{p,a}$, $E_{p,c}$, $E_{T,½}$, ΔE, $i_{p,a}$, $i_{p,c}$ and $i_{p,a}/i_{p,c}$ ratio of the TEMPOOSO$_3^-$/TEMPO$^+$OSO$_3^-$ redox couple obtained from CVs measured at 5 mV s^{-1} of 10 mmol dm^{-3} [C_4HIm][TEMPOOSO$_3$] dissolved in [C_4HIm][NTf$_2$]. All potentials are relative to that of dmFc/dmFc$^+$.

Parameter, units	
$E_{p,a}$, mV	763
$E_{p,c}$, mV	695
$E_{1/2}$, mV	729
ΔE, mV	68
$I_{p,a}$, μA	+2.80
$I_{p,c}$ μA	-2.79
$I_{p,a}/I_{p,c}$	1.00

Figure B.1: Last 40 min of bulk electrolysis of a 10 cm^3 solution of 0.6 mol dm^{-3} benzyl alcohol, 0.06 mol dm^{-3} TEMPO and 2.4 mol dm^{-3} 2,6-lutidine dissolved in a [C_8C_1Im][DCA]. Total electrolysis time 5.5 hrs with an applied current of 100 mA. The increase in potential at the end of the electrolysis indicate the consumption of the alcohol substrate.

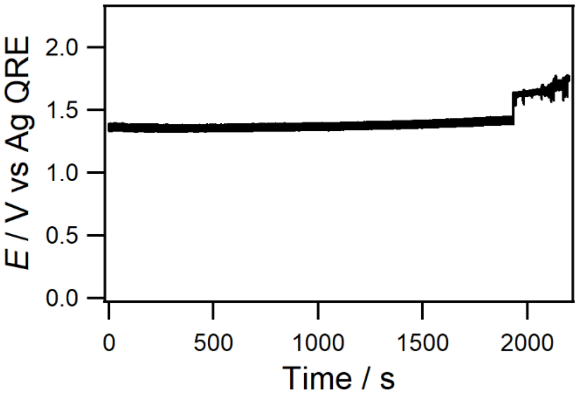

Figure B.2: 10 cm^3 solutions of 0.6 mol dm^{-3} benzyl alcohol, 0.06 mol dm^{-3} TEMPO and 2.4 mol dm^{-3} 2,6-lutidine dissolved in a [C_8C_1Im][DCA] before (solution to the left) and after (solution to the right) prolonged bulk electrolysis time, 37 hours at an applied current of 50 mA.

Figure B.3: GC-FID calibration curves for a) benzyl alcohol, b) benzaldehyde, c) 1-phenylethanol and d) acetophenone. The calibration curves were obtained by measuring the peak area ratio of benzyl alcohol, benzaldehyde, 1-phenylethanol or acetophenone with the reference ($A_{substrqte} \div A_{Ref}$) of solutions containing varying concentrations of the substrate. Tert-butylbenzene was used as the reference. The conditions of GC-FID injections are detailed in chapter 2.